Aspectos não perturbativos da QCD em espalhamentos elásticos hadrônicos

Mateus Broilo da Rocha

Porto Alegre

2017

FEDERAL UNIVERSITY OF RIO GRANDE DO SUL

INSTITUTE OF PHYSICS

DOCTORAL QUALIFYING EXAM

Non-perturbative QCD aspects of elastic hadronic scatterings [*]

Mateus Broilo da Rocha

Supervisor: Prof. Dr. Emerson Gustavo de Souza Luna

Doctoral Qualifying Thesis submitted to the Institute of Physics, Federal University of Rio Grande do Sul, in partial fulfillment of the requirements to proceed to the final exam for the degree of Doctor of Science.

Porto Alegre

September 25, 2017

To all whom I love,
no more nor less.

"*What befell the weakling youth lifting the dread goddess's veil at Lais?*"
– Moby Dick, Herman Melville.

List of Abbreviation

CERN   *Conseil Européen pour la Recherche Nucléaire*

CM   *Centre of Mass*

DIS   *Deep Inelastic Scattering*

DGM   *Dynamical Gluon Mass*

DGLAP   *Dokshitzer-Gribov-Lipatov-Altarelli-Parisi*

dof   *degree of freedom*

FMLt   *Froissart-Martin-Łukaszuk Theorem*

HERA   *Hadron Electron Ring Accelerator*

ISR   *Intersecting Storage Ring*

LHC   *Large Hadron Collider*

lhs   *left-hand side*

LO   *Leading Order*

NLO   *Next to Leading Order*

OPE   *Operator Product Expansion*

PDF   *Parton Distribution Function*

pQCD   *Perturbative Quantum Chromodynamics*

QCD   *Quantum Chromodynamics*

QED   *Quantum Electrodynamics*

QIM   *QCD Inspired Model*

rhs   *right-hand side*

SLAC   *Stanford Linear Accelerator*

TOTEM   *TOTal Elastic and diffractive cross section Measurement*

Resumo

Nos últimos anos, o LHC tem divulgado medições precisas de espalhamentos elásticos próton-próton que tem se tornado um guia importante na busca pela seleção de modelos fenomenológicos e abordagens teóricas para se entender, de uma vez por todas, a teoria das interações fortes. Através da formulação de dois modelos compatíveis com analiticidade e unitaridade, sendo estes um baseado em teoria de Regge e outro inspirado em Cromodinâmica Quântica, estudamos alguns aspectos relacionados à Física por trás das interações hadrônicas. Em modelos de polos de Regge, o crescimento das seções de choque hádron-hádron é relacionado à troca de um estado sem cor possuindo os números quânticos do vácuo. Na perspectiva da QCD, o Pomeron pode ser entendido como a troca de pelo menos dois glúons em um estado de singleto de cor, desta forma a teoria de Regge atua como um importante manual no desenvolvimento de uma teoria fundamental para processos suaves baseada em QCD. Em modelos inspirados em QCD, o crescimento das seções de choque é associado ao espalhamento semiduro de pártons que compõem os hádrons. A dependência com energia da seção de choque é devida principalmente à processos elementares que possuem ao menos um glúon no estado incial, entretanto estes processos apresentam divergências em pequenos valores dos momenta transferido.

Em altas energias, o Pomeron desempenha um papel crucial na descrição das interações suaves. À luz desses novos dados, que de fato fornecem um vínculo único aos parâmetros do Pomeron, realizamos uma análise detalhada aos dados de espalhamentos próton-próton e antipróton-próton de forma a determinar o *intercept* e o *slope* da trajetória do Pomeron suave. Esta análise foi realizada baseada em teoria de Regge usando amplitudes a nível de Born e amplitudes eiconalizadas. No primeiro caso, estimamos a contibuição da troca de dois Pomerons, e no último caso investigamos o papel que desempenha a forma do vértice próton-Pomeron e também demos atenção particular à singularidade mais próxima no canal t da trajetória do Pomeron. Examinamos também os efeitos de Reggeons secundários ao introduzir as contribuições das trocas de mésons com maiores valores de *spin*, sendo estes, os mésons com assinatura positiva a_2 e f_2, e com assinatura negativa ω e ρ.

Usando um modelo eiconal baseado em QCD, estudamos as contribuições infravermelhas às interações párton-párton semiduras considerando uma carga efetiva cujo comportamento infravermelho é vinculado à uma escala de massa dinâmica, que é um efeito puramente não perturbativo, e sua existência é fortemente sustentada por simulações recentes de QCD na

rede. O modelo é construído através do modelo a pártons, usando seções de choque elementares de processos partônicos de QCD, funções de distribuição atualizadas de quarks e glúons, sendo estas CTEQ6L, CTEQ6L1 e MSTW, e cortes cinemáticos fisicamente motivados que restringem os processos elementares partônicos ao regime semiduro. Discutimos os aspectos teóricos deste formalismo e consideramos as implicações fenomenológicas de uma classe de fatores de forma dependentes de energia no limite de altas energias da amplitude de espalhamento frontal. De forma a conectar a dinâmica de pártons semiduros com o espalhamento hádron-hádron, introduzimos relações de dispersão integrais especialmente construídas para relacionar a parte real e a parte imaginária das eiconais com fatores de forma com dependência em energia. Em nosso modelo, a eiconal é escrita em termos de partes par e ímpar conectadas pela simetria de cruzamento. Esta conexão, entre a função eiconal complexa com uma relação de dispersão integral, é somente possível porque em primeira ordem de aproximação da série da eiconal, suas partes par e ímpar, respectivamente, assumirão valores reais em um segmento do eixo real com a mesma estrutura de corte que a amplitude de espalhamento.

Discutimos as implicações dos nossos resultados e apresentamos previsões para a seção de choque total, para a razão entre parte real e imaginária da amplitude de espalhamento frontal considerando os dados recentes obtidos pela colaboração TOTEM no LHC e também em energias de raios cósmicos, obtidos pelos experimentos AUGER e *Tellescope array*. Também apresentamos algumas previsões aos dados recentes de seção de choque diferencial elástica em colisões próton-próton obtidas no LHC.

Como este é um trabalho que está em progresso, nós ainda temos muito o que fazer. Desta forma, algumas perspectivas, possíveis mudanças nos modelos e algumas futuras intuições também são discutidas nas observações finais no final deste texto. Nada aqui deve ser tomado como uma verdade absoluta. Este é um estudo com perspectivas futuras, e por esta razão nada é imutável.

Abstract

In the last couple of years, the LHC has released precise measurements of elastic proton-proton scattering which has become an important guide in the search for selecting phenomenological models and theoretical approaches to understand, once and for all, the theory of strong interactions. By means of the formulation of two based-models compatible with analyticity and unitarity constraints, namely, one based upon Regge theory and another inspired by Quantum Chromodynamics, we study some aspects concerning the Physics behind hadronic interactions. In Regge pole models, the increase of hadron-hadron cross-sections is related to the exchange of a colourless state having the quantum numbers of the vacuum, the Pomeron. In the QCD framework the Pomeron can be understood as the exchange of at least two gluons in a colour singlet state, hence Regge theory acts as an important enchiridion in the development towards a fundamental theory for soft process based upon QCD. In QCD-inspired models, the increase of cross-sections is associated with semi-hard scattering of partons within hadrons. The energy dependence of the cross-section is driven mainly by elementary processes which have at least one gluon in the initial state, however these processes are potentially divergent at low transfered momenta.

At high energies the Pomeron plays a crucial part in describing the soft interactions. At the light of these recent data, which in fact provide a unique constraint on the Pomeron parameters, we perform a detailed analysis of proton-proton and also antiproton-proton scattering data in order to determine the intercept and the slope of the soft Pomeron trajectory. This analysis is performed based on Regge theory using Born-level and eikonalised amplitudes. In the former case we estimate the contribution of double Pomeron exchange and in the latter one we investigate the role of eikonalisation in both one- and two-channel models. The role of the proton-Pomeron vertex form and of the nearest t-channel singularity in the Pomeron trajectory receive particular attention. We also examine the effects of the secondary Reggeons by introducing the exchange contribution of the highest-spin meson trajectories, namely the positive-signature mesons a_2 and f_2, and the negative ones ω and ρ.

Using an eikonal QCD-based model, we study infrared contributions to semi-hard parton-parton interactions by considering an effective charge whose infrared behaviour is constrained by a dynamical mass scale, which is a purely non-perturbative dynamical effect and its existence is strongly supported by some recent QCD lattice simulations. The model is built

from the parton model using standard QCD elementary parton-level processes, updated sets of quarks and gluon distribution functions, namely CTEQ6L, CTEQ6L1 and MSTW, and physically motivated kinematic cutoffs that restrict the elementary partonic process to semi-hard ones. We discuss the theoretical aspects of this formalism and consider the phenomenological implications of a class of energy-dependent form factors in the high-energy limit of the forward scattering amplitude. In order to connect the semi-hard parton-level dynamics to the hadron-hadron scattering, we introduce integral dispersion relations specially tailored to relate the real and imaginary parts of eikonals with energy-dependent form factors. In our model the eikonals are written in terms of even and odd parts connected by crossing symmetry. This connection between the complex eikonal function with integral dispersion relations is only possible because at first-order of approximation in the eikonal series, its even and odd parts, respectively, will take real values on a real axis segment with the same cut structure of the scattering amplitude.

We discuss the implications of our results and present predictions for the total cross-section, the ratio of the real to imaginary part of the forward scattering amplitude considering the recent data obtained by the TOTEM Collaboration at the LHC and also at cosmic-ray energies data obtained by the AUGER and Telescope Array experiments. We also present some predictions for the recent elastic differential cross-section data in proton-proton collisions obtained at LHC.

Since this is a work in progress, we still have much to do. Therefore, some perspectives, possible changes in the models and future insights are also discussed in the concluding remarks at the end of the text. Nothing here should be taken as an absolute, and unrestricted, cornerstone of truth. This is a study with future prospects, for this reason nothing is unchangeable.

Contents

List of Figures

List of Tables

Chapter 1

Introduction

Traditionally, the theory of elementary particle Physics and fields is devoted to study the structure of matter and its interactions at subatomic levels. The whole work and research performed in theoretical particle Physics over the last century has lead the scientific community towards the formulation of a well-grounded theory describing three of the four fundamental forces, the so-called Standard Model of elementary particles, or simply known as Standard Model. Speaking of which, these primary fundamental forces are the electromagnetic, weak and strong interactions. More specifically, it is understood that the electromagnetic and weak interactions are different manifestations of the same fundamental force called electroweak interaction, as it was discovered in the early 60's by Sheldon Glashow. Although the Higgs mechanism was incorporated into the electroweak sector in the late 60's by Steven Weinberg and Abdus Salam, only a couple of years ago it was indeed observed the spontaneous symmetry breaking mechanism as the most probable mass generation mechanism for the elementary particles.

Despite this last breakthrough within the observation of the Higgs boson there are still open problems, specially in the nuclear-strong sector which is described by a Yang-Mills $SU(3)$ theory known as Quantum Chromodynamics. The QCD is considered as the standard theory of strong interactions. It is a local non-Abelian field theory based on the invariant properties of an exact gauge symmetry $SU(3)$ [1, 2]. This theory describes the interaction among partons within hadrons and its principal characteristic is the asymptotic freedom of quarks and gluons in the limit of high momentum transfer, which is equivalent to the limit of short distances. However, the non-observation of free physical parton fields in nature implies the hypothesis that confinement sets up a threshold in the limit of low momentum transfer, or the limit of long distances. Therefore, the existence of two different interaction scales, with unique regimes, lead to the central problem in QCD which is the lack of a global method to study strong interactions, since it is physically inconsistent to apply a perturbative approach into confinement region.

One of the challenges faced by the particle Physics scientific community concerns the non-perturbative aspects of nuclear interactions, which are manifested in processes invol-

ving low momenta transfer, defined as soft processes. An example of soft process is the diffractive hadronic scattering, which can be separated into elastic scattering and single- or double-diffraction dissociation [3]. The elastic hadronic scattering at high energies represents a rather simple kinematic process, however its complete dynamical description is a fundamental problem in QCD, since the confinement phenomena prohibits a perturbative approach, which is a characteristic of processes with high momenta transfer, also known as hard processes, and a consequence of asymptotic freedom [4, 5]. The region of low momentum transfer is important not only because confinement is an intrinsically and exclusive characteristic of strong interactions, but rather because diffractive processes are dominant in high-energy scatterings. Such process is defined as a reaction in which no quantum numbers are exchanged between the colliding particles where its experimental signature is the presence of large gaps in the rapidity distribution, *i.e.*, the absence of hadronic activity in some regions of the phase space.

An alternative approach to the description of elastic hadronic scattering, and independent from QCD, is the Regge theory. This is a rather old mathematical framework originally formulated in the picture of non-relativistic Quantum Mechanics by Tulio Regge [6, 7]. Priorly, it was used to study the bound states of an attractive well-behaved spherically symmetric potential in such a way that the partial-wave amplitude can be properly analytically continued to complex values of angular momenta. Latter on, Regge theory was translated into the language of particle Physics by means of the properties of the scattering S-matrix [8–10]. Regge theory belongs to the class of t-channel models and is the theoretical framework used to study diffraction. The bound states, or even sometimes a whole family of resonances, which is known as Regge poles, are related to the description of strong interactions by means of the exchange of Regge trajectories [11–14].

The usual methodology and schemes adopted to tackle diffractive processes are based on general fundamental principles associated with axiomatic field theory, as for example, the principles of analyticity, unitarity and crossing symmetry of the scattering S-matrix. By means of phenomenological models, we seek connections among these fundamental principles and field theories. Our work so far is related to the study of elastic hadronic scatterings, namely the elastic pp and $\bar{p}p$ scatterings, by means of two different phenomenological approaches based on those properties of the scattering amplitudes: a Regge-Gribov inspired model, based on Regge theory, and a QCD inspired model, based the parton model of QCD.

In Regge pole models, the increase of the hadronic cross-section with increasing energy is associated with the exchange of a colourless state with the quantum numbers of the vacuum, which is the leading singularity in the t-channel, *i.e.* the leading Regge pole, the so-called Pomeron [15, 16]. It is common to find in the literature that diffraction is synonym of Pomeron Physics in the Regge language. However, Regge theory and QCD are two completely different approaches, in the QCD perspective the Pomeron can be described as

bound states of gluons, at least two gluons in a colour singlet state. Therefore, the former serves as an important guide in the search towards a fundamental theory for soft hadronic process.

At the light of the recent LHC data [17–22], the first part of this Thesis is devoted to study the role that the soft Pomeron plays in strong interaction, which is indisputably of extreme importance. Therefore, by means of Born-level amplitudes with single and double Pomeron exchange, where the latter is used to restore the unitarity bound since the Pomeron intercept is an effective power and valid only over a limited range of energies, and also by means of an eikonalised amplitude, which is unitary by construction, we study the effects of the extrema bounds of the soft Pomeron to forward physical observables, namely the total pp and $\bar{p}p$ cross-section as well as the ρ-parameter, and also we give predictions for the elastic differential cross-section. More precisely, we consider the possibilities of different combinations of vertices and trajectories for the Pomeron, as for instance we give particular attention to the nearest t-channel singularity in the Pomeron trajectory [23], and examine the effects of secondary Reggeons, namely the degenerate meson trajectories with positive-signatures, f_2 and a_2, and the negative ones, ω and ρ.

In the QCD-inspired eikonal model the connection between the elementary dynamics of QCD to physical processes involving hadrons, where the hadronic interactions are described by means of interactions among quarks and gluons, respectively, is made by means of the QCD parton model [24–32]. Therefore, the behaviour of physical observables is derived using standard QCD cross-section for elementary partonic subprocesses, updated sets of quarks and gluon distribution functions and physically motivated cutoffs that restricts the parton-level processes to semi-hard ones. In this picture, the increase of the total cross-section is associated with parton-parton semi-hard scatterings, and the high-energy dependence of the cross-sections is driven mainly by processes involving gluons. This is quite well understood in the framework of perturbative QCD, but since at high energies there is a close relation between the soft and the semi-hard components, then the non-perturbative dynamics of the theory is also manifest at the elementary level. However, these elementary processes are plagued by infrared divergences and one natural way to regularise these divergences is by means of a purely non-perturbative effect, the mechanism of gluon mass generation [33,34].

Within this revised version of the dynamical gluon mass model, the main focus in the second part of this Thesis is to explore the non-perturbative dynamics of QCD. We bring up the infrared properties of QCD by considering the possibility that these non-perturbative dynamics generates an effective gluons mass scale. The dynamical gluon mass is intrinsically related to an infrared finite strong coupling. Considering the recent LHC elastic data sets in pp and $\bar{p}p$ collision obtained by the TOTEM Collaboration [17–22], the description of the forward observables follows by considering the eikonal representation, the unitarity condition of the scattering S-matrix and the existence of a class of energy-dependent semi-hard form

factors [28, 29]. These form factors represent the overlap distribution of partons within hadrons at a given impact parameter. We are also considering the effects of updated sets of partonic distribution functions in the forward observables, namely CTEQ6L, CTEQ6L1 and MSTW, respectively.

The outline of this Thesis is organised as follows: Chapter 2 introduces some topics related to the formal theory of scattering as well as a brief discussion concerning the kinematics of scattering process, the partial-wave expansion and the eikonal formalism. The closing section presents the experimental data compiled and analysed by the Particle Data Group [35] and also the recent elastic data sets obtained by the TOTEM Collaboration at the LHC considered in both parts of the Thesis. More precisely, these recent data sets correspond to the highest collider CM energy.

In Chapter 3, it is introduced the idea behind Regge theory. It is described the mathematical construction that beggins as an analytical continuation of the partial-wave amplitudes to complex values of angular momenta, by bringing up informations how it effects the convergence domains, and goes to the introduction of a new quantum number called signature and how it puts through the problem of analytically continuation in relativistic scattering.

Chapter 4 is the kernel of the first part proposed in the Thesis. Here, it is described the Regge-Gribov formalism used to model Born-level amplitudes and eikonalised amplitudes. We study the effect of the contribution of double-Pomeron exchange in the Born-level analysis at the limit of high energies and how it is supposed to restore unitarity. We consider also the effects of a non-linear term corresponding to a two-pion loop in the Pomeron trajectory. We present the first results obtained by means of both eikonalised and non-eikonalised amplitudes.

In Chapter 5, it is presented a brief introduction to Quantum Chromodynamics, the original parton model and the parton model of QCD, where the Bjorken scaling is broken by means of logarithms divergences. It is also shown a brief deduction concerning the leading order and the next-to-leading order expressions for the QCD coupling, a fundamental parameter in the Standard Model.

Chapter 6 corresponds to the second part of the Thesis, a revised study of the original dynamical gluon mass model. The non-perturbative QCD effects is introduced by means of a QCD-inspired eikonal model whereupon a momentum-dependent gluon mass scale is used to deal with the infrared divergences that usually plague the elementary partonic subprocesses. By means of a class of factorised energy-dependent form factors and also considering updated sets of partonic distribution function constrained by physically motivated kinematic cutoff, we give predictions to forward observables, namely total cross-section and ρ-parameter for pp and $\bar{p}p$ interactions. We compare these new results to our previous ones.

In Chapter 7, without formality, it is discussed some perspectives about our work so far.

It is presented some possible changes concerning our both phenomenological-based models, or even sometimes just ideas that we still need to put forward. These are just hint that perhaps we might follow in the next couple of months.

The Appendixes are there just to give a more mathematical meaning to our calculations and to show that everything is precisely well grounded. And most of all, it is used in the attempt to not overload the text.

Chapter 2

Kinematics of scattering processes

There is no doubt that the cross-sections are the most important physical observables in general scattering processes since it is related to the scattering occurrence probability. This first Chapter is fully dedicated to show in detail the aspects of these physical observables. Within the Quantum Mechanical approach in the high-energy limit, and also by means of the semi-classical approximation, it will be shown that the scattering amplitude, which is the function that defines all the scattering, turns out to be represented in the impact parameter plane by means of an eikonal function. However, before studying the impact parameter representation and the eikonal formalism, there are some basic and essential features concerning the physics behind it.

2.1   Preliminaries

From Optics to Quantum Mechanics and from nuclear to hadron Physics, diffraction covers a large set of phenomena [3]. There are many physical experiments concerning the different kinds of collision processes and particles. At high energies, there is the possibility that the final result be a composite system of many new particles. Usually it is said that these collisions lead to scatterings. An easy way to represent it and to understand what is going on mathematically speaking, but not quite so, is by means of a reaction equation,

$$1 + 2 \rightarrow 3 + 4 + 5 + ...,\tag{2.1}$$

where it represents the collision between particles of types 1 and 2 leading to a composite state of new particles $3 + 4 + 5 + ...$ as the final product, *i.e.* the post-scattering result.

In the 60's, W.L. Good & W.D. Walker [36], were the first authors to give a precise description, and also a modern one, of hadronic diffraction:

"A phenomenon is predicted in which a high-energy particle beam undergoing diffraction scattering from a nucleus will acquire components corresponding to various products of the virtual dissociations of the incident particles [...] These diffraction-produced systems would

have a characteristic extremely narrow distribution in transverse momentum and would have the same quantum numbers of the initial particle."

Although, even today this definition is still pretty much the same, it is possible to exploit it by introducing two other different, but equivalent definitions. In the theoretical point of view, a hadronic diffractive process is in general defined as follows [3]:

I. *"A reaction in which no quantum numbers are exchanged between the colliding particles is, at high energies, a diffractive reaction."*

This definition is simple and general enough so that it can cover all the diffractive collision cases at high energies, as depicted in Figure 2.1:

i. Elastic scattering $- 1 + 2 \rightarrow 1' + 2' -$ when the incident particles correspond exactly to those ones in the final state.

ii. Single-diffraction $- 1 + 2 \rightarrow 1' + X_2$ ou $1 + 2 \rightarrow X_1 + 2' -$ when one of the incident particles remains the same after the collision whilst the other one produces a set X of new particles, or a resonance, preserving the quantum numbers of the initial state.

iii. Double-diffraction $- 1 + 2 \rightarrow X_1 + X_2 -$ when both the incident particles give rise to new sets of different particles, or to a resonance, preserving the quantum numbers of the initial state.

In the experimental point of view, the complete identification of the final state is not always possible to obtain. Hence, in practice it is needed to provide an operational definition of hadronic diffraction which is equivalent to the one given before [3, 37]:

II. *"A diffractive reaction is characterised by a large, non-exponentially suppressed, rapidity gap in the final state."*

This definition expresses the fact that the request of a large final state rapidity gap non-exponentially suppressed, $dN/d\Delta\eta \sim constant$, defines the reaction as a diffractive one. Since, contaminations from the distribution of non-diffractive events are of the form $dN/d\Delta\eta \sim e^{-\Delta\eta}$. Therefore, diffractive contributions can be distinguished only asymptotically from non-diffractive ones, after all the latter decrease with energy.

Particularly, the main focus of this Thesis are the diffractive scatterings where the two particles remain unaltered after the collision, but in a different kinematic configuration. More specifically, the Thesis kernel is the study of a two-body exclusive scattering special case *viz.* the elastic scattering,

$$1 + 2 \rightarrow 1' + 2'. \tag{2.2}$$
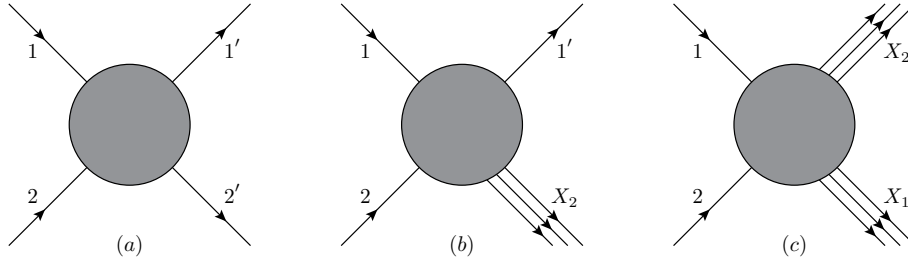
Figure 2.1: (a) Elastic scattering, (b) single-diffraction and (c) double-diffraction.

Despite the fact that it is viewed as the simplest process concerning the kinamatics, the theoretical description of elastic scattering is extremely difficult [3], because it is linked to processes with low-momentum transfer q^2. These processes are usually called soft ones. The description of hadronic scattering with low-q^2 actually is one of the most important and challenging concerning the active field of high-energy physics.

There is a property called asymptotic freedom of QCD which states that in a well defined energy range the partons can be viewed as free objects, *i.e* as the energy increases the bounds between partons become asymptotically weaker and the corresponding length scale decreases [4,5]. This feature is valid for hard processes, meaning high-q^2. Although part of the process is still of non-perturbative origin the high-q^2 value allows one to use perturbative QCD. Soft processes are the opposite because confinement, which states that the bounds between partons do not weaken as the energy increases [2], prevents a perturbative approach and then new calculation methods are required.

In what follows, it will be shown the basics of two-particles elastic scattering via the Quantum Mechanical formalism by means of the formal theory of scattering.

2.2 The Lippmann-Schwinger equation

There are some basic hypotheses simplifying the scattering, such as one can disregard the coherence effects in the scattered wave function. Therefore, instead of looking at the whole beam one might deal only with two particles interacting, since the scattered flux of N particles equals to N times the flux scattered by one particle. The problem is much simpler then, and the Hamiltonian describing this system is simply

$$H = H_0 + V(\mathbf{r}), \tag{2.3}$$

where $V(\mathbf{r})$ is the potential and H_0 stands for the kinetic-energy operator,

$$H_0 = \frac{\mathbf{P}^2}{2M}, \tag{2.4}$$

and $\mathbf{P} = \mathbf{P}_1 + \mathbf{P}_2$ is the total momentum, $M = m_1 m_2 / (m_1 + m_2)$ is the reduced mass and $\mathbf{r} = \mathbf{r}_1 - \mathbf{r}_2$ is the relative distance between particles.

The absence of a scatter implies that $V(\mathbf{r})$ be zero,

$$H_0 |\phi\rangle = E|\phi\rangle, \tag{2.5}$$

where $|\phi\rangle$ are the energy eigenkets of H_0. The presence of $V(\mathbf{r})$ leads just to a different energy eigenstate from the one usual of a free-particle state. But, when considering elastic scattering processes, one might be interested in obtaining the stationary solution of the full-Hamiltonian Schrödinger equation[1],

$$(H_0 + V)|\psi\rangle = E|\psi\rangle \ , \ \ E = \frac{\hbar^2 k^2}{2M}. \tag{2.6}$$

Working with scattering problems always demands a careful look at the boundary conditions so that the evolution description of the wave function is correctly written. Then, the first assumption made is that the initial state should be a state without interaction, *i.e.*, a plane-wave at asymptotically $r \to -\infty$. The second assumption made is to consider the potential interacting on the initial state and in the range $r \leq r_0$ of $V(\mathbf{r})$. For this reason, asymptotically when $r \to \infty$, the wave function of the whole system is the superposition of the non-scattered and the scattered components, *i.e*, the limit $V \to 0$ implies $|\psi\rangle \to |\phi\rangle$.

Within these two assumptions it may be argued that a possible solution for expression (2.6) is

$$|\psi\rangle = |\phi\rangle + \frac{1}{E - H_0} V |\psi\rangle, \tag{2.7}$$

even though there is a singularity in the *rhs*. To avoid further and unnecessary complications one might use a prescription for dealing with the singular operator $1/(E - H_0)$. A nice and easy way to do it is by making the eigenenergy E slightly complex,

$$|\psi^{\pm}\rangle = |\phi\rangle + \frac{1}{E \pm i\epsilon - H_0} V |\psi^{\pm}\rangle. \tag{2.8}$$

The trick used here will not cause any trouble at all, after all the limit $\epsilon \to 0^{\pm}$ will always be taken once the singularity can be properly contoured using the residue theorem [38]. Looking at expression (2.8) it is easy to see that it does not depend on particular representation, this is known as the Lippmann-Schwinger equation. The physical meaning of $\pm$ will be discussed in the following section, but it is related with time $t \gg t_0$ and $t \ll t_0$, where t_0 stands for the precise moment when the interaction occurred.

---

[1] Henceforth, it will be used the natural system of units, however in this section it was explicitly written all the factors $\hbar$ to avoid any kind of confusion. Otherwise, when not mentioned, we consider $\hbar = c = 1$.

2.2.1 The scattering amplitude

Working on the position basis, expression (2.8) can be written as an integral equation,

$$\langle \mathbf{r}|\psi^{\pm}\rangle = \frac{e^{i\mathbf{p}\cdot\mathbf{r}/\hbar}}{(2\pi\hbar)^{3/2}} + \frac{2M}{\hbar^2} \int d^3\mathbf{r}' \, G_{\pm}(\mathbf{r},\mathbf{r}') \, \langle \mathbf{r}'|V|\psi^{\pm}\rangle, \tag{2.9}$$

where $G_{\pm}(\mathbf{r},\mathbf{r}')$ is defined as

$$G_{\pm}(\mathbf{r},\mathbf{r}') \equiv \frac{\hbar^2}{2M} \left\langle \mathbf{r} \left| \frac{1}{E \pm i\epsilon - H_0} \right| \mathbf{r}' \right\rangle. \tag{2.10}$$

It is straightforward to show that $G_{\pm}(\mathbf{r},\mathbf{r}')$ can easily be projected into momentum basis,

$$G_{\pm}(\mathbf{r},\mathbf{r}') = -\frac{1}{(2\pi)^3} \int d^3\mathbf{q} \, \frac{e^{i\mathbf{q}\cdot|\mathbf{r}-\mathbf{r}'|}}{q^2 - (k \mp i\epsilon)^2} \quad , \quad (k \mp i\epsilon)^2 \simeq k^2 \mp i\epsilon, \tag{2.11}$$

where it was set $\mathbf{p}' \equiv \hbar\mathbf{q}$. As it was mentioned before, the singularity must be properly contoured using the residue theorem, then by doing so and after taking the limit $\epsilon \to 0^{\pm}$ one finds that

$$G_{\pm}(\mathbf{r},\mathbf{r}') = -\frac{1}{4\pi} \frac{e^{\pm ik|\mathbf{r}-\mathbf{r}'|}}{|\mathbf{r}-\mathbf{r}'|}, \tag{2.12}$$

meaning that $G_{\pm}(\mathbf{r},\mathbf{r}')$ is nothing more than the Green's function for the Helmholtz's equation.

There is a definition which states that a given operator is local if, and only if, it can be written as $\langle \mathbf{r}'|\hat{A}|\mathbf{r}''\rangle = \hat{A}(\mathbf{r}')\delta^{(3)}(\mathbf{r}'-\mathbf{r}'')$. In the case where this operator is $V(\mathbf{r})$, then a set of local potentials are defined as those ones which are functions of the position operator $\mathbf{r}$ only, and as a result $\langle \mathbf{r}'|V|\psi^{\pm}\rangle = V(\mathbf{r}')\langle \mathbf{r}'|\psi^{\pm}\rangle$. Then, finally the expression for the total wave function (2.9) is given by

$$\langle \mathbf{r}|\psi^{\pm}\rangle = \frac{e^{i\mathbf{k}\cdot\mathbf{r}}}{(2\pi\hbar)^{3/2}} - \frac{2M}{\hbar^2} \int d^3\mathbf{r}' \, \frac{e^{\pm ik|\mathbf{r}-\mathbf{r}'|}}{4\pi|\mathbf{r}-\mathbf{r}'|} \, V(\mathbf{r}') \, \langle \mathbf{r}'|\psi^{\pm}\rangle, \tag{2.13}$$

where $\mathbf{k} \equiv \mathbf{p}/\hbar$. It is important to remember that the wave function $\langle \mathbf{r}|\psi^{\pm}\rangle$ was written in the presence of a scatterer, then the first term in the *rhs* of expression (2.13) represents the incident wave $\langle \mathbf{r}|\phi\rangle$ whilst the second term represents the effect of scattering.

What is really interesting to study in scattering processes is the effect of the scatterer far outside its range. Therefore, in the asymptotic limit where the detector is placed very far away from the scatterer, or similarly $\mathbf{r} \gg \mathbf{r}'$, it can be easily shown that

$$|\mathbf{r}-\mathbf{r}'| \simeq r - \mathbf{r}'\cdot\hat{\mathbf{r}}, \tag{2.14}$$

so, finally the wave function turns out to be given by

$$
\begin{aligned}
\langle \mathbf{r}|\psi^+\rangle \underset{r\to\infty}{\sim}\ & \frac{e^{i\mathbf{k}\cdot\mathbf{r}}}{(2\pi\hbar)^{3/2}} - \frac{1}{4\pi}\frac{2M}{\hbar^2}\frac{e^{ikr}}{r}\int d^3\mathbf{r}'\, e^{-i\mathbf{k}'\cdot\mathbf{r}'}\, V(\mathbf{r}')\langle\mathbf{r}'|\psi^+\rangle \\
=\ & \frac{1}{(2\pi\hbar)^{3/2}}\left[e^{i\mathbf{k}\cdot\mathbf{r}} + \frac{e^{ikr}}{r}\, f(\mathbf{k},\mathbf{k}')\right].
\end{aligned}
\tag{2.15}
$$

In the aforementioned expression, and as it was already mentioned before, it is clear that $\langle\mathbf{r}|\psi^+\rangle$ corresponds to the original plane-wave in propagation direction $\mathbf{k}$ plus an outgoing spherical wave with spatial dependence e^{ikr}/r and amplitude $f(\mathbf{k},\mathbf{k}')$. This is usually referred as the scattering amplitude and it contains all the dynamic information of the collision process. In general it is written as a function of the wave vectors $\mathbf{k}$ and $\mathbf{k}'$, or similarly as a function of k and the respectively scattering angles of $\mathbf{k}'$ relative to $\mathbf{k}$,

$$
f(\mathbf{k},\mathbf{k}') \equiv -\frac{1}{4\pi}\frac{2M}{\hbar^2}(2\pi)^3\int d^3\mathbf{r}'\, e^{-i\mathbf{k}'\cdot\mathbf{r}'}\, V(\mathbf{r}')\langle\mathbf{r}'|\psi^+\rangle = -\frac{4\pi^2 M}{\hbar^2}\langle\mathbf{k}'|V|\psi^+\rangle.
\tag{2.16}
$$

From the same point of view $\langle\mathbf{r}|\psi^-\rangle$ represents the original plane-wave in propagation direction $\mathbf{k}$ and an incoming spherical wave with spatial dependence e^{-ikr}/r and amplitude proportional to $\langle-\mathbf{k}'|V|\psi^-\rangle$.

2.3   Cross-sections

In a simple way, we may say that the differential cross-section is viewed as the ratio of the number of particles scattered into an element of solid-angle $d\Omega$ per unit of time to the number of incident particles crossing an unit area per unit of time. It is equivalent to say it represents the occurrence of detected events per $d\Omega$,

$$
\frac{d\sigma}{d\Omega}\, d\Omega = \frac{r^2\,|\mathbf{j}_{scatt}|\, d\Omega}{|\mathbf{j}_{inc}|},
\tag{2.17}
$$

where $|\mathbf{j}_{scatt}|$ and $|\mathbf{j}_{inc}|$ account for the scattered and the incident density flux, respectively, and they can be calculated by means of the relation

$$
\mathbf{j} = -\frac{i\hbar}{2M}\left(\psi^*\nabla\psi - \psi\nabla\psi^*\right),
\tag{2.18}
$$

which is obtained from Schrödinger's equation.

Within expressions (2.15) and (2.18), it is easily seen that[2]

$$
\mathbf{j}_{scatt} = \frac{\hbar k}{r^2 M}\,|f(\mathbf{k},\mathbf{k}')|^2\,\hat{\mathbf{r}},
\tag{2.19}
$$

---

[2] Considering an incident plane-wave in the z direction.

$$\mathbf{j}_{inc} = \frac{\hbar k}{M} \, \hat{\mathbf{z}}, \tag{2.20}$$

and hence, the elastic differential cross-section is given by

$$\frac{d\sigma}{d\Omega} = |f(\mathbf{k}, \mathbf{k}')|^2. \tag{2.21}$$

Before pressing on, it should be clear that the elastic scattering processes ought to be only one accessible channel, whereupon the possibility of inelastic events must be taken into account, so that the total cross-section constains a probability interpretation of the scattering process. Integrating (2.21) over the whole solid-angle it leads to the elastic cross-section , σ_{el}. Hence,

$$\sigma_{tot} = \sigma_{el} + \sigma_{in}, \tag{2.22}$$

or in the probabilistic interaction form,

$$\frac{\sigma_{el}}{\sigma_{tot}} + \frac{\sigma_{in}}{\sigma_{tot}} = 1, \tag{2.23}$$

which in a sense tells that the total cross-section measures the overall probability of interaction. This relation represents the unitarity principle, where in the quantum mechanical context it is linked to conservation of probabilities whilst in classical mechanics it is linked to conservation of energy.

There is still an expression, also known as the optical theorem [3, 38], which relates the total cross-section to the imaginary part of the forward scattering amplitude $f(\mathbf{k}, \mathbf{k}) = f(\theta = 0)$,

$$\sigma_{tot} = \frac{4\pi}{k} \operatorname{Im} f(\mathbf{k}, \mathbf{k}). \tag{2.24}$$

2.4 Asymptotic theorems

It was decided to save this section in the attempt to make a brief discussion about three important theorems which one frequently encounters in particle Physics. These theorems have been derived using the fundamental principles of analyticity, unitarity and crossing symmetry, and usually they are expressed by a set of mathematically rigorous inequalities in which the scattering amplitudes must satisfy.

2.4.1 Optical theorem

In the beginning of this chapter, it was mentioned that the most important physical observables in diffraction were the cross-sections, provided that they are associated with the occurrence probability of one certain scattering process. There is a basic and fundamental

relationship usually attributed to Bohr, Peierls, Placzek and Feenberg, known as the optical theorem [3, 38], see expression (2.24).

Starting with Lippmann-Schwinger's equation (2.8), the imaginary part of the scattering amplitude can be written as

$$
\begin{aligned}
\operatorname{Im}\langle\mathbf{k}|V|\psi^+\rangle &= -\pi\langle\mathbf{k}|V\delta(E-H_0)V|\psi^+\rangle \\
&= -\pi\int d\Omega'\,\frac{Mk}{\hbar^2}\,|\langle\mathbf{k}'|V|\psi^+\rangle|^2,
\end{aligned}
\tag{2.25}
$$

where it was used that

$$
\lim_{\epsilon\to0^+}\left(\frac{1}{E\pm i\epsilon-H_0}\right)=\lim_{\epsilon\to0^+}\int_\infty^\infty dE'\,\frac{\delta(E-E')}{E\pm i\epsilon-H_0}=i\pi\delta(E-H_0).
\tag{2.26}
$$

Thus, by means of the expression for the differential cross-section (2.21) and bearing in mind that $\mathbf{k}'=\mathbf{k}$ imposes scattering in the forward direction, *i.e*,

$$
\sigma_{tot}=\int\frac{d\sigma}{d\Omega}\,d\Omega,
\tag{2.27}
$$

it is found that

$$
\begin{aligned}
\operatorname{Im} f(\mathbf{k},\mathbf{k}) &= -\frac{\hbar^2}{4\pi^2 M}\left(-\pi\frac{Mk}{\hbar^2}\int d\Omega'\,|\langle\mathbf{k}'|V|\psi^+\rangle|^2\right) \\
&= \frac{k}{4\pi}\,\sigma_{tot}.
\end{aligned}
\tag{2.28}
$$

2.4.2 The Froissart-Martin-Łukaszuk bound

For many years and since the early days of the ISR, it has been known that the pp total cross-section starts rising after attaining a minimum in the region of $35-40$ mb [35]. It was found that the σ_{tot}^{pp} has a typical-like $\ln^\gamma s$ growing behaviour with $\gamma\sim2$ [3, 39]. As a matter of fact, the Froissart-Martin-Łukaszuk bound is much more general, actually, assuming the analyticity and unitarity properties of the scattering S-matrix, it states that for any hadronic cross-section there is a limit in which cannot grow faster than $\ln^2 s$ [40–42],

$$
\sigma_{tot}(s)\le(const)\cdot\ln^2 s.
\tag{2.29}
$$

By considering first the asymptotic representation of partial-wave amplitudes[3] in the s-channel,

$$
A_\ell(s)\underset{\ell,s\to\infty}{\sim}f(s)\exp[-\ell\zeta(z_0)],
\tag{2.30}
$$

---

[3] The partial-wave expansion will be shown in Section 2.5

where $\zeta(z) = \ln[z + (z^2 - 1)^{1/2}]$, $z_0 = 1 + 2t/s$ and $f(s)$ is a function with a power-like s-dependence. And afterwards, expanding $\zeta(z)$ as $\ln(1 + x)$ and taking the limit $s \to \infty$, expression (2.30) can be rewritten as

$$A_\ell(s) \sim \exp\left[-\left(\frac{2t}{\sqrt{s}}\right)\ell + \delta \ln s\right].$$ (2.31)

In the limit of high energies one can neglect the partial waves with angular momentum values of $\ell \gtrsim c\sqrt{s}\ln s$ in such a way that the amplitude series can be truncated as

$$A(s,t) \underset{s \to \infty}{\simeq} \sum_{\ell=0}^{c\sqrt{s}\ln s} (2\ell + 1)A_\ell(s)P_\ell(z) \lesssim 16i\,\pi \sum_{\ell=0}^{c\sqrt{s}\ln s} (2\ell + 1) \sim i\,Cs\ln^2 s, \;\; \text{para} \;\; s \to \infty,$$ (2.32)

where it was used the unitarity bound $0 \le ImA_\ell(s)/16\pi \le 1$ and also that the associated Legendre polynomial of ℓ-order are $|P_\ell(z)| \le 1$ for $-1 \le z \le 1$. The optical theorem finally leads to expression (2.29) as $s \to \infty$.

2.4.3   The (revised) Pomeranchuk theorem for total cross-sections

What is usually called today as the original Pomeranchuk theorem [43] states that generally if ab and $a\bar{b}$ cross-sections become asymptotically constant and if the ρ-parameter, *i.e* the ratio of the real to imaginary part of the forward scattering amplitude, increases slower than $\ln s$, hence the two cross-sections become asymptotically equal. This definition of the theorem was quite nice when the highest-energy available data came from Serpukhov $\sqrt{s} \sim 70$ GeV, where the σ_{tot}^{pp} seemed to become constant with increasing energy.

Nowadays this scenario has changed since it is seen that cross-sections keep rising as the energy increases. Thus, the original Pomeranchuk theorem must be carefully modified. The scattering processes like ab and $a\bar{b}$ at high energies still obey asymptotically,

$$\lim_{s \to \infty} \frac{\sigma_{tot}^{ab}(s)}{\sigma_{tot}^{a\bar{b}}(s)} \to 1.$$ (2.33)

The revised version of the theorem [44, 45] states that if ab and $a\bar{b}$ cross-sections grow as $\ln^\gamma s$, then[4] the difference between them should be bounded as

$$\Delta\sigma \le (const) \cdot \ln^{\gamma/2} s.$$ (2.34)

More specifically, Pomeranchuk's theorem relies on the fact that there is the possibility to write dispersion relations tailored to relate the real and imaginary part of the scattering

---

[4] For a better understanding if the cross-sections will eventually approach each other, maybe a good thing to do is to look for Fischer's theorem.

amplitude, and also in some assumptions concerning the energy-dependence of the amplitudes [3].

There is an asymptotic relation similar to (2.33), but relating the elastic differential cross-section known as Cornille-Martin theorem [46],

$$\lim_{s\to\infty}\left[\frac{d\sigma_{ab}(s,t)}{d|t|}\bigg/\frac{d\sigma_{a\bar{b}}(s,t)}{d|t|}\right]\to 1, \tag{2.35}$$

even though the difference of the differential cross-sections at fixed t may not go to zero, in fact it grows as $\ln^2 s$ [39]. As a consequence of this theorem the forward slope $B(s)$ goes to unity,

$$\lim_{s\to\infty}\frac{B_{ab}(s,t=0)}{B_{\bar{a}b}(s,t=0)}\to 1. \tag{2.36}$$

Using the relation between the forward differential and total cross-section, one can easily show that [39]

$$\lim_{s\to\infty}\left(\frac{\rho_{ab}(s)}{\rho_{a\bar{b}}(s)}\right)^2\to 1. \tag{2.37}$$

Perhaps the optical theorem is one of the most important relation in diffraction, however the further results shown here have a limited applicability range in the experimental data analysis. Although they are valid in the asymptotic limit $s\to\infty$, one can use them to study asymptotic cross-section properties and extrema bounds.

2.5 Partial-wave expansion

The rotational invariance from a spherically symmetric potential implies an elastic scattering amplitude decomposed as a summation of angular momentum components [3,38, 39]. This decompositon, also known as partial-wave expansion, is written as

$$f(\mathbf{k},\mathbf{k}')=f(k,\theta)=\sum_{\ell=0}^{\infty}(2\ell+1)\,a_\ell(k)P_\ell(\cos\theta), \tag{2.38}$$

where the sum is over all possible values of angular momentum ℓ, k is the momentum in the CM frame and $a_\ell(k)$ is the partial-wave amplitude.

To understand the physical meaning of $a_\ell(k)$ once again it is useful to analyse the asymptotic behaviour of $\langle\mathbf{r}|\psi^+\rangle$. Substituting the partial-wave expanded scattering amplitude (2.38) into expression (2.15), and also using the expansion of a plane wave in term of

spherical waves, one finds that in the limit of large distances [38],

$$
\langle \mathbf{r} | \psi^+ \rangle \underset{r \to \infty}{\sim} \frac{e^{i\mathbf{k} \cdot \mathbf{r}}}{(2\pi\hbar)^{3/2}} - \frac{1}{4\pi} \frac{2M}{\hbar^2} \frac{e^{ikr}}{r} \int d^3\mathbf{r}' \, e^{-i\mathbf{k}' \cdot \mathbf{r}'} V(\mathbf{r}') \langle \mathbf{r}' | \psi^+ \rangle
$$

$$
= \frac{1}{(2\pi)^{3/2}} \sum_{\ell=0}^{\infty} (2\ell+1) \frac{P_\ell(\cos\theta)}{2ik} \left\{ [1 + 2ika_\ell(k)] \frac{e^{ikr}}{r} - \frac{e^{-i(kr-\ell\pi)}}{r} \right\}. \quad (2.39)
$$

Then, the interacting potential acting on the scattering process changes only the coefficient of the outgoing wave, i.e. $1 \to 1 + 2ika_\ell(k)$, whilst the incoming wave remains unaltered. By conservation of current the initial incoming flux must equal the outgoing flux, and this must hold for each partial wave because of angular momentum conservation. In principle one could define a quantity $S(k)$ such that [3]

$$
S_\ell(k) \equiv 1 + 2ika_\ell(k), \quad (2.40)
$$

this means that by conservation of probability,

$$
|S_\ell(k)| = 1, \quad (2.41)
$$

thus, the most that can happen between the wave functions before and after the scattering is a change in the phase of the outgoing wave. Expression (2.41) is known as the unitarity relation for the ℓ-th partial wave where $S_\ell(k)$ stands for the ℓ-th diagonal element of the scattering S-matrix. Defining this phase shift as $2\delta_\ell(k)$ so that

$$
S_\ell(k) = e^{2i\delta_\ell(k)}, \quad (2.42)
$$

hence the amplitudes $a_\ell(k)$ can be rewritten in the following way

$$
a_\ell(k) = \frac{e^{2i\delta_\ell(k)} - 1}{2ik}. \quad (2.43)
$$

By means of expression (2.21) one finds the elastic cross-section,

$$
\begin{aligned}
\sigma_{el} &= \int d\Omega \, \frac{d\sigma_{el}}{d\Omega} = \int d\Omega \, |f(k,\theta)|^2 = \int d\Omega \left| \sum_{\ell=0}^{\infty} (2\ell+1) a_\ell(k) P_\ell(\cos\theta) \right|^2 \\
&= 2\pi \sum_{\ell,\ell'=0}^{\infty} (2\ell+1)(2\ell'+1) |a_\ell(k)|^2 \int_{-1}^{+1} d(\cos\theta) \, P_\ell(\cos\theta) P_{\ell'}^*(\cos\theta) \\
&= 4\pi \sum_{\ell=0}^{\infty} (2\ell+1) |a_\ell(k)|^2, \quad (2.44)
\end{aligned}
$$

where it was used $P_\ell(\cos\theta) = P_\ell^*(\cos\theta)$ and the orthogonality of Lengendre polynomials,

$$\int_{-1}^{+1} d(\cos\theta)\, P_\ell(\cos\theta) P_{\ell'}(\cos\theta) = \frac{2}{2\ell+1}\, \delta_{\ell\ell'}. \tag{2.45}$$

Finally, the total cross-section is found, as usual, by means of the optical theorem (2.24),

$$\begin{aligned} \sigma_{tot} &= \frac{4\pi}{k} \operatorname{Im} f(k, \theta = 0) \\ &= \frac{4\pi}{k} \sum_{\ell=0}^{\infty} (2\ell+1)\operatorname{Im} a_\ell(k). \end{aligned} \tag{2.46}$$

Consider the case where only elastic collisions take place, then expression (2.44) equals expression (2.46). Thus,

$$\operatorname{Im} a_\ell(k) = k|a_\ell(k)|^2, \tag{2.47}$$

this is what is usually called as elastic unitarity condition. This condition holds for those cases where the phase shits $\delta_\ell(k)$ are real quantities, and then the validity of unitarity relation (2.41) is ensured only when $\delta_\ell(k)$ is real.

In high-energy physics essentially there are two kinds of collisions: elastic ones, where there are conservation of incident particles quantum numbers and the initial and final states are the same; and inelastic ones, where there are changes in incident particles quantum numbers and the initial and final state are not necessarily the same. In the general case when the inelastic channels are open, the elastic conditions (2.41) and (2.47) are no longer true, and somehow absorption effects must be introduced in the region near the potential [3]. In this case, the unitarity condition implies that

$$|S_\ell(k)| \leq 1, \tag{2.48}$$

where now the phase shifts $\delta_\ell(k)$ are complex quantities. Then, expression (2.42) must be rewritten as

$$S_\ell(k) = \eta_\ell(k) e^{2i\zeta_\ell(k)}, \tag{2.49}$$

where $\eta_\ell(k) \equiv e^{-2\operatorname{Im}\{\delta_\ell(k)\}}$, with $\operatorname{Im}\delta_\ell(k) \geq 0$ and $\zeta_\ell(k) \equiv \operatorname{Re}\delta_\ell(k)$ are real quantities. Therefore, in the general case the elastic unitarity condition (2.47) is given by

$$\operatorname{Im} a_\ell(k) \geq k|a_\ell(k)|^2. \tag{2.50}$$

Within these relations, the general unitarity condition satisfied by the partial-wave amplitudes reads

$$\operatorname{Im} a_\ell(k) - k|a_\ell(k)|^2 = \frac{1 - \eta_\ell^2(k)}{4k}, \tag{2.51}$$
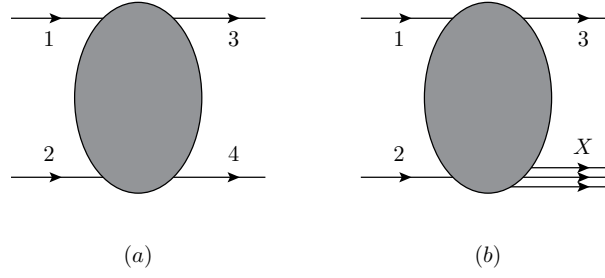
Figure 2.2: (a) Two-body exclusive scattering and (b) single-particle inclusive scattering.

where $0 \leq \eta_\ell(k) \leq 1$, are usually called as absorption (or inelastic) coefficients. It is straightforward to see that in the elastic limit, $\eta_\ell(k) = 1$, its *rhs* reduces to zero and expression (2.47) is a particular case of (2.51).

Bearing in mind that $S_\ell(k)$ is a diagonal element of the scattering S-matrix and it is accordingly written by expression (2.49) when both elastic and inelastic channels are open, the cross-sections can be properly written in terms of the absorption coefficients $\eta_\ell(k)$ and the real phase shifts $\zeta_\ell(k)$,

$$\sigma_{tot} = \sigma_{el} + \sigma_{in} = \frac{2\pi}{k^2} \sum_{\ell=0}^{\infty} (2\ell + 1)[1 - \eta_\ell(k) \cos 2\zeta_\ell(k)], \tag{2.52}$$

$$\sigma_{el}(k) = \frac{\pi}{k^2} \sum_{\ell=0}^{\infty} (2\ell + 1)[1 - 2\eta_\ell(k) \cos 2\zeta_\ell(k) + \eta_\ell^2(k)], \tag{2.53}$$

$$\sigma_{in}(k) = \frac{\pi}{k^2} \sum_{\ell=0}^{\infty} (2\ell + 1)[1 - \eta_\ell^2(k)]. \tag{2.54}$$

2.6 Two-body processes and the Mandelstam invariants

Each diffractive process has its own experimental signature consisting in an unique final kinamatic configuration. However, once it is settled the basic fundamental hypothesis that physical observables are independent from the inertial reference frame, the necessary requirement is that these physical quantities must be grounded on a set of symmetry operations associated with 4-dimensional space-time which maintains the physics invariant. This means that symmetry operations can be defined simply as an operation leading a physical system to another, but conditioned that the same properties are preserved and the same equations are satisfied. In summary, it must be invariant under Lorentz transformations [47]. Relying on this, it is often used the Mandelstam invariants.

In a two-body exclusive scattering process, see Figure 2.2(a),[5]

$$1 + 2 \to 3 + 4, \quad (s - \text{channel}), \tag{2.55}$$

only two independent kinamatic variables are needed[6]. As mentioned, these variables are usually chosen among the three Mandelstam invariants defined as [48]

$$s = (p_1 + p_2)^2 = (p_3 + p_4)^2 , \tag{2.56}$$

$$t = (p_1 - p_3)^2 = (p_2 - p_4)^2 , \tag{2.57}$$

$$u = (p_1 - p_4)^2 = (p_2 - p_3)^2 , \tag{2.58}$$

and by means of energy-momentum conservation and considering the particles on-shell, then the identity,

$$s + t + u = \sum_{i=1}^{4} m_i^2, \tag{2.59}$$

must be respected. Respectively, p_i, $i = 1, ..., 4$, are the 4-momenta of particles $1, ..., 4$. In
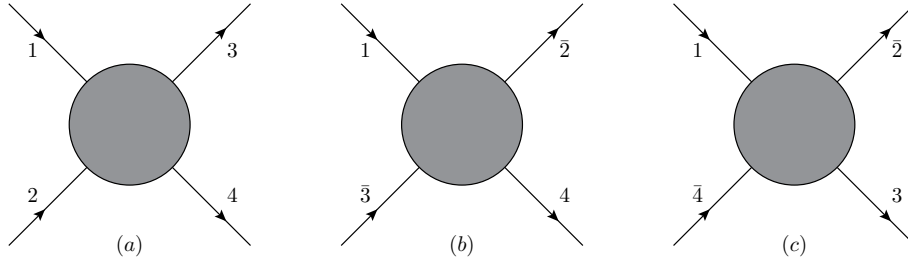
Figure 2.3: (a) s-channel, (b) t-channel and (c) u-channel. Here, as for example, $\bar{2}$ means that the momentum of particle 2 has been reversed and all additive quantum numbers have changed sign, *i.e.* $\bar{2}$ is the antiparticle of 2.

general, s and t are the chosen independent variables. Where in reaction (2.55) s is the square of the total CM energy and t is the squared momentum transfer. This reaction is referred to an s-channel process. Analogously, for t-channel process (and u-channel process) means that t (u) defined by expression (2.57) and (2.58), is the total squared CM energy, see Figure 2.3,

$$1 + \bar{3} \to \bar{2} + 4, \quad (t - \text{channel}), \tag{2.60}$$

$$1 + \bar{4} \to \bar{2} + 3, \quad (u - \text{channel}). \tag{2.61}$$

---

[5] And for completeness (b) was depicted just to show the class where single-diffractive dissociation falls into

[6] In a generic reaction of the type $1 + 2 \to 3 + 4 + ... + N$, the number of independent Lorentz invariants is $3N - 10$.

2.6.1   The centre-of-mass reference frame

By taking as an example the s-channel process (2.55), the momentum conservation relation in the CM frame, see Figure 2.4, by definition is

$$\mathbf{p}_1 = -\mathbf{p}_2 = \mathbf{k}, \tag{2.62}$$

$$\mathbf{p}_3 = -\mathbf{p}_4 = \mathbf{k}', \tag{2.63}$$

where the 4-momenta of the particles can be written as

$$\begin{aligned}
p_1 &= (E_1, \mathbf{k}) \ , \ \ p_2 = (E_2, -\mathbf{k}), \\
p_3 &= (E_3, \mathbf{k}') \ , \ \ p_4 = (E_4, -\mathbf{k}').
\end{aligned} \tag{2.64}$$

Moreover, the energies E_i can be written in terms of the total squared CM energy s,

$$E_1 = \frac{1}{2\sqrt{s}}(s + m_1^2 - m_2^2), \tag{2.65}$$

$$E_2 = \frac{1}{2\sqrt{s}}(s + m_2^2 - m_1^2), \tag{2.66}$$

$$E_3 = \frac{1}{2\sqrt{s}}(s + m_3^2 - m_4^2), \tag{2.67}$$

$$E_4 = \frac{1}{2\sqrt{s}}(s + m_4^2 - m_3^2). \tag{2.68}$$

The momenta $\mathbf{k}$ and $\mathbf{k}'$, and also the momentum transfer t, are expressed by means of the mass-shell condition $p_\nu p^\nu = p^2 = m^2$, then

$$|\mathbf{k}| = \frac{1}{2\sqrt{s}} \lambda^{1/2}(s, m_1^2, m_2^2), \tag{2.69}$$

$$|\mathbf{k}'| = \frac{1}{2\sqrt{s}} \lambda^{1/2}(s, m_1^2, m_4^2), \tag{2.70}$$

$$t = m_1^2 + m_3^2 - 2E_1 E_3 + 2|\mathbf{k}||\mathbf{k}'| \cos\theta, \tag{2.71}$$

and $\cos\theta$ can be written in terms of s and t variables,

$$\cos\theta = \frac{s^2 + s(2t - \Sigma_i m_i^2) + (m_1^2 - m_2^2)(m_3^2 - m_4^2)}{\lambda^{1/2}(s, m_1^2, m_2^2)\lambda^{1/2}(s, m_1^2, m_4^2)}, \tag{2.72}$$

where $\lambda(x, y, z)$ is a function defined as

$$\lambda(x, y, z) = x^2 + y^2 + z^2 - 2xy - 2yz - 2xz. \tag{2.73}$$

In the high-energy limit, $s \to \infty$, the masses can be neglected and one finds that $E_i \simeq \sqrt{s}/2$ and $|\mathbf{k}|, |\mathbf{k}'| \simeq \sqrt{s}/2$.

An important two-body exclusive scattering case, which is the mains focus of this Thesis is the elastic scattering represented by Figure 2.2. The relations between the CM variables, $\mathbf{k}$ and θ can be much simplified considering the elastic scattering of particles with the same mass,

$$|\mathbf{k}| = \frac{1}{2}\sqrt{s - 4m^2}, \tag{2.74}$$

$$\cos\theta = 1 + \frac{2t}{s - 4m^2}. \tag{2.75}$$

It is straightforward to see the following reverse relations,

$$s = 4(k^2 + m^2), \tag{2.76}$$

$$t = -4k^2 \sin^2\left(\frac{\theta}{2}\right), \tag{2.77}$$

$$u = -2k^2(1 + \cos\theta), \tag{2.78}$$

where in the last one it was used the identity (2.59).
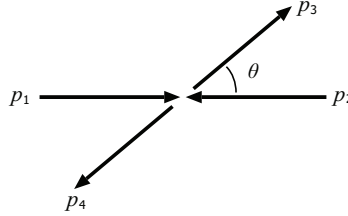
Figure 2.4: The CM reference frame.

2.6.2 Physical domains

Also by considering the case where the collision process is an equal-mass scattering, then the physical domain is simply found by means of the kinamatic limits of k and θ in expression (2.76-2.78). For $k \geq 0$, $-1 \leq \cos\theta \leq 1$ and $0 \leq \sin^2(\theta/2) \leq 1$, one finds that for the s-channel,

$$s \geq 4m^2 \ , \ t \leq 0 \ , \ u \leq 0. \tag{2.79}$$

Following the same path, for a t-channel reaction (2.60), the squared CM energy is now written as $t = (p_1 + p_{\bar{3}})^2 = (p_1 - p_3)^2$ and the momentum transfer $s = (p_1 - p_{\bar{2}})^2 = (p_1 + p_2)^2$,

$$t = 4(k_t^2 + m^2), \tag{2.80}$$

$$s = -4k_t^2 \sin^2\left(\frac{\theta_t}{2}\right), \tag{2.81}$$

where the t subscript means t-channel, respectively. The physical domains are then

$$t \geq 4m^2 \ , \ s \leq 0 \ , \ u \leq 0. \tag{2.82}$$

Similarly, for the u-channel reaction (2.61),

$$u = 4(k_u^2 + m^2), \tag{2.83}$$

$$t = -4k_u^2 \sin^2\left(\frac{\theta_u}{2}\right), \tag{2.84}$$

$$u \geq 4m^2 \ , \ s \leq 0 \ , \ t \leq 0. \tag{2.85}$$
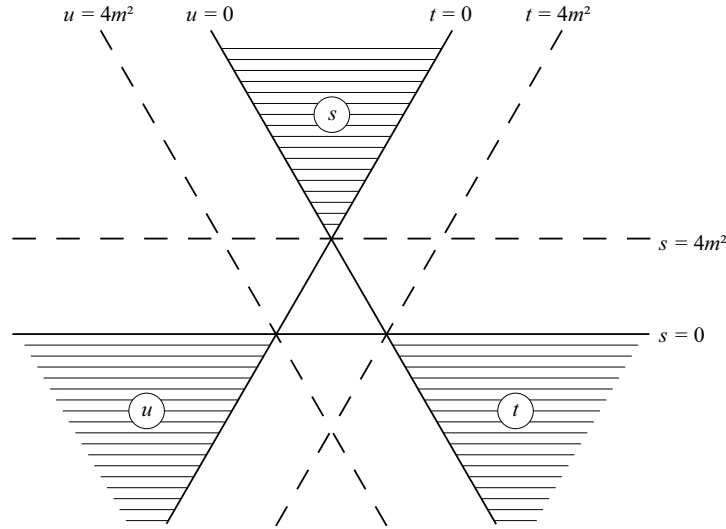
Figure 2.5: The Mandelstam plot and the physical domains of s, t and u channels.

Although s, t, u-channel processes have different and non-overlapping physical domains, see Figure 2.5, the crossing symmetry of the S-matrix ensures they are described by the same scattering amplitude. Hence,

$$F_{1+2 \to 3+4}(s, t, u) = F_{1+\bar{3} \to \bar{2}+4}(t, s, u), \tag{2.86}$$

and for the u-channel,

$$F_{1+2 \to 3+4}(s, t, u) = F_{1+\bar{4} \to \bar{2}+3}(u, t, s). \tag{2.87}$$

Thus, it is easy to see that processes such as those ones given by reactions (2.55) and

(2.60) are simply related by the change of s and t. Usually it is said that (2.60) is the crossed channel of (2.55). Our main focus is on pp and $\bar{p}p$ elastic scattering described by

$$s\text{-channel}: \quad p + p \rightarrow p + p, \tag{2.88}$$

$$t\text{-channel}: \quad \bar{p} + p \rightarrow \bar{p} + p. \tag{2.89}$$

As a function of the Mandelstam variables, the elastic differential cross-section (2.21) and the total cross-section (2.24) can be written as

$$\frac{d\sigma}{dt}(s,t) = \pi \, |F(s,t)|^2, \tag{2.90}$$

$$\sigma_{tot}(s) = 4\pi \, \text{Im} \, F(s, t = 0), \tag{2.91}$$

where it was used $\pi dq^2 \simeq k^2 d\Omega$ and $q^2 = -t$, and also the normalisation $f = (\sqrt{s}/2)F \simeq kF$ for the scattering amplitude. Beyond these two physical observables, there is another quantity of particular interest in elastic hadronic scattering which defines the phase of the forward amplitude called the ρ-parameter and written as the ratio of the real to imaginary part of the forward scattering amplitude,

$$\rho(s) = \frac{\text{Re} \, F(s, t = 0)}{\text{Im} \, F(s, t = 0)}. \tag{2.92}$$

Strictly and rigorously speaking, this is not a physical quantity in a sense that it is not obtained as a direct measurement, but as a parameter to adjust the elastic differential cross-section in the Coulombian-nuclear region. Experimentally, it is known that the nuclear (hadronic) elastic differential cross-section can be parametrised in the low-$|t|$ region, $0.02 < |t| < 0.5$ GeV^2, as

$$\frac{d\sigma_n}{dt}(s,t) = \left[\frac{d\sigma_n}{dt}\right]_{t=0} e^{Bt}, \tag{2.93}$$

where $B(s)$ is the forward slope, *i.e.* a plot $\ln(d\sigma_{nucl}/dt) \times t$ in the low-t region would give a straight line of slope B. In this case, the slope can be written as

$$B(s) = \left[\frac{d}{dt} \ln \frac{d\sigma_n}{dt}(s,t)\right]_{t=0} = \left[\left(\frac{d\sigma_n}{dt}\right)^{-1} \frac{d}{dt}\left(\frac{d\sigma_n}{dt}\right)\right]_{t=0}. \tag{2.94}$$

By means of expressions (2.90) and (2.91), the nuclear differential cross-section can be written in terms of the ρ-parameter as

$$\frac{d\sigma_n}{dt}(s,t) = \pi \, \left|(\rho + i)\frac{\sigma_{tot}}{4\pi} e^{Bt/2}\right|^2. \tag{2.95}$$

The simultaneous presence of Coulombian and nuclear fields does not allow one to disregard interference effects. Instead, the complete differential cross-section is given by

$$\frac{d\sigma}{dt} = \frac{d\sigma_{coulomb}}{dt} + \frac{d\sigma_{cn}}{dt} + \frac{d\sigma_n}{dt}, \tag{2.96}$$

where the interference term is

$$\frac{d\sigma_{cn}}{dt} \approx \pi(\rho + \alpha\varphi)\left(\frac{\alpha\sigma_{tot}}{t}\right), \tag{2.97}$$

and α stands for the fine-structure constant and φ is the phase factor in the Coulombian region. The interference cross-section implies into the direct measure of the quantity $(\rho + \alpha\varphi)$, thus if one knows σ_{tot}, then the ρ-parameter can be evaluated. What is usually called as the elastic differential cross-section, see expression (2.90), is indeed the nuclear differential cross-section [39].

2.7 Impact-parameter representation and the eikonal formalism

In the high-energy limit the ℓ-th partial-wave bounds the cross section as a decreasing function of the energy as, see expression (2.52),

$$\sigma_{tot} \leq \frac{2\pi}{k^2}\left(2\ell + 1\right), \tag{2.98}$$

then a huge increasing number of partial-waves must contribute to the high-energy amplitude. There is a subtlety that in this high-energy limit it is possible to construct a geometrical representation based on the impact-parameter space, which is the 2-dimensional space orthogonal to the beam of particles, known as the impact-parameter representation.

The scattering amplitude is written as a sum over all possible values of angular momentum ℓ, however for finite potentials the energy is bounded by a maximum value ℓ_{max}, given by $\sqrt{\ell_{max}(\ell_{max}+1)} \simeq kr_0$, where r_0 stands for the potential range. At high energies $kr_0 \gg 1$, *i.e.* when the energy of the scattering particles is higher than the interacting potential, $E \geq |V(\mathbf{r})|$, implies the condition $\ell_{max} \gg 1$. Thus, it is sensible to convert the discrete sum over ℓ into an integral of element $d\ell$,

$$\sum_{\ell=0}^{\ell_{max}} \rightarrow \int_0^\infty d\ell,$$

then the scattering amplitude is written as an integral,

$$f(\mathbf{k}, \mathbf{k}') = \frac{i}{2k} \int_0^\infty d\ell\, (2\ell + 1) \left[1 - e^{i\chi(k,\ell)}\right] P_\ell(\cos\theta), \tag{2.99}$$

where it was defined $\chi(k, \ell)$ as the continuum form of the phase-shifts, also known as the eikonal function[7]. For $\ell \gg 1$ and small angles the Legendre polynomials can be written in terms of Bessel's functions of zeroth order,

$$P_\ell(\cos\theta) \approx J_0\left[(2\ell + 1)\sin(\theta/2)\right] \approx J_0(kb\theta).$$

By means of the semi-classical approximation $bk = \ell + 1/2$, where the impact-parameter b is viewed as the minimal transverse distance between two particles in a collision, then $\int d\ell$ can be properly replaced by $\int db\, k$. Finally, by using expressions (2.76) and (2.77) for the energy s and the momentum transfer q ($\equiv \sqrt{-t}$), the scattering amplitude can be rewritten as

$$f(s, q) = ik \int_0^\infty db\, b\, J_0(qb) \left[1 - e^{i\chi(s,b)}\right], \tag{2.100}$$

and through the normalisation $f = kF$,

$$F(s, t) = i \int_0^\infty db\, b\, J_0(b\sqrt{-t})\, \Gamma(s, b). \tag{2.101}$$

In the eikonal formalism, the quantity $1 - e^{i\chi(s,b)}$ is known as the profile function,

$$\Gamma(s, b) = 1 - e^{i\chi(s,b)}, \tag{2.102}$$

which describes the absorption resulting from the opening of inelastic channels by means of a simple optical-geometrical property namely shadowing, a clear bridge towards diffraction [3]. It is easily seen the aforementioned expression is the Fourier-Bessel transform of the scattering amplitude $F(s, t)$,

$$\Gamma(s, b) = -i \int_0^\infty d\sqrt{-t}\, \sqrt{-t}\, J_0(b\sqrt{-t})\, F(s, t). \tag{2.103}$$

Expression (2.102) tells that the profile function is a complex function, and hence in principle that is nothing wrong rewriting it as a combination of a real and a imaginary part,

$$\Gamma(s, b) = \operatorname{Re}\Gamma(s, b) + i\operatorname{Im}\Gamma(s, b), \tag{2.104}$$

---

[7] In the literature sometimes one may also find it by the name of opacity function, because it is related to shadowing, and defined as $\Omega(s, b) = -i\chi(s, b)$.

which in a sense it is equivalently of writing,

$$
\Gamma(s,b) = 1 - e^{i\operatorname{Re}\chi(s,b) - \operatorname{Im}\chi(s,b)}
$$
$$
= \underbrace{\left(1 - e^{-\chi_I}\cos\chi_R\right)}_{\operatorname{Re}\Gamma(s,b)} + i\underbrace{\left(-e^{-\chi_I}\sin\chi_R\right)}_{\operatorname{Im}\Gamma(s,b)}, \tag{2.105}
$$

where it was written $\operatorname{Re}\chi(s,b) \equiv \chi_R$ and $\operatorname{Im}\chi(s,b) \equiv \chi_I$ just for not to overload the notation. Continuing, the square modulus of $\Gamma(s,b)$,

$$
|\Gamma(s,b)|^2 = [\operatorname{Re}\Gamma(s,b)]^2 + [\operatorname{Im}\Gamma(s,b)]^2
$$
$$
= 2\underbrace{\left(1 - e^{-\chi_I}\cos\chi_R\right)}_{\operatorname{Re}\Gamma(s,b)} - \left(1 - e^{-2\chi_I}\right), \tag{2.106}
$$

so, the real part of the profile function, related to the imaginary part of $F(s,t)$, is associated with contributions from the elastic and inelastic channels via unitarity [3], in other words the unitarity of the S-matrix requires that the absorptive part of the elastic scattering amplitude receives contributions from both the elastic and the inelastic channels. In impact parameter space this condition may be written as

$$
2\operatorname{Re}\Gamma(s,b) = |\Gamma(s,b)|^2 + \left(1 - e^{-2\chi_I}\right). \tag{2.107}
$$

The cross-sections in the impact-parameter representation are then written by means of the optical theorem (2.46), the eikonal representation (2.102) and the unitarity principle (2.23),

$$
\begin{aligned}
\sigma_{el}(s) &= 2\pi \int_0^\infty db\, b\, |\Gamma(s,b)|^2 \\
&= 2\pi \int_0^\infty db\, b\, |1 - e^{-\chi_I + i\chi_R}|^2 \\
&= 2\pi \int_0^\infty db\, b\, \left[2\left(1 - e^{-\chi_I}\cos\chi_R\right) - \left(1 - e^{-2\chi_I}\right)\right],
\end{aligned} \tag{2.108}
$$

$$
\begin{aligned}
\sigma_{in}(s) &= 2\pi \int_0^\infty db\, b\, \left[2\operatorname{Re}\Gamma(s,b) - |\Gamma(s,b)|^2\right] \\
&= 2\pi \int_0^\infty db\, b\, \left(1 - e^{-2\chi_I}\right),
\end{aligned} \tag{2.109}
$$

$$\sigma_{tot}(s) = 2\pi \int_0^\infty db\, b\, 2\,\mathrm{Re}\Gamma(s,b)$$

$$= 4\pi \int_0^\infty db\, b\, \left(1 - e^{-\chi_I} \cos\chi_R\right). \tag{2.110}$$

The ρ-parameter will be given by

$$\rho(s) = \frac{\mathrm{Re}\left\{i \int_0^\infty db\, b\, \left(1 - e^{i\chi(s,b)}\right)\right\}}{\mathrm{Im}\left\{i \int_0^\infty db\, b\, \left(1 - e^{i\chi(s,b)}\right)\right\}}$$

$$= \frac{\int_0^\infty db\, b\, e^{-\chi_I} \sin\chi_R}{\int_0^\infty db\, b\, \left(1 - e^{-\chi_I} \cos\chi_R\right)} \tag{2.111}$$

the elastic differential cross-section,

$$\frac{d\sigma}{dt}(s,t) = \pi \left| i \int_0^\infty db\, b\, J_0(b\sqrt{-t})\, \left[1 - e^{i\chi(s,b)}\right] \right|^2$$

$$= \pi \left\{ \left[\int_0^\infty db\, b\, J_0(b\sqrt{-t})\, \left(e^{-\chi_I} \sin\chi_R\right)\right]^2 + \left[\int_0^\infty db\, b\, J_0(b\sqrt{-t})\, \left(1 - e^{-\chi_I} \cos\chi_R\right)\right]^2 \right\} \tag{2.112}$$

and the B-slope,

$$B(s) = \frac{1}{2} \left\{ \frac{\int_0^\infty db\, b\, e^{-\chi_I} \sin\chi_R \int_0^\infty db\, b^3\, e^{-\chi_I} \sin\chi_R}{[\int_0^\infty db\, b\, e^{-\chi_I} \sin\chi_R]^2 + [\int_0^\infty db\, b\, (1 - e^{-\chi_I} \cos\chi_R)]^2} \right. $$
$$\left. + \frac{\int_0^\infty db\, b\, (1 - e^{-\chi_I} \cos\chi_R) \int_0^\infty db\, b^3\, (1 - e^{-\chi_I} \cos\chi_R)}{[\int_0^\infty db\, b\, e^{-\chi_I} \sin\chi_R]^2 + [\int_0^\infty db\, b\, (1 - e^{-\chi_I} \cos\chi_R)]^2} \right\}. \tag{2.113}$$

Notice that, by using the unitarity principle (2.23) the structure of the cross-sections (2.108-2.110) could be written in terms of distribution functions, also known as overlap functions defined as

$$G_{tot}(s,b) = 2\,\mathrm{Re}\,\Gamma(s,b), \tag{2.114}$$

$$G_{el}(s,b) = |\Gamma(s,b)|^2, \tag{2.115}$$

$$G_{in}(s,b) = G_{tot}(s,b) - G_{el}(s,b) = 2\mathrm{Re}\,\Gamma(s,b) - |\Gamma(s,b)|^2. \tag{2.116}$$

In this picture the inelastic overlap function $G_{in}(s,b)$ is the probability occurrence of at least one inelastic event at impact-parameter b, or in the same way the probability that neither hadron is broken up in a collision at impact-parameter b is therefore given by $P(s,b) = e^{-2\chi_I(s,b)}$. One direct physical consequence is that no scattering process can be uniquely inelastic, and thus the usual statement that the elastic amplitude results from the shadow scattering from the inelastic channels. Similarly in classical optical theory,

according to Babinet's principle, the incidence of plane-waves into an obstacle is equivalent to the diffraction by its complementary object. Henceforth, the scattering amplitude tends to be purely imaginary and the elastic scattering purely diffractive with increasing energy.

2.8 Experimental data

The behaviour of the hadronic cross-sections with increasing CM energy is extremely important to get a good understanding of high-energy diffraction physics. Through out the whole information one can obtain from regions of low and high momentum transfer, the cross-sections play a fundamental role in the study of the smooth transition to perturbative QCD.

The experimental data used in the Thesis so far are from pp and $\bar{p}p$ elastic scattering obtained by dedicated experiments in colliders over the past few years. These are the reactions with the highest CM energy that have ever been measured in laboratory.

§ Forward physical quantities

It will be shown here the experimental data of $\sigma_{tot}^{pp,\bar{p}p}$ and $\rho^{pp,\bar{p}p}$. Despite the fact that the complete set of experimental data for these both forward quantities is huge, for some reasons it will not be entirely considered the whole set. First, because the very low-energy data corresponds to the Coulombian-nuclear interference region and we are mainly focused on elastic diffractive processes. Second, because the very high-energy data, higher than the LHC present energies, corresponds to cosmic-ray CM energies[8]. However, cosmic-ray predictions are strongly dependent on the Monte Carlo generator for extracting the σ_{tot}^{pp} from measurements of proton-air production cross-section σ_{prod}^{p-air}, which causes uncertainties larger than those ones from colliders.

The complete set of $\sigma_{tot}^{pp,\bar{p}p}$, according to the Particle Data Group [35], has 283 and 444 data points, respectively. The complete set of $\rho^{pp,\bar{p}p}$, 118 and 91 data points, respectively, see Figures 2.6 and 2.7. This is the reason why we decided to use forward data only in the energy region $\sqrt{s} \geq 10$ GeV. Just as a matter of comparison, we extrapolate our results in the energy region far beyond LHC. However, these cosmic-ray data, respectively the AUGER experimental datum at $\sqrt{s} = 57$ TeV with $\sigma_{tot}^{pp} = 133.0 \pm 29.0$ mb [49] and the Telescope Array (TA) datum at $\sqrt{s} = 95$ TeV with $\sigma_{tot}^{pp} = 170.0 \pm 51.0$ mb [50], are not being considered in our fitting. Thus, with the constraint $\sqrt{s} \geq 10$ GeV, now the set of $\sigma_{tot}^{pp,\bar{p}p}$ has 73 and 30 data points, respectively, and for the set of $\rho^{pp,\bar{p}p}$, 50 and 12 data points, respectively, see Figures 2.8, 2.9 and 2.10, and Tables 2.1-2.5.

---

[8] There are some cosmic-ray data points in the middle energy region, but smaller than the typical Tevatron energies and one point approximately at $\sqrt{s} = 6$ TeV.

In the case of $\bar{p}p$ scattering, there are results for $\sigma_{tot}^{\bar{p}p}$ and $\rho^{\bar{p}p}$ only at energies $\sqrt{s} \leq 1.8$ TeV, which represents the CM energy of Tevatron at Fermilab. However, in the case of pp scattering, the σ_{tot}^{pp} and ρ^{pp} results at energies $\sqrt{s} \leq 62.8$ were obtained at CERN-ISR, and the recent TOTEM measurements at the LHC at energies $\sqrt{s} = 7 - 8$ TeV. It is shown in Table 2.1 the compiled set of the highest collider energy data for σ_{tot}^{pp} obtained by the TOTEM Collaboration [17–21] by means of three specific methods:

I. Elastic scattering extrapolating to the optical point $(t = 0)$

The elastic differential cross-section can be written, according to expression (2.90), in terms of the scattering amplitude as

$$\frac{d\sigma}{dt}(s,t) = \pi \left| F(s,t) \right|^2.$$

The optical theorem (2.91) gives a relation between the total cross-section and the imaginary part of the forward scattering amplitude,

$$\sigma_{tot}(s) = 4\pi \operatorname{Im} F(s, t = 0) = \frac{4\sqrt{\pi}}{\sqrt{1 + \rho^2}} \left[\frac{d\sigma}{dt} \bigg|_{t=0} \right]^{1/2}, \tag{2.117}$$

where it was used $F(s,0) = (\rho + i) \operatorname{Im} F(s,0)$ and ρ stands for the ratio of the real to imaginary part of the scattering amplitude. Exponentially extrapolating the elastic differential cross-section to $t = 0$, see expression (2.93), and using the prediction of $\rho \simeq 0.145 \pm 0.007$ at $\sqrt{s} = 7$ TeV from the COMPETE Group [51], the TOTEM Collaboration arrived at $\sigma_{tot}^{pp} = 98.30 \pm 2.80$ mb [17] and $\sigma_{tot}^{pp} = 98.58 \pm 2.23$ mb [18], both using the luminosity provided by the CMS [52]. At $\sqrt{s} = 8$ TeV the TOTEM Collaboration arrived at $\sigma_{tot}^{pp} = 102.90 \pm 2.3$ mb and $\sigma_{tot}^{pp} = 103.0 \pm 2.3$ mb where the ρ-parameter was for the first time at the LHC extracted via the Coulombian-nuclear interference region, *viz.* $\rho = 0.120 \pm 0.030$ [21].

II. ρ-independent determination

The measured quantity in a scattering experiment is a counting rate and not a cross-section *per se*. Thus, for an elastic scattering, the quantity measured is the (number of counts)/seconds/(interval of time),

$$\Delta N(t) = \mathcal{L}_{int} \frac{d\sigma}{dt}, \tag{2.118}$$

where $\mathcal{L}_{int}$ is the integrated luminosity with units $(area)^{-1} \times (time)^{-1}$. The cross-section can be obtained by summing directly the elastic and inelastic cross-section,

$$\sigma_{tot} = \frac{N_{el} + N_{in}}{\mathcal{L}_{int}^{CMS}} = \sigma_{el} + \sigma_{in}, \tag{2.119}$$

where N_{el} and N_{in} represents, respectively, the elastic and inelastic rates integrated over a given data taking period. Using this technique the TOTEM Collaboration arrived at $\sigma_{tot}^{pp} = 99.10 \pm 4.30$ mb at $\sqrt{s} = 7$ TeV [19]. It is included in the data set the first estimate for the ρ-parameter made by the TOTEM Collaboration in their ρ-independent measurement. Then, by combining the elastic and inelastic measurements in order to determine ρ^2,

$$\rho^2 = 16\pi \left(\hbar c\right)^2 \mathcal{L}_{int}^{CMS} \frac{dN_{el}/dt|_{t=0}}{(N_{el} + N_{in})^2} - 1, \tag{2.120}$$

yields $\rho^2 = 0.009 \pm 0.056$. Taking a uniform $|\rho|$ distribution, then at $\sqrt{s} = 7$ TeV, $\rho = 0.145 \pm 0.091$ [19].

III. Luminosity-independent technique

Using the optical theorem (2.91), the elastic and inelastic measurements can be combined in such a way that total cross-section can be written without the knowledge of the luminosity,

$$\sigma_{tot} = \frac{16\pi(\hbar c)^2}{1 + \rho^2} \frac{dN_{el}/dt|_{t=0}}{N_{el} + N_{in}}. \tag{2.121}$$

Taking $\rho \simeq 0.141 \pm 0.007$ from the COMPETE [51] extrapolation at $\sqrt{s} = 7$ TeV yields the luminosity-independent total cross section $\sigma_{tot}^{pp} = 98.0 \pm 2.5$ mb [19]. At the energy $\sqrt{s} = 8$ TeV and taking $\rho \simeq 0.140 \pm 0.007$ from COMPETE [51] preferred model extrapolation, the TOTEM Collaboration arrived at $\sigma_{tot}^{pp} = 101.7 \pm 2.9$ [20].

§ The elastic differential cross-section

As it was mentioned above, the fundamental quantity measured in an elastic scattering experiment is the counting rate in a fixed energy. By means of expression (2.118) the differential cross-section can be determined as

$$\frac{d\sigma}{dt} = \frac{1}{\mathcal{L}_{int}} \frac{dN_{el}}{dt}. \tag{2.122}$$

In general, the elastic differential cross-section can be divided in three well behaved and specific contributions, see expression (2.96), and written as

$$\frac{d\sigma}{dt} = \pi \left| F_c \, e^{i\alpha\varphi(t)} + F_n \right|^2 , \qquad (2.123)$$

where F_c and F_n stands for the scattering amplitudes. In the case of pp scattering [39]:

i. $d\sigma_c/dt \sim 4\pi^2(\alpha/|t|)^2$, which is the purely Coulombian component and dominates in the region $|t| < 10^{-3}$ GeV^2.

ii. $d\sigma_{cn}/dt \sim \pi(\rho + \alpha\varphi)(\alpha\sigma_{tot}/|t|)$, which is the Coulombian-nuclear interference component and dominates in the region $|t| \simeq 10^{-3}$ GeV^2. The term $\alpha\varphi$ leads to the distortion in the purely hadronic component induced by the presence of the Coulombian field.

iii. $d\sigma_n/dt = (1 + \rho^2)\,\sigma_{tot}^2\,e^{-B|t|}/16$, which is the purely hadronic component parametrised in the region of the diffractive peak and dominates at $|t| > 10^{-2}$ GeV^2.

Thus in the region where the momentum transfer is typically higher than 10^{-2} GeV^2, the elastic differential cross-section is completely determined only by the purely hadronic component. The consequence is that the diffraction pattern observed in Figure 2.11 is exclusively due to the strong interaction dynamical evolution as a functionof momentum transfer in the collision.

The experimental data set for elastic differential cross-section used in this Thesis so far corresponds to the recent measurements made by the TOTEM Collaboration at CM energies $\sqrt{s} = 7$ TeV [18, 22] and $\sqrt{s} = 8$ TeV [21], corresponding to 165 and 27 data points respectively, see Figures 2.12 and 2.13, and Tables 2.6-2.8.
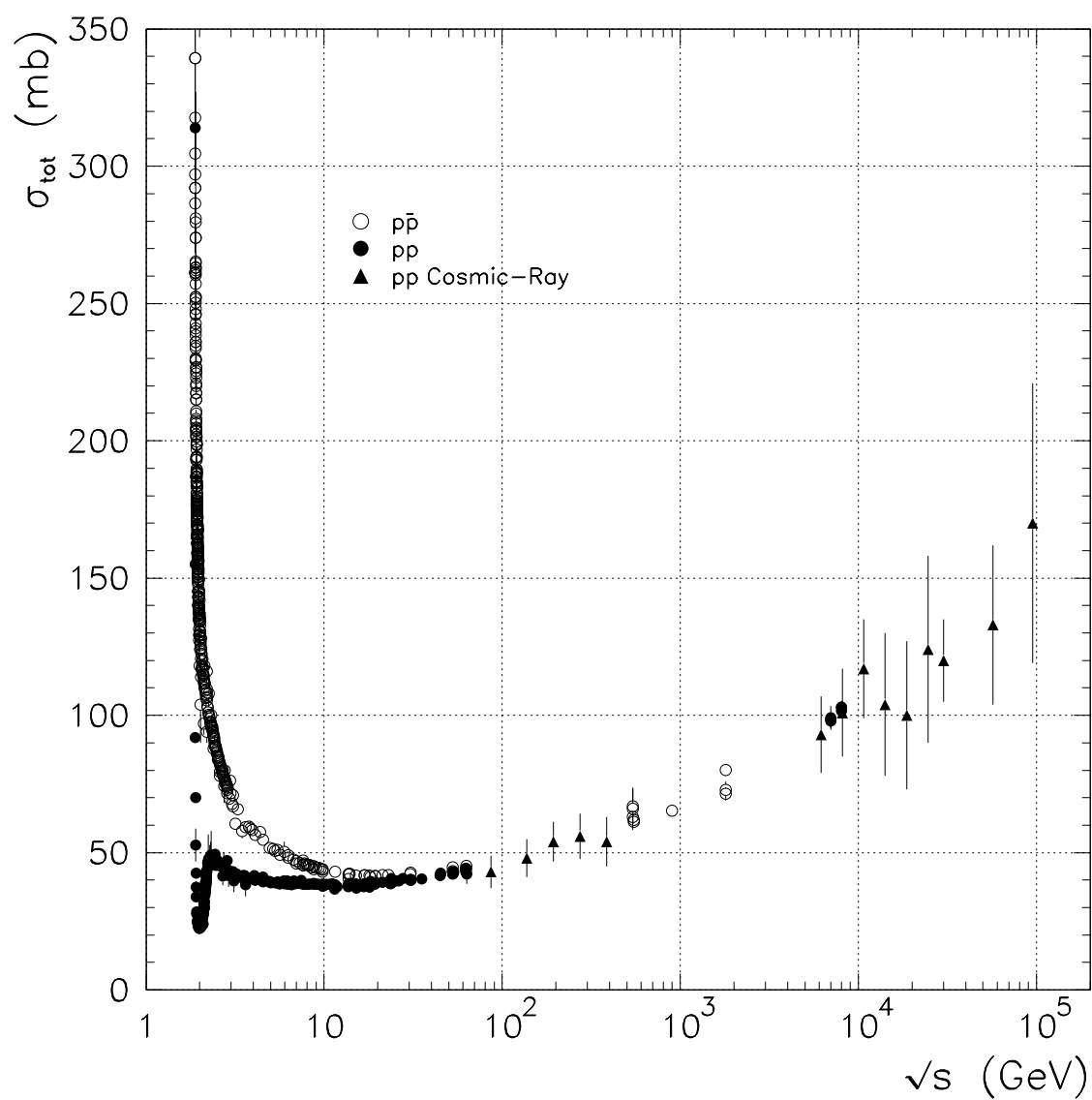
Figure 2.6: The complete data set of pp (filled circle) and $\bar{p}p$ (open circle) total cross-section.
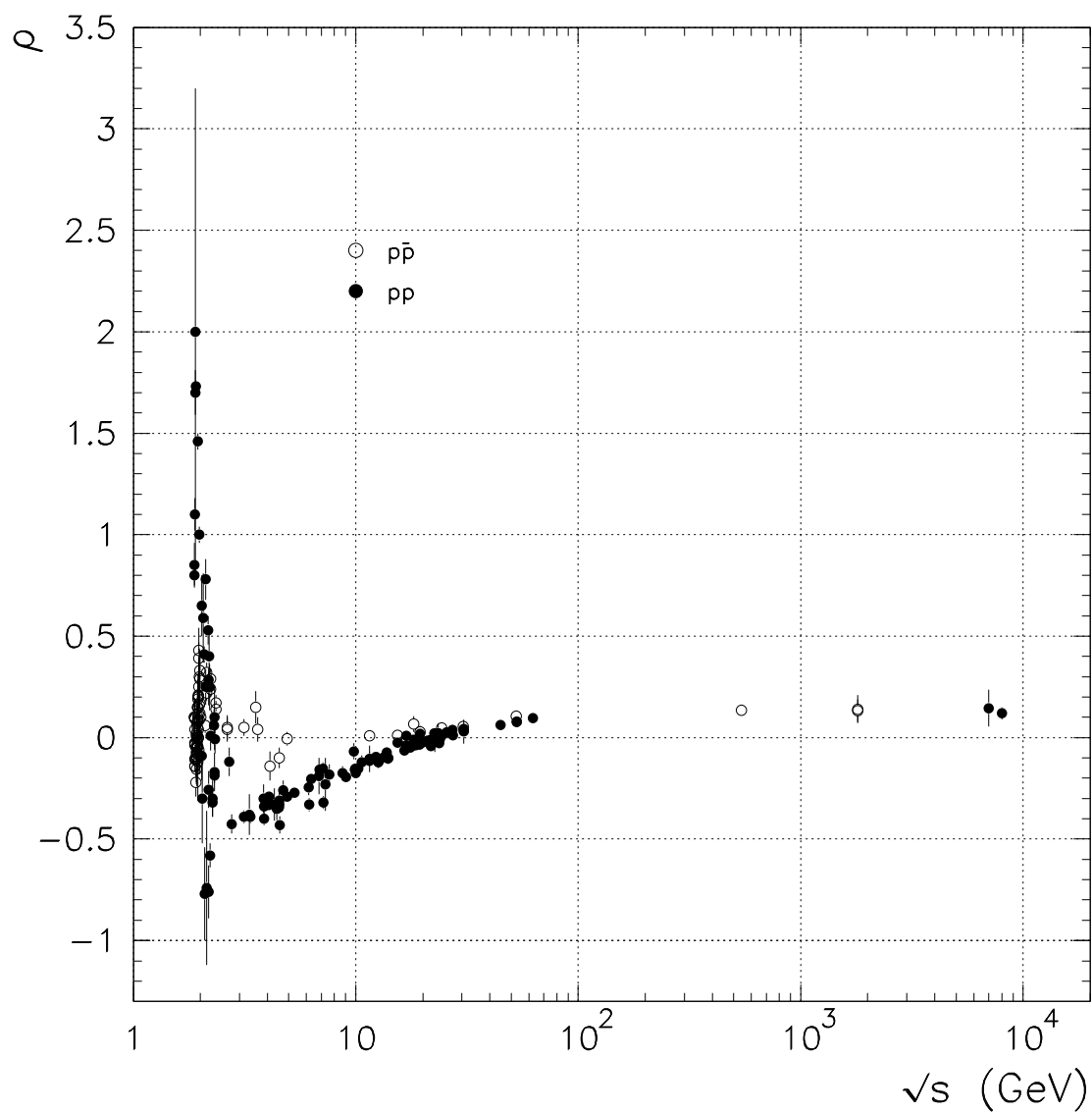
Figure 2.7: The complete data set of the ratio of the real to imaginary part of the forward scattering amplitude for pp (filled circle) and $\bar{p}p$ (open circle).
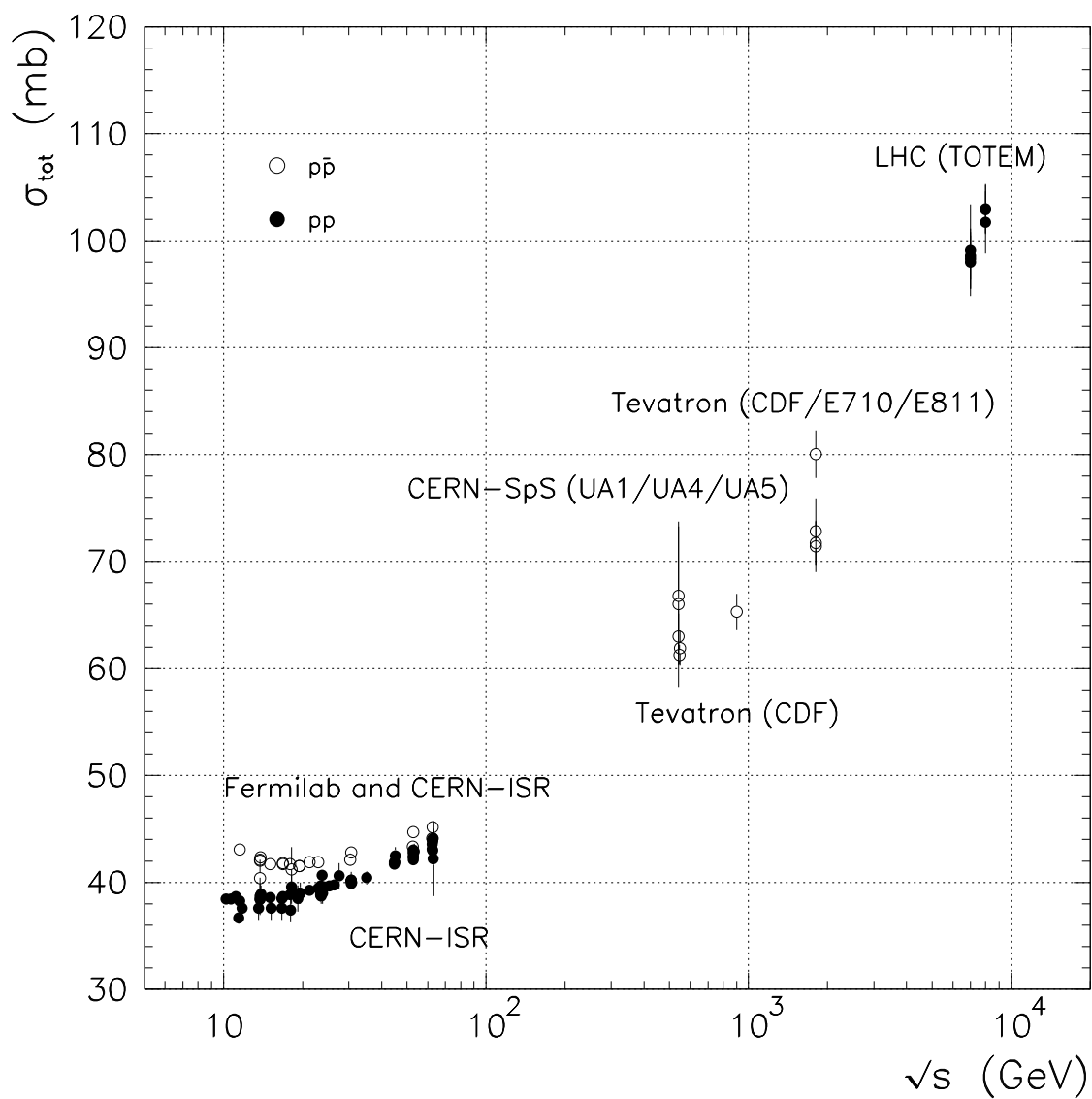
Figure 2.8: Total cross-section experimental data set at energies $\sqrt{s} \geq 10$ GeV with statistical and systematic uncertainties combined in quadrature. The corresponding collaborations are properly identified.
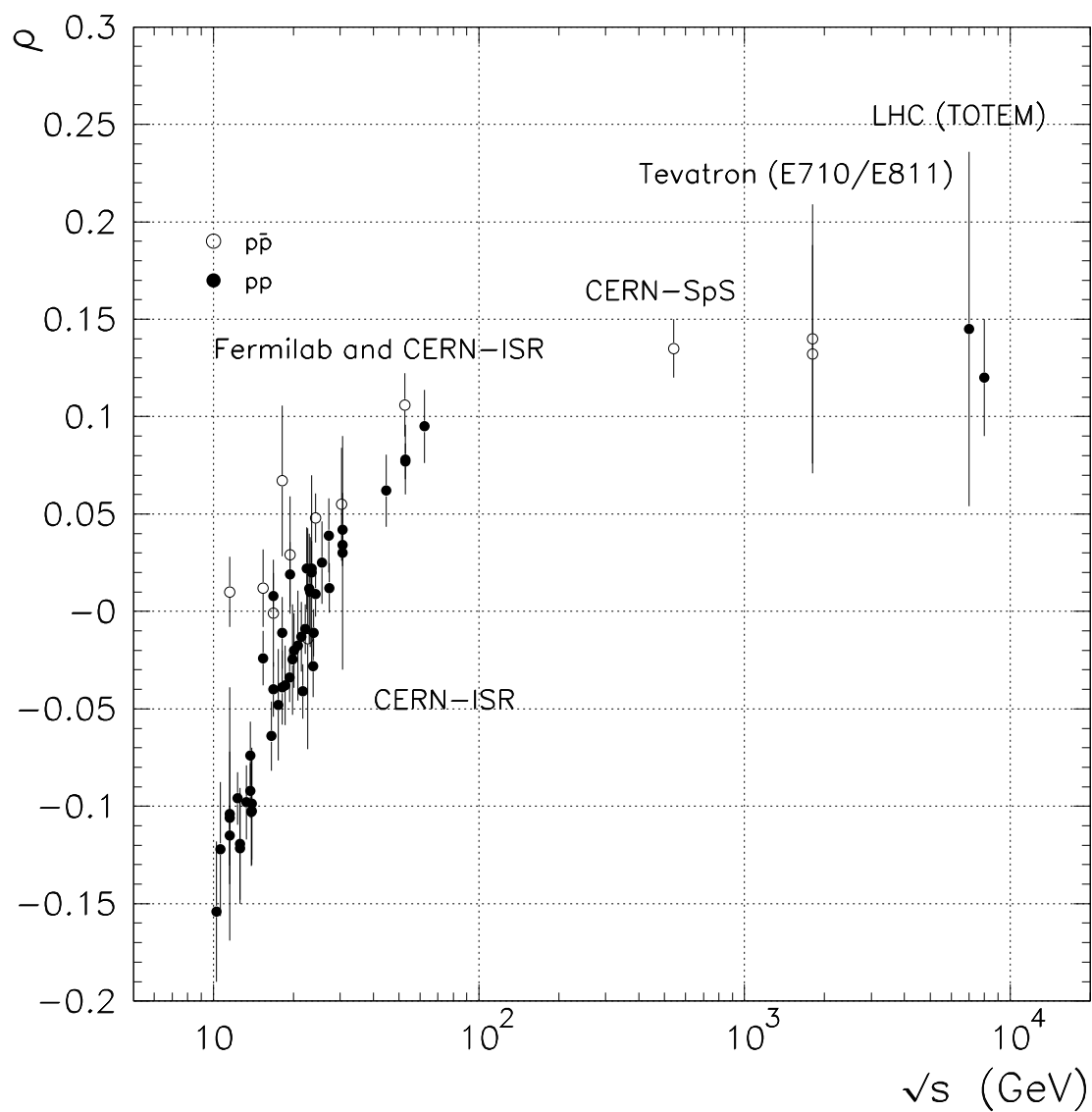
Figure 2.9: Ratio of the real to imaginary part of the scattering amplitude experimental data set at energies $\sqrt{s} \geq 10$ GeV with statistical and systematic uncertainties combined into quadrature. As in the last caption, the corresponding collaborations are properly identified.
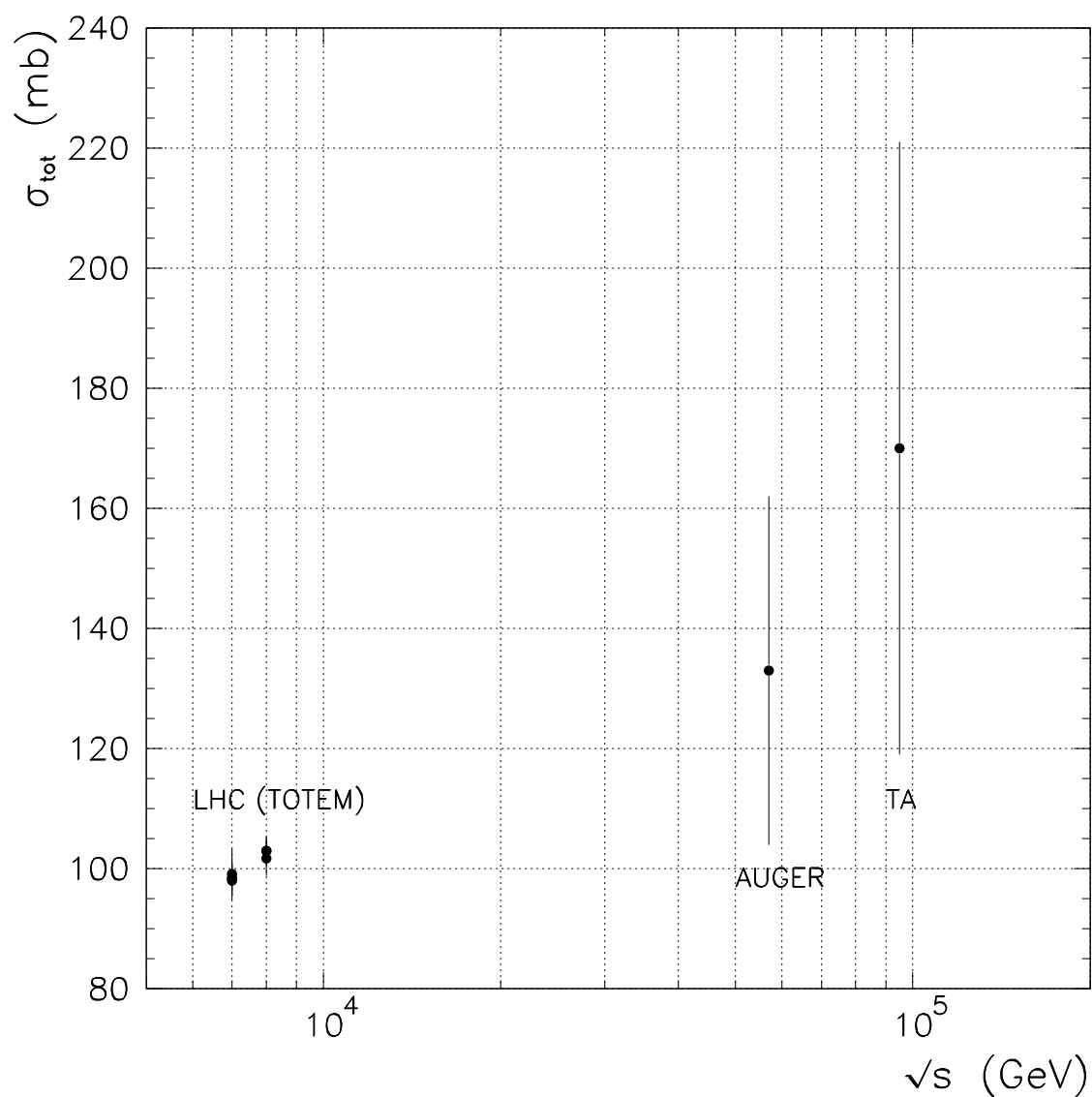
Figure 2.10: Experimental data points at cosmic-ray energies obtained by The Pierre Auger Collaboration [49], datum at $\sqrt{s} = 57$ TeV, and by the Telescope Array (TA) [50], datum at $\sqrt{s} = 95$ TeV. The statistical and systematic uncertainties were combined into quadrature.

Collaboration	Reference	$\sqrt{s}$ (TeV)	σ_{tot} (mb)
	[17]	7	98.30 ± 2.80
	[18]	7	98.58 ± 2.23
	[19]	7	99.10 ± 4.30
TOTEM	[19]	7	98.00 ± 2.50
	[20]	8	101.70 ± 2.90
	[21]	8	102.90 ± 2.30
	[21]	8	103.00 ± 2.30

Collaboration	Reference	$\sqrt{s}$ (TeV)	ρ
TOTEM	[19]	7	0.145 ± 0.091
TOTEM	[21]	8	0.120 ± 0.030

Table 2.1: Total cross-section and the ratio of the real to imaginary part of the forward scattering amplitude data obtained by the TOTEM experiment at the LHC at energies $\sqrt{s} =$ 7 TeV e 8 TeV, respectively. The statistical and systematic uncertainties were combined into quadrature.
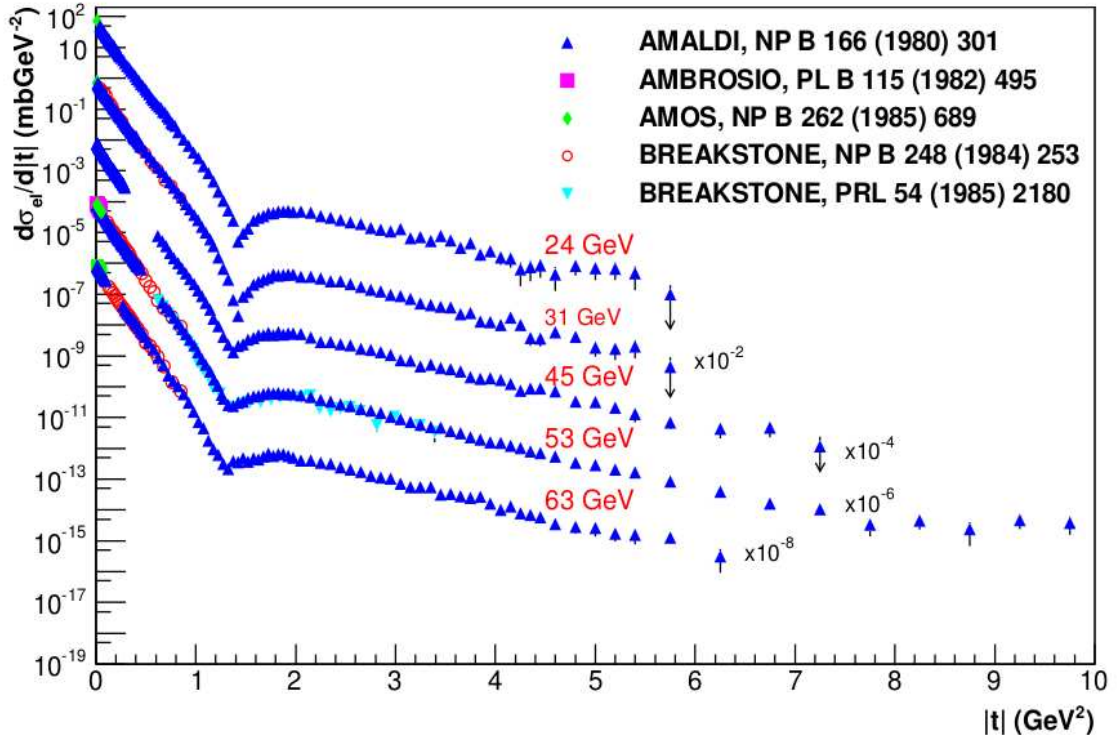
Figure 2.11: Experimental elastic differential cross-section data set at $\sqrt{s} = 24 - 63$ GeV, obtained by ISR experiment at CERN [53–57]. This figure was taken from Reference [58].
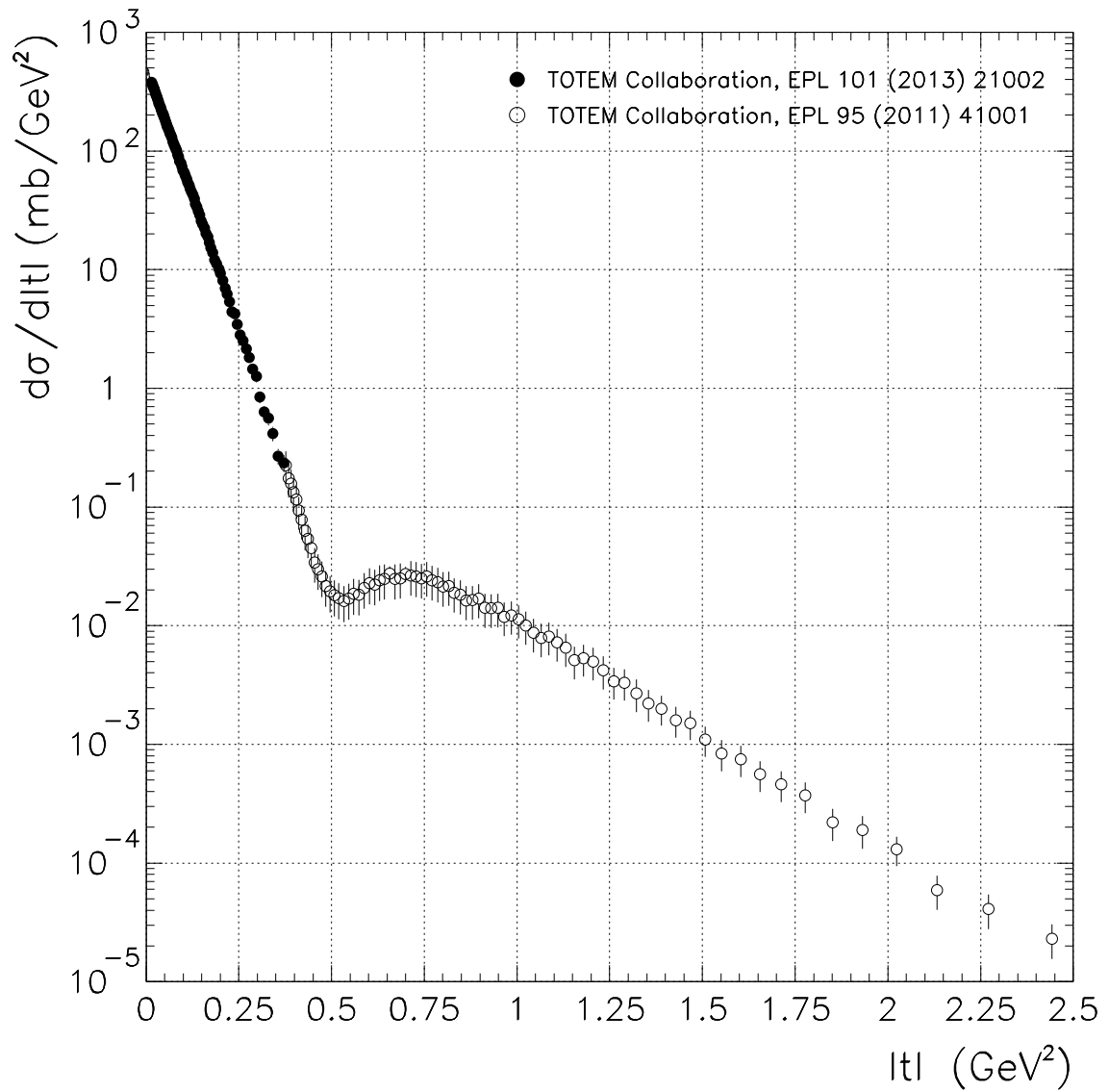
Figure 2.12: Experimental data set for *pp* elastic differential cross-section at $\sqrt{s} = 7$ TeV [18, 22] with statistical and systematic uncertainties combined into quadrature.
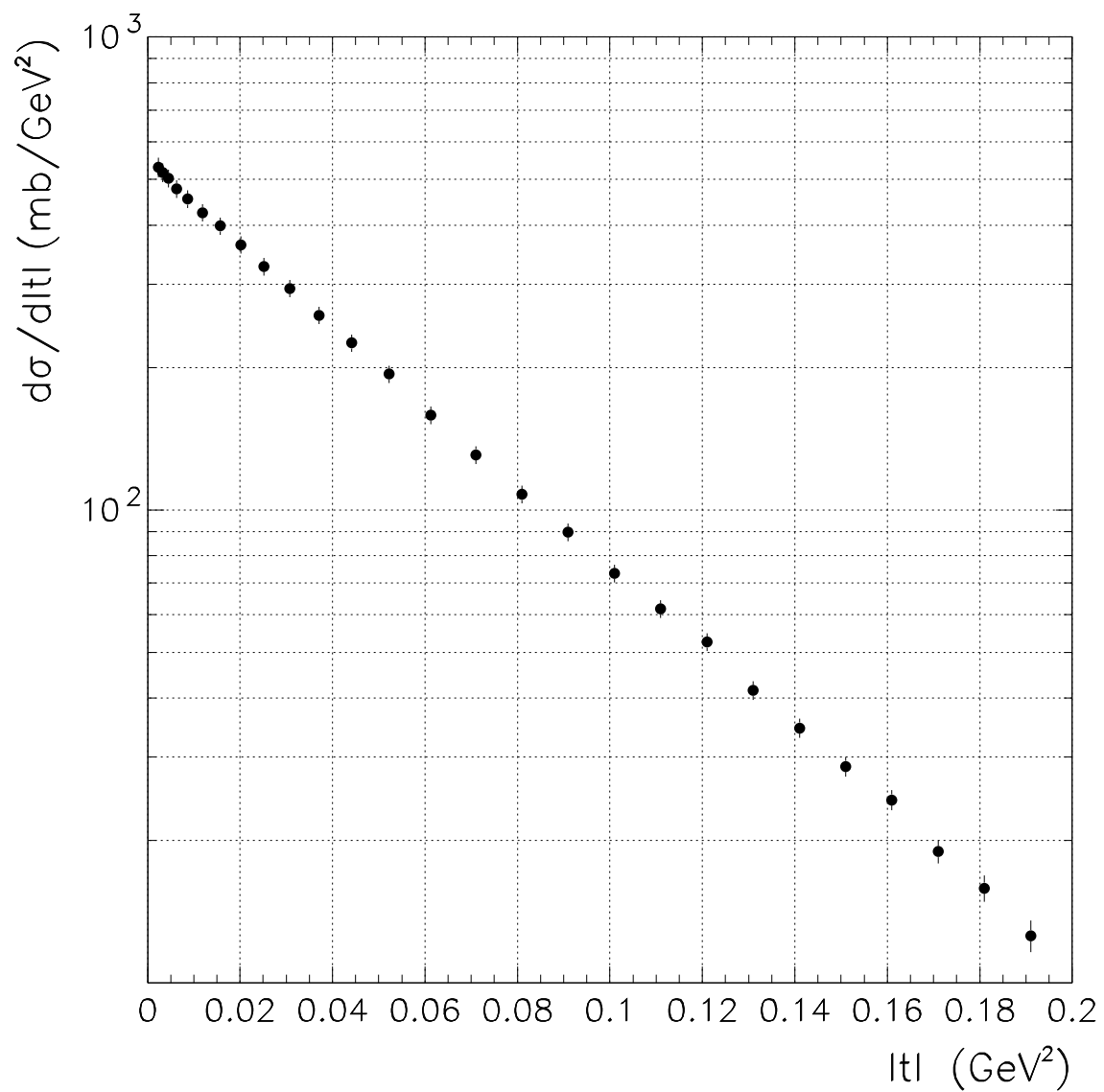
Figure 2.13: Experimental data set for pp elastic differential cross-section at $\sqrt{s} = 8$ TeV [21] with statistical and systematic uncertainties combined into quadrature.

$\sqrt{s}$ (GeV)	σ_{tot}^{pp} (mb)	$\sqrt{s}$ (GeV)	σ_{tot}^{pp} (mb)
10.25	38.43 ± 0.20	26.39	39.77 ± 0.17
10.70	38.44 ± 0.19	27.60	40.60 ± 1.20
11.12	38.65 ± 0.21	30.60	40.22 ± 0.21
11.46	36.68 ± 0.53	30.60	40.11 ± 0.19
11.54	38.28 ± 0.16	30.60	39.91 ± 0.41
11.78	37.60 ± 1.12	30.60	40.07 ± 0.24
13.63	37.60 ± 1.12	30.60	40.20 ± 0.80
13.76	38.70 ± 1.74	30.60	40.10 ± 0.40
13.76	38.46 ± 0.16	30.70	40.10 ± 0.20
13.77	38.39 ± 0.20	30.80	40.00 ± 0.60
13.90	38.90 ± 0.80	35.20	40.42 ± 0.62
15.06	38.59 ± 0.16	44.70	41.70 ± 0.40
15.19	37.60 ± 1.12	44.70	41.90 ± 0.24
16.66	37.60 ± 1.12	44.90	41.89 ± 0.40
16.66	38.47 ± 0.58	45.20	42.50 ± 0.80
16.83	38.69 ± 0.16	52.80	43.01 ± 0.26
16.83	38.62 ± 0.20	52.80	42.38 ± 0.17
17.91	38.83 ± 0.16	52.80	42.10 ± 0.20
18.01	37.40 ± 1.12	52.80	42.85 ± 0.42
18.17	39.60 ± 1.62	52.80	42.71 ± 0.35
19.22	38.50 ± 1.22	52.90	42.40 ± 0.40
19.42	38.98 ± 0.16	53.20	42.90 ± 0.70
19.42	38.90 ± 0.20	62.30	43.55 ± 0.32
19.66	39.00 ± 1.00	62.40	43.10 ± 0.40
21.26	39.24 ± 0.16	62.50	44.00 ± 0.45
22.96	39.42 ± 0.16	62.70	43.82 ± 0.32
23.50	39.65 ± 0.23	62.70	42.96 ± 0.38
23.50	39.40 ± 0.30	62.80	44.10 ± 0.90
23.50	39.13 ± 0.40	63.00	42.20 ± 3.50
23.50	38.80 ± 0.25	7000	98.58 ± 2.23
23.50	38.90 ± 0.70	7000	98.00 ± 2.50
23.60	38.70 ± 0.70	7000	99.10 ± 4.30
23.76	39.21 ± 0.92	7000	98.30 ± 2.80
23.76	40.68 ± 0.55	8000	101.70 ± 2.90
23.88	39.00 ± 1.00	8000	102.90 ± 2.30
24.16	39.59 ± 0.17	8000	103.00 ± 2.30
25.30	39.69 ± 0.17		

Table 2.2: The pp total cross-section data set obtained from colliders, totalising a number of #73 points.

$\sqrt{s}$ (GeV)	ρ^{pp}	$\sqrt{s}$ (GeV)	ρ^{pp}
10.29	-0.154 ± 0.036	20.12	-0.020 ± 0.019
10.64	-0.122 ± 0.034	20.81	-0.018 ± 0.028
11.52	-0.106 ± 0.034	21.42	-0.013 ± 0.018
11.54	-0.115 ± 0.015	21.70	-0.041 ± 0.014
11.54	-0.104 ± 0.065	22.17	-0.009 ± 0.013
12.32	-0.096 ± 0.013	22.50	0.022 ± 0.021
12.63	-0.122 ± 0.028	23.00	0.012 ± 0.028
12.63	-0.119 ± 0.029	23.20	0.010 ± 0.028
13.34	-0.098 ± 0.019	23.50	0.022 ± 0.014
13.76	-0.092 ± 0.014	23.50	0.020 ± 0.050
13.76	-0.074 ± 0.017	23.76	-0.028 ± 0.016
13.90	-0.103 ± 0.028	23.88	-0.011 ± 0.012
13.97	-0.099 ± 0.029	24.30	0.009 ± 0.012
13.97	-0.102 ± 0.028	25.61	0.025 ± 0.021
15.37	-0.024 ± 0.014	27.18	0.039 ± 0.019
16.52	-0.064 ± 0.018	27.36	0.012 ± 0.012
16.83	-0.040 ± 0.014	30.60	0.030 ± 0.060
16.83	0.008 ± 0.012	30.60	0.034 ± 0.008
17.54	-0.048 ± 0.029	30.60	0.042 ± 0.019
18.14	-0.039 ± 0.019	44.70	0.062 ± 0.018
18.17	-0.011 ± 0.018	52.80	0.077 ± 0.009
18.68	-0.038 ± 0.020	52.90	0.078 ± 0.018
19.37	-0.034 ± 0.013	62.40	0.095 ± 0.019
19.42	0.019 ± 0.017	7000	0.145 ± 0.091
19.85	-0.025 ± 0.028	8000	0.120 ± 0.030

Table 2.3: The corresponding data set of the ratio of the real to imaginary part of the forward scattering amplitude in pp interactions, totalising a number of #50 points.

$\sqrt{s}$ (GeV)	$\sigma_{tot}^{\bar{p}p}$ (mb)	$\sqrt{s}$ (GeV)	$\sigma_{tot}^{\bar{p}p}$ (mb)
11.54	43.05 ± 0.18	30.60	42.80 ± 0.35
13.76	40.40 ± 1.71	52.60	43.32 ± 0.34
13.76	42.12 ± 0.18	52.80	44.71 ± 0.46
13.76	42.04 ± 0.23	62.30	44.12 ± 0.40
13.87	42.33 ± 0.14	62.70	45.14 ± 0.37
15.07	41.70 ± 0.22	540	66.80 ± 6.48
16.83	41.79 ± 0.24	540	66.00 ± 7.74
16.83	41.72 ± 0.28	541	63.00 ± 2.10
17.91	41.69 ± 0.22	546	61.26 ± 0.93
18.17	41.20 ± 2.10	547	61.90 ± 1.62
19.42	41.51 ± 0.22	900	65.30 ± 1.66
19.42	41.54 ± 0.36	1800	71.71 ± 2.02
21.26	41.90 ± 0.26	1800	80.03 ± 2.24
22.96	41.91 ± 0.27	1800	72.80 ± 3.10
30.40	42.13 ± 0.58	1800	71.42 ± 2.41

Table 2.4: The $\bar{p}p$ total cross-section data set obtained from colliders, totalising a number of #30 points.

$\sqrt{s}$ (GeV)	$\rho^{\bar{p}p}$	$\sqrt{s}$ (GeV)	$\rho^{\bar{p}p}$
11.54	0.010 ± 0.018	24.30	0.048 ± 0.013
15.37	0.012 ± 0.020	30.40	0.055 ± 0.029
16.83	-0.001 ± 0.028	52.60	0.106 ± 0.016
18.17	0.067 ± 0.038	541	0.135 ± 0.015
19.42	0.029 ± 0.030	1800	0.140 ± 0.069
22.63	-0.014 ± 0.057	1800	0.132 ± 0.056

Table 2.5: The corresponding data set of the ratio of the real to imaginary part of the forward scattering amplitude in $\bar{p}p$ interactions, totalising a number of #12 points.

$|t|$ (GeV^2)	$d\sigma/d|t|$ (mb/GeV^2)	$|t|$ (GeV^2)	$d\sigma/d|t|$ (mb/GeV^2)
5.15×10^{-3}	465.00 ± 34.20	0.106	61.90 ± 2.72
6.50×10^{-3}	465.00 ± 23.71	0.109	58.11 ± 2.56
8.18×10^{-3}	437.50 ± 19.74	0.112	54.11 ± 2.39
9.95×10^{-3}	411.00 ± 18.01	0.116	51.21 ± 2.26
1.17×10^{-2}	402.30 ± 17.54	0.119	48.24 ± 2.13
1.35×10^{-2}	384.50 ± 16.70	0.122	44.99 ± 2.01
1.54×10^{-2}	378.00 ± 16.38	0.126	42.74 ± 1.94
1.72×10^{-2}	360.30 ± 15.57	0.130	39.49 ± 1.82
1.91×10^{-2}	348.10 ± 15.06	0.133	35.75 ± 1.69
2.10×10^{-2}	337.00 ± 14.55	0.137	33.63 ± 1.61
2.29×10^{-2}	325.00 ± 14.04	0.141	31.08 ± 1.53
2.48×10^{-2}	307.90 ± 13.24	0.145	28.91 ± 1.44
2.68×10^{-2}	296.70 ± 12.83	0.149	25.65 ± 1.31
2.87×10^{-2}	285.90 ± 12.33	0.153	24.16 ± 1.25
3.07×10^{-2}	275.30 ± 11.82	0.157	22.35 ± 1.18
3.28×10^{-2}	263.00 ± 11.31	0.162	20.22 ± 1.09
3.48×10^{-2}	252.00 ± 10.82	0.166	19.01 ± 1.05
3.69×10^{-2}	242.80 ± 10.41	0.171	16.92 ± 0.96
3.90×10^{-2}	231.60 ± 9.91	0.175	15.20 ± 0.88
4.11×10^{-2}	222.20 ± 9.50	0.180	13.90 ± 0.83
4.33×10^{-2}	210.90 ± 9.01	0.185	12.09 ± 0.74
4.55×10^{-2}	204.80 ± 8.80	0.190	11.26 ± 0.71
4.77×10^{-2}	197.20 ± 8.40	0.196	10.11 ± 0.65
4.99×10^{-2}	187.50 ± 8.01	0.201	9.31 ± 0.61
5.22×10^{-2}	178.10 ± 7.60	0.207	8.07 ± 0.55
5.45×10^{-2}	168.80 ± 7.20	0.213	6.98 ± 0.49
5.69×10^{-2}	162.50 ± 6.89	0.219	6.22 ± 0.45
5.92×10^{-2}	155.50 ± 6.60	0.225	5.38 ± 0.40
6.16×10^{-2}	149.40 ± 6.40	0.232	4.40 ± 0.34
6.41×10^{-2}	140.20 ± 5.98	0.239	4.25 ± 0.34
6.66×10^{-2}	135.10 ± 5.79	0.246	3.47 ± 0.29
6.91×10^{-2}	129.00 ± 5.53	0.253	2.82 ± 0.25
7.16×10^{-2}	120.53 ± 5.18	0.261	2.52 ± 0.22
7.42×10^{-2}	115.10 ± 4.96	0.270	2.14 ± 0.20
7.69×10^{-2}	109.63 ± 4.73	0.278	1.82 ± 0.18
7.95×10^{-2}	104.97 ± 4.54	0.287	1.45 ± 0.16
8.23×10^{-2}	100.22 ± 4.34	0.297	1.26 ± 0.13
8.50×10^{-2}	93.18 ± 4.04	0.307	$0.85 \pm 9.79 \times 10^{-2}$
8.78×10^{-2}	89.16 ± 3.88	0.318	$0.63 \pm 7.80 \times 10^{-2}$
9.07×10^{-2}	81.78 ± 3.57	0.330	$0.56 \pm 7.22 \times 10^{-2}$
9.36×10^{-2}	78.85 ± 3.45	0.342	$0.42 \pm 5.90 \times 10^{-2}$
9.66×10^{-2}	73.92 ± 3.24	0.356	$0.27 \pm 4.04 \times 10^{-2}$
9.96×10^{-2}	68.77 ± 3.02	0.371	$0.24 \pm 3.75 \times 10^{-2}$
0.103	65.53 ± 2.88		

Table 2.6: The elastic differential cross-section data set at $\sqrt{s} = 7$ TeV as given in [18], totalising a number of #87 points.

$\|t\|$ (GeV^2)	$d\sigma/d\|t\|$ (mb/GeV^2)	$\|t\|$ (GeV^2)	$d\sigma/d\|t\|$ (mb/GeV^2)
0.377	$0.225 \pm 6.88 \times 10^{-2}$	0.847	$(1.83 \pm 0.589) \times 10^{-2}$
0.384	$0.174 \pm 5.37 \times 10^{-2}$	0.863	$(1.63 \pm 0.519) \times 10^{-2}$
0.391	$0.157 \pm 4.87 \times 10^{-2}$	0.880	$(1.64 \pm 0.519) \times 10^{-2}$
0.398	$0.133 \pm 4.12 \times 10^{-2}$	0.897	$(1.69 \pm 0.538) \times 10^{-2}$
0.405	$0.116 \pm 3.61 \times 10^{-2}$	0.913	$(1.41 \pm 0.449) \times 10^{-2}$
0.412	$(9.30 \pm 2.87) \times 10^{-2}$	0.931	$(1.40 \pm 0.444) \times 10^{-2}$
0.420	$(7.80 \pm 2.46) \times 10^{-2}$	0.948	$(1.41 \pm 0.444) \times 10^{-2}$
0.430	$(6.30 \pm 2.01) \times 10^{-2}$	0.966	$(1.19 \pm 0.373) \times 10^{-2}$
0.436	$(5.40 \pm 1.71) \times 10^{-2}$	0.985	$(1.22 \pm 0.383) \times 10^{-2}$
0.445	$(4.50 \pm 1.45) \times 10^{-2}$	1.005	$(1.13 \pm 0.354) \times 10^{-2}$
0.454	$(3.40 \pm 1.10) \times 10^{-2}$	1.024	$(1.00 \pm 0.313) \times 10^{-2}$
0.464	$(3.00 \pm 1.01) \times 10^{-2}$	1.044	$(8.70 \pm 2.73) \times 10^{-3}$
0.474	$(2.60 \pm 8.56) \times 10^{-2}$	1.065	$(7.90 \pm 2.48) \times 10^{-3}$
0.485	$(2.16 \pm 7.21) \times 10^{-2}$	1.086	$(8.10 \pm 2.48) \times 10^{-3}$
0.496	$(1.95 \pm 6.56) \times 10^{-2}$	1.108	$(7.20 \pm 2.22) \times 10^{-3}$
0.508	$(1.80 \pm 6.05) \times 10^{-2}$	1.131	$(6.50 \pm 2.02) \times 10^{-3}$
0.520	$(1.71 \pm 5.76) \times 10^{-2}$	1.155	$(5.10 \pm 1.58) \times 10^{-3}$
0.533	$(1.61 \pm 5.41) \times 10^{-2}$	1.179	$(5.30 \pm 1.58) \times 10^{-3}$
0.547	$(1.69 \pm 5.66) \times 10^{-2}$	1.205	$(5.00 \pm 1.53) \times 10^{-3}$
0.560	$(1.85 \pm 6.22) \times 10^{-2}$	1.232	$(4.20 \pm 1.32) \times 10^{-3}$
0.574	$(1.83 \pm 6.12) \times 10^{-2}$	1.261	$(3.40 \pm 1.02) \times 10^{-3}$
0.588	$(2.08 \pm 6.91) \times 10^{-2}$	1.290	$(3.30 \pm 0.971) \times 10^{-3}$
0.602	$(2.28 \pm 7.62) \times 10^{-2}$	1.322	$(2.70 \pm 0.825) \times 10^{-3}$
0.616	$(2.22 \pm 7.37) \times 10^{-2}$	1.355	$(2.20 \pm 0.658) \times 10^{-3}$
0.629	$(2.42 \pm 8.10) \times 10^{-2}$	1.390	$(2.00 \pm 0.559) \times 10^{-3}$
0.643	$(2.47 \pm 8.16) \times 10^{-2}$	1.428	$(1.60 \pm 0.461) \times 10^{-3}$
0.657	$(2.74 \pm 4.10) \times 10^{-2}$	1.467	$(1.50 \pm 0.412) \times 10^{-3}$
0.671	$(2.48 \pm 8.16) \times 10^{-2}$	1.507	$(1.10 \pm 0.316) \times 10^{-3}$
0.685	$(2.51 \pm 8.26) \times 10^{-2}$	1.552	$(8.40 \pm 2.50) \times 10^{-4}$
0.700	$(2.73 \pm 4.03) \times 10^{-2}$	1.603	$(7.50 \pm 2.21) \times 10^{-4}$
0.714	$(2.65 \pm 8.66) \times 10^{-2}$	1.656	$(5.60 \pm 1.63) \times 10^{-4}$
0.728	$(2.59 \pm 8.46) \times 10^{-2}$	1.713	$(4.60 \pm 1.35) \times 10^{-4}$
0.742	$(2.50 \pm 8.15) \times 10^{-2}$	1.777	$(3.70 \pm 1.06) \times 10^{-4}$
0.757	$(2.60 \pm 8.40) \times 10^{-2}$	1.851	$(2.20 \pm 0.671) \times 10^{-4}$
0.771	$(2.41 \pm 7.80) \times 10^{-2}$	2.024	$(1.30 \pm 0.361) \times 10^{-4}$
0.801	$(2.13 \pm 6.85) \times 10^{-2}$	2.133	$(5.90 \pm 1.90) \times 10^{-5}$
0.816	$(2.16 \pm 6.95) \times 10^{-2}$	2.272	$(4.10 \pm 1.32) \times 10^{-5}$
0.831	$(1.89 \pm 6.04) \times 10^{-2}$	2.443	$(2.30 \pm 0.743) \times 10^{-5}$

Table 2.7: The elastic differential cross-section data set at $\sqrt{s} = 7$ TeV as given in [22], totalising a number of #78 points.

$|t|$ (GeV^2)	$d\sigma/d|t|$ (mb/GeV^2)	$|t|$ (GeV^2)	$d\sigma/d|t|$ (mb/GeV^2)
2.298×10^{-3}	529.76 ± 25.09	7.098×10^{-2}	130.78 ± 5.64
3.240×10^{-3}	516.92 ± 23.29	8.098×10^{-2}	107.80 ± 4.67
4.535×10^{-3}	502.29 ± 21.72	9.098×10^{-2}	89.71 ± 3.88
6.266×10^{-3}	477.43 ± 20.57	0.10	73.41 ± 3.23
8.628×10^{-3}	454.13 ± 19.49	0.11	61.78 ± 2.69
1.183×10^{-2}	424.90 ± 18.17	0.12	52.55 ± 2.27
1.576×10^{-2}	398.49 ± 16.73	0.13	41.52 ± 1.91
2.019×10^{-2}	363.33 ± 15.30	0.14	34.58 ± 1.62
2.517×10^{-2}	327.03 ± 13.87	0.15	28.69 ± 1.37
3.077×10^{-2}	293.88 ± 12.35	0.16	24.37 ± 1.20
3.709×10^{-2}	257.86 ± 10.93	0.17	18.95 ± 1.08
4.419×10^{-2}	225.35 ± 9.46	0.18	15.86 ± 1.01
5.220×10^{-2}	193.69 ± 8.09	0.19	12.59 ± 0.96
6.121×10^{-2}	158.48 ± 6.80		

Table 2.8: The elastic differential cross-section data set at $\sqrt{s} = 8$ TeV as given in [21], totalising a number of #27 points.

Chapter 3

Regge theory

Traditionally, Regge theory is the theoretical framework used to study diffraction, and it belongs to the class of t-channel models, where the description of strong interactions is performed by means of the exchange of something which in fact is not viewed as particles with a definite spin, but rather by a class of objects known as Regge trajectories [3,11–13]. In the particle physics terminology, Regge trajectories are often called Reggeons. Asymptotically, the Reggeon with the vacuum quantum numbers which dominates at increasing energy is the so-called Pomeron, thus in the Regge language diffractive reactions are those ones which are described by Pomeron exchange between particles 1 and 2 whereas no quantum numbers are exchanged in the reaction.

Through out the scientific community, many consider the Pomeron as a misleading, an ill-defined or even in some cases a meaningless concept. However, one cannot dispute the phenomenological success of Regge theory in describing a wide class of reactions in which no other framework was capable of. Once it was said by A. Donnachie and P.V. Landshoff [16] that although this less optimistic point of view "*Regge theory remains one of the great truths of particle Physics*", moreover because a large class of processes are very well described using just simple predictions. On the other hand, it is worth mentioning that when extended to high energies, it relies on a series of assumptions, such as, for instance, the introduction of a new quantum number called signature. Therefore, its merging with a fundamental theory as QCD would be definitely a huge step towards a full description and understanding of strong interactions. This remains as one of the open problems in the physics of $20th$ century, and with a little bit of luck and huge effort by the community perhaps it might be solved in the $21th$ one. In simple words it could be stated that: is Regge theory the limit of QCD at $q \to 0$?

3.1   Regge poles

Despite the fact that the main ideas of Regge theory have been used in the theoretical field of particle physics, more specifically in the study of hadronic phenomena, it was origi-

nally formulated in the context of non-relativistic Quantum Mechanics [6,7]. The basic idea of T. Regge was to study the bound states for an attractive spherically symmetric potential which appears as poles of the partial-wave amplitude $a_\ell(k)$ for integer values of ℓ, and then analytically to continue these values to complex ones, therefore obtaining an interpolating function $a(\ell, k)$, which reduces to $a_\ell(k)$ for $\ell = 0, 1, 2, ...$, respectively. In the case of well behaved potential, $i.e.$ $V(\mathbf{r}) \to 0$ at $r \to \infty$, Yukawa-type potentials, and in order to constrain the functional form of the scattering amplitude when analytically continued to complex ℓ values the general mathematical properties of the S-matrix, namely unitarity, analyticity, and crossing symmetry, are essentials to define the singularities of the resulting function $a(\ell, k)$. More specifically, they will be given by simple removable poles, which is known as Regge poles, and located at values defined by a relation such as

$$\ell = \alpha(k), \tag{3.1}$$

where $\alpha(k)$ is a function of the energy and called Regge trajectory. Each bound state or resonance corresponds to a single Regge trajectory as given by expression (3.1). By giving integer values to the angular momentum ℓ, $i.e.$ by attributing a physical value, then it can be properly obtained the energy of each state.

In the picture of relativistic scattering, and by means of the general properties of the S-matrix, it can be demonstrated that the relativistic scattering amplitude $A_\ell(t)$ can be analytically continued to complex ℓ values, thus obtaining an interpolation function $A(\ell, t)$, still having simple poles defined by

$$\ell = \alpha(t). \tag{3.2}$$

The contribution of each singularity to the scattering amplitude is given by

$$\lim_{s \to \infty} A(s, t) \sim s^{\alpha(t)}, \tag{3.3}$$

where the singularity with the largest real part, or the leading singularity in the t-channel, determines the asymptotic behaviour of the scattering amplitude in the s-channel.

3.2 Partial-wave expansion and the complex angular momenta

Although the idea of complex angular momenta is rather old and originally due to Poincaré, and latter used by Sommerfeld to study the propagation of electromagnetic waves, this technique is central in Regge theory. However, the continuation to complex angular momenta naturally emerges when studying the convergence domain of the scattering ampli-

tude, in a sense that it allows a correct analytic continuation to arbitrarily large energies, $s \to \infty$. To find out the convergence domain, the starting point is the partial-wave expansion of the scattering amplitude in the t-channel [3],

$$A(s,t) = \sum_{\ell=0}^{\infty} (2\ell + 1)\, A_\ell(t) P_\ell(z), \qquad (3.4)$$

where the partial-wave amplitude is given by

$$A_\ell(t) = \frac{1}{2} \int_{-1}^{+1} dz\, P_\ell(z)\, A(s(z,t),t), \qquad (3.5)$$

with

$$z \equiv \cos \vartheta_t = 1 + \frac{2s}{t - 4m^2}. \qquad (3.6)$$

Although expression (3.4) is a correct representation of scattering in the physical t-channel domain $t \geq 4m^2$ and $-1 \leq z \leq 1$, this partial-wave series cannot be readily used to represent the t-channel exchange crossing symmetric amplitude for high-energy s-channel scattering. This is due to the singularities of $A(s,t)$ defined by expression (3.4) appearing in the partial-wave amplitude $A_\ell(t)$ and the s dependence embodied in the Legendre polynomials, which are entire functions of z. More specifically, as $s \to \infty$, z becomes proportional to s and the series diverges. Thus, the partial-wave series does not converge in a domain of the complex s, t and u variables larger than the physical t-channel domain.

3.2.1   Convergence domain

The asymptotic behaviour of $P_\ell(z)$ for real ℓ is given by [3]

$$\lim_{\ell \to \infty} P_\ell(\cos \vartheta) = \mathcal{O}(e^{\ell |\mathrm{Im}\, \vartheta|}), \qquad (3.7)$$

thus the partial-wave series in expression (3.4) at $\ell \to \infty$ converges only if $A_\ell(t)\, e^{\ell |\mathrm{Im}\, \vartheta|} \leq 1$. By using these relation and also writing the partial-wave amplitude as

$$\lim_{\ell \to \infty} A_\ell(t) \sim e^{-\ell \eta(t)}, \qquad (3.8)$$

one finds that the corresponding convergence region of $A(s,t)$ in the complex plane is $|\mathrm{Im}\, \vartheta| \leq \eta(t)$, which represents a symmetric horizontal line in the imaginary ϑ-axis of width $\eta(t)$.

By rewriting $z = \cos \vartheta = x + i\, y$, and also $\vartheta = \mathrm{Re}\, \vartheta + i\, \mathrm{Im}\, \vartheta$, then,

$$z = \cos(\mathrm{Re}\, \vartheta) \cosh(\mathrm{Im}\vartheta) - i\, \sin(\mathrm{Re}\, \vartheta) \sinh(\mathrm{Im}\, \vartheta), \qquad (3.9)$$
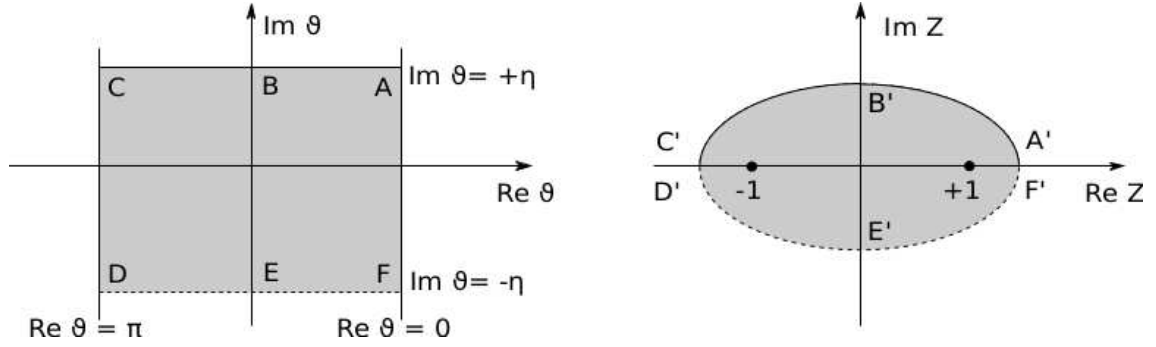
Figure 3.1: The convergence domain of the partial-wave scattering amplitude for $|\text{Im}\,\vartheta| \leq \eta(t)$.

a straightforward calculation shows that the convergence domain of the partial-wave expansion in expression (3.4) in the complex plane is given by an ellipse with foci $z = \pm 1$, see Figure 3.1,

$$\frac{x^2}{\chi^2} + \frac{y^2}{\chi^2 - 1} = 1, \tag{3.10}$$

where this quantity $\chi = \cosh \eta(t)$ was defined. This result implies that the partial-wave expansion converges in a domain slightly larger than the elementary physical domain $-1 \leq z \leq 1$, but never to arbitrarily large values of z. This means that expression (3.4) cannot be continued to regions where s and u becomes arbitrarily large.

In the opposite case, where the partial-wave series is obtained using purely imaginary values of ℓ, then the asymptotic behaviour of the Legendre polynomials would be given by [3]

$$\lim_{\ell \to i\infty} P_\ell(\cos \vartheta) = \mathcal{O}(e^{|\ell||\text{Re}\,\vartheta|}). \tag{3.11}$$

In this case, and provided that the partial-wave amplitude behaves as

$$\lim_{\ell \to i\infty} A_{|\ell|}(t) \sim e^{-|\ell|\delta(t)}, \tag{3.12}$$

the convergence condition for $A(s,t)$ in the complex plane would be ensured in a symmetric vertical line in the real ϑ-axis of width $\delta(t)$, *i.e* in $|\text{Re}\,\vartheta| \leq \delta(t)$. Following the same procedure as before, a straightforward calculation would show that the convergence domain is given by an hyperbola with foci $z = \pm 1$, where convergence is ensured outside its halves, see Figure 3.2,

$$\frac{x^2}{\xi^2} + \frac{y^2}{1 - \xi^2} = 1, \tag{3.13}$$

where it was defined $\xi = \cos \delta(t)$. The difference with respect to the previous case where the values of ℓ were purely real, is that here the hyperbola has an open domain and also it
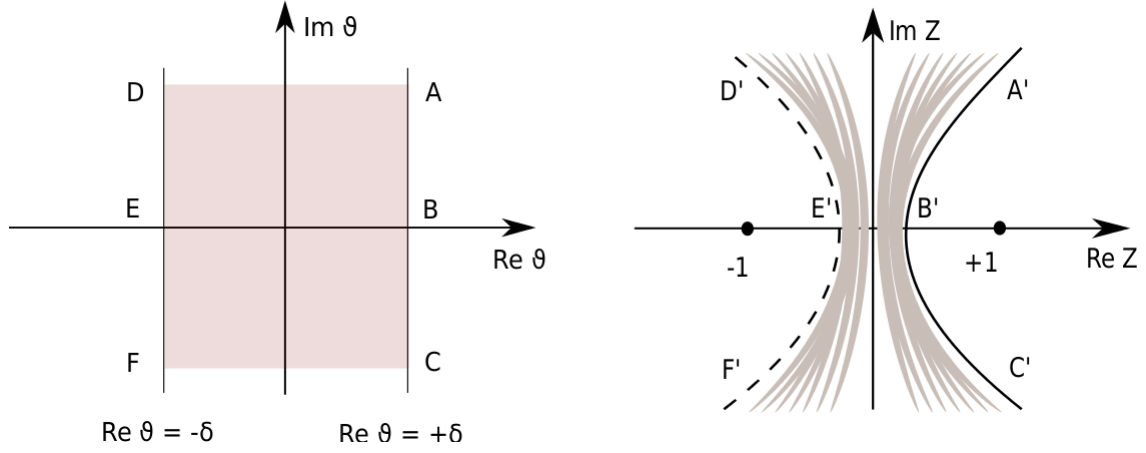
Figure 3.2: The convergence domain of the partial-wave scattering amplitude for $|\mathrm{Re}\,\vartheta| \leq \delta(t)$.

overlaps the ellipse which guarantees that the analytic continuation of the partial-wave series over complex values of ℓ. The new expansion will represent the same scattering function in a domain where s or u can become arbitrarily large.

3.2.2 Introduction of complex angular momenta

Henceforth, it is known the convergence region where an analytic continuation of the partial-wave series is valid in all channels. However, the introduction of complex angular momenta rely on a series of assumptions, such as assuming that it is possible to continue the partial-wave amplitude $A_\ell(t)$ to complex values of ℓ and construct an interpolating function $A(\ell, t)$ which reduces to $A_\ell(t)$ for real integer values of ℓ and has the following properties [3]:

   I. $A(\ell, t)$ has only simple singularities in the complex ℓ-plane.

  II. $A(\ell, t)$ is analytic for $\mathrm{Re}\,\ell \geq L$.

 III. $\lim\limits_{|\ell| \to \infty} A(\ell, t) = 0$ for $\mathrm{Re}\,\ell > 0$.

It is possible to show that if $A(\ell, t)$ exists and it satisfies properties II and III, then is uniquely determined by the values it takes for integer ℓ [59]. By using I and II the partial-wave expansion (3.4) can be rewritten as

$$A(s, t) = \sum_{\ell=0}^{N-1} (2\ell + 1) A_\ell(t) P_\ell(z) + \sum_{\ell=N}^{\infty} (2\ell + 1) A_\ell(t) P_\ell(z), \qquad (3.14)$$

where N is the first integer value of momenta greater than L, and the second sum in the *rhs* represents the contribution of the amplitude which carries the singularity in the real axis.

Using the relation for the Legendre polynomials $P_\ell(-z) = (-1)^\ell P_\ell(z)$, and also that [12],

$$\sum_\ell (2\ell+1)A_\ell(t)P_\ell(z) = \frac{i}{2}\int_C d\ell \, \frac{(-1)^\ell(2\ell+1)A(\ell,t)P_\ell(z)}{\sin\pi\ell}, \tag{3.15}$$

one finds that expression (3.14) is written in terms of an integral over a contour C which avoids all singularities of $A(\ell,t)$, see Figure 3.3,

$$A(s,t) = \sum_{\ell=0}^{N-1}(2\ell+1)A_\ell(t)P_\ell(z) + \frac{i}{2}\int_C d\ell \, (2\ell+1)A(\ell,t)\frac{P_\ell(-z)}{\sin\pi\ell}. \tag{3.16}$$

In order to involve all the singularities of $A(\ell,t)$ in the complex plane, the contour C is deformed into a line parallel to the imaginary ℓ-axis, namely $C' = (a-i\infty, a+i\infty)$. Thus, this new contour C' is located to the right of all singularities, see Figure 3.3. The property III and the asymptotic behaviour of the Legendre polynomials in the limit at $\ell \to \infty$, $|P_\ell(-z)/\sin\pi\ell| < \mathcal{O}(\ell^{-1/2})$, ensures that the semicircle integral which closes C' at infinity vanishes, and then [3],

$$A(s,t) = \sum_{\ell=0}^{N-1}(2\ell+1)A_\ell(t)P_\ell(z) + \frac{i}{2}\int_{a-i\infty}^{a+i\infty} d\ell \, (2\ell+1)A(\ell,t)\frac{P_\ell(-z)}{\sin\pi\ell}. \tag{3.17}$$

If the singularities of the partial-wave series are simple poles, and if the contour is moved towards to even smaller values, then the contributions from the residues of the poles together with the residues from the poles of $\sin^{-1}\pi\ell$ cancel some of the terms of the truncated series in the above expression. Thus, by displacing the contour C' to the left in the interval $-1/2 \le \mathrm{Re}\,\ell < 0$, then,
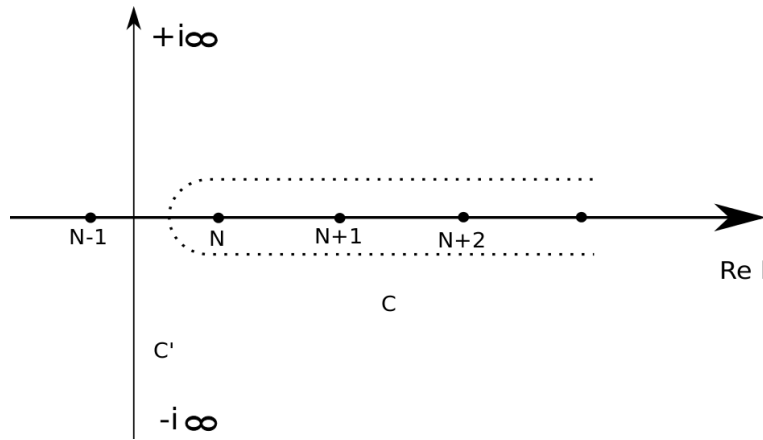
Figure 3.3: The integration contour for the Watson-Sommerfeld representation of the scattering amplitude.

$$
\begin{aligned}
A(s,t) &= \sum_{\ell=N}^{\infty}(2\ell+1)A_\ell(t)P_\ell(z) + \frac{i}{2}\int_{a-i\infty}^{a+i\infty} d\ell\,(2\ell+1)A(\ell,t)\frac{P_\ell(-z)}{\sin\pi\ell} \\
&= \frac{i}{2}\int_C d\ell\,(2\ell+1)A(\ell,t)\frac{P_\ell(-z)}{\sin\pi\ell} + \frac{i}{2}\int_{a-i\infty}^{a+i\infty} d\ell\,(2\ell+1)A(\ell,t)\frac{P_\ell(-z)}{\sin\pi\ell}. \quad (3.18)
\end{aligned}
$$

By means of the residue theorem, where it states that the line integral of a function is related to the sum of the residues of the function at the poles,

$$
\int_C d\ell\, f(\ell) = 2\pi i \sum_i \operatorname{Res} f(\ell)|_{\ell\to\alpha_i}, \qquad (3.19)
$$

where α_i stands for the i-th pole of $A(\ell,t)$. The residue can be calculated by means of the following relation [60],

$$
\operatorname{Res} f(\ell)|_{\ell\to\alpha_i} = \frac{1}{(k-1)!}\lim_{\ell\to\alpha_i}\frac{d^{k-1}}{d\ell^{k-1}}\left[(\ell-\alpha_i)^k f(\ell)\right], \qquad (3.20)
$$

where for a simple pole α_i, $i.e$ $k=1$, the residue of the first integral in the rhs of expression (3.18) is given by

$$
\operatorname{Res} f(\ell)|_{\ell\to\alpha_i} = \gamma_i(t)\frac{(2\alpha_i+1)P_{\alpha_i}(-z)}{\sin\pi\alpha_i}, \qquad (3.21)
$$

and the residue function at that pole is defined by

$$
\gamma_i(t) = \lim_{\ell\to\alpha_i}(\ell-\alpha_i)A(\ell,t). \qquad (3.22)
$$

Therefore, substituting the last result (3.21) into expression (3.18) one finds [3, 11],

$$
A(s,t) = -\pi\sum_i \gamma_i(t)\frac{(2\alpha_i(t)+1)P_{\alpha_i}(-z)}{\sin\pi\alpha_i(t)} + \frac{i}{2}\int_{a-i\infty}^{a+i\infty} d\ell\,(2\ell+1)A(\ell,t)\frac{P_\ell(-z)}{\sin\pi\ell}, \qquad (3.23)
$$

which is known as the Watson-Sommerfeld transformation of the scattering amplitude $A(s,t)$, where α_i represents the location in the complex ℓ-plane of the i-th pole of $A(\ell,t)$, called Regge pole. As previously shown in the case of purely imaginary angular momenta, the convergence domain of expression (3.23) is valid outside the halves of the hyperbola in the z-plane, see expression (3.13).

The large-s behaviour of the Watson-Sommerfeld transformed amplitude for fixed t, which is exactly the same as large-z, is given by [61]

$$
\lim_{|z|\to\infty} P_\ell(z)\sim z^\ell, \quad \operatorname{Re}\ell\geq -\frac{1}{2}. \qquad (3.24)
$$

Therefore, in the large $|z|$-limit the integral in the rhs of expression (3.23) behaves asymp-

totically as $|z|^{-1/2}$ and gives a negligible contribution to the scattering amplitude $A(s,t)$, where only the pole contribution survives,

$$\lim_{|z|\to\infty} A(s,t) \simeq -\pi \sum_i \gamma_i(t)(2\alpha_i(t)+1)\frac{(-z)^{\alpha_i(t)}}{\sin \pi\alpha_i(t)}. \tag{3.25}$$

The dominant term will be the one with the largest $\mathrm{Re}\,\alpha_i$. Thus, in the case of a t-channel exchange, and by taking into account only the right-most Regge trajectory $\alpha(t)$, the asymptotic behaviour of the scattering amplitude for fixed t will be written as [3]

$$A(s,t) \underset{s\to\infty}{\simeq} -\gamma(t)\frac{s^{\alpha(t)}}{\sin \pi\alpha(t)}, \tag{3.26}$$

where some constants and t-dependent factors were absorbed into $\gamma(t)$. Since the convergence domain relies outside of the halves of the hyperbola, then the asymptotic amplitude in the crossed s-channel exchange for asymptotic large-t behaviour can be properly obtained by changing $t \leftrightarrow s$, *i.e.* by invoking the property of crossing symmetry of the scattering S-matrix,

$$A(s,t) \underset{t\to\infty}{\simeq} -\gamma(s)\frac{t^{\alpha(s)}}{\sin \pi\alpha(s)}. \tag{3.27}$$

Hence, expression (3.26) represents the prediction of the Regge theory for the large-s behaviour of the scattering amplitude, and also that the leading singularity governs the asymptotic behaviour of $A(s,t)$ as $s \to \infty$.

3.3   Regge poles in relativistic scattering

If the scattering amplitude admits the existence of N-times subtracted dispersion relation, the partial-wave scattering amplitude can be written as an integral representation for $A(s,t)$ valid for $\ell \geq N$, known as the Froissart-Gribov projection [8, 40],

$$A_\ell(t) = \frac{1}{\pi}\int_{z_0}^{+\infty} dz_t\, D_s(s(z_t,t),t)\, Q_\ell(z_t) + \frac{1}{\pi}\int_{-z_0}^{-\infty} dz_t\, D_u(u(z_t,t),t)\, Q_\ell(z_t), \tag{3.28}$$

where z_t is the scattering angle in the t-channel,

$$z_t \equiv \cos\vartheta_t = 1 + \frac{2s}{t - 4m^2}, \tag{3.29}$$

$Q_\ell(z_t')$ stands for the Legendre function of the second kind,

$$Q_\ell(z_t') = \frac{1}{2}\int_{-1}^{1} dz_t\, P_\ell(z_t)\frac{z_t^N}{z_t'^N(z_t'^N - z_t)}, \tag{3.30}$$

and finally, $D_s(s,t)$ and $D_u(u,t)$ are the discontinuity functions in the s and u channels. Respectively, they are given by [3]

$$D_s(s,t) = \frac{1}{2i} \lim_{\epsilon \to 0^+} \left[A(s+i\epsilon, t) - A(s - i\epsilon, t) \right], \tag{3.31}$$

$$D_u(u,t) = \frac{1}{2i} \lim_{\epsilon \to 0^+} \left[A(4m^2 - u - t - i\epsilon, t) - A(4m^2 - u - t + i\epsilon, t) \right], \tag{3.32}$$

and it coincides with the imaginary part of the scattering amplitude, $D_s(s,t) = \mathrm{Im}\, A(s,t)$. By rewriting the second integral in expression (3.28) with the change of variables $z_t \to -z_t$, and using $u(-z_t, t) = s(-z_t, t)$, one finds that

$$Q_\ell(-z_t) = -e^{-i\pi\ell} Q_\ell(z_t), \tag{3.33}$$

and the partial-wave scattering amplitude can be written as [3]

$$A_\ell(t) = \frac{1}{\pi} \int_{z_0}^{+\infty} dz_t \left[D_s(s(z_t, t), t) + e^{-i\pi\ell} D_u(u(z_t, t), t) \right] Q_\ell(z_t), \tag{3.34}$$

where $e^{-i\pi\ell} = (-1)^\ell$ for integer values of ℓ. The first term in the *rhs* of the above expression vanishes exponentially, because of the asymptotic behaviour of $Q_\ell(z)$ at $\ell \to \infty$ [61],

$$\lim_{\ell \to \infty} Q_\ell(z_t) \sim \ell^{-1/2} \exp\left\{ - \left(\ell + \frac{1}{2} \right) \ln \left[z_t + (z_t^2 - 1)^{1/2} \right] \right\}. \tag{3.35}$$

The amplitude cannot be continued to complex values of ℓ, because the second term in expression (3.34) diverges when $\mathrm{Im}\,\ell$ becomes asymptotically large at $\ell \to \infty$,

$$\lim_{\ell \to \infty} A_\ell(t) = \lim_{\ell \to \infty} \frac{1}{\pi} \int_{z_0}^{+\infty} dz_t \, e^{-i\pi(\mathrm{Re}\,\ell + i\mathrm{Im}\,\ell)} D_u(u(z_t, t), t) \, Q_\ell(z_t). \tag{3.36}$$

The way to overcome this problem can be properly done by introducing a new quantum number, the signature $\xi = \pm 1$ [3, 11, 12], in such a form that the amplitude is written by means of crossing-even and crossing-odd terms,

$$A_\ell^\xi(t) = \frac{1}{\pi} \int_{z_0}^{\infty} dz_t \, D_s^\xi(s, t) \, Q_\ell(z_t), \tag{3.37}$$

where the signature discontinuity function $D_s^\xi(s,t)$ is defined as

$$D_s^\xi(s, t) = D_s(s, t) + \xi D_u(s, t). \tag{3.38}$$

Thus, expression (3.37) coincides with expression (3.34) for even and odd integer ℓ-values,

$$A_\ell^+(t) = A_\ell(t), \quad \text{for} \quad \ell \text{ even}, \tag{3.39}$$

$$A_\ell^-(t) = A_\ell(t), \quad \text{for} \quad \ell \text{ odd}, \tag{3.40}$$

where it is usually said that the even-amplitude has positive signature, $\xi = +1$, whereas the odd-amplitude has negative signature, $\xi = -1$. By means of expressions (3.37) and (3.38), and notice that $D_s + \xi D_u = D_s + (-1)^\ell D_u$, then,

$$
\begin{aligned}
\sum_{\xi=\pm 1} \left(1 + \xi e^{-i\pi\ell}\right) A_\ell^\xi(t) &= \frac{1}{\pi} \int_{z_0}^\infty dz_t \sum_{\xi=\pm 1} \left(1 + \xi e^{-i\pi\ell}\right) \left[D_s(s,t) + (-1)^\ell D_u(s,t)\right] Q_\ell(z_t) \\
&= \frac{2}{\pi} \int_{z_0}^\infty dz_t \left[D_s(s,t) + (-1)^\ell D_u(s,t)\right] Q_\ell(z_t), \tag{3.41}
\end{aligned}
$$

where the last line is simply the partial-wave amplitude as given by expression (3.34). Therefore, we obtain

$$A_\ell(t) = \frac{1}{2} \sum_{\xi=\pm 1} \left(1 + \xi e^{-i\pi\ell}\right) A_\ell^\xi(t). \tag{3.42}$$

It can be defined a function called definite-signature scattering amplitude which is written by the partial-wave expansion,

$$A^\xi(t) = \sum_{\ell=0}^\infty (2\ell+1) A_\ell^\xi(t) P_\ell(z_t), \tag{3.43}$$

where it is a well-behaved function at $\ell \to \infty$, and hence can be analytically continued to the complex ℓ-plane by means of the Watson-Sommerfeld transform,

$$A^\xi(z_t, t) = \frac{i}{2} \int_C d\ell \, (2\ell+1) A^\xi(\ell, t) \frac{P_\ell(-z_t)}{\sin \pi\ell}, \tag{3.44}$$

and following the same procedure as before [3],

$$A^\xi(z_t, t) = \frac{i}{2} \int_C d\ell \, (2\ell+1) A^\xi(\ell, t) \frac{P_\ell(-z_t)}{\sin \pi\ell} + \frac{i}{2} \int_{c-i\infty}^{c+i\infty} d\ell \, (2\ell+1) A^\xi(\ell, t) \frac{P_\ell(-z_t)}{\sin \pi\ell}, \tag{3.45}$$

where the first integral is calculated by means of the theorem of residues at $\ell \to \alpha_{i_\xi}$, and α_{i_ξ} defines the location of the i-th pole of the definite-signature amplitude $A^\xi(z_t, t)$,

$$A^\xi(z_t, t) = -\pi \sum_{i_\xi} \gamma_{i_\xi}(t) \left(2\alpha_{i_\xi}(t) + 1\right) \frac{P_{\alpha_{i_\xi}}(-z_t)}{\sin \pi\alpha_{i_\xi}} + \frac{i}{2} \int_{c-i\infty}^{c+i\infty} d\ell \, (2\ell+1) A(\ell, t) \frac{P_\ell(-z_t)}{\sin \pi\ell}. \tag{3.46}$$

with the summation taken over definite-signature Regge poles. It is easy to show that the full amplitude can be obtained by applying $(2\ell + 1)P_\ell(z_t)$ in expression (3.42),

$$A(z_t, t) = \sum_{\ell=0}^{\infty}(2\ell+1)A_\ell(t)P_\ell(z_t) = \frac{1}{2}\sum_{\xi=\pm1}\sum_{\ell=0}^{\infty}\left(1+\xi e^{-i\pi\ell}\right)(2\ell+1)A_\ell(t)P_\ell(z_t), \quad (3.47)$$

and now, the full amplitude is given by

$$A(z_t, t) = -\pi\sum_{\xi=\pm1}\sum_{i_\xi}\frac{1+\xi e^{-i\pi\ell}}{2}\gamma_{i_\xi}(t)\left(2\alpha_{i_\xi}(t)+1\right)\frac{P_{\alpha_{i_\xi}}(-z_t)}{\sin\pi\alpha_{i_\xi}(t)} +$$
$$+ \frac{i}{2}\sum_{\xi=\pm1}\int_{c-i\infty}^{c+i\infty}d\ell\,\frac{1+\xi e^{-i\pi\ell}}{2}(2\ell+1)A(\ell,t)\frac{P_\ell(-z_t)}{\sin\pi\ell}d\ell. \quad (3.48)$$

There are two asymptotic limits to analyse in the above expression. The first one is the behaviour of the full amplitude at large-$|z_t|$, which is given by the Legendre polynomials,

$$\lim_{z_t\to\infty}A(z_t,t)\simeq -\sum_{\xi=\pm1}\sum_{i_\xi}\gamma_{i_\xi}(t)\frac{1+\xi e^{-i\pi\alpha_{i_\xi}(t)}}{\sin\pi\alpha_{i_\xi}(t)}(-z_t)^{\alpha_{i_\xi}(t)}$$
$$+ \frac{i}{2}\sum_{\xi=\pm1}\int_{c-i\infty}^{c+i\infty}d\ell\,\frac{1+\xi e^{-i\pi\ell}}{2}(2\ell+1)A(\ell,t)\frac{(-z_t)^\ell}{\sin\pi\ell}, \quad (3.49)$$

where some factors have been absorbed into the residue function $\gamma_{i_\xi}(t)$. The argument of the integral in the above expression vanishes exponentially in the limit at $\ell\to\infty$, therefore the pole series gives the dominant contribution,

$$A(z_t,t)\underset{z_t\to\infty}{\simeq}\sum_{\xi=\pm1}\sum_{i_\xi}\gamma_{i_\xi}(t)\frac{1+\xi e^{-i\pi\alpha_{i_\xi}(t)}}{\sin\pi\alpha_{i_\xi}(t)}(-z_t)^{\alpha_{i_\xi}(t)}, \quad (3.50)$$

by keeping only the leading pole, respectively it is the pole with the largest $\mathrm{Re}\,\alpha_{i_\xi}$, and defining $\alpha(t)$ as its trajectory and $\gamma(t)$ the residue. Thus, in the case of a t-channel exchange the asymptotic scattering amplitude at large-s will be given by [3]

$$A(s,t)\underset{s\to\infty}{\simeq}-\gamma_i(t)\frac{1+\xi e^{-i\pi\alpha(t)}}{\sin\pi\alpha(t)}s^{\alpha(t)}. \quad (3.51)$$

As before, the amplitude in the crossed s-channel for asymptotic large-t can be obtained by the exchange of $t\leftrightarrow s$,

$$A(s,t)\underset{t\to\infty}{\simeq}-\gamma_i(s)\frac{1+\xi e^{-i\pi\alpha(s)}}{\sin\pi\alpha(s)}t^{\alpha(s)}. \quad (3.52)$$

These expressions express a fundamental result of Regge theory which states that the leading complex angular momentum singularity of the partial-wave amplitude in a given

channel, that is precisely the Regge pole, determines the asymptotic behaviour of the scattering amplitude in the crossed channels.

3.4   Regge trajectories

The partial-wave amplitude, which asymptotically is given by $A(\ell, t) \propto s^\alpha$ for $s \to \infty$, in the presence of a Regge pole at $\ell \to \alpha(t)$ behaves as [3, 13]

$$A(\ell, t) \underset{\ell \to \alpha(t)}{\sim} \frac{\gamma(t)}{\ell - \alpha(t)}, \tag{3.53}$$

where for real and positive values of t the Regge poles represent resonances or bound states of increasing angular momentum, spin. Thus, the Regge trajectory $\alpha(t)$, or Reggeons as it is usually called in the particle physics language, interpolates such bound states. In relativistic scattering theory the Reggeons are associated with the exchange of families of particles. Values of t such that $\alpha(t)$ in a non-negative integer correspond to the squared mass of a bound state or resonance with that spin.

The denominator in the scattering amplitude in expression (3.51) vanishes whenever $\alpha(t)$ crosses an integer. But, as a consequence, to avoid that the same thing happens to the numerator at every other integer value of ℓ, it is imposed that a trajectory with positive signature, $\xi = +1$, interpolates between resonances with non-negative even integer angular momentum, whereas trajectories with negative signatures, $\xi = -1$, interpolates positive odd integer angular momentum resonances. Summarising, one needs to identify the poles with the exchange of physical particles of spin $J_i^\pm$, where it represents positive integer values, and mass m_i, where $\alpha(m_i^2) = J_i$. Therefore, the s-channel asymptotic behaviour of the amplitude is determined by the exchange of a whole family of resonances in the crossed t-channel.

A simple way to visualise the Regge trajectories, is to expand $\alpha(t)$ in power series around $t = 0$, thus for small values of t,

$$\alpha(t) = \alpha(0) + \alpha' t \tag{3.54}$$

where $\alpha(0)$ and α' are known as the intercept and the slope of the trajectory, respectively. Although the above linear expansion for the Regge trajectory was supposed to be justified only for low-t, it can be seen, by means of Chew & Frautschi [62,63] plots of the spins of low lying mesons against square mass, that by interpolating resonances with the same quantum numbers one finds that they lie in a straight line, and hence expression (3.54) holds for rather larger values of t. As a matter of fact, this linearity continues for negative values of t. More specifically, at $t = -0.64$ GeV^2 the trajectory passes through zero, this is an example of a nonsense pole since there cannot be a resonance with negative square mass. Therefore,

this non-physical pole must decouples from the amplitude.

By means of the optical theorem, and considering the simplest version of t-channel models where nuclear forces are usually attributed to the exchange of mesons, the total cross-section would be given by $\sigma_{tot} \sim s^{2J-2}$ at large-s. The exchange of a spin-1 meson, such as ρ would require the cross-section to increase linearly with s and the exchange of a spin-2 meson like the f_2 would therefore require the cross-section to increase quadratically with s. It is clear that this simplest model leads to violation of the Froissart-Martin-Łukaszuk bound, *i.e.* violation of unitarity. In the Regge language, the cross-section is given asymptotically by $\sigma_{tot} \sim s^{\alpha(0)-1}$. All the leading mesonic trajectories have $\alpha(0) \simeq 0.45$ and $\alpha' \simeq 0.93$ GeV^{-2}, following the Donnachie-Landshoff model where all the leading mesonic trajectories are degenerate and lie on a exchange-degenerate linear trajectory [16]. By considering only the leading mesonic exchange, it leads to total cross-sections decreasing with energy and experimentally none of this is observed. Total cross-section do not vanish asymptotically, but rather rise slowly as s increases. An indication that something else must contribute to the observed rise of hadronic total cross-section. Moreover, by retaining the picture of particle exchange then all the resonance contributions in the t-channel must act collectively and combine in a way, or another, to give the observed energy dependence. This is Regge theory, the mathematical framework for adding resonances together.

However, in the 60's Foldy & Peierls [15] noticed that if for a particular scattering the cross-section does not fall with increasing energy then that process must be dominated by the exchange of vacuum quantum numbers. Thus, by attributing this rise to the exchange of a single Regge pole it follows that the exchange corresponds to a Reggeon whose intercept is greater than 1 and carries the quantum numbers of the vacuum. This trajectory is called the Pomeron. The physical particles which would provide the resonances for integer values of the Pomeron trajectory for positive t have not been yet identified. Particles with the quantum numbers of the vacuum are difficult to detect, but such particles can exist in QCD as bound states of gluons, also known as glueballs.

Chapter 4

Regge-Gribov based model

It is well known that good descriptions of forward data up to the Tevatron energy have been obtained by using a linear Pomeron trajectory [16,51,64–69], namely $\alpha_{\mathbb{P}}(t) = 1+\epsilon+\alpha'_{\mathbb{P}}t$. The energy dependence of the total and diffractive cross-sections is driven by ϵ while $\alpha'_{\mathbb{P}}$ determines the energy dependence of the forward slopes. However, for example, ZEUS and H1 low-t data for exclusive ρ and ϕ photoproduction call forth a rather non-linear Pomeron trajectory [70–72]. Most recently, the TOTEM experiment at the CERN LHC has released new data on total cross-sections and diffractive processes that have enhanced the interest in high-energy hadron physics and become a pivotal source of information for selecting theoretical methods and models.

Currently, these measurements provide a unique constraint on the Pomeron parameters and allow us to study its behaviour more thoroughly since the contribution of the Pomeron component to the χ^2 is absolutely dominant in the LHC regime. Hence, the TOTEM data allow us to address more effectively the question of linearity versus non-linearity of the Pomeron trajectory. Moreover, the small value of $\alpha'_{\mathbb{P}}$ usually obtained from screened Regge models indicates that the soft Pomeron may be treated perturbatively since in the Gribov Reggeon calculus the mean transverse momentum of the partons is given by $\langle p_T \rangle = 1/\sqrt{\alpha'_{\mathbb{P}}}$ [8–10,73]. This perturbative approach sets up the stage for building a fundamental theory for soft processes based upon QCD. The screening effects can be calculated in terms of a two-channel eikonal model and again the TOTEM data are instrumental in determining the effects of the eikonalisation on the Pomeron parameters in both the one- and two-channel models.

Given the central role that the soft Pomeron plays in strong processes, its close scrutiny continues to be a core task in hadron physics. The first part of this Thesis is then devoted to a detailed study of the soft Pomeron at the light of these recent LHC data. More precisely, it will be evaluated the relative plausibilities of different combinations of vertices and trajectories of the soft Pomeron.

4.1 Phenomenology

Diffraction processes account for a substantial fraction of hadron-hadron total cross-section at high energies. These processes, which include elastic scattering or single- or double-diffractive dissociation, are characterised by the presence of one or more large rapidity gaps, which in turn are associated with the exchange of a colourless state having the quantum numbers of the vacuum, namely the Pomeron ($\mathbb{P}$). In the soft regime, *i.e.* low-t domain, diffractive processes are described by Regge theory [3, 11–14], in which the high-energy behaviour of the scattering amplitude is described by singularities of the amplitude in the complex plane of angular momentum. In the simplest scenario the diffractive processes are driven by an isolated pole at $J = \alpha(t)$, resulting in an elastic amplitude $A(s,t)$ written in terms of the Regge pole trajectory $\alpha(t)$, where $A(s,t) \propto s^{\alpha(t)}$. However, if more than one pole contributes, the elastic scattering amplitude is expressed in the s-channel as a descending asymptotic series of powers of s,

$$A(s,t) = \sum_i \gamma_i(t)\eta_i(t)s^{\alpha_i(t)}, \tag{4.1}$$

where $\gamma_i(t)$ is the residue function and $\eta_i(t)$ is the signature factor, respectively. The signature factor, which completely defines the phase of the scattering amplitude, because the Regge trajectories and the residue functions are expected to be real below the threshold, is given by [3, 11–14]

$$\eta_i(t) = -\frac{1 + \xi e^{-i\pi\alpha_i(t)}}{\sin(\pi\alpha_i(t))}. \tag{4.2}$$

Straightforward calculation shows that the signature factor for even- and odd-trajectory can be written respectively as, see Appendix B.1

$$
\begin{aligned}
\eta(t) &= -\frac{e^{-i\pi\alpha_i(t)/2}}{\sin\left(\frac{\pi}{2}\alpha_i(t)\right)}, \quad \text{for} \quad \xi = +1, \\
\eta(t) &= -i\,\frac{e^{-i\pi\alpha_i(t)/2}}{\cos\left(\frac{\pi}{2}\alpha_i(t)\right)}, \quad \text{for} \quad \xi = -1.
\end{aligned}
\tag{4.3}
$$

The ratio of the real to imaginary part of $A(s,t)$, by considering a single Regge pole exchange, is written as

$$\frac{\text{Re}\,A(s,t)}{\text{Im}\,A(s,t)} = -\frac{1 + \xi\cos\pi\alpha(t)}{\sin\pi\alpha(t)}, \tag{4.4}$$

in the forward direction, $t = 0$, this expression defines the ρ-parameter. In Regge theory it is determined by the intercept of the exchanged trajectory.

4.1.1 The Pomeron

As it was already mentioned in the concluding remarks of the last section in Chapter 3, Regge theory predicts that the cross-section decreases with increasing energy for Reggeons with intercepts lower than 1. There was a time where the total cross-section seemed to become constant with increasing energy when the highest CM energy data came from Serpukhov. This is the basis of the Pomeranchuk theorem which states that the cross-section for ab and $a\bar{b}$ should become asymptotically equal. In 1961, in order to account for the asymptotically constant total cross-section, Chew, Frautschi and Gribov introduced a Regge trajectory with intercept 1. This Reggeon was named Pomeron, after its inventor I. Ya. Pomeranchuk, who idealised its concept in 1958.

The Pomeron trajectory does not correspond to any known particle, and from fitting elastic scattering data, it was found that its trajectory is much flatter than the one from other Reggeons, $\alpha'_{\mathbb{P}} \simeq 0.25 \text{ GeV}^{-2}$. As consequence of the constancy required of the total cross-section, it implies that $\alpha_{\mathbb{P}}(0) \simeq 1$. Pomeron exchange dominates in elastic and diffractive processes, which are known to proceed via exchange of vacuum quantum numbers in the t-channel. There are no changes in the quantum numbers of the interacting particles and the Pomeron is defined by

$$\mathbb{P}: \quad P = +1, \; C = +1, \; G = +1, \; I = 0, \; \xi = +1, \tag{4.5}$$

whereas for the other leading Reggeon trajectories, they are defined by the following quantum numbers,

$$
\begin{aligned}
f_2 \quad &: \quad P = +1, \; C = +1, \; G = +1, \; I = 0, \; \xi = +1, \\
\rho \quad &: \quad P = -1, \; C = -1, \; G = +1, \; I = 1, \; \xi = -1, \\
\omega \quad &: \quad P = -1, \; C = -1, \; G = -1, \; I = 0, \; \xi = -1, \\
a_2 \quad &: \quad P = +1, \; C = +1, \; G = -1, \; I = 1, \; \xi = +1,
\end{aligned}
$$

Since the Pomeron has a positive-signature trajectory, then in the limit $\alpha_{\mathbb{P}}(0) \to 1$, for an asymptotically constant cross-sections, the signature factor behaves as

$$\lim_{\alpha_{\mathbb{P}}(0) \to 1} \eta_{\mathbb{P}}(0) = -\frac{1 + e^{-i\pi\alpha_{\mathbb{P}}(0)}}{\sin \pi\alpha_{\mathbb{P}}(0)} = i, \tag{4.6}$$

where it was used the L'Hopital rule. Thus the leading $\mathbb{P}$ scattering amplitude has $\eta(0) = i$, and for large-s at $t = 0$ behaves as a purely imaginary amplitude,

$$A_{\mathbb{P}}(s, t = 0) \underset{s \to \infty}{\sim} i\gamma_{\mathbb{P}}(0)s^{\alpha_{\mathbb{P}}(0)}. \tag{4.7}$$

However, total cross-section are known to rise with increasing energy, see Figures 2.6, 2.8 and 2.10. This would therefore imply an intercept $\alpha_{\mathbb{P}}(0) > 1$ and will eventually lead to a violation of the Froissart-Martin-Lukaszuk bound. Since the intercept is only very slightly above 1, at the present highest CM energies in colliders or even in cosmic-ray we are still far from asymptopia, and therefore some, unknown, mechanism should eventually unitarise cross-sections. There are some beliefs that going beyond the exchange of single Pomeron pole preservation of unitarity will be obtained. In fact, multiple Pomeron exchanges are able to tame the asymptotic rise of cross-section. Regge poles are only part of the possible singularities allowed by Regge theory. There are other types of singularities in the complex ℓ-plane which correspond to the exchange of two or more Reggeon, as for example the afore-mentioned multiple-Pomeron exchange. This is known as Regge cuts, and its existence is a phenomenological issue, since there are failures in factorisation which cannot be explained by pole singularities alone, and also as a tool to unitarise total cross-sections. In the case of double-Pomeron exchange in the t-channel, this Regge cut structure leads to scattering amplitudes which behaves asymptotically at $s \to \infty$ as $A_{\mathbb{PP}}(s,t) \sim -s^{\alpha_{\mathbb{PP}}(t)}/\ln s$, where $\alpha_{\mathbb{PP}}(t) = 2\alpha_{\mathbb{P}}(0) - 1 + \alpha'_{\mathbb{P}}t/2$. Another possibility to take into account unitarity restoration is to construct an eikonalised amplitude, which is unitarised by definition. In this picture the eikonal expansion could be related somehow to the exchanged series.

If, however, the high-energy behaviour of the total cross-section is indeed a result of the superposition of various Reggeon exchanges, and since the intercepts are universal, then one should therefore expect that they are able to contribute in the description of other total hadronic processes,

$$
\begin{aligned}
\pi^- p &\sim \mathbb{P} + f_2 + \rho, \\
\pi^+ p &\sim \mathbb{P} + f_2 - \rho, \\
K^- p &\sim \mathbb{P} + f_2 + \rho + a_2 + \omega, \\
K^+ p &\sim \mathbb{P} + f_2 - \rho + a_2 - \omega, \\
pp &\sim \mathbb{P} + f_2 - \rho + a_2 - \omega, \\
pp &\sim \mathbb{P} + f_2 + \rho + a_2 + \omega, \\
pn &\sim \mathbb{P} + f_2 + \rho - a_2 - \omega.
\end{aligned}
$$

In the particle-particle and antiparticle-particle total cross-section differences the Pomeron

contribution cancels out,

$$\sigma(\pi^- p) - \sigma(\pi^+ p) \sim 2\rho,$$
$$\sigma(K^- p) - \sigma(K^+ p) \sim 2(\omega + \rho),$$
$$\sigma(\bar{p}p) - \sigma(pp) \sim 2(\omega + \rho),$$
$$\sigma(pn) - \sigma(pp) \sim 2(\rho - a_2).$$

Since these total cross-section differences are determined by sub-leading Regge trajectories which vanish at the asymptotic limit $s \to \infty$, in agreement with the revised Pomeranchuk theorem.

4.1.2   Total and elastic cross-section

Each term of the series in expression (4.1) represents a specific exchange in the t-channel. From the optical theorem, the cross-section reads

$$\sigma_{tot}(s) = 4\pi \sum_i g_i s^{\alpha_i(0)-1}, \tag{4.8}$$

with $g_i \equiv \gamma_i(0)\mathrm{Im}\,\eta_i(0)$. The Pomeron as it emerges from fits to forward observables is called soft Pomeron. The magnitude of its intercept $\alpha_{\mathbb{P}}$ plays a central role in Regge theory, since de Pomeron is the Reggeon with the largest intercept, originally $\alpha_{\mathbb{P}} = 1$. However, in order to describe the observed increase with s of all hadronic cross-sections at high-energy, the Pomeron should have an effective intercept such that $\alpha_{\mathbb{P}} = 1 + \epsilon$, with $\epsilon > 0$. This supercritical intercept value is arrived at by taking into account, in addition to Regge poles, multi-Pomeron cuts in the complex angular momentum plane.

The elastic differential cross-section is given by expression (2.90) and its form in Regge theory is written as

$$\frac{d\sigma}{d|t|}(s,t) = F(t)\, s^{2\alpha(t)-2}, \tag{4.9}$$

where $F(t)$ is a function of t and it has absorbed the residue function, the signature factor and other constants. In general, if many poles contribute, then interference terms will appear. By considering only one single Reggeon with linear trajectory, see expression (3.54), then the elastic differential cross-section can be rewritten as

$$\frac{d\sigma}{d|t|}(s,t) = F(t)\, s^{2\alpha(0)-2}\, e^{-2\alpha'|t|\ln s}, \tag{4.10}$$

where it was written $s^{\alpha^{2\prime}t} = e^{2\alpha' t \ln s}$. If the colliding particles are alike and by assuming a

simple exponential parametrisation for the residue function, such as $\gamma(t) = \gamma(0)e^{B_0 t}$, thus

$$\frac{d\sigma}{d|t|}(s,t) \sim s^{2\alpha(0)-2} e^{-B|t|}, \tag{4.11}$$

where $B = B_0 + 2\alpha' \ln s$ is the t-slope of the scattering amplitude. The width of the forward peak, $\Delta|t| = (B_0 + 2\alpha' \ln s)^{-1}$ decreases with increasing energy. This phenomena is known as the shrinkage of the forward diffraction peak, and it can be interpreted as an increase of the interaction radius $R_{int} \sim \sqrt{\alpha' \ln s}$ at $s \to \infty$. This shrinkage is indeed observed, however it is not suggested by any optical analogy.

4.2 Born-level analysis

The forward Born-level Regge amplitude introduced some time ago by Donnachie and Landshoff has two contributions [16], one representing an effective single Pomeron and the other representing the exchange of the highest-spin meson trajectories, namely a_2, f_2, ω and ρ. However, more recent analysis have indicated that the assumption of degeneracy of the mesons trajectories is not supported by the forward data [64–68]. The best result are obtained with a Born-level amplitude decomposed into three contributions,

$$A_B(s,t) = A_{\mathbb{P}}(s,t) + A_+(s,t) + \tau A_-(s,t). \tag{4.12}$$

The term $A_{\mathbb{P}}(s,t)$ represents the exchange of the Pomeron, $A_+(s,t)$ the exchange of the Reggeons with $C = +1$, namely a_2 and f_2, and $A_-(s,t)$ that of the Reggeons with $C = -1$, namely ω and ρ. Specifically, the amplitude for single exchange is

$$A_i(s,t) = \beta_i^2(t)\eta_i(t) \left(\frac{s}{s_0}\right)^{\alpha_i(t)}, \tag{4.13}$$

where β_i is the elastic proton-Reggeon vertex, $\eta_i(t)$ is the signature factor and $\alpha_i(t)$ is the Regge pole trajectory, with $i = \mathbb{P}, +, -$. Here s_0 is a mass scale usually chosen to be of the order of 1 GeV^2. By comparing expressions (4.1) and (4.13) it can be seen that the residue function factorises as $\gamma_i(t) = \beta_i^2(t)$. The signature factor is given by expression (4.2), where $\xi = +1$ for the Pomeron and the Reggeons a_2 and f_2, and $\xi = -1$ for the Reggeons ω and ρ. Thus, the pp and $\bar{p}p$ scatterings are described in terms of Pomeron, positive- and negative-signature Regge exchange.

However, in order to simplify the numerical calculations involved in the forthcoming eikonal analysis, it was adopted, so far, the asymptotic form of the signatures at the very low-t region, namely $\eta_i(t) = -e^{-i\pi\alpha_i(t)/2}$ for even-signature trajectories and $\eta_i(t) = ie^{-i\pi\alpha_i(t)/2}$ for odd-signature ones [65], see Appendix B.2. The choice of these simplified signatures do not

affect the Pomeron parameters ϵ and $\alpha'_{\mathbb{P}}$, but simply introduces the vertex transformations,

$$
\begin{aligned}
\beta_{\mathbb{P}}^2(t) &\to \sin\left(\frac{\pi}{2}\alpha_{\mathbb{P}}(t)\right)\beta_{\mathbb{P}}^2(t), \\
\beta_+^2(t) &\to \sin\left(\frac{\pi}{2}\alpha_+(t)\right)\beta_+^2(t), \\
\beta_-^2(t) &\to -\cos\left(\frac{\pi}{2}\alpha_-(t)\right)\beta_-^2(t).
\end{aligned}
\tag{4.14}
$$

Therefore, using these simplified form of the Reggeon signatures, each term in the Born-level amplitude, see expression (4.3), can be separated into its real and imaginary parts, respectively. For the Pomeron contribution,

$$
A_{\mathbb{P}}(s,t) = -\beta_{\mathbb{P}}^2(t)\cos\left(\frac{\pi}{2}\alpha_{\mathbb{P}}(t)\right)\left(\frac{s}{s_0}\right)^{\alpha_{\mathbb{P}}(t)} + i\beta_{\mathbb{P}}^2(t)\sin\left(\frac{\pi}{2}\alpha_{\mathbb{P}}(t)\right)\left(\frac{s}{s_0}\right)^{\alpha_{\mathbb{P}}(t)},
\tag{4.15}
$$

for Reggeons with $C = +1$,

$$
A_+(s,t) = -\beta_+^2(t)\cos\left(\frac{\pi}{2}\alpha_+(t)\right)\left(\frac{s}{s_0}\right)^{\alpha_+(t)} + i\beta_+^2(t)\sin\left(\frac{\pi}{2}\alpha_+(t)\right)\left(\frac{s}{s_0}\right)^{\alpha_+(t)},
\tag{4.16}
$$

and the term corresponding to Reggeons with $C = -1$,

$$
A_-(s,t) = \beta_-^2(t)\sin\left(\frac{\pi}{2}\alpha_-(t)\right)\left(\frac{s}{s_0}\right)^{\alpha_-(t)} + i\beta_-^2(t)\cos\left(\frac{\pi}{2}\alpha_-(t)\right)\left(\frac{s}{s_0}\right)^{\alpha_-(t)}.
\tag{4.17}
$$

Thus the complete real and imaginary Born-level amplitude is written by

$$
\mathrm{Re}\, A_B(s,t) = \mathrm{Re}\, A_{\mathbb{P}}(s,t) + \mathrm{Re}\, A_+(s,t) + \tau\, \mathrm{Re}\, A_-(s,t),
\tag{4.18}
$$

$$
\mathrm{Im}\, A_B(s,t) = \mathrm{Im}\, A_{\mathbb{P}}(s,t) + \mathrm{Im}\, A_+(s,t) + \tau\, \mathrm{Im}\, A_-(s,t),
\tag{4.19}
$$

where τ flips sign when going from $pp\,(\tau = -1)$ to $\bar{p}p\,(\tau = +1)$.

The positive-signature secondary Reggeons, namely a_2 and f_2, are taken to have an exponential form for the proton-Reggeon vertex,

$$
\beta_+(t) = \beta_+(0)\exp(b_+t/2),
\tag{4.20}
$$

and to lie on an exchange-degenerate linear trajectory of form,

$$
\alpha_+(t) = 1 - \eta_+ + \alpha'_+ t,
\tag{4.21}
$$

where $\alpha_+(0) = 1 - \eta_+$. Similarly, the exchange-degenerate negative-signature secondary Reggeons, namely ω and ρ, are described by the parameters $\beta_-(0)$, b_-, η_- and α'_-.

For Pomeron exchange it will be investigated two different types of proton-Pomeron vertex and two different types of trajectory, one of which being non-linear. The methodology is, using the standard statistical χ^2 test, to evaluate the relative plausibilities of these vertices and trajectories in the light of the LHC data, *i.e.* to consider different combinations of $\beta_\mathbb{P}$ and $\alpha_\mathbb{P}(t)$, and the effectiveness of these combinations at describing the high-energy forward data. In the first combination, referred to as "BI model", it will be adopted an exponential form for the proton-Pomeron vertex,

$$\beta_\mathbb{P}(t) = \beta_\mathbb{P}(0)\exp(b_\mathbb{P}t/2), \tag{4.22}$$

and a linear Pomeron trajectory,

$$\alpha_\mathbb{P}(t) = \alpha_\mathbb{P}(0) + \alpha'_+ t, \tag{4.23}$$

where henceforth is defined $\alpha_\mathbb{P}(0) \equiv 1 + \epsilon$. In the second model, called "BII", it will be adopted an exponential vertex, see expression (4.15) and the non-linear Pomeron trajectory [23, 74–76],

$$\alpha_\mathbb{P}(t) = \alpha_\mathbb{P}(0) + \alpha'_\mathbb{P}t - \frac{\beta_\pi^2 m_\pi^2}{32\pi^3}\, h\left(\frac{4m_\pi^2}{|t|}\right), \tag{4.24}$$

where

$$h(x) = \frac{4}{x}\, F_\pi^2(t)\left[2x - (1+x)^{3/2}\ln\left(\frac{\sqrt{1+x}+1}{\sqrt{1+x}-1}\right) + \ln\left(\frac{m^2}{m_\pi^2}\right)\right], \tag{4.25}$$

with $x = 4m_\pi^2/|t|$, $m_\pi = 139.6$ MeV and $m = 1$ GeV. The non-linear term in the Pomeron trajectory comes from the nearest t-channel singularity, a two-pion loop [23]. In the above expression $F_\pi(t)$ is the form factor of the pion-Pomeron vertex, for which it will be taken the standard pole expression $F_\pi(t) = \beta_\pi/(1 - t/a_1)$. The coefficient β_π specifies the value of the pion-Pomeron coupling and for this it will be adopted the additive quark model relation $\beta_\pi/\beta_\mathbb{P} = 2/3$. In the third combination, called "BIII model", we adopt the non-linear Pomeron trajectory, see expression (4.17) and the power-like form for the proton-Pomeron vertex [23, 74–77],

$$\beta_\mathbb{P}(t) = \frac{\beta_\mathbb{P}(0)}{(1 - t/a_1)(1 - t/a_2)}, \tag{4.26}$$

where the free parameter a_1 is the same as the one in the form factor of the pion-Pomeron vertex $F_\pi(t)$. The total cross-section, the elastic differential cross-section and the ratio of the real to imaginary part of the forward scattering amplitude are expressed in terms of the amplitude in expression (4.3),

$$\begin{aligned}\sigma_{tot}(s) &= \frac{4\pi}{s}\,\text{Im}\,A(s, t=0)\\ &= Xs^\epsilon + Y_+ s^{-\eta_+} + \tau\, Y_- s^{-\eta_-},\end{aligned} \tag{4.27}$$

$$\frac{d\sigma}{d|t|}(s,t) = \frac{\pi}{s^2}\,|\text{Im}\,A(s,t)|^2\,, \tag{4.28}$$

$$\rho(s) = \frac{\text{Re}\,A(s,t=0)}{\text{Im}\,A(s,t=0)}, \tag{4.29}$$

where $X \equiv 4\pi\beta_{\mathbb{P}}^2(0)\sin(\pi\alpha_{\mathbb{P}}(0)/2)s_0^{-(1+\epsilon)}$ and $Y_{\pm}$ represents the imaginary part of the forward, $t=0$, scattering amplitude, respectively, where $Y_{+} \equiv 4\pi\beta_{+}^2(0)\sin(\pi\alpha_{+}(0)/2)s_0^{-(1+\eta_+)}$ and $Y_{-} \equiv 4\pi\beta_{-}^2(0)\cos(\pi\alpha_{-}(0)/2)s_0^{-(1+\eta_-)}$. In the above expressions the scattering amplitude is $A(s,t) = A_B(s,t)$.

4.2.1   Double-Pomeron exchange

The lack of a footprint of unitarisation breaking up to LHC energies can be confirmed by investigating the role of multiple Pomeron exchanges on the scattering amplitude. Unfortunately, despite the advances in theoretical understanding of the Pomeron in the last four decades, we still do not know how to do it. However, there is a consensus that the contribution of the double-Pomeron exchange ($\mathbb{PP}$) is negative and has energy dependence $s^{\alpha_{\mathbb{PP}}(t)}$ divided by some function of $\ln s$ [87], where

$$\alpha_{\mathbb{PP}}(t) = 1 + 2\epsilon + \frac{1}{2}\,\alpha_{\mathbb{P}}'t. \tag{4.30}$$

Thus, the $\mathbb{PP}$ contribution is flatter in t than the single $\mathbb{P}$ exchange, becoming more important for higher values of t. In order to estimate an upper bound on the ratio $R \equiv \beta_{\mathbb{PP}}^2(0)/\beta_{\mathbb{P}}^2(0)$, it was added the phenomenological term to the amplitude in expression (4.3),

$$A_{\mathbb{PP}}(s,t) = -\beta_{\mathbb{PP}}^2(t)\,\eta_{\mathbb{PP}}(t)\frac{s}{s_0}^{\alpha_{\mathbb{PP}}(t)}\left[\ln\left(-i\frac{s}{s_0}\right)\right]^{-1}, \tag{4.31}$$

where $\eta_{\mathbb{PP}}(t) = -e^{-i\pi\alpha_{\mathbb{PP}}(t)/2}$, $\beta_{\mathbb{PP}} = \exp(b_{\mathbb{P}}t/4)$ and $\ln(-ix) = \ln(x) - i\pi/2$. From the model BI it was obtained, after a global fit, the result

$$R = \frac{\beta_{\mathbb{PP}}^2(0)}{\beta_{\mathbb{P}}^2(0)} = \frac{|\mathbb{PP}_{coupling}|}{\mathbb{P}_{coupling}} < 0.2\%. \tag{4.32}$$

4.2.2   First results using Born-level amplitudes

In our analyses we carried out global fits to forward pp and $\bar{p}p$ scattering data above $\sqrt{s} = 10$ GeV and to the elastic differential scattering cross-section for pp, namely the total cross-section $\sigma_{pp,\bar{p}p}$, the ratio of the real to imaginary part of the forward scattering amplitude $\rho^{pp,\bar{p}p}$ and the differential elastic cross-section $d\sigma^{pp}/d|t|$ at $\sqrt{s} = 7$ and 8 TeV with $t \leq 0.2$ GeV^2.

We used data sets compiled and analysed by the Particle Data Group [35] as well as the recent data at LHC from the TOTEM Collaboration [17–22], with the statistic and systematic errors added into quadrature. More specifically, the TOTEM data set includes the first and second measurements ot the total pp cross-section at $\sqrt{s} = 7$ TeV, namely $\sigma_{tot}^{pp} = 98.30 \pm 2.8$ mb [17] and $\sigma_{tot}^{pp} = 98.58 \pm 2.23$ mb [18], both using the optical theorem together with the luminosity provided by the CMS [52], the luminosity-independent measurement at $\sqrt{s} = 7$ TeV, namely $\sigma_{tot}^{pp} = 98.0 \pm 2.5$ mb [19], the ρ-independent measurements at $\sqrt{s} = 7$ TeV of σ_{pp} and ρ-parameter, namely $\sigma_{tot}^{pp} = 98.0 \pm 2.5$ mb and $\rho^{pp} = 0.145 \pm 0.091$ [19], the luminosity-independent measurement at $\sqrt{s} = 8$ TeV, namely $\sigma_{tot}^{pp} = 101.7 \pm 2.9$ mb [20], and the measurement in the Coulombian-nuclear interference region at $\sqrt{s} = 8$ TeV of σ_{pp} and ρ-parameter, namely $\sigma_{tot}^{pp} = 102.0 \pm 2.3$ mb and $\sigma_{tot}^{pp} = 103.0 \pm 2.3$ mb, for central and peripheral phase formulations, respectively, and $\rho^{pp} = 0.120 \pm 0.03$ [21]. The TOTEM Collaboration has also measured elastic differential cross-section at $\sqrt{s} = 7$ TeV and 4-momentum transfers squared $|t|$ in the intervals $0.00515 \leq |t| \leq 0.235$ GeV^2 [18] and $0.377 \leq |t| \leq 2.443$ GeV^2 [22], and at $\sqrt{s} = 8$ TeV in the intervals $6 \times 10^{-4} \leq |t| \leq 0.2$ GeV^2 [21].

In all the fits performed was used a χ^2 fitting procedure, where the value of χ^2_{min} is distributed as a χ^2 distribution with N degrees of freedom. The fits to the experimental data sets were performed adopting an interval $\chi^2 - \chi^2_{min}$ corresponding, in the case of normal errors, to the projection of χ^2 hypersurface containing 90% of probability. This corresponds to $\chi^2 - \chi^2_{min} = 12.02$ and 13.36 in the case of 7 and 8 free parameters, respectively.

Following the methodology of using the minimum number of free parameters, in the following analyses the slopes of the secondary-Reggeon linear trajectories, namely α'_+ and α'_-, are fixed at 0.9 GeV^{-1}. These values are in agreement with those usually obtained in Chew-Frautschi plots. Also, the slopes associated with the form factors are fixed at $b_+ = 0.5$ GeV^{-2} and $b_- = 3.1$ GeV^{-2}. These values are consistent with those obtained in previous studies [65, 75, 76] and do not have enough statistical weight to constrain the Pomeron parameters. It was also fixed the scale of the pion-Pomeron vertex at $a_1 = m_\rho^2 = 0.776$ GeV^2 [77].

In the case of Born-level amplitudes, the values of the Regge parameters determined by global fits to pp and $\bar{p}p$ data are listed in Table 4.1. The descriptions of the data are displayed in Figure 4.1 for BI and BII models (solid curves), and BIII model (dashed curves). Notice that in the case of BI and BII models we fixed the parameter $b_{\mathbb{P}}$ at 5.5 GeV^{-2} since, as discussed in Reference [74], it is the natural choice for the computation of double-diffractive central Higgs production via WW-fusion (since the W boson is radiated from a quark, like the photon). Moreover, at this value, which corresponds to the slope of the electromagnetic proton form factor, the Pomeron is described by trajectories with $\alpha'_{\mathbb{P}} \simeq 0.25$ GeV^{-2}. Interestingly enough, this value is consistent with the estimates of $\alpha'_{\mathbb{P}}$

recently obtained from holographic QCD models [78–82]. However, if we perform the global fit at another value of $b_\mathbb{P}$, say 4.0 GeV^{-2} (which is not atypical [74]), we obtain the values $\alpha'_\mathbb{P} = 0.3346 \pm 0.0085$ GeV^{-2} and 0.3339 ± 0.0085 GeV^{-2} in the case of BI and BII models, respectively, whilst the remaining free parameters remain with the same values.

It is important to notice that the Pomeron intercept $\alpha_\mathbb{P}(0) = 1 + \epsilon$ is an effective power, valid over a limited range of energies, otherwise the forward amplitude $A(s, t = 0)$ would grow so large that unitarity bound would be violated. Thus, the parameter ϵ represents not only the exchange of s single Pomeron, but also n-Pomeron exchange processes, $n \geq 2$. These multiple exchanges must tame the rise of the total cross-section so that the breakdown of unitarity is avoided and, as a consequence, the value of ϵ should decrease slowly with increasing energy. However, the results already seen in Figure 4.1 clearly indicate that a very good description of forward data up to LHC energy is obtained using a constant value of ϵ.

The values of the Regge parameters arising from this double-Pomeron analysis are shown in the last column of Table 4.1. The description of σ_{tot} and ρ is displayed in Figure 4.1. Our results show that the simple introduction of the nearest-t channel singularity in the Pomeron trajectory, i.e, just by considering a non-linear trajectory for single-Pomeron exchange, is not sufficient to play a substantial statistical weight when compared to the fitted results from model BI. The same happens with the inclusion of double-Pomeron exchange in model BI+$\mathbb{PP}$. Although each one of the four Born-level amplitudes are built in a unique form, the curves obtained in models BI, BII and BI+$\mathbb{PP}$ are indistinguishable from each other. For these reasons we decided to use a solid curve to correspond these three models whereas a dashed one was used for BIII, respectively. Therefore, these pictorical smooth differences among these Born-level models depicted in Figure 4.1 must be attributed mainly to the presence of the power-like proton-Pomeron vertex plus the introduction of a non-linear Pomeron trajectory. Bearing in mind that Figure 4.1 corresponds to forward observables, we must take into account the significant t dependence in the Born-level amplitude, more precisely in the Pomeron contribution since it gives the asymptotic high-energy behaviour. The fits to the $d\sigma/dt$ are responsible for this small difference. More specifically, the small deviations in the central values of the Pomeron intercept and in the coupling of the $p - \mathbb{P}$ vertex at $t = 0$, $\beta_\mathbb{P}(0)$, as listed in Table 4.1.

The Born-level fit results for the total cross-section are summarised below, where it was used only the central values listed in Table 4.1, s is in GeV^2 and the total cross-section in mb,

$$\text{(BI)} \quad \sigma_{tot}^{pp,\bar{p}p} = 18.382\, s^{0.0945} + 57.298\, s^{-0.329} \mp 30.097\, s^{-0.527}, \tag{4.33}$$

$$\text{(BII)} \quad \sigma_{tot}^{pp,\bar{p}p} = 18.364\, s^{0.0945} + 56.986\, s^{-0.329} \mp 30.097\, s^{-0.527}, \tag{4.34}$$

$$\text{(BIII)} \quad \sigma_{tot}^{pp,\bar{p}p} = 18.114\, s^{0.0958} + 56.664\, s^{-0.323} \mp 30.053\, s^{-0.526}, \tag{4.35}$$

$$(\text{BI+}\mathbb{PP}) \ \sigma_{tot}^{pp,\bar{p}p} = 18.401 \, s^{0.0945} - 3.381 \times 10^{-2} \, s^{1.189} \, \text{Im} \left[\frac{i}{\ln s - i\frac{\pi}{2}} \right] + 57.298 \, s^{-0.329} \mp 30.097 \, s^{-0.527}.$$

$$(4.36)$$

	Born-level amplitudes			
	BI	BII	BIII	BI + $\mathbb{PP}$
ϵ	0.0945±0.0035	0.0945±0.0033	0.0958±0.0039	0.0945±0.0038
$\alpha'_{\mathbb{P}}$ [GeV^{-2}]	0.2502±0.0085	0.2495±0.0085	0.3788±0.0088	0.4469±0.0094
$\beta_{\mathbb{P}}(0)$ [GeV^{-1}]	1.949±0.057	1.948±0.052	1.935±0.062	1.950±0.060
$b_{\mathbb{P}}$ [GeV^{-2}]	5.5 [fixed]	5.5 [fixed]	-	5.5 [fixed]
η_+	0.329±0.055	0.329±0.049	0.323±0.059	0.329±0.057
$\beta_+(0)$ [GeV^{-1}]	3.67±0.41	3.66±0.37	3.64±0.44	3.67±0.43
η_-	0.527±0.084	0.527±0.080	0.526±0.090	0.527±0.089
$\beta_-(0)$ [GeV^{-1}]	2.89±0.51	2.89±0.49	2.89±0.54	2.89±0.54
a_1 [GeV^2]	-	m_ρ^2 [fixed]	m_ρ^2 [fixed]	-
a_2 [GeV^2]	-	-	7.5±3.9	-
$\beta_{\mathbb{PP}}(0)$	-	-	-	0.085±0.022
χ^2/dof	0.79	0.79	0.79	0.79

Table 4.1: The values of the Pomeron and secondary Reggeon parameters obtained in global fits to the $\sigma_{tot}^{pp,\bar{p}p}$, $\rho^{pp,\bar{p}p}$ and $d\sigma^{pp,\bar{p}p}/dt$ data. The errors correspond to a 90% confidence level. The parameters α'_+, α'_-, b_+ and b_- and a_1 are fixed.
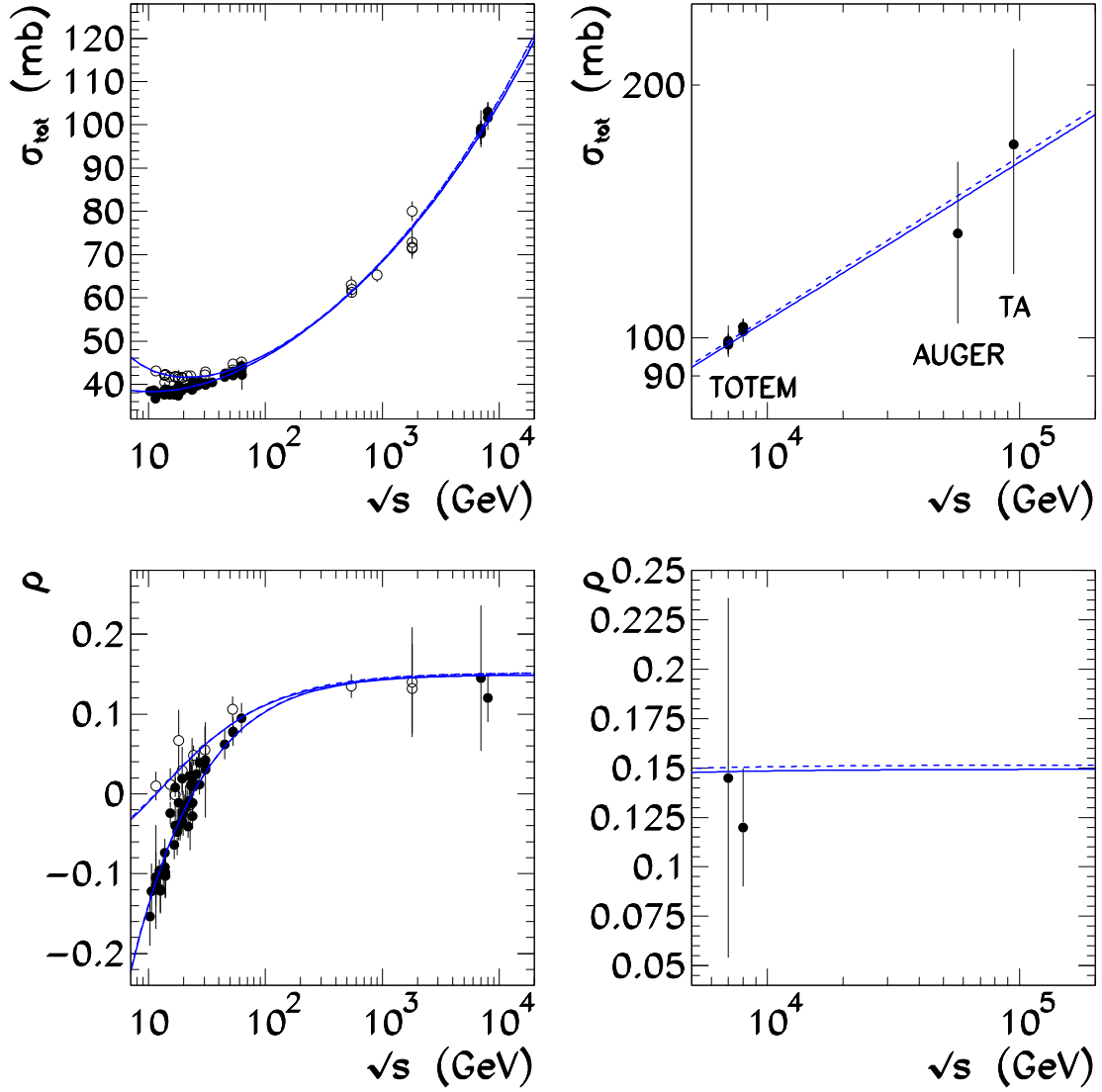
Figure 4.1: Predictions for the forward observables, namely total cross-section and ρ-parameter for pp and $\bar{p}p$ scattering by means of the results obtained through out the Born-level analysis. It is also depicted the region of high energies. In the case of the ρ-parameter, it is possible to see that asymptotically at the Born-level $\rho \to constant$, which is an expected result in such analysis. Respectively, the solid curves corresponds to BI, BII and BI+$\mathbb{PP}$ models whereas dashed ones is associated with BIII model.

4.3 Eikonal analysis

It is well known that expression (4.13) leads to total cross-sections which violate the Froissart-Martin bound. The usual justification for using such Born-level models is that it is viewed as an effective scattering amplitude where the unitarity violation only occurs at extremely high energies far beyond LHC.

As it was mentioned in the previous section, in the case of Born-level amplitudes the breakdown of unitarity can be avoided by introducing the exchange series $\mathbb{P}+\mathbb{PP}+\mathbb{PPP}+...$ in such a way that the amplitude in expression (4.13) is some kind of "Born approximation", that is why it is usually called as Born-level amplitude. Although some general analytic properties of these multiple-exchange terms are known, it is less clear how to carry out a full computation of them. On the other hand, it is well established that eikonalisation is an effective procedure to take into account some properties of high-energy s-channel unitarity.

Thus in the sense to restore the Froissart-Martin bound, the Born-level amplitude is eikonalised using the impact parameter representation, see expression (2.100),

$$A_{eik}(s,t) = is \int_0^\infty db\, b\, J_0(b\sqrt{-t}) \left[1 - e^{i\chi(s,b)} \right], \tag{4.37}$$

where the eikonalised amplitude is written in terms of a complex eikonal function $\chi(s,b) = \chi_R(s,b) + i\chi_I(s,b)$. As long as the Pomeron term in the Born-level amplitude represents a single-Pomeron exchange, one in principle could expand $1 - e^{i\chi(s,b)}$ and connect each term to the exchange series,

$$1 - \sum_{n=0}^\infty \frac{(i\chi)^n}{n!} = -i\chi + \frac{\chi^2}{2!} + \frac{i\chi^3}{3!} + ... \leftrightarrow \mathbb{P} + \mathbb{PP} + \mathbb{PPP} + ... \tag{4.38}$$

This is not an absolute truth, because the analyticity properties of poles and cuts in multiple-Pomeron exchange is much more complicated than a simple exponential expansion, and therefore does not tell the whole story. Despite the criticism, this is just a phenomenological way to give some meaning to eikonal unitarisation, which, by the way, is just one possible solution of the unitarity equation [88–90]. So, the procedure consists by expanding the exponential up to the first order, *i.e.* retaining only the first term which is linear in χ, then the first-approximation amplitude, identified as the Born-level amplitude, is given by

$$A_B(s,t) = s \int_0^\infty db\, b\, J_0(b\sqrt{-t})\, \chi(s,b), \tag{4.39}$$

hence, the eikonal function is related to the Born-level amplitude by the Fourier-Bessel

transform,

$$\chi(s,b) = \frac{1}{s} \int_0^\infty d\sqrt{-t}\,\sqrt{-t}\,J_0(b\sqrt{-t})\,A_B(s,t), \tag{4.40}$$

and then it is inserted back into expression (4.30) to provide the "full eikonalised" amplitude. The total cross-section, the elastic differential cross-section and the ρ-parameter are calculated using expressions (4.20)-(4.22) with $A(s,t) = A_{eik}(s,t)$, see expressions (2.110)-(2.112).

4.3.1 Two-channel eikonal model

As it was mentioned in the Section 4.2.2, an effective Pomeron intercept $\alpha_\mathbb{P}(0) > 1$ is obtained taking into account multi-Pomeron cuts (moving branch points) in the j-plane. These singularities are required in order to assure s-channel unitarity. In the models considered in the preceding sections we have not accounted for the possibility of diffractive proton excitation in intermediate states, such as $p \to N^*$. However, it is possible to incorporate the s-channel unitarity with elastic and a low-mass intermediate state N^* by using a two-channel eikonal approach. The Good-Walker formalism [83] provides an elegant and convenient form to incorporate $p \to N^*$ diffractive dissociation. In this approach we introduce diffractive eigenstates $|\phi_i\rangle$ that diagonalise the T-matrix. Thus, the incoming hadron wave functions $|h\rangle$ (in our case the 'beam' and 'target' proton wave functions) can be written as superpositions of these diffractive eigenstates, namely

$$|h\rangle_{beam} = \sum_i a_{ki}|\phi_i\rangle, \quad \text{and} \quad |h\rangle_{target} = \sum_k a_{ik}|\phi_k\rangle. \tag{4.41}$$

Since we need at least two diffractive eigenstates, in a two-channel eikonal model $i, k = 1, 2$. The extension to n-channel eikonal models is straightforward, however, it is well known that a two-channel model is sufficient to capture the single- or double-diffractive dissociation behaviour very accurately [74–77, 84–86]. In this Thesis we adopt a two-channel eikonal model in which the Pomeron couplings to the two diffractive eigenstates k are

$$\beta_{\mathbb{P},k}(t) = (1 \pm \gamma)\beta_\mathbb{P}(t), \tag{4.42}$$

i.e., the eigenvalues of the two-channel vertex are $1\pm\gamma$, where $\gamma \simeq 0.55$ [75,76]. This value is in accordance with $p \to N^*$ dissociation observed at CERN-ISR energies, more specifically, it is the value required in order to obtain the experimental value of the cross-section for low-mass diffraction, namely $\sigma_{SD}^{lowM} \simeq 2$ mb, measured at $\sqrt{s} = 31$ GeV.

Since each amplitude has two vertices, the total cross-section is controlled by an elastic

scattering amplitude with three different exponents,

$$A_{eik}(s,t) = is \int_0^\infty b\, db\, J_0(bq) \left[1 - \frac{1}{4} e^{i(1+\gamma)^2 \chi(s,b)} - \frac{1}{2} e^{i(1+\gamma^2)\chi(s,b)} - \frac{1}{4} e^{i(1-\gamma)^2 \chi(s,b)} \right]. \quad (4.43)$$

4.3.2 First results using eikonalised amplitudes

In the calculation of the eikonal function (4.40) the input amplitudes $(A_{Born}(s,t))$ are simply the ones related to BI, BII and BIII models. These single-channel eikonal models are referred to, respectively, as EI, EII and EIII models, and as for the case of the two-channel ones, DI, DII and DIII models, respectively.

The values of the Regge parameters obtained using the eikonalised amplitude $A_{eik}(s,t)$ is listed in Table 4.2, for the single-channel analysis, and in Table 4.3, in the case of two-channel analysis. Similarly to the case of the Born-level analysis, here we found a similar behaviour. The single-channel description of the data is displayed in Figure 4.2, and as before our results reveal that practically there is no difference between EI and EII models, and once again the difference is properly constrained by the functional form of the third one, EIII model. Despite the fact that in the eikonal formalism there is a "running" in t, see expression (4.40), and only after is setted $t = 0$, at least for the description of the forward physical observables, it is not strong enough, per se, to distinguish between EI and EII results. Even though, the eikonalised amplitude is build up from the Born-level amplitude, however, we could not say that such results were then expected. By following the same methodology as the one in Figure 4.1, we used in Figure 4.2 a solid curve to fit the results obtained by EI and EII models, since they are essentially indistinguishable, and a dashed one to EIII, respectively. Once more, the role of a power-like proton-Pomeron vertex within the nearest-t channel singularity in the Pomeron trajectory accounts for the dynamical differences. We obtained higher values for the χ^2/dof in the two-channel analysis, at least for DI and DII models, than the ones we have obtained before, respectively. Therefore, we did not carry to perform the fit to the data using these two models, because in our understanding they will not correspond to a good or accurate fit to the experimental data. The solid curve depicted in Figure 4.3 refers only to the DIII model.

The descriptions for the elastic differential cross-section is displayed in Figure 4.4. For consistency, we decided to perform the fits following the same methodology as previously discussed in the construction of the aforementioned figures, *i.e*, in the case of the Born-level amplitudes the solid (dashed) curves corresponds to BI, BII and BI+$\mathbb{PP}$ (BIII), see Figure 4.4(a), for the single-channel models solid (dashed) curves corresponds to EI and EII (EIII), see Figure 4.4(b), respectively. Since we have not fitted the results to the forward physical observables using DI and DII models, we decided to depict only the description achieved

by means of DIII model, see Figure 4.4(c). As a matter of comparison, it is displayed in Figure 4.4(d) the corresponding predictions obtained through out the analysis of BIII, EIII and DIII models for the elastic differential cross-section at CM energies of $\sqrt{s} = 7, 8$ and 13 TeV. The solid, dashed and dotted curves correspond to BIII, EIII and DIII, respectively.

	Single-channel eikonalised amplitudes		
	EI	EII	EIII
ϵ	0.1103±0.0020	0.1091±0.0094	0.1213±0.0052
$\alpha'_{\mathbb{P}}$ [GeV^{-2}]	0.2484±0.0010	0.266±0.012	0.1375±0.0057
$\beta_{\mathbb{P}}(0)$ [GeV^{-1}]	2.066±0.012	2.090±0.17	1.917±0.084
$b_{\mathbb{P}}$ [GeV^{-2}]	2.899±0.011	2.56±0.96	-
η_+	0.3563±0.0051	0.360±0.060	0.322±0.054
$\beta_+(0)$ [GeV^{-1}]	4.870±0.056	4.94±0.72	4.56±0.49
η_-	0.5509±0.0027	0.552±0.088	0.544±0.087
$\beta_-(0)$ [GeV^{-1}]	3.760±0.022	3.78±0.70	3.65±0.66
a_1 [GeV^2]	-	m_ρ^2 [fixed]	m_ρ^2 [fixed]
a_2 [GeV^2]	-	-	0.369 ±0.012
χ^2/dof	1.11	1.09	0.80

Table 4.2: The values of the Pomeron and secondary Reggeon parameters obtained in global fits to the $\sigma_{tot}^{pp,\bar{p}p}$, $\rho^{pp,\bar{p}p}$ and $d\sigma^{pp,\bar{p}p}/dt$ data. The errors correspond to a 90% confidence level. The parameters α'_+, α'_-, b_+, b_- and a_1 are fixed.
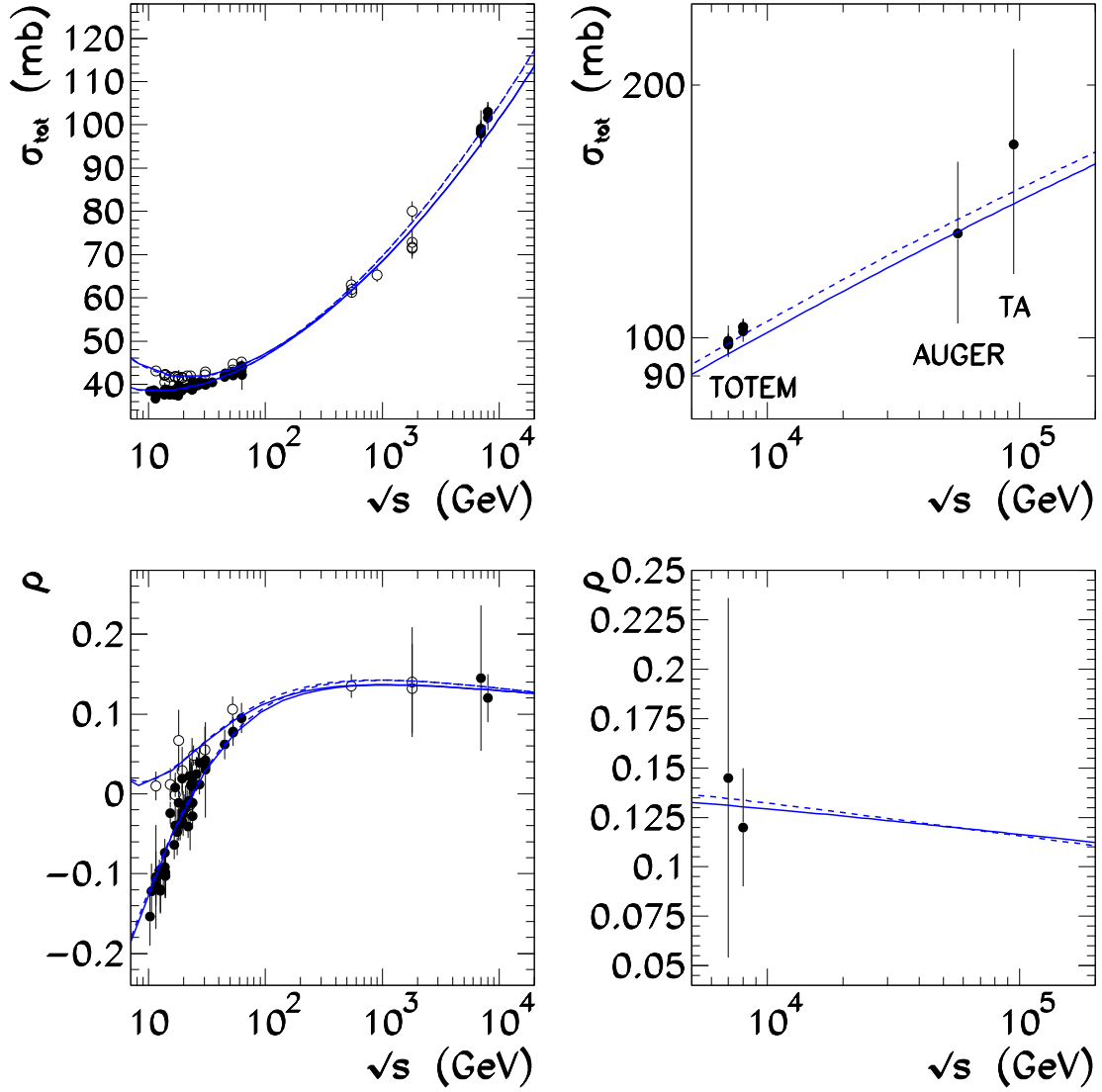
Figure 4.2: Predictions for the forward observables, namely total cross-section and ρ-parameter for pp and $\bar{p}p$ scattering by means of the results obtained through out the single-channel eikonal analysis. It is also depicted the region of high energies. Here, it possible to see that the high-energy behaviour of the ρ-parameter is in accordance with the theoretical predictions. Respectively, the solid curves corresponds to EI, and BII models whereas dashed ones is associated with EIII model.

	Two-channel eikonalised amplitudes		
	DI	DII	DIII
ϵ	0.1383±0.0038	0.1393±0.0014	0.1472±0.0044
$\alpha'_{\mathbb{P}}$ [GeV^{-2}]	0.0909±0.00020	0.0703±0.00075	0.0447±0.00048
$\beta_{\mathbb{P}}(0)$ [GeV^{-1}]	1.948±0.027	1.919±0.26	1.896±0.011
$b_{\mathbb{P}}$ [GeV^{-2}]	4.42±0.16	4.787±0.033	-
η_{+}	0.3314±0.0072	0.3284±0.0055	0.3287±0.0057
$\beta_{+}(0)$ [GeV^{-1}]	5.261±0.099	5.218±0.039	5.314±0.014
η_{-}	0.5487±0.0037	0.5475±0.0011	0.5547±0.0022
$\beta_{-}(0)$ [GeV^{-1}]	4.15±0.50	4.122±0.025	4.165±0.094
a_1 [GeV^2]	-	m_ρ^2 [fixed]	m_ρ^2 [fixed]
a_2 [GeV^2]	-	-	0.383±0.010
χ^2/dof	1.42	1.42	0.85

Table 4.3: The values of the Pomeron and secondary Reggeon parameters obtained in global fits to the $\sigma_{tot}^{pp,\bar{p}p}$, $\rho^{pp,\bar{p}p}$ and $d\sigma^{pp,\bar{p}p}/dt$ data using eikonalized amplitudes. The parameters α'_{+}, α'_{-}, b_{+}, b_{-} and a_1 are fixed..

	BIII model		EIII model		DIII model	
$\sqrt{s}$ [TeV]	σ_{tot} [mb]	ρ	σ_{tot} [mb]	ρ	σ_{tot} [mb]	ρ
7.0	98.9±3.9	0.150±0.006	98.4±3.9	0.135±0.005	96.1±3.8	0.135±0.005
8.0	101.5±7.2	0.150±0.011	100.7±7.2	0.134±0.010	98.4±7.0	0.135±0.010
13.0	111.3±10.2	0.151±0.014	109.3±10.0	0.130±0.012	106.3±9.7	0.135±0.012
14.0	112.9±10.7	0.151±0.014	110.6±10.5	0.130±0.012	107.7±10.3	0.135±0.013
57.0	148±18	0.151±0.019	138±17	0.120±0.015	133±17	0.135±0.017
95.0	163±23	0.151±0.021	149±21	0.116±0.016	144±20	0.135±0.019

Table 4.4: Predictions for the forward scattering quantities σ_{tot}^{pp} and ρ^{pp} using different Regge-Gribov based models.
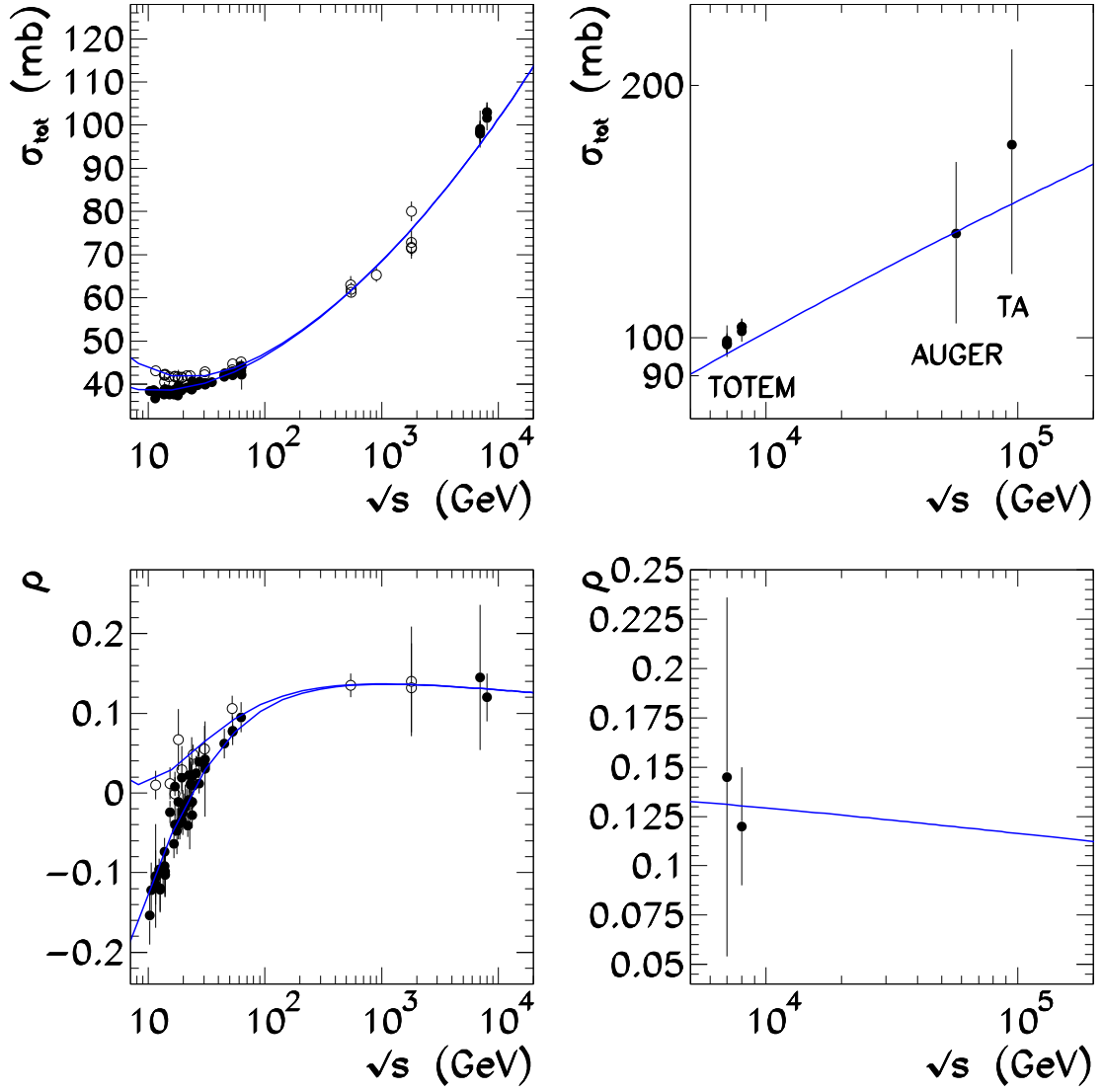
Figure 4.3: The corresponding results for $\sigma_{tot}^{pp,\bar{p}p}$ and $\rho^{pp,\bar{p}p}$ by means of the results obtained through out the double-channel eikonal analysis. The filled circles refers to pp data whereas open ones to $\bar{p}p$ data, respectively. It is depicted only the result obtained in the DIII model.
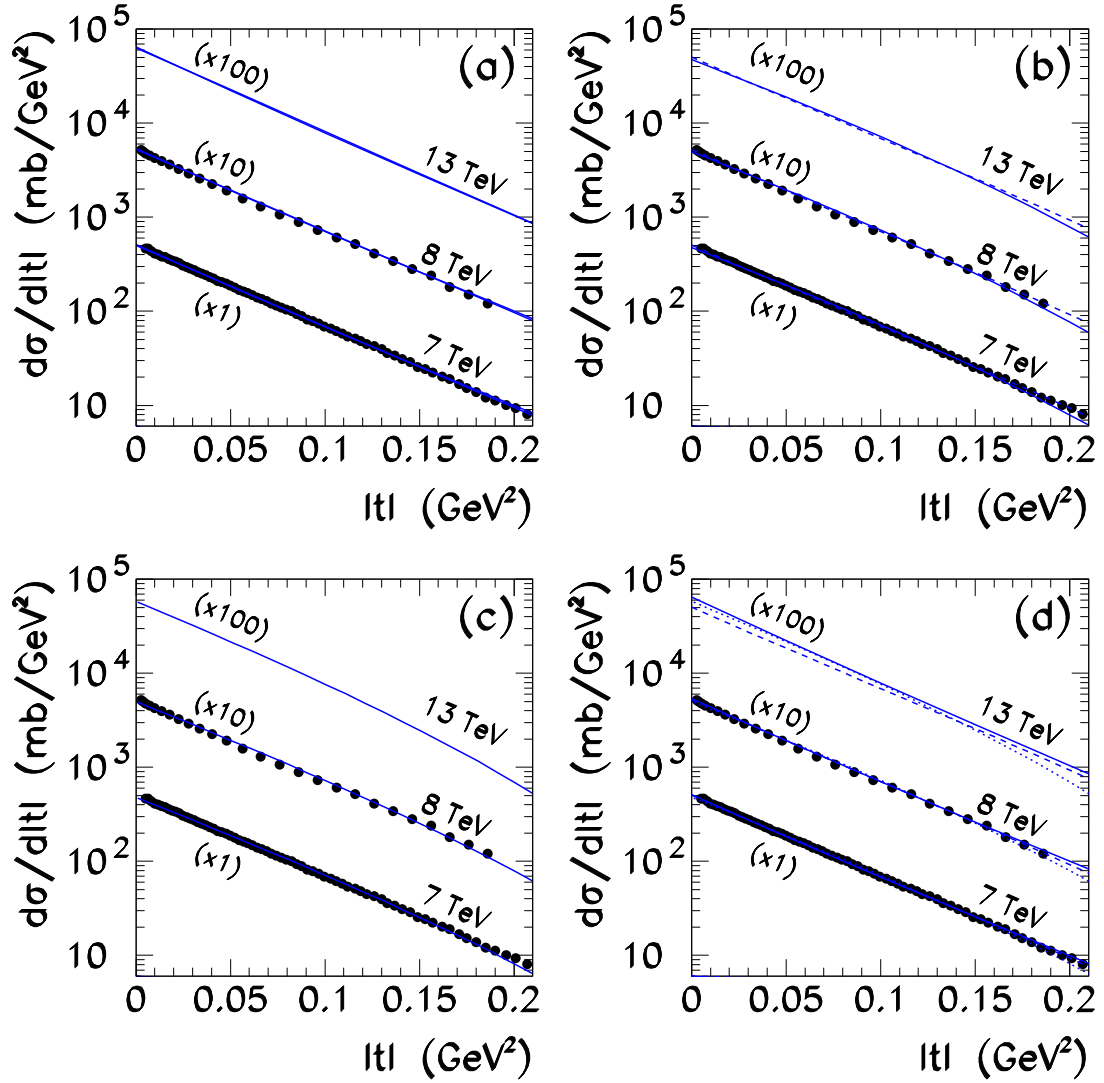
Figure 4.4: Fits to the elastic differential *pp* cross-section for different Regge-Gribov based models. (a) corresponds to Born-level analysis, solid curves are related to BI, BII and BI+$\mathbb{PP}$ and dashed to BIII; (b) corresponds to single-channel eikonal models, solid curves are related to EI and EII and dashed to EIII; and (c) corresponds to the two-channel analysis where it is shown only the predictions for DIII. (d) gives the comparison results among BIII (solid), EIII (dashed) and DIII (dotted).

Chapter 5

QCD parton model

Quantum Chromodynamics is the non-Abelian gauge theory that describes the strong interaction among quarks and gluons, which collectively are called partons, and it is one of the pillars of the Standard Model of elementary particles [1, 2]. The QCD is described by means of the invariant properties of the symmetry group $SU(N_c)$, where $N_c = 3$ defines the dimension of the group and introduces a new quantum number, the colour charge. Historically, the colour degrees of freedom appeared as a solution to the problem of the barion Δ^{++} wave function. This barion is compounded by three u quarks, and therefore has spin 3/2. It is well known that quarks has spin 1/2, so the Fermi-Dirac statistics properly implies a antisymmetric wave function, and beyond that the Pauli exclusion principle assures that each one of the three quarks must exhibit distinct quantum numbers. And in fact they do, once it is considered that the wave function is totally antisymmetric with respect to the colour degrees of freedom.

The quark fields transform following the $SU(3)_c$ fundamental representation and given by the spinors ψ_q, where each quark's flavour has one in three possible colour charges. The gauge fields are represented by the T^A generator matrices of $SU(3)_c$, and given by eight generators, or also by eight vector gluons, identified by $A = 1, ..., 8$. However, quarks were never measured as free particles, but as hadronic states of colour singlet linear combinations of quarks, antiquarks and gluons. Then, the interaction force among quarks should increase with increasing distances, and this behaviour can be explained by means of a mechanism called confinement. The non-Abelian nature of the gauge group allows the existence of coloured gluons and also that they can interact with each other, therefore leading to a property known as asymptotic freedom, where the strong coupling, calculated by means of perturbation theory and renormalisation group, monotonically decreases in short distances or equivalently at high values of momentum transfer.

5.1   Quantum Chromodynamics

There are two distinct categories in QCD: the ultraviolet regime, also known as perturbative, and the infrared regime, called non-perturbative. The former is characterised by the asymptotic free behaviour of the theory, *i.e.* it is identified by processes where the mass scale is higher than $\Lambda_{QCD} \sim 200$ MeV. The latter one, instead of what usually happens in short distance regime, the quarks and gluons are not observed as free states of particles, therefore hadrons are not considered as colour states. Moreover, the gauge symmetry implies that gluons are massless, but recent studies indicate that the gluons may develop a dynamical momentum-dependent mass in the infrared sector [24, 27–29] by means of Dyson-Schwinger equations and its existence is strongly supported by QCD lattice simmulations [91–101].

5.1.1   The Lagrangian of QCD

The Feynman rules required for a perturbative analysis of QCD can be derived from a Lagrangian density, which is given by

$$\mathcal{L}_{QCD} = \mathcal{L}_{classical} + \mathcal{L}_{gauge-fixing} + \mathcal{L}_{ghost}. \tag{5.1}$$

The classical Lagrangian term corresponding to the dynamics of massive quarks and massless gluons is

$$\mathcal{L}_{cl}(x) = -\frac{1}{4}F_{\mu\nu}^A(x)F_A^{\mu\nu}(x) + \sum_q \bar{\psi}_q^r(x)(i\slashed{D} - m)_{rs}\psi_q^s(x), \tag{5.2}$$

where $r, s = 1, 2, 3$ are colour index and $q = u, d, s, c, b, t$ is the flavour and $\slashed{D} = \gamma^\mu D_\mu$. The Dirac matrices satisfy the Clifford algebra anti-commutation relation $\{\gamma^\mu\gamma^\nu\} = 2g^{\mu\nu}$, where the metric is $g^{\mu\nu} = \text{diag}(1, -1, -1, -1)$. The quark fields ψ_q^r are in the triplet representation of the colour group. Then, the covariant derivative acting on triplet fields takes the form,

$$(D_\mu)_{rs} = \partial_\mu\delta_{rs} + ig_s(t^C G_\mu^C(x))_{rs}, \tag{5.3}$$

and similarly acting on octet fields,

$$(D_\mu)_{AB} = \partial_\mu\delta_{AB} + ig_s(T^C G_\mu^C(x))_{AB}, \tag{5.4}$$

where t and T are matrices in the fundamental and adjoint representations of $SU(3)_c$ respectively,

$$[\lambda^A, \lambda^B] = if^{ABC}\lambda^C, \tag{5.5}$$

and a representation for the generators t^A is provided by the eight Gell-Mann matrices, which are hermitian and traceless [1]

$$t^A = \frac{1}{2}\lambda^A. \tag{5.6}$$

By convention, it is chosen that the t^A generators of $SU(N_c)$ are normalised as

$$Tr(t^A t^B) = \frac{1}{2}\delta^{AB}, \tag{5.7}$$

and obey the following relations,

$$t^A_{ab} t^A_{bc} = C_F \delta_{ac}, \tag{5.8}$$

$$Tr(T^C T^D) = f^{ABC} f^{ABD} = C_A \delta^{CD}, \tag{5.9}$$

where

$$C_F = \frac{N_c^2 - 1}{2N_c}, \quad C_A = N_c. \tag{5.10}$$

The field strength tensor is derived from the gluon field G_μ^A,

$$F_{\mu\nu}^A(x) = \partial_\mu G_\nu^A(x) - \partial_\nu G_\mu^A(x) - g_s f^{ABC} G_\mu^B G_\nu^C, \tag{5.11}$$

where g_s is the strong coupling, which determines the strength of the interaction between coloured fields, and f^{ABC}, with $A, B, C = 1, ...8$, are the structure functions of QCD which satisfy the Jacobi identity,

$$f_{ABE} f_{ECD} + f_{CBE} f_{AED} + f_{DBE} f_{ACE} = 0. \tag{5.12}$$

The Feynman rules for qq, qg and gg interactions can then be obtained by expanding expression (5.2) term by term,

$$\mathcal{L}_{cl} = \underbrace{-\frac{1}{4}\left(\partial_\mu G_\nu^A(x) - \partial_\nu G_\mu^A(x)\right)\left(\partial^\mu G_A^\nu(x) - \partial^\nu G_A^\mu(x)\right)}_{\text{kinetic gluon term}} +$$

$$\underbrace{\sum_q \bar{\psi}_q^r(x)\left(i\gamma^\mu \partial_\mu - m_q\right)_{rs}\psi_q^s(x)}_{\text{kinetic and massive quark term}} \underbrace{-g_s G_\mu^A(x)\sum_q \bar{\psi}_q^r(x)\gamma^\mu \left(\frac{\lambda^A}{2}\right)_{rs}\psi_q^s(x)}_{\text{quark-gluon interaction term}} +$$

$$\underbrace{+\frac{g_s}{2} f^{ABC}\left(\partial_\mu G_\nu^A(x) - \partial_\nu G_\mu^A(x)\right)G_\mu^B(x)G_\nu^C(x)}_{\text{3-gluon interaction term}} \underbrace{-\frac{g_s}{4} f^{ABC} f^{ADE} G_\mu^B(x)G_\nu^C(x)G_\mu^D(x)G_\nu^E(x)}_{\text{4-gluon interaction term}}.$$

$$\tag{5.13}$$

QCD is a local gauge theory, therefore one can perform a redefinition of the fields independently at every point in space and time without changing the physical content of the theory. Thus, these redefinitions of the quark and gluon field leads to transformations like,

$$
\begin{aligned}
\psi_q(x) &\to \psi_q'(x) = U(x)\left[\psi_q(x)\right] = \left[e^{i g_s t^A \theta^A(x)}\right] \psi_q(x), \\
G_\mu^A &\to G_\mu'^A(x) = G_\mu^A + \partial_\mu \theta^A(x) + g_s f^{ABC} \theta^B(x) G_\mu^C(x),
\end{aligned}
\tag{5.14}
$$

where $\theta^A(x)$ stands for the set of arbitrarily infinitesimal functions known as gauge angle, from which the physical observables are independent. The covariant derivative transforms in the same way as the field itself,

$$
D_\mu \psi_q(x) \to D'_\mu \psi_q'(x) = \left(\partial_\mu + i g_s t^A G_\mu'^A\right) \psi_q'(x) = U(x)\left[D_\mu\right] \psi_q(x),
\tag{5.15}
$$

then the transformation property for the gluon field is given by

$$
t^A G_\mu'^A = U(x)\, t^A G_\mu^A U^{-1}(x) + \frac{i}{g_s} \left[\partial_\mu U(x)\right] U^{-1}(x).
\tag{5.16}
$$

A straightforward calculation shows that the transformation property of the non-Abelian field strength tensor is

$$
T^A F_{\mu\nu}'^A = U(x) T^A F_{\mu\nu}^A U^{-1}(x).
\tag{5.17}
$$

It is impossible to define a gluon propagator without fixing the gauge first. The Feynman rules can only be properly deduced after a previous insertion of a gauge-fixing term $\mathcal{L}_{gf}$. One possible choice is the Lorenz gauge $\partial_\mu G_A^\mu = 0$,

$$
\mathcal{L}_{fc} = -\frac{1}{2\lambda}(\partial_\mu G_A^\mu)^2,
\tag{5.18}
$$

where λ is a gauge parameter. The Lorenz gauge defines the class of the so-called covariant gauges [103]. By means of expression (5.16), the gluon propagator is written as

$$
i\Delta^{\mu\nu}(k) = -\frac{i}{k^2}\left(g^{\mu\nu} + (\lambda - 1)\frac{k^\mu k^\nu}{k^2}\right),
\tag{5.19}
$$

where k^μ stands for the particles 4-momenta. It is usually defined that $\lambda = 1$ ($\lambda = 0$) represents the Feynman (Landau) gauge. However, in a non-Abelian theory, such as QCD, the gauge-fixing term must be accompanied by terms involving complex scalar fields η^A,

$$
\mathcal{L}_{gt} = \partial_\mu \eta^{A\dagger}(D_{AB}^\mu \eta^B),
\tag{5.20}
$$

and usually called as ghost fields or Faddeev-Popov fields [104, 105]. In fact, it is required the presence of these fields because they properly cancel the non-physical degrees of freedom that one usually encounters in working with covariant gauges[1].

Another possible choice for the gauge-fixing term is the axial gauges,

$$\mathcal{L}_{fc} = \partial_\mu (n^\mu G_\mu^A)^2. \tag{5.21}$$

This kind of choice has the advantage of avoiding the presence of non-physical degrees of freedom, but the disadvantage is that the gluon propagator is more complicated,

$$i\Delta^{\mu\nu}(k) = \frac{i}{k^2} \left(-g^{\mu\nu} + \frac{n^\mu k^\nu + n^\nu k^\mu}{n \cdot k} - \frac{(n^2 + \lambda k^2) k^\mu k^\nu}{(n \cdot k)^2} \right). \tag{5.22}$$

Assuming that $n^2 = 0$ and $\lambda = 0$, then it is called the light-cone gauge also called the physical gauge, because at $k^2 \to 0$ there are only two polarisations,

$$k \cdot \epsilon^{(i)}(k) = 0 \quad \text{and} \quad n \cdot \epsilon^{(i)}(k) = 0, \tag{5.23}$$

where $\epsilon(k)$ stands for the polarisation states.

5.1.2   Renormalisation and the effective coupling

The calculation of Feynman diagrams with loops leads to divergences in the 4-momentum integrals, which must be properly regularised. These divergences can be treated by means of regularisation processes, for instance: adding extra parameters into the theory (infrared mass scale m_g), imposing an *ad hoc* upper integration limit (regularisation with a momentum cutoff in the ultraviolet region) or even working in a space with non-integer dimensions (dimensional regularisation $D = 4 - 2\epsilon$).

An alternative process is the possibility to perform a field rescaling in such a way that the divergences can be absorbed into redefined physical quantities, such as mass, coupling constant and field strength, by means of a renormalisation process of the theory[2]. Although the physical quantities must be independent of the renormalisation scheme, the choice of the perturbative expansion parameter is not unique. Even the renormalisation scales (subtraction points that remove the ultraviolet divergences) are not necessarily the same whenever applied into different processes. The renormalisation process introduces one, or more than

---

[1] This brief introduction on QCD does not aim to discuss Gribov's copies, therefore, it will not be considered here.

[2] Formally, the renormalisation is performed by adding connected Feynman diagrams, *i.e.*, irreducible 2-point Green functions. In a theory such as QCD, it is possible to define a renormalised propagator using products of $\gamma_\Gamma(g_s)$ known as anomalous dimension. Therefore, one is able to find the class of equations which defines the renormalisation group, the Callan-Szymanski equations.

one, scale parameter with mass dimension, but as mentioned the physical observables must be not scale-dependent, and this invariance can be studied by means of the renormalisation group equations. Therefore, the subtraction of ultraviolet divergences leads to the emergence of a renormalisation scale μ, thus all the renormalised quantities turn out to be scale-dependent.

By considering a dimensionless physical observable $\mathcal{R}$, which depends on a single energy scale Q, calculated as a perturbation series in the effective coupling $\alpha_s \equiv \alpha_s(\mu^2) = g_s^2/4\pi$, and supposing either that Q is much bigger than all other dimensionful parameters. Since this renormalisation scale introduces a second mass scale μ, then in the general case $\mathcal{R}$ depends only on the ratio Q^2/μ^2 and the renormalised coupling α_s, but not μ itself,

$$\mathcal{R} \equiv \mathcal{R}\left(\frac{Q^2}{\mu^2}, \alpha_s(\mu^2)\right), \tag{5.24}$$

mathematically, the μ-independence is given by

$$\mu^2 \frac{d}{d\mu^2}\mathcal{R}(Q^2/\mu^2, \alpha_s) = \left(\mu^2 \frac{\partial}{\partial\mu^2} + \mu^2 \frac{\partial\alpha_s}{\partial\mu^2}\frac{\partial}{\partial\alpha_s}\right)\mathcal{R}(Q^2/\mu^2, \alpha_s) = 0. \tag{5.25}$$

This expression can be rewritten in a more compact form,

$$\frac{d}{d\mu^2}\mathcal{R}(e^\tau, \alpha_s) = \left(\frac{\partial e^\tau}{\partial\mu^2}\frac{\partial}{\partial\alpha} + \frac{\partial\alpha}{\partial\mu^2}\frac{\partial}{\partial\alpha}\right)\mathcal{R}(e^\tau, \alpha_s) = 0, \tag{5.26}$$

where it was defined,

$$\tau \equiv \ln\left(\frac{Q^2}{\mu^2}\right), \quad \text{and} \quad \beta(\alpha_s) \equiv \mu^2 \frac{\partial\alpha_s}{\partial\mu^2} = \frac{\partial\alpha_s}{\partial\ln\mu^2}. \tag{5.27}$$

where τ is just a parameter and $\beta(\alpha_s)$ is the so-called beta function of the renormalisation group, and it gives the asymptotic behaviour of the theory in the ultraviolet regime. Since $\partial e^\tau/\partial\mu^2 = -Q^2/\mu^2$, then expression (5.26) can be written as

$$\left(-\frac{Q^2}{\mu^2}\frac{\partial}{\partial\tau} + \mu^2\frac{\partial\alpha_s}{\partial\mu^2}\frac{\partial}{\partial\alpha_s}\right)\mathcal{R}(e^\tau, \alpha_s) = 0, \tag{5.28}$$

hence, taking the limit at $\mu^2 \to Q^2$,

$$\left(-\frac{\partial}{\partial\tau} + \beta(\alpha_s)\frac{\partial}{\partial\alpha_s}\right)\mathcal{R}(e^\tau, \alpha_s) = 0, \tag{5.29}$$

which is known as the renormalisation equation of the QCD group. It is possible to show that $\mathcal{R}(e^\tau, \alpha_s) = \mathcal{R}(1, \alpha_s(\tau)) = \alpha_s(\tau)$ is solution of the above expression (5.29) with boundary condition $\alpha_s(\tau = 0) = \alpha_s(\mu^2) = \alpha_s$. By implicitly defining a new function, the running

coupling $\alpha_s(\tau)$, such that

$$\tau = \int_{\alpha_s(0)}^{\alpha_s(\tau)} \frac{d\alpha'}{\beta(\alpha')}, \tag{5.30}$$

then all the scale dependence in $\mathcal{R}$ enters through the running of the coupling constant. Hence, by taking $\mathcal{R} \equiv \alpha(\tau)$ in expression (5.29) and differentiating (5.30),

$$\frac{d\alpha_s(\tau)}{d\tau} = \beta(\alpha_s(\tau)), \quad \text{and} \quad \frac{d\alpha_s(\tau)}{d\alpha_s} = \frac{\beta(\alpha_s(\tau))}{\beta(\alpha_s)}. \tag{5.31}$$

Once it is known the behaviour of the running coupling then one can predict the variation of $\mathcal{R}$ with any given Q.

The running of the coupling constant is determined by the renormalisation group equation once it is known the β function. In QCD, the β function has the perturbative expansion [1, 4, 5, 106],

$$-\beta(\alpha_s(\tau)) = b_0\alpha_s^2(\tau) + b_1\alpha_s^3(\tau) + b_2\alpha_s^4(\tau) + ..., \tag{5.32}$$

where

$$b_0 = \frac{\beta_0}{4\pi} = \frac{1}{4\pi}\left(11 - \frac{2}{3}N_f\right), \tag{5.33}$$

$$b_1 = \frac{\beta_1}{16\pi^2} = \frac{1}{16\pi^2}\left(102 - \frac{38}{3}N_f\right), \tag{5.34}$$

and N_f stands for the number of active light flavours, $m_q \ll Q$ and terms $b_{\geq 2}$ are dependent on the renormalisation scheme.

By means of the perturbative expansion of the β function, see expression (5.32), and rewriting expression (5.31) as

$$\frac{d\alpha_s(\tau)}{d\tau} \rightarrow \frac{d\alpha_s(Q^2)}{dQ^2/Q^2}, \tag{5.35}$$

then the running of the coupling with the energy scale Q is given by

$$\frac{d\alpha_s(\tau)}{d\tau} = \beta(\alpha_s(\tau)) = Q^2\frac{d\alpha_s(Q^2)}{dQ^2} = -b_0\alpha_s^2(Q^2)\left(1 + \frac{b_1}{b_0}\alpha_s(Q^2) + \frac{b_2}{b_0}\alpha_s^2(Q^2) + ...\right). \tag{5.36}$$

The perturbative expansion of the β function can be truncated so that only the terms b_0 and b_1 survive. As a matter of fact, it is possible to do such thing because physical quantities are usually known up to NLO in perturbative calculations. Therefore, in phenomenology only LO and NLO terms are considered. The corresponding behaviour of $\alpha_s(Q^2)$ can be calculated rewriting expression (5.36) as a geometric series,

$$Q^2\frac{d\alpha_s(Q^2)}{dQ^2} = -b_0\,\alpha_s^2(Q^2)\sum_{n=0}^{\infty}\left(\frac{b_1}{b_0}\,\alpha_s(Q^2)\right)^n = -\frac{b_0\,\alpha_s^2(Q^2)}{1 - \frac{b_1}{b_0}\alpha_s(Q^2)}, \tag{5.37}$$

where it was considered only the first order of perturbation, and the b_n terms in expression (5.32) are written as [1,2]

$$b_n = b_0 \left(\frac{b_1}{b_0} \right)^n . \tag{5.38}$$

Since expressions (5.36) and (5.38) are equivalent up to $\mathcal{O}(\alpha_s^3)$, then the latter one can be used to calculate $\alpha_s^{LO}(Q^2)$ and $\alpha_s^{NLO}(Q^2)$. Hence, the integration of expression (5.31) where the lower limit is the cutoff μ^2, and by means of the definition of the parameter τ, see expression (5.27), takes the form

$$\int_{\alpha_s(\mu^2)}^{\alpha_s(Q^2)} \frac{d\alpha_s(Q^2)}{\beta(\alpha_s)} = \tau = \ln\left(\frac{Q^2}{\mu^2} \right), \tag{5.39}$$

and by expression (5.37),

$$\int_{\alpha_s(\mu^2)}^{\alpha_s(Q^2)} d\alpha_s(Q^2) \left(-\frac{1 - \frac{b_1}{b_0}\alpha_s(Q^2)}{b_0 \alpha_s^2(Q^2)} \right) = \ln\left(\frac{Q^2}{\mu^2} \right), \tag{5.40}$$

where the solution can be obtained by solving the integral. Thus, one gets

$$\frac{1}{b_0 \alpha_s(Q^2)} - \frac{1}{b_0 \alpha_s(\mu^2)} + \frac{b_1}{b_0^2} \ln\left(\frac{\alpha_s(Q^2)}{\alpha_s(\mu^2)} \right) = \ln\left(\frac{Q^2}{\mu^2} \right). \tag{5.41}$$

Collecting terms with explicit dependence on the energy scale Q and on the subtraction point μ, then one finds,

$$-\frac{1}{b_0 \alpha_s(Q^2)} - \frac{b_1}{b_0^2} \ln \alpha_s(Q^2) + \ln Q^2 = -\frac{1}{b_0 \alpha_s(\mu^2)} - \frac{b_1}{b_0^2} \ln \alpha_s(\mu^2) + \ln \mu^2 = C, \tag{5.42}$$

and this expression is nothing more than a c-number. So in principle there ought not to be a problem at all to equal the above expression to a constant C.

The perturbative QCD tells us how the coupling does behave with the renormalisation scale, but it says nothing on the scale itself. Therefore, this scale must be chosen as a fundamental parameter in the theory so that the coupling is set at some reference scale defined by convention. One common choice is to use the neutral vector Z boson mass as reference, $\mu = M_Z \simeq 92$, GeV, which is larger than the typical QCD scale, and thus it is sufficient to ensure that the calculations lies in the perturbative region. Hence, the QCD fundamental parameter is given by the experimental value of $\alpha_s(M_Z^2)$.

A clever way to deal with that arbitrarily C constant is to introduce a dimensional parameter Λ into the definition of the effective coupling $\alpha_s(Q^2)$. This parameter sets the

scale at $\alpha_s \to \infty$. Then expression (5.30) can be rewritten as

$$\ln\left(\frac{Q^2}{\Lambda^2}\right) = \int_{\infty}^{\alpha_s(Q^2)} \frac{d\alpha_s(Q^2)}{\beta(\alpha_s(Q^2))} = \int_{\alpha_s(Q^2)}^{\infty} \frac{d\alpha_s(Q^2)}{b_0\alpha_s^2(\tau) + b_1\alpha_s^3(\tau) + b_2\alpha_s^4(\tau) + \ldots}, \tag{5.43}$$

thus, using the perturbative expansion of the β function, see expression (5.32), and integrating up to $\mathcal{O}(\alpha_s^3)$, one arrives at the precise functional forms at LO and NLO for the running coupling.

Alternatively, it is possible to obtain the same result for the running coupling at LO level, and an approximate one at NLO [1], by defining the constant C as

$$C = \ln\Lambda^2 + \frac{b_1}{b_0^2}\ln b_0, \tag{5.44}$$

so that expression (5.42) are given by

$$\alpha_s(Q^2) = \frac{1}{b_0\left[\ln\left(\frac{Q^2}{\Lambda^2}\right) - \frac{b_1}{b_0^2}\ln(b_0\,\alpha_s(Q^2))\right]} = \frac{1}{b_0\ln\left(\frac{Q^2}{\Lambda^2}\right)\left[1 - \frac{b_1}{b_0^2}\ln(b_0\,\alpha_s(Q^2))/\ln\left(\frac{Q^2}{\Lambda^2}\right)\right]}. \tag{5.45}$$

Expanding into inverse powers of $\ln\left(Q^2/\Lambda^2\right)$ up to 1-order, and using that $1/(1-x) = 1 + x + x^2 + \ldots$, one arrives at the following result

$$\alpha_s(Q^2) = \frac{1}{b_0\ln\left(\frac{Q^2}{\Lambda^2}\right)}\left[1 + \frac{\frac{b_1}{b_0^2}\ln(b_0\,\alpha_s(Q^2))}{\ln\left(\frac{Q^2}{\Lambda^2}\right)}\right] = \underbrace{\frac{1}{b_0\ln\left(\frac{Q^2}{\Lambda^2}\right)}}_{\text{LO term}} + \underbrace{\frac{\frac{b_1}{b_0^2}\ln(b_0\,\alpha_s(Q^2))}{b_0\ln\left(\frac{Q^2}{\Lambda^2}\right)\ln\left(\frac{Q^2}{\Lambda^2}\right)}}_{\text{NLO term}}. \tag{5.46}$$

Hence, the running coupling at LO is obtained by considering only the first term in the *rhs*,

$$\alpha_s^{LO}(Q^2) = \frac{4\pi}{\beta_0\ln\left(\frac{Q^2}{\Lambda^2}\right)}, \tag{5.47}$$

whereas for the case of the running coupling at NLO, both terms must be taken into account, then

$$\alpha_s^{NLO}(Q^2) = \frac{1}{b_0\ln\left(\frac{Q^2}{\Lambda^2}\right)}\left[1 + \frac{\frac{b_1}{b_0^2}\ln(b_0\,\alpha_s^{LO}(Q^2))}{\ln\left(\frac{Q^2}{\Lambda^2}\right)}\right], \tag{5.48}$$

and a straightforward calculation leads to

$$\alpha_s^{NLO}(Q^2) = \frac{4\pi}{\beta_0\ln\left(\frac{Q^2}{\Lambda^2}\right)}\left[1 - \frac{\beta_1}{\beta_0^2}\frac{\ln\ln\left(\frac{Q^2}{\Lambda^2}\right)}{\ln\left(\frac{Q^2}{\Lambda^2}\right)}\right]. \tag{5.49}$$

It is usually said that expressions (5.47) and (5.49) are the 1-loop and 2-loop approximations in perturbation theory.

5.2 The parton model

Confinement prohibits the formation of free states of quarks an gluons, therefore the colourless hadrons observed in laboratory must be somehow linked to coloured quarks and gluons described by QCD. The mechanism, which establishes this link, is known as the parton model and it was built under the hypothesis that hadrons are compounded by punctual particles collectively called partons, thus hadron-hadron interactions results from interactions among these partons. This hypothesis was verified in the late 60's by means of deep inelastic experiments at SLAC [108], and since then many other experiments have performed deep inelastic lepton-hadron scattering at increasingly higher energies and provided some of the most precise tests of perturbative QCD. It also represents the most direct way to probe the internal structure of hadrons

5.2.1 Deep inelastic scattering

It is described by the interaction of a high-energy charged lepton off a nucleon target. This interaction occurs by means of gauge bosons exchange (γ^*, Z^0 for neutral current and $W^{\pm}$ for charged current), where the process with virtual photon exchange has significant contributions for the cross-section compared to those ones with Z^0 and $W^{\pm}$, because massive vector bosons are suppressed due to their mass appearing as a pole in the propagator $1/(Q^2 + M^2)$ [1, 3, 47]. In the final state, it is measured a lepton ℓ and a hadronic state X formed by the nucleon fragmentation,

$$\ell + N \rightarrow \ell' + X. \tag{5.50}$$

There are different names for different kinds of processes. For instance, processes where it is measured only the lepton beyond the final hadronic state X, are usually called as inclusive, see Figure 2.2. There are also the class of semi-inclusive process where it is selected a given final X state or even the exclusive one described by a particular configuration where the nucleon is not completely dissociated.

The inclusive process in reaction (5.50) is represented by the LO perturbative diagram in Figure 5.1, where the incoming and outgoing lepton $4-$momenta (assumed hereafter to be an electron) are labeled by k^{μ} and k'^{μ}, respectively, the momentum of the target (assumed hereafter to be a proton) by P^{μ} and the momentum transfer by $q^{\mu} = k^{\mu} - k'^{\mu}$. Then the standard deep inelastic variables are described by three kinematic invariants, where one
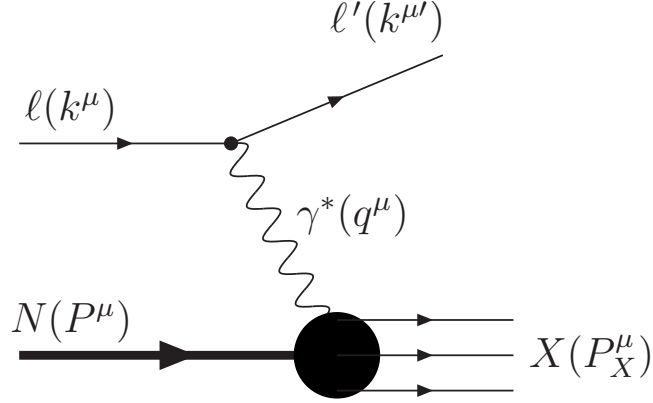
Figure 5.1: LO perturbative Feynman diagram for DIS $ep \to eX$.

of them is the incoming lepton energy E, or alternatively the Mandelstam invariant that represents the CM energy [3, 47],

$$s = (k + P)^2, \tag{5.51}$$

and the other two are usually chosen among the following,

$$Q^2 = -q^2 = (k - k')^2 > 0, \tag{5.52}$$

$$W^2 = (P + q)^2 \tag{5.53}$$

$$\nu = \frac{P \cdot q}{m_p} = \frac{W^2 + Q^2 - m_p^2}{2m_p}, \tag{5.54}$$

$$x = \frac{Q^2}{2P \cdot q} = \frac{Q^2}{2m_p\nu} = \frac{Q^2}{W^2 + Q^2 - m_p^2}, \tag{5.55}$$

$$y = \frac{\nu}{E} = \frac{P \cdot q}{P \cdot k} = \frac{W^2 + Q^2 - m_p^2}{s - m_p^2}, \tag{5.56}$$

where the energy variables refer to the target rest frame, m_p is the proton mass, W^2 is the CM energy squared of γ^*p system, that is the invariant mass squared of the hadronic system X, $\nu = E - E'$ is the transferred energy.

DIS is described by the dimensionless Bjorken variable x defined by expression (5.55). Since $W^2 \geq m_p^2$ and by means of expression (5.55), one finds that $W^2 = m_p^2 + 2p \cdot q(1 - x)$ and hence the Bjorken x variable takes values $0 \leq x \leq 1$. The variable $y = \nu/E$, sometimes called inelasticity, is the fraction of the incoming lepton energy carried by the exchanged photon and also takes values $0 \leq y \leq 1$. A useful relation connecting x, y and Q^2 is

$$xy = \frac{Q^2}{s - m_p^2} \simeq \frac{Q^2}{s}, \quad s \gg m_p. \tag{5.57}$$

The term deep inelastic is related to the kinematic regime where both $m_p \nu \gg m_p^2$ and $Q^2 \gg m_p^p$, with x fixed and finite. Thus one can safely neglect the proton mass with respect to other large energy scales in the process [3].

In the lowest order the inclusive QED cross-section for the $ep \to eX$ scattering can be written in terms of the leptonic $L_{\mu\nu}$ and hadronic $W_{\mu\nu}$ tensors,

$$\frac{d^2\sigma}{dE'd\Omega} = \frac{\alpha_{em}^2}{2m_p Q^4} \frac{E'}{E} L^{\mu\nu} W_{\mu\nu}, \tag{5.58}$$

where $\alpha_{em} = e^2/4\pi \sim 1/137$ is the fine structure constant, also called the electromagnetic coupling constant, and $\Omega \equiv (\theta, \phi)$ is the scattering solid angle. The leptonic tensor is calculated by means of the QED Feynman rules [47],

$$L_{\mu\nu} = \frac{1}{2} \text{Tr} \left[\not{k}\gamma_\mu \not{k}'\gamma_\nu \right] = 2(k_\mu k'_\nu + k_\nu k'_\mu - g_{\mu\nu}k \cdot k'), \tag{5.59}$$

and the hadronic tensor is given by [3]

$$W_{\mu\nu} = \frac{1}{2\pi} \int d^4z \, e^{iq\cdot z} \, \langle P | J_\mu(z) J_\nu(0) | P \rangle, \tag{5.60}$$

where J_μ stands for the current density operator and represents the probability of transition between the initial to the final state, and $|P\rangle$ is the proton eigenstate. The leptonic tensor can be explicitly calculated in any type of vertex. However, since it is not fully understood the confinement mechanism, the hadronic tensor must be written as a parametrisation combining all the possibilities between its 4-momenta P and q in the $\gamma^* p$ vertex [47],

$$W_{\mu\nu} = W_1 g_{\mu\nu} + \frac{W_2}{m_p^2} P_\mu P_\nu + \frac{W_3}{m_p^2} q_\mu q_\nu + \frac{W_4}{m_p^2} \left(q_\mu P_\nu + q_\nu P_\mu \right), \tag{5.61}$$

where W_i are scalar functions of P and q. By means of some constraints, such that: the hadroninc tensor is symmetric, $W_{\mu\nu} = W_{\nu\mu}$; the electromagnetic density current is hermitian, $W_{\mu\nu} = W_{\mu\nu}^*$; and the electromagnetic density current is conserved, $q^\mu W_{\mu\nu} = q^\nu W_{\mu\nu} = 0$. One has that one possible parametrisation is [3, 47, 107]

$$\frac{1}{2m_p} W_{\mu\nu} = \left(-g_{\mu\nu} + \frac{q_\mu q_\nu}{q^2} \right) W_1(P \cdot q, q^2) +$$
$$+ \left[\left(P_\mu - \frac{P \cdot q}{q^2} q_\mu \right) \left(P_\nu - \frac{P \cdot q}{q^2} q_\nu \right) \right] \frac{W_2(P \cdot q, q^2)}{m_p^2}. \tag{5.62}$$

Therefore, the cross-section is written in terms of the two structure functions W_1 and W_2,

$$\frac{d^2\sigma}{dE'd\Omega} = \frac{4\alpha_{em}^2 E'^2}{Q^4} \left(2W_1 \sin^2 \frac{\theta}{2} + W_2 \cos^2 \frac{\theta}{2} \right), \tag{5.63}$$

where θ is the electron scattering angle. It is customary to introduce the dimensionless structure functions,

$$F_1(x, Q^2) \equiv m_p W_1(\nu.Q^2), \tag{5.64}$$

$$F_2(x, Q^2) \equiv \nu W_2(\nu.Q^2). \tag{5.65}$$

In terms of F_1 and F_2, the hadronic tensor reads,

$$W_{\mu\nu} = 2 \left(-g_{\mu\nu} + \frac{q_\mu q_\nu}{q^2} \right) F_1(x, Q^2) + \frac{2}{P \cdot q} \left[\left(P_\mu - \frac{P \cdot q}{q^2} q_\mu \right) \left(P_\nu - \frac{P \cdot q}{q^2} q_\nu \right) \right] F_2(x, Q^2). \tag{5.66}$$

An usual form of the DIS inclusive $ep \to eX$ cross-section, which is typically found in the literature [1, 3, 47, 107], is given in terms of the dimensionless structure function and also x and y variables. But first, one might be able to rewrite the cross-section into cylindric symmetry coordinates,

$$\frac{d^2\sigma}{dE'd\Omega} = \frac{d^2\sigma}{dE'2\pi \sin\theta d\theta}, \tag{5.67}$$

and by means of the Jacobi's determinant,

$$
\begin{aligned}
\frac{d^2\sigma}{dE'd\Omega} &= \frac{1}{2\pi \sin\theta} \left| \frac{\partial(x,y)}{\partial(E',\theta)} \right| \frac{d^2\sigma}{dxdy} \\
&= \frac{1}{2\pi \sin\theta} \left| \begin{matrix} \frac{\partial x}{\partial E'} & \frac{\partial x}{\partial \theta} \\ \frac{\partial y}{\partial E'} & \frac{\partial y}{\partial \theta} \end{matrix} \right| \frac{d^2\sigma}{dxdy} \\
&= \frac{1}{2\pi \sin\theta} \left| \begin{matrix} \frac{2E \sin^2 \frac{\theta}{2}}{M} \left[\frac{E'+(E-E')}{(E-E')^2} \right] & \frac{2EE'}{(E-E')M} \sin\frac{\theta}{2}\cos\frac{\theta}{2} \\ -\frac{1}{E} & 0 \end{matrix} \right| \frac{d^2\sigma}{dxdy} \\
&= \frac{1}{2\pi \sin\theta} \frac{2E'}{(E-E')M} \frac{\sin\theta}{2} \frac{d^2\sigma}{dxdy} \\
&= \frac{E'}{2\pi MEy} \frac{d^2\sigma}{dxdy}. \tag{5.68}
\end{aligned}
$$

Finally, the inclusive cross-section in terms of x and y is given by

$$\frac{d^2\sigma}{dxdy} = \frac{4\pi\alpha_{em}^2 s}{Q^4} \left[xy^2 F_1(x, Q^2) + \left(1 - y - \frac{xym_p^2}{s} \right) F_2(x, Q^2) \right]. \tag{5.69}$$

An alternative derivation of these results is given in terms of the invariants of Mandelstam,

$$s \simeq 2k \cdot P = 2m_p E, \tag{5.70}$$

$$t \simeq -Q^2 = -4EE' \sin^2 \frac{\theta}{2}, \tag{5.71}$$

$$u \simeq -2k' \cdot P = -2m_p E'. \tag{5.72}$$

A straightforward calculation gives,

$$\frac{d^2\sigma}{dtdu} = \frac{4\pi\alpha_{em}^2}{t^2s^2}\frac{1}{s+u}\left[(s+u^2)xF_1(x,t) - usF_2(x,t)\right],\tag{5.73}$$

where there is a relation among the Bjorken variable x and the invariants of Mandelstam,

$$x = \frac{Q^2}{2P\cdot q} = \frac{Q^2}{2k\cdot p - 2k'\cdot p} = \frac{-t}{s+u}.\tag{5.74}$$

In principle, measurements of cross-section (5.69) at different values of x and y, or either the cross-section as given by expression (5.73), allows one to determine the structure functions $F_1(x,Q^2)$ and $F_2(x,Q^2)$. However, since the contribution of $F_1(x,Q^2)$ to the cross-section is relatively small, the measurements are usually performed only to determine $F_2(x,Q^2)$, thus $F_1(x,Q^2)$ is theoretically estimated. In Figure 5.2 is depicted different measurements of $F_2(x,Q^2)$ at different values of x and Q^2, obtained by ZEUS, H1, NMS, BDCMS and E665 experiments [109]. The values of F_2 at $x \sim 0.25$ are in the region where it was originally observed the scaling invariance at SLAC.

5.2.2   Bjorken scaling

In DIS, the signal that there are actually structureless particles inside the proton is that a short wavelength photon beam resolves the quarks within the proton provided that $\lambda(\simeq 1/\sqrt{Q^2}) \ll 1$ fermi. Thus, the $ep \to eX$ cross-section described by expression (5.64), or similarly by expressions (5.69) and (5.73), suddenly starts behaving like that one for free Dirac particle, and expression (5.64) turns into the cross-section for a generic electron-lepton elastic scattering process, as in the case of $e\mu \to e\mu$ given by the Mott formula [47],

$$\frac{d^2\sigma}{dE'd\Omega} = \frac{4\alpha^2 E'^2}{q^2}\left(\cos^2\frac{\theta}{2} - \frac{q^2}{2m^2}\sin^2\frac{\theta}{2}\right)\delta\left(\nu + \frac{q^2}{2m^2}\right).\tag{5.75}$$

Thus, the proton structure functions become,

$$2m_p W_1^{point}(\nu, Q^2) = 2F_1^{point}(\nu, Q^2) = \frac{Q^2}{2m_p^2\nu}\delta\left(1 - \frac{Q^2}{2m_p\nu}\right)$$

$$\nu W_1^{point}(\nu, Q^2) = F_2^{point}(\nu, Q^2) = \delta\left(1 - \frac{Q^2}{2m_p\nu}\right).\tag{5.76}$$

Therefore, these point-like structure functions depend only on the ratio $Q^2/2m_p\nu$, instead of Q^2 and ν, independently. However, this is not the case in elastic ep scattering, because protons actually have structure and it can be properly implemented by introducing

a form factor $G^2(Q^2)$,

$$
\begin{aligned}
2m_p W_1^{elastic}(\nu, Q^2) = 2F_1^{elastic}(\nu, Q^2) &= \frac{Q^2}{2m_p^2\nu} G^2(Q^2)\delta\left(1 - \frac{Q^2}{2m_p\nu}\right) \\
\nu W_1^{elatic}(\nu, Q^2) = F_2^{elastic}(\nu, Q^2) &= G^2(Q^2)\delta\left(1 - \frac{Q^2}{2m_p\nu}\right),
\end{aligned}
\tag{5.77}
$$

thus the structure functions cannot be rearranged to be functions of a single dimensionless variable. When Q^2 increases above 0.71 GeV^2, as a dipole-like picture for the form factor this value reflects the inverse size of the proton, the form factor weaken the chance of elastic scattering, so the proton is more likely to break up. Hence, at the high-energy limit, when asymptotically one has

$$
\nu, Q^2 \to \infty, \quad \text{but the ratio} \quad x = \frac{Q^2}{2m_p\nu} \to \text{fixed},
\tag{5.78}
$$

now called the Bjorken limit, structure functions F_1 and F_2 should approximately scale, *i.e.* depend only on x [110, 111],

$$
F_i(x, Q^2) \to F_i(x).
\tag{5.79}
$$

One might be able to conclude that in a process such as DIS, the virtual photon probes the proton as a bag of spin $1/2$ particles.

5.3 The original parton model

In the late 60's, the experimental verification that in the Bjorken limit the structure functions are only x-dependent gave birth to the parton model. It is based on the assumption that the virtual photon incoherently scatters off the constituents of the nucleon, which in the limit at $Q^2 \to \infty$ are treated as free particles, see Figure 5.3. The parton model is most easily formulated in the infinite momentum frame in which the proton is moving very fast, $p^\mu = (P, 0, 0, P)$ with $P \gg m_p$. In this picture, the quarks are essentially free during the time interval of interaction with the virtual photon, since there are effects of Lorentz contraction (the longitudinal size of the proton is contracted by a factor of m_p/P with respect to its original size in the rest frame), therefore the $\gamma^* p$ interaction time scales are much smaller than the interaction time among quarks itself [1, 112].

Various types of point partons make up the proton, and each one of them carry a small fraction x of their host proton's momentum and energy. Following this line of thought, the ep interaction can be properly written as an incoherent sum of scattering probabilities

ZEUS
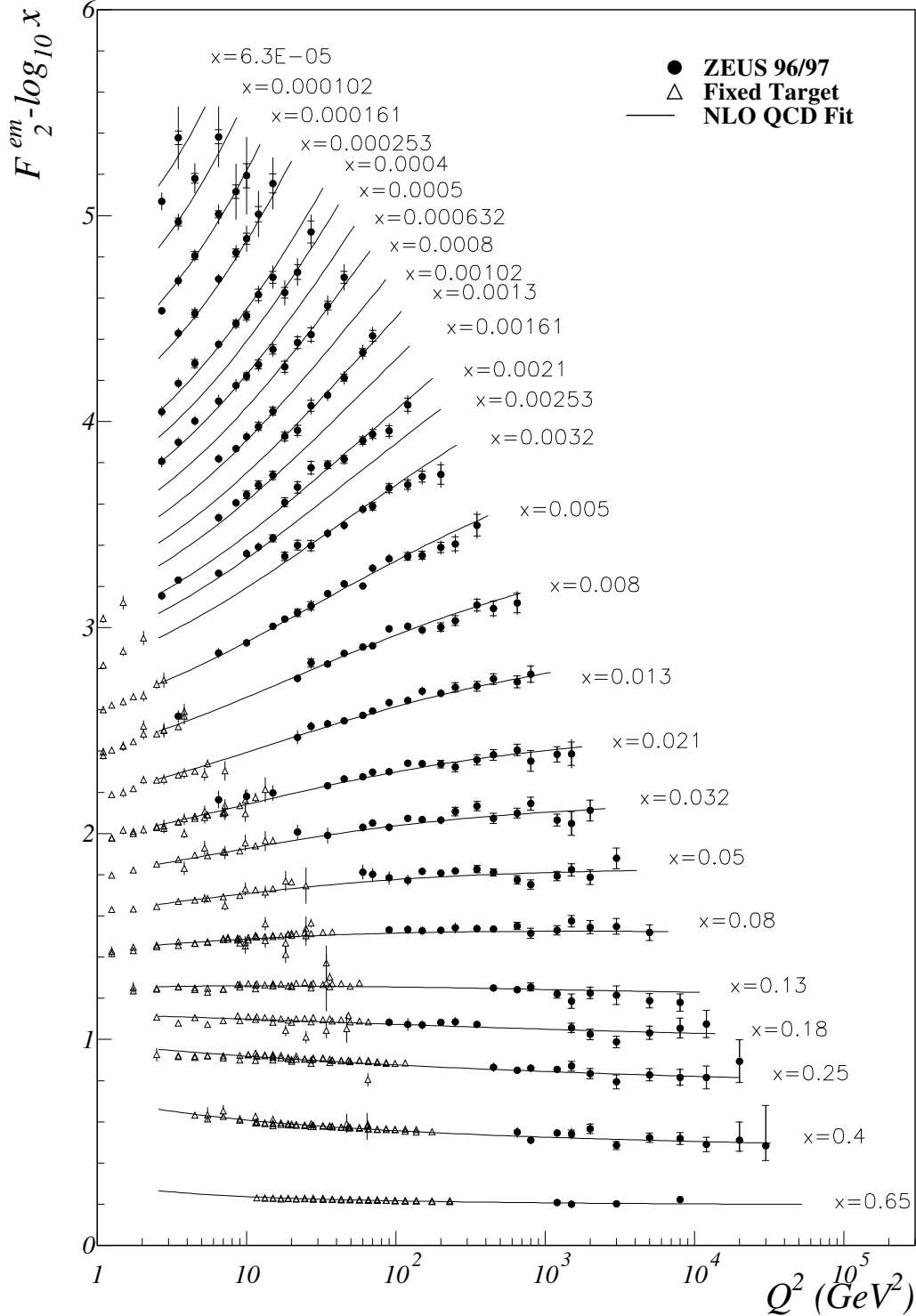
Figure 5.2: Measurements of the structure function $F_2(x, Q^2)$ for several x-values. Respectively, measurements at at low-Q^2 were obtained by the NMS, BDCMS and E665 fixed target experiments, and those ones at high-Q^2 were obtained by the ZEUS and H1 experiments [109].

among the electrons and free quarks,

$$\left(\frac{d^2\sigma}{dxdy}\right)_{ep\to eX} = \sum_q \int_0^1 d\xi \, f_q(\xi) \left(\frac{d^2\sigma}{dxdy}\right)_{eq_i\to eq_i}, \tag{5.80}$$

where $f_q(\xi)$ are the quark distribution functions and $d\xi \, f_q(\xi)$ are the probability to find a quark q carrying a fraction of the proton's momentum between ξ e $\xi + d\xi$, with $0 \le \xi \le 1$. The actual number of partons within the proton is given by [47]

$$N_q = \int_0^1 d\xi \, f_q(\xi), \tag{5.81}$$

and by conservation of momentum, the sum over all fractions carried by each partons must equal the proton's momentum,

$$\sum_q \int_0^1 d\xi \, \xi \, f_q(\xi) = 1. \tag{5.82}$$

To obtain the structure function $F_2(x, Q^2)$, first it is necessary to calculate the elementary $eq_i \to eq_i$ cross-section [1, 107],

$$\left(\frac{d^2\sigma}{dxdy}\right)_{eq} = \frac{2\pi\alpha_{em}^2 e_q^2}{Q^4}\left[1 + (1-y)^2\right]\delta(x - \xi), \tag{5.83}$$

where e_q stands for the quark electric charge. The mass-shell condition[3] for the outgoing
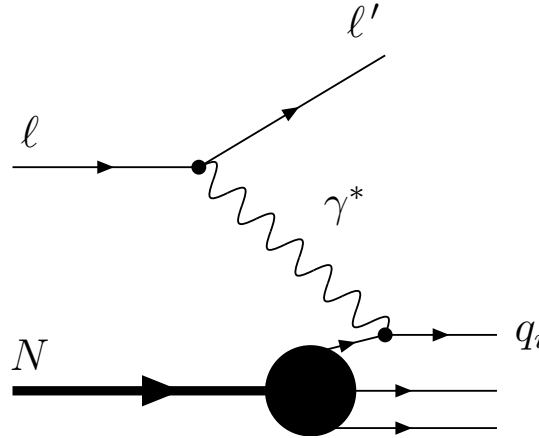
Figure 5.3: Parton model DIS diagram. The virtual photon interacts with a parton within the proton.

---

[3] A real particle is in the mass-shell when $p^\mu = p = (E, \vec{p})$ and satisfies $p^2 \equiv p \cdot p = E^2 - \vec{p}^2 = m^2 = m^2$. In the case of a virtual particle, $p^2 \ne m^2$. More specifically, for a virtual photon $q^2 \ne 0$.

quark with $Q^2 \gg m_q^2$,

$$p_q' = (p_q + q)^2 = q^2 + 2p_q \cdot q = -2P \cdot q(x - \xi) = 0, \tag{5.84}$$

implies $x = \xi$, and justifies $\delta(x - \xi)$ in expression (5.84). Within the elementary $eq_i \to eq_i$ cross-section, see expression (5.83), the differential cross-section for the quark scattering is written as

$$\frac{d^2\sigma}{dxdy} = \sum_q \int_0^1 d\xi \, f_q(\xi) \frac{2\pi\alpha_{em}^2 e_q^2}{Q^4} \left[1 + (1 - y)^2\right] \delta(x - \xi). \tag{5.85}$$

By comparing this result with expression (5.69), and neglecting the m_p, one finds the parton model prediction for the structure functions,

$$F_2(x) = 2xF_1(x) = x \sum_q e_q^2 \int_0^1 d\xi \, f_q(\xi) \, \delta(x - \xi) = \sum_q e_q^2 \, x \, f_q(x). \tag{5.86}$$

This result is known as the Callan-Gross relation [113] and suggests that the structure function $F_2(x)$ probes a quark with momentum fraction $x = \xi$. Therefore, the measured structure function is in fact a distribution in x rather than a delta function, such that the quarks carry a range of momentum fractions, see Figure 5.2. The Callan-Gross relation is a direct consequence of the fermionic nature of the quarks [1, 3].

The measurements of the structure function F_2 can be used to reveal the internal structure of hadrons. In the case of $ep \to eX$ process, neglecting the presence of c quarks and also heavier quarks, expression (5.86) can be written as [1, 47]

$$\frac{1}{x}F_2^{ep}(x) = \left(\frac{2}{3}\right)^2 [u^p(x) + \bar{u}^p(x)] + \left(\frac{1}{3}\right)^2 [d^p(x) + \bar{d}^p(x)] + \left(\frac{1}{3}\right)^2 [s^p(x) + \bar{s}^p(x)]. \tag{5.87}$$

where it was used the following notation for the quark distribution functions,

$$\begin{aligned} f_u(x) &= u(x) = u_V(x) + u_S(x) \\ f_{\bar{u}}(x) &= \bar{u}(x) = u_S(x) \\ f_d(x) &= d(x) = d_V(x) + d_S(x) \\ f_{\bar{d}}(x) &= \bar{d}(x) = \bar{d}_S(x) \\ f_s(x) &= s(x) = s_S(x) = \bar{s}(x). \end{aligned} \tag{5.88}$$

Hadrons are formed by two different kinds of quarks: the valence ones (V), which define each type of known hadron, and the sea quarks (S), which come in pairs of virtual $q\bar{q}$ created by the vacuum polarisation of the colour field. Since protons and neutrons form a isospin doublet (same spin-1/2, $m_p \sim m_n$, and interacts by means of the strong force) it is said

that protons and neutrons are different quantum states of the same entity called nucleon. Therefore, its structure functions are correlated. Since there are many u quarks within the proton as d quarks within the neutron, then the distribution functions of these quarks will be the same, $u^p(x) = d^n(x)$, and in the same way $d^p(x) = u^n(x)$ e $s^p(x) = s^n(x)$. So, the structure function of neutrons is given by [47]

$$\frac{1}{x} F_2^{en}(x) = \left(\frac{2}{3}\right)^2 [u^n(x) + \bar{u}^n(x)] + \left(\frac{1}{3}\right)^2 [d^n(x) + \bar{d}^n(x)] + \left(\frac{1}{3}\right)^2 [s^n(x) + \bar{s}^n(x)]. \quad (5.89)$$

In first approximation, one can consider that sea quark constituents, which are lighter than the valence ones, occur with the same frequency and same momentum distribution,

$$u_M(x) = \bar{u}_S(x) = d_S(x) = \bar{d}_S(x) = s_S(x) = \bar{s}_S(x) = S(x), \quad (5.90)$$

where $S(x)$ stands for the momentum distribution of the sea quarks. Moreover, since protons and neutrons do not have valence $\bar{u}, \bar{d}$ and $\bar{s}$ quarks, hence

$$\begin{aligned} u - \bar{u} &= u - \bar{u}_M = u - u_M = u_V, \\ d - \bar{d} &= d - \bar{d}_M = d - d_M = d_V, \\ s - \bar{s} &= s_M - \bar{s}_M = 0. \end{aligned} \quad (5.91)$$

By integrating these relations, one obtains the number of valence quarks in a proton (neutron),

$$\int_0^1 dx \, [u(x) - \bar{u}(x)] = 2 \, (1) \quad (5.92)$$

$$\int_0^1 dx \, [d(x) - \bar{d}(x)] = 1 \, (2) \quad (5.93)$$

$$\int_0^1 dx \, [s(x) - \bar{s}(x)] = 0. \quad (5.94)$$

Respectively, the proton structure function, see expression (5.87), can be written in the form,

$$\begin{aligned} \frac{1}{x} F_2^{ep} &= \left(\frac{2}{3}\right)^2 [u_V + u_S + \bar{u}_V + \bar{u}_S] + \left(\frac{1}{3}\right)^2 [d_V + d_S + \bar{d}_V + \bar{d}_S] + \left(\frac{1}{3}\right)^2 [S + S] \\ &= \left(\frac{2}{3}\right)^2 [u_V + S + S] + \left(\frac{1}{3}\right)^2 [d_V + S + S] + \left(\frac{1}{3}\right)^2 [S + S] \\ &= \frac{1}{9} [4u_V + d_V] + \frac{4}{9} S, \end{aligned} \quad (5.95)$$

and for the neutron structure function, see (5.89),

$$\frac{1}{x}F_2^{en}(x) = \frac{1}{9}\left[u_V + 4d_V\right] + \frac{4}{9}S. \tag{5.96}$$

It is expected that $S(x)$ has a *Bremsstrahlung* spectrum in the region of small-x, since gluons create $q\bar{q}$ sea pairs. The number of sea quarks grows logarithmically at $x \to 0$. Then, in the region $x \sim 0$, the momentum fraction of the valence quarks are much smaller than the one of the sea quark pairs,

$$\lim_{x \to 0} \frac{F_2^{en}(x)}{F_2^{ep}(x)} \to 1, \tag{5.97}$$

as for the case at $x \to 1$, the valence quarks u_V and d_V have most of the hadron's momentum fraction leaving a small amount for the sea, hence [47],

$$\lim_{x \to 1} \frac{F_2^{en}(x)}{F_2^{ep}(x)} \to \frac{u_V + 4d_V}{4u_V + d_V}. \tag{5.98}$$

Although the success of the parton model with respect to the experimental verification of Bjorken scaling, there was still some kind of anxiety by the scientific community. The hypothesis that quarks behave like free particles in small distances seems inconsistent with the lack of direct measurements of quarks, whose confinement suggested a different behaviour. Despite the theoretical issues, the DIS measurements have shown that the sum over all fraction of momentum carried by the quarks within the proton did not equal to 1, see expression (5.82), but only 50% of the total proton's momentum. By summing up all the parton's momenta, one should arrive at the total proton's momentum,

$$\int_0^1 dx\, xp\left[u + \bar{u} + d + \bar{d} + s + \bar{s}\right] = p - p_g, \tag{5.99}$$

therefore this difference must be related to the momentum of neutral partons. However, they are not detected in direct measurements of DIS. By multiplying expression (5.99) and defining the neutral parton's momentum fraction $\epsilon_g \equiv p_g/p$,

$$\int_0^1 dx\, x\left[u + \bar{u} + d + \bar{d} + s + \bar{s}\right] = 1 - \epsilon_g. \tag{5.100}$$

By means of expressions (5.95) and (5.96), and neglecting the s quark's momentum since their contribution are rather small, then

$$\begin{aligned}
\int_0^1 dx\, xF_2^{ep}(x) &= \frac{4}{9}\int_0^1 dx\, x\left[u + \bar{u}\right] + \frac{1}{9}\int_0^1 dx\, x\left[d + \bar{d}\right] = \frac{4}{9}\epsilon_u + \frac{1}{9}\epsilon_d = 0.18, \\
\int_0^1 dx\, xF_2^{en}(x) &= \frac{1}{9}\int_0^1 dx\, x\left[u + \bar{u}\right] + \frac{4}{9}\int_0^1 dx\, x\left[d + \bar{d}\right] = \frac{1}{9}\epsilon_u + \frac{4}{9}\epsilon_d = 0.12,
\end{aligned} \tag{5.101}$$
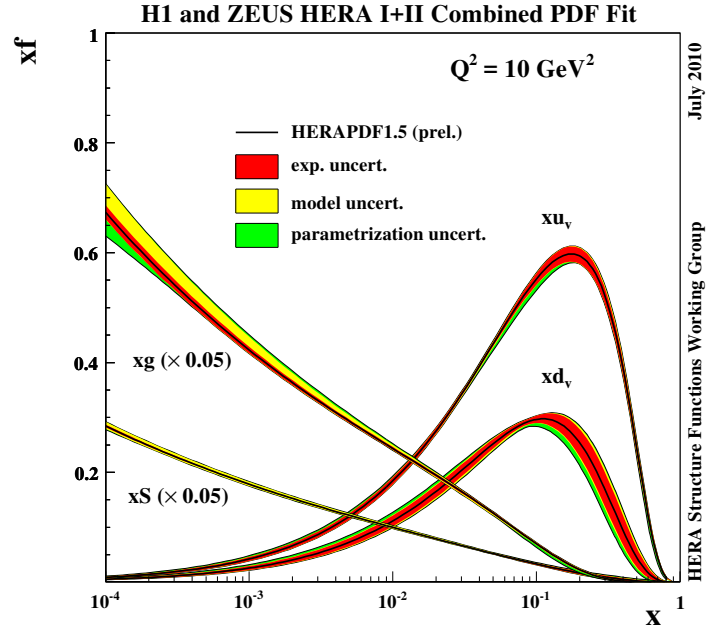
Figure 5.4: Partons distribution within a proton [114].

where ϵ_u and ϵ_d stand for the momentum fractions carried by $(u + \bar{u})$ and $(d + \bar{d})$, and $\epsilon_g \sim 1 - \epsilon_u - \epsilon_d$, thus one arrives at $\epsilon_u = 0.36$, $\epsilon_d = 0.18$ and $\epsilon_g = 0.48$, respectively.

Therefore, half of the total amount of the proton's momentum is carried by these neutral partons, which in fact were not detected in DIS ep experiments. Only with QCD and the asymptotic behaviour of the effective coupling at $\alpha_s(Q^2 \to \infty) \to 0$ justifies the theoretical hypothesis that quarks are asymptotic free in small distances of order Q^{-1}. In addition, the presence of gluons, which evince that they carry the other half of the proton's momentum, and also they are the gauge bosons of the strong force where the coupling is therefore given by the colour quantum number. These results, plus the experimental verification that in some kinematic regions the Bjorken scaling is broken has led to the formulation of the QCD parton model. In Figure 5.4 are depicted the partons distributions, respectively [114].

5.4   The parton model and QCD

The original parton model, see Figure 5.3, is only the zeroth-order approximation of the $\gamma^* N$ scattering. After all, the partonic constituents within hadrons are not free objects, they are in fact described by QCD. It was shown in the last section that at the asymptotic Bjorken limit the structure functions scale, *i.e.* $F(x, Q^2) \to F(x)$. However, one observes that this scaling is broken in QCD and structure functions appear to depend on logarithms
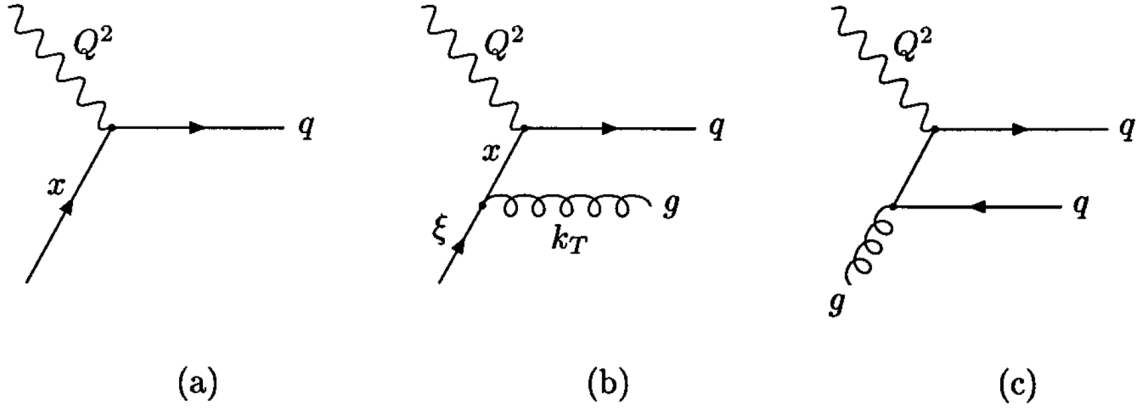
Figure 5.5: DIS partonic process diagrams: (a) zeroth-order diagram related to the original parton model, (b,c) QCD $\mathcal{O}(\alpha_s)$ diagrams related to the QCD parton model.

of Q^2. According to perturbative QCD, new subprocess can contribute to the DIS cross-sections, *e.g.*, a quark can emit a gluon and acquire large transverse momentum k_T, see Figure 5.5(b), thus the integrals extend up to the kinematic limit at $k_T^2 \sim Q^2$ and leads to contributions proportional to $\alpha_s \ln Q^2$, which break scaling.

In the case of collinear singularity, *i.e.* in the limit at $t \to 0$ the gluon is emitted parallel to the quark, the contribution of diagram (b) from Figure 5.5 to the structure function $F_2(x, Q^2)$ leads to divergences at $k_T^2 = 0$. To calculate this emission, one must take into account all the possible values of ξ and k_T that describe the collinear gluon. More specifically, the logarithms of Q^2 appear through out the integration over the gluon momentum spectrum emission [115],

$$\frac{\alpha_s}{2\pi} \int_{\kappa^2}^{Q^2} \frac{dk_T^2}{k_T^2} = \frac{\alpha_s}{2\pi} \ln\left(\frac{Q^2}{\kappa^2}\right), \tag{5.102}$$

where the upper limit of integration is defined by the photon virtuality Q^2 interacting within the quarks, and the κ in the lower limit stands for an infrared arbitrary parameter responsible to regularise the divergence at $k_T^2 = 0$. Hence, once it is known the single gluon vertex contribution[4], see expression (5.102), it can be shown that the structure function is given by [3]

$$F_2(x, Q^2) = \sum_q e_q^2 \, x \int_x^1 \frac{d\xi}{\xi} f_q(\xi) \left\{ \delta\left(1 - \frac{x}{\xi}\right) + \frac{\alpha_s}{2\pi}\left[P_{qq}\left(\frac{x}{\xi}\right)\ln\left(\frac{Q^2}{\kappa^2}\right) + h\left(\frac{x}{\xi}\right)\right] + ... \right\}, \tag{5.103}$$

where P_{qq} are the splitting functions and $h(x/\xi)$ is a finite function, respectively. The

---

[4] The contribution of diagram with n-gluon emission is proportional to $[\alpha_s \ln(Q^2/\kappa^2)]^n$.

zeroth-order term in expression (5.103) reflects the original parton model[5], see expression (5.86), with $\xi = x$. After the gluon emission, the momentum fraction ξ carried by the quark reduces to x, then the integration limit is now given at $x \leq \xi < 1$.

The presence of logarithms of Q^2 and κ implies the non-convergence of the perturbative expansion in expression (5.103), as the $\ln Q^2$ terms can be rather large. Following the same path as the renormalisation of the ultraviolet divergences [3], the collinear divergences can be properly absorbed by defining a factorisation scale μ_f, which plays a similar role to the renormalisation scale,

$$\ln\left(\frac{Q^2}{\kappa^2}\right) = \ln\left(\frac{Q^2}{\mu_f^2}\right) + \ln\left(\frac{\mu_f^2}{\kappa^2}\right), \tag{5.104}$$

and by convenience the $h(x/\xi)$ will be rewritten as

$$h(z) = h^{(1)}(z) + h^{(2)}(z), \tag{5.105}$$

where the singularity $\ln\left(\mu^2/\kappa\right)$ and the term $h^{(2)}(z)$ will be absorbed into a redefinition of the quark distribution function,

$$f_q(x, \mu_f^2) = f_q(x) + \frac{\alpha_s}{2\pi} \int_x^1 \frac{d\xi}{\xi} f_q(\xi) \left[P_{qq}\left(\frac{x}{\xi}\right) \ln\left(\frac{\mu_f^2}{\kappa^2}\right) + h^{(2)}\left(\frac{x}{\xi}\right) \right] + \dots \tag{5.106}$$

The separation in expression (5.105) defines the factorisation scheme, and in this case, the structure function F_2 can be written in terms of this renormalised quark distribution,

$$F_2(x, Q^2) = \sum_q e_q^2 x \int_x^1 \frac{d\xi}{\xi} f_q(x, \mu_f^2) C\left(\frac{x}{\xi}, Q^2, \mu_f^2\right), \tag{5.107}$$

where this result is known as the collinear factorisation theorem [1, 3]. The $C\left(z, Q^2, \mu_f^2\right)$, called coefficient function, is given by the renormalised partonic structure function,

$$C\left(z, Q^2, \mu_f^2\right) = \delta(1 - z) + \frac{\alpha_s}{2\pi} \left[P_{qq}(z) \ln\left(\frac{Q^2}{\mu_f^2}\right) + h^{(1)}(z) \right] + \dots \tag{5.108}$$

5.4.1   Scaling violation

Since $F_2(x, Q^2)$ is a physical observable which cannot depend on the unphysical quantity μ^2, then expression (5.107) implies that $f_q(x, \mu_f^2)$ must be finite and analytic. The κ

---

[5] Delta function property,

$$\delta[f(x)] = \sum_i \frac{\delta(x - x_i)}{|f^{(\prime)}(x = x_i)|}, \quad \text{then} \quad \delta\left(1 - \frac{x}{\xi}\right) = \xi\delta(x - \xi).$$

.

parameter can be removed by differentiating expression (5.106) with respect to $\ln Q^2$ at the limit at $\mu_f \to Q^2$,

$$\frac{\partial f_q(x, Q^2)}{\partial \ln Q^2} = \frac{\alpha_s}{2\pi} \int_x^1 \frac{d\xi}{\xi} f_q(\xi, Q^2) P_{qq}\left(\frac{x}{\xi}\right). \tag{5.109}$$

This integral-differential equation is a LO example of a class of evolution equations, namely DGLAP equation [116–119], and it describes how $f_q(x, Q^2)$ evolves with Q^2 by means of an initial scale Q_0, once it is known $f_q(x, Q_0^2)$. The DGLAP equations describe the perturbative QCD correction to the partonic distribution functions effectively resuming contributions of the type $[\alpha_s \ln Q^2]^n$.

At the limit where Q^2 is bigger than the quark masses, the gluon distribution affects the quark and antiquark distributions Q^2-dependence. As a matter of fact the gluon distribution receives contributions from quark and antiquark distributions. Taking into account the diagram (c) from Figure 5.5, where the gluon produces a $q\bar{q}$ pair, therefore complete evolution equation for f_q is given by

$$\frac{\partial f_q(x, Q^2)}{\partial \ln Q^2} = \frac{\alpha_s}{2\pi} \int_x^1 \frac{d\xi}{\xi} \left[f_q(\xi, Q^2) P_{qq}\left(\frac{x}{\xi}\right) + 2N_f\, f_g(\xi, Q^2) P_{qg}\left(\frac{x}{\xi}\right) \right] + \mathcal{O}(\alpha_s^2), \tag{5.110}$$

where $f_g(x, Q^2)$ stands for the renormalised gluon distribution function,

$$\frac{\partial f_g(x, Q^2)}{\partial \ln Q^2} = \frac{\alpha_s}{2\pi} \int_x^1 \frac{d\xi}{\xi} \left[f_q(\xi, Q^2) P_{gq}\left(\frac{x}{\xi}\right) + f_g(\xi, Q^2) P_{gg}\left(\frac{x}{\xi}\right) \right] + \mathcal{O}(\alpha_s^2). \tag{5.111}$$

At leading order the splitting functions are given by

$$P_{qq}(z) = \frac{4}{3} \left(\frac{1 + z^2}{1 - z} \right)_+, \tag{5.112}$$

$$P_{qg}(z) = \frac{1}{2}[z^2 + (1 - z)^2], \tag{5.113}$$

$$P_{gq}(z) = \frac{4}{3} \frac{[1 + (1 - z)^2]}{z}, \tag{5.114}$$

$$P_{gg} = 6 \left[\frac{1 - z}{z} + z(1 - z) + \frac{z}{(1 - z)_+} + \left(\frac{11}{12} - \frac{N_f}{3} \right) \delta(1 - z) \right], \tag{5.115}$$

where the "plus" distributions are defined as

$$\int_0^1 dx\, \frac{f(x)}{(1 - x)_+} = \int_0^1 dx\, \frac{f(x) - f(1)}{1 - x}, \quad \text{where} \quad \frac{1}{(1 - x)_+} = \frac{1}{1 - x}, \quad \text{para } 0 \le x < 1. \tag{5.116}$$

It is possible to properly summarise this result by defining,

$$\mathcal{U}(x, Q^2) = \begin{pmatrix} f_q(x, Q^2) \\ f_g(x, Q^2) \end{pmatrix}, \tag{5.117}$$

thus, expressions (5.110) and (5.111) will be rewritten as

$$\frac{\partial \mathcal{U}(x, Q^2)}{\partial \ln Q^2} = \frac{\alpha_s}{2\pi} \int_x^1 \frac{d\xi}{\xi} \, \mathcal{P}\left(\frac{x}{\xi}, Q^2\right) \mathcal{U}(\xi, Q^2), \tag{5.118}$$

where,

$$\mathcal{P}(z, Q^2) = \begin{pmatrix} P_{qq}(z, Q^2) & 2N_f P_{qg}(z, Q^2) \\ P_{gq}(z, Q^2) & P_{gg}(z, Q^2) \end{pmatrix}. \tag{5.119}$$

The above relation is called splitting matrix, because P_{ij} physically represents the probability that each elementary vertex "j emits i" and has its momentum fraction reduced by a factor z.

The predictions with respect to hard and semi-hard scatterings of hadrons are related to the precise knowledge of the partonic distribution functions. These are universal functions, since they describe the partonic hadronic content at any given scattering. The PDF's, $f_q(x, Q^2)$ and $f_g(x, Q^2)$, used in our QCD-inpired eikonal model are specific for pp and $\bar{p}p$ collisions, where they were obtained by means of a global analysis of all data involving deep inelastic process and some other process involving protons. The better the precision which the data are obtained, and the wider the kinematic region, will lead the scientific community a better understanding of the PDF's. The parametrisation of the PDF reflects its x dependence in an initial Q_0 scale, where its value must be high enough to be in the perturbative region. Some authors adopt $Q_0 = 1$ GeV and parametrisations such that [120]

$$x f_i(x, Q_0^2) = A_i x^{-\lambda_i} (1 - x)^{\eta_i} (1 + \epsilon_i \sqrt{x} + \gamma_i x), \tag{5.120}$$

with $i = u_V, d_V, S$, where S stands for the total sea quark distribution, and $A_i, \lambda_i, \epsilon_i, \eta_i$ e γ_i are determined by the best fit to the data. By means of this parametrisation, it is used the DGLAP equations to evolve $f_i(x, Q^2)$ in all values of x and Q^2 in which there are available experimental data.

It is most noteworthy to state that several authors use different sets of parametrisations, and different choices to deal with uncertainties and correlated systematic errors between new and previous experimental data.

Chapter 6

QCD-inspired eikonal model

It is well known that processes with low-q^2 contribute to most of the total cross-section and also that diffractive reactions cannot be treated perturbatively and calculated in reliable way within QCD. A wide variety of models in high-energy particle scattering belong to the so-called class of QCD-inspired models [121]. These type of models represent an attempt to create a solid background towards a future theoretical description fully based on QCD. Moreover, they aim to describe some hadronic processes linked to the transition region between the perturbative and non-perturbative domains by means of the QCD parton model [122].

The unitarity condition of the scattering S-matrix demands that the absorbed part of the elastic scattering amplitude receives contributions from both the elastic and inelastic channel. Following the impact-parameter picture, this condition can be seen by expressions (2.107) and (2.116). In the QIM the description of the elastic scattering appears as the shadow of the inelastic processes and the diffracted waves will be added up coherently in the forward direction giving rise to a sharp peak at the optical point. Therefore, it implies that the scattering amplitude can be properly addressed in the eikonal approximation, see expression (2.100). A common feature in this kind of models is to consider that part of the growth of the total cross-section at high energies is associated with the rapidly increase of the PDF's, mainly gluons, at small-x.

An analysis made by Amaldi and Schubert [53] at the ISR energy region showed that those models which were constructed through out factorised eikonals in energy and impact-parameter, $e.g.$ $\chi(s,b) = f(s)w(b)$, were incompatible with the experimental results. Henceforth, the QIM narrows the choice of physically motivated eikonals with some kind of hybrid properties, or either sometimes called as semi-factorised, in energy and impact-parameter by means of the QCD parton-model.

Various models fall into the class of QIM [24–29, 123–126]. Albeit they often lack of mathematical rigor, they claim to reformulate old concepts in a modern approach based on QCD. Over the past few decades other attempts have been made to provide a picture of soft diffraction based upon QCD, for instance considering that the growth of the total cross-

section with energy is intrinsically driven by the rise of the gluon contribution, since it gives the dominant contribution at small-x. The break in this kind of approach lies in the well known fact that perturbative QCD is inadequate to deal with low-$|t|$ processes and hence in order to obtain quantitative results each model is strongly dependent on assumptions.

6.1 Non-perturbative QCD effects

The recent measurements of pp elastic, inelastic and total cross-sections at the LHC by the TOTEM Collaboration [17–22] have enhanced the interest in the theoretical and experimental study of hadron-hadron interactions. By the way, it also has become a pivotal source of information for selecting models and theoretical methods. Presently, the LHC provides us with the highest available collider CM energy, $\sqrt{s} = 8$ TeV, but with the possibility to achieve $\sqrt{s} = 13$ TeV latter in the future. At present, one of the main theoretical approaches for the description of the observed increase of hadron-hadron total cross-sections, which was predicted many years ago [127] and accurately verified by experiment [35], is the QCD-inspired formalism, as well as the class of Regge-pole models.

The latter attributes the increase of the total cross-section to the exchange of a colorless state having the quantum numbers of the vacuum, *viz.* the Pomeron [3,11–13]. In the QCD framework a possible interpretation for the Pomeron is that it can be understood as the exchange of at least two gluons in a color-singlet state [128,129]. An interesting model for the Pomeron was evaluated in reference [130], where it was pointed out the importance of the QCD non-perturbative vacuum. One important aspect of this non-perturbative-type physics appears as an infrared gluon mass scale which regulates the divergent behaviour of the Pomeron exchange.

In the QIM approach the energy dependence of the total cross-sections is obtained from the QCD using an eikonal formulation compatible with analyticity and unitarity constraints, as it was already shown before. More precisely, the behaviour of the forward observables is derived from the QCD parton model using standard QCD cross-sections for elementary parton-parton processes, updated sets of PDF's and physically motivated cutoffs that restrict the parton-level processes to semi-hard ones.

These semi-hard processes arise from hard scatterings of partons carrying very small fraction of their host hadron's momenta, leading to the appearance of jets with transverse energy E_T much smaller than the total CM energy available in the hadronic collision. In this picture the scattering of hadrons is an incoherent summation over all possible constituent scattering and the increase of the total cross-sections is directly associated with parton-parton semi-hard scatterings. As it was repeatedly mentioned before, the high-energy dependence of the cross-sections is driven mainly by processes involving the gluon

contribution, since it gives the dominant contribution at small-x. However, despite this scenario being quantitatively understood in the framework of perturbative QCD, the non-perturbative character of the theory is also manifest at the elementary level since at high energies the soft and the semi-hard components of the scattering amplitude are closely related [131, 132]. Thus, in considering the forward scattering amplitude, it becomes important to distinguish between semi-hard gluons, which participate in hard parton-parton scattering, and soft gluons, emitted in any given parton-parton QCD radiation process.

There is no easy way out on the task of describing forward observables in hadron-hadron collision bringing up information about the infrared properties of QCD, but fortunately it can be properly addressed by considering the possibility that the non-perturbative dynamics of QCD generate an effective gluon mass. This dynamical gluon mass is intrinsically related to an infrared finite strong coupling constant, and its existence is strongly supported by recent QCD lattice simulations [91–102] as well as by phenomenological results [24–32, 133–143]. More specifically, a global description of $\sigma_{tot}^{pp,\bar{p}p}(s)$ and $\rho^{pp,\bar{p}p}(s)$ can succeed in a consistent way by introducing a non-perturbative QCD effective charge in the calculation of the parton-level processes involving gluons, which dominate at high-energy and determine the asymptotic behaviour of hadron-hadron cross-sections.

6.1.1 Infrared mass scale

Recently, it has been discussed in the literature some possible ways of merging the non-perturbative aspects of QCD with the perturbative expansion. Somehow, the freezing of the QCD running coupling constant at low-energy scales suggests that, in principle, it could be possible to capture non-perturbative effects in a reliable way [33,34]. The existence of a dynaminal gluon mass is intimately related with the freezing of the running coupling constant [144]. Therefore, it should systematically be present in the perturbative expansion.

One attempt to understand the effects of dynamically massive gluons was performed by Forshaw *et al.* [145]. They have introduced bare massive gluons and study the amplitude for some tree and one-loop diagrams that could be relevant for diffractive scattering. Despite to be instructive, the calculation does not recover the massless QCD result, *i.e.* it does not reproduce the high-energy limit of massless gluons with 2 degrees of freedom. By the way, this is a very good question because in principle for a gluon with a momentum-dependent dynamical mass, even though it is not a physical mass, in the literal and strictly precise meaning of mass, it should still have 3 degrees of freedom. Actually the dynamical masses go to zero at large momenta and it should be expected to recover the elementary cross-sections of perturbative QCD in the high-energy limit. So, how exactly happens this transition $3 \rightarrow 2$ degrees of freedom?

The elementary processes are plagued by infrared divergences, which have to be regu-

larised by means of some cutoff procedure. One natural regulator for these infrared diver-
gences was introduced some time ago [146, 147] and has become an important ingredient
to the class of dynamical mass eikonal models [24–32]. It is based on the increasing evi-
dence that the QCD develops an effective, momentum-dependent mass for the gluons, while
preserving the local $SU(3)_c$ invariance of the theory. This dynamical gluon mass $M_g(Q^2)$
introduces a natural scale that, in principle, sets up a threshold for gluons to pop up from
the vacuum [148, 149]. Moreover, it is intrinsically linked to an infrared-finite QCD effec-
tive charge $\bar{\alpha}_s(Q^2)$, therefore being the natural infrared regulator in this new class of DGM
eikonal model.

Since the gluon mass generation is purely a dynamical effect, the formal tool for tackling
this non-perturbative phenomenon, in the continuum, is provided by the Dyson-Schwinger
equations [150, 151]. These equations constitute an infinite set of coupled nonlinear integral
equation governing the dynamics of QCD Green's functions. The functional forms of M_g
and $\bar{\alpha}_s$, obtained by J.M. Cornwall through the use of the pinch technique in order to derive
a gauge invariant Dyson-Schwinger equation for the gluon propagator and the triple gluon
vertex, are given by [146, 147]

$$\bar{\alpha}_s(Q^2) = \frac{4\pi}{\beta_0 \ln\left[\left(Q^2 + 4M_g^2(Q^2)\right)/\Lambda^2\right]}, \tag{6.1}$$

$$M_g^2(Q^2) = m_g^2 \left[\frac{\ln\left[\left(Q^2 + 4M_g^2(Q^2)/\Lambda^2\right]\right]}{\ln\left(4m_g^2/\Lambda^2\right)}\right]^{-12/11}, \tag{6.2}$$

where $\Lambda(\equiv \Lambda_{QCD})$ is the QCD scale parameter, $\beta_0 = 11 - (2/3)n_f$, n_f stands for the number
of flavors and m_g is an infrared mass scale to be adjusted in order to provide reliable results
concerning calculations of strongly interacting processes. As mentioned in the previous
section, the existence of the gluon mass scale m_g is strongly supported by QCD lattice
simulations and phenomenological results, and its value is typically found to be of the order
$m_g = 500 \pm 200$ MeV. Note that in the limit $Q^2 \gg \Lambda^2$ the dynamical mass $M_g^2(Q^2)$ vanishes
and the effective charge matches with the one-loop perturbative QCD coupling $\alpha_s^{pQCD}(Q^2)$.
It means that the asymptotic ultraviolet behaviour of the LO running coupling, obtained
from the renormalisation group equation perturbation theory, is reproduced in solutions of
Dyson-Schwinger equations,

$$\bar{\alpha}_s(Q^2 \gg \Lambda^2) \sim \frac{4\pi}{\beta_0 \ln(Q^2/\Lambda^2)} = \alpha_s^{pQCD}(Q^2), \tag{6.3}$$

provided only that the truncation method employed in the analysis preserves the multiplica-
tive renormalisability [32]. There is also a different functional expression for the dynamical

gluon mass [152, 153] given by

$$M_g^2(Q^2) = \frac{m_g^4}{Q^2 + m_g^2},\tag{6.4}$$

which is consistent with the asymptotic behaviour of $M_g^2(Q^2)$ in the presence of the gluon condensates [154]. Even though the calculation of the hadronic cross-section does not depend strongly on the specific form of $M_g(Q^2)$, but more on its infrared mass-scale value m_g [24, 27–29, 154].

However, in the infrared region, the coupling $\alpha_s^{pQCD}(Q^2)$ has Landau singularities on the spacelike semiaxis $0 \leq Q^2 \leq \Lambda^2$, *i.e.,* it has a nonholomorphic (singular) behaviour at low Q^2 [155]. This problem has been faced in the past years with analytic versions of QCD whose coupling $\alpha_s(Q^2)$ is holomorphic (analytic) in the entire complex plane except the timelike axis ($Q^2 < 0$) [156–167]. The effective charge $\bar{\alpha}_s(Q^2)$, on the other hand, shows the existence of an infrared fixed point as $Q^2 \to 0$, *i.e.,* the dynamical mass term tames the Landau pole and $\bar{\alpha}_s$ freezes at a finite value in the infrared limit. Thus, providing that the gluon mass scale is set larger than half of the QCD scale parameter, namely $m_g/\Lambda > 1/2$, the analyticity of $\bar{\alpha}_s(Q^2)$ is preserved. This ratio is also phenomenologically determined [24–27, 30–32, 133–143] and typically lies in the interval $m_g/\Lambda \in [1.1; 2]$. More over, as recently pointed out by G. Cvetič [168], the evaluation of renormalisation scale-invariant spacelike quantities at low-Q^2, in terms of infrared freezing couplings, can be done as a truncated series in derivatives of the coupling with respect to the logarithm of Q^2, which in turn exhibit significantly better convergence properties.

6.2   The revised dynamical gluon mass model

In the QCD-based (or "minijet") models the increase of the total cross-sections is associated with semi-hard scatterings of partons in the hadrons. These models incorporate soft and semi-hard processes in the treatment of high-energy hadron-hadron interactions and a consistent calculation must take into account a formulation compatible with analyticity and unitarity constraints.

Following the L. Durand & H. Pi model prescription [124–126], *i.e.* $\Gamma(s, b) = 1 - e^{-\chi(s,b)}$, in the eikonal representation, the cross-sections, ρ-parameter and B-slope still will be written according to expressions (2.108-2.113), but changing $\mathrm{Re}\,\chi \to -\mathrm{Im}\,\chi$ and $\mathrm{Im}\,\chi \to \mathrm{Re}\,\chi$, thus,

$$\sigma_{tot}(s) = 4\pi \int_0^\infty db\, b \left[1 - e^{-\chi_R(s,b)} \cos \chi_I(s, b) \right],\tag{6.5}$$

$$\begin{aligned} \sigma_{inel}(s) &= \sigma_{tot}(s) - \sigma_{el}(s) \\ &= 2\pi \int_0^\infty db\, b \left[1 - e^{-2\chi_R(s,b)} \right], \end{aligned}\tag{6.6}$$

as well as the ρ-parameter,

$$\rho(s) = \frac{-\int_0^\infty db\, b\, e^{-\chi_R(s,b)} \sin\chi_I(s,b)}{\int_0^\infty db\, b\, \left[1 - e^{-\chi_R(s,b)} \cos\chi_I(s,b)\right]}, \tag{6.7}$$

respectively, where as usual s is the square of the total CM energy, b is the impact parameter, the quantity in square brackets in the *rhs* of expression (6.6) stands for the inelastic overlap function $G_{in}(s,b)$, and the complex eikonal function is written as

$$\chi(s,b) = \operatorname{Re}\chi(s,b) + i\operatorname{Im}\chi(s,b) \equiv \chi_R(s,b) + i\,\chi_I(s,b). \tag{6.8}$$

In this picture the probability that neither hadron is broken up in a collision at impact parameter b is therefore given by $P(s,b) = e^{-2\chi_R}(s,b)$.

In this newest version of the DGM model, it was assumed that the eikonal function for pp and $\bar{p}p$ scattering is additive with respect to the soft and semi-hard parton interactions in the hadron-hadron collision,

$$\chi(s,b) = \chi_{soft}(s,b) + \chi_{SH}(s,b). \tag{6.9}$$

In the semi-hard limit of strong interactions hadron-hadron collisions can be treated as an incoherent sum of the interactions among quarks and gluons. More specifically, the QCD cross-section σ_{QCD} is obtained by convoluting the cross-section $\hat{\sigma}$ for the QCD subprocesses with their associated parton distributions. It follows from the QCD parton model that the eikonal $\chi_{SH}(s,b)$ can be factorised as [124–126]

$$\operatorname{Re}\chi_{SH}(s,b) = \frac{1}{2} W_{SH}(b)\,\sigma_{QCD}(s), \tag{6.10}$$

where $W_{SH}(b)$ is an overlap density for the partons at impact parameter space b,

$$W_{SH}(b) = \int d^2 b'\, \rho_A(|\mathbf{b} - \mathbf{b}'|)\, \rho_B(b'), \tag{6.11}$$

and $\sigma_{QCD}(s)$ is the usual QCD cross-section,

$$\begin{aligned}
\sigma_{QCD}(s) = \sum_{ij} \frac{1}{1+\delta_{ij}} \int_0^1 dx_1 \int_0^1 dx_2 \int_{Q_{min}^2}^\infty d|\hat{t}|\, \frac{d\hat{\sigma}_{ij}}{d|\hat{t}|}(\hat{s},\hat{t}) \\
\times f_{i/A}(x_1,|\hat{t}|,|)\, f_{j/B}(x_2,|\hat{t}|)\, \Theta\left(\frac{\hat{s}}{2} - |\hat{t}|\right),
\end{aligned} \tag{6.12}$$

with $|\hat{t}| \equiv Q^2$ and $i,j = q,\bar{q},g$. In the above expression the integration limits satisfy $x_1 x_2 s > 2|\hat{t}| > 2Q_{min}^2$, where Q_{min}^2 is a minimum momentum transfer in the semi-hard

scattering, $\hat{s}$ and $\hat{t}$ are the Mandelstam variables of the parton-parton subsystem, and x_1 and x_2 are the fractions of the momenta of the host hadrons A and B carried by the partons i and j. The term $d\hat{\sigma}_{ij}/d|\hat{t}|$ is the differential cross-section for ij scattering, and $f_{i/A}(x_1, |\hat{t}|)$ $(f_{j/B}(x_2, |\hat{t}|))$ is the usual parton i (j) distribution in the hadron A (B).

The eikonal function is written in terms of even and odd eikonal parts connected by crossing symmetry, similarly to the case of the Durand & Pi model. In the case of the pp and $\bar{p}p$ scatterings, this combination reads

$$\chi^{\bar{p}p}_{pp}(s,b) = \chi^+(s,b) \pm \chi^-(s,b), \tag{6.13}$$

with the even part written in term of soft and semi-hard even eikonals

$$\chi^+(s,b) = \chi^+_{soft}(s,b) + \chi^+_{SH}(s,b), \tag{6.14}$$

and similarly the odd eikonal,

$$\chi^-(s,b) = \chi^-_{soft}(s,b) + \chi^-_{SH}(s,b). \tag{6.15}$$

In the QCD parton model $\chi^-_{SH}(s,b)$ decreases rapidly with increasing s, since the difference between pp and $\bar{p}p$ cross-sections is due only to the different weighting of the quark-antiquark (valence) annihilation cross-sections in the two channels. Hence the crossing-odd eikonal $\chi^-(s,b)$ receives no contribution from semi-hard processes at high energies. As a result, it is sufficient to take $\chi_{SH} = \chi^+_{SH}$ and, consequently, $\chi^- = \chi^-_{soft}$, since the main interest relies on the high-energy scattering region. The connection between the real and imaginary parts of $\chi^+(s,b)$ and $\chi^-(s,b)$ was obtained by means of dispersion relations. It deserves a careful reading, thus it will be discussed in a separated section elsewhere in the text. Henceforth, further details on integral and derivative dispersion relations are in Appendix A.

6.2.1 Energy-dependent form factors

For the overlap densities, the simplest hypothesis is to assume $W_{SH}(b)$ is the same as $W_{soft}(b)$. This prescription is not however true in the QCD parton model, since soft interactions are mainly related to interactions among valence quarks, whilst semi-hard interactions are dominated by gluons. Moreover, a scenario where quarks and gluons exhibit a somewhat different spatial distribution seems plausible [126], since gluons are expected to be distributed around the quarks. Furthermore, in contrast with gluons, quarks have electric charges, and the (matter) distribution of the valence quarks can be associated in a reasonable way with the proton's charge distribution. As a consequence, a commonly used

choice for the soft overlap densities $W^-_{soft}(b)$ and $W^+_{soft}(b)$ comes from the charge dipole approximation to the form factors $G_A(k_\perp)$ and $G_B(k_\perp)$ of the colliding hadrons A and B, see Appendix C.1,

$$
\begin{aligned}
A(b) &= \int d^2 b' \, \rho_A(|\mathbf{b} - \mathbf{b}'|) \, \rho_B(b') \\
&= 2\pi \int_0^\infty dk_\perp \, k_\perp \, J_0(k_\perp b) \, G_A(k_\perp) \, G_B(k_\perp),
\end{aligned}
\tag{6.16}
$$

and

$$
G_A(k_\perp) = G_B(k_\perp) \equiv G_{dip}(k_\perp; \mu) = \left(\frac{\mu^2}{k_\perp^2 + \mu^2} \right)^2.
\tag{6.17}
$$

Here, $\rho(b)$ is the parton density, which gives the probability density for finding a parton in the area $d^2 b$ at impact parameter b, In terms of the form factor it is simply written as

$$
\rho(b) = \frac{1}{2\pi} \int d^2 k_\perp \, G(k_\perp) e^{i\mathbf{k}_\perp \cdot \mathbf{b}}.
\tag{6.18}
$$

Thus, using the dipole form factor $G_{dip}(k_\perp; \mu)$, see Appendix C.2.2,

$$
\begin{aligned}
W^+_{soft}(b; \mu^+_{soft}) &= \frac{1}{2\pi} \int_0^\infty dk_\perp \, k_\perp \, J_0(k_\perp b) \, G^2_{dip}(k_\perp; \mu^+_{soft}) \\
&= \frac{(\mu^+_{soft})^2}{96\pi} (\mu^+_{soft} b)^3 K_3(\mu^+_{soft} b),
\end{aligned}
\tag{6.19}
$$

where μ^+_{soft} is a free adjustable parameter that accounts for the matter (valence quark) distribution inside the hadron. The $W(b; \mu)$ function is normalised so that $\int d^2 W(b; \mu) = 1$. In the same way, the odd soft density is written as

$$
W^-_{soft}(b; \mu^-_{soft}) = \frac{(\mu^-_{soft})^2}{96\pi} (\mu^-_{soft} b)^3 K_3(\mu^-_{soft} b),
\tag{6.20}
$$

where $\mu^-_{soft} \equiv 0.5$ GeV, its value is fixed since the odd eikonal just accounts for the difference between pp and $\bar{p}p$ channels at low energies.

In the case of semi-hard gluons, which dominate at high-energy, it was considered the possibility of a "broadening" of the spatial distribution. Our assumption suggests an increase of the average gluon radius when $\sqrt{s}$ increases. The way for introducing this effect can be paved by looking at previous approaches, particularly in geometrical ones, in which the role of phenomenological energy-dependent form factors is central [169–175]. The assumption considered in this version of the DGM model, based on the QCD parton model, can be properly implemented using two *Ansätze* for the energy-dependent form factors, namely a

monopole,

$$G_{SH}^{(m)}(s, k_\perp; \nu_{SH}) = \frac{\nu_{SH}^2}{k_\perp^2 + \nu_{SH}^2}, \tag{6.21}$$

and a dipole,

$$G_{SH}^{(d)}(s, k_\perp; \nu_{SH}) = \left(\frac{\nu_{SH}^2}{k_\perp^2 + \nu_{SH}^2}\right)^2, \tag{6.22}$$

where $\nu_{SH} = \nu_1 - \nu_2 \ln(s/s_0)$, with $\sqrt{s_0} \equiv 5$ GeV. Here, ν_1 and ν_2 are constants to be fitted. In the case of the monopole the overlap density is, see Appendix C.2.1,

$$
\begin{aligned}
W_{SH}^{(m)}(s, b; \nu_{SH}) &= \frac{1}{2\pi} \int_0^\infty dk_\perp \, k_\perp \, J_0(k_\perp b) \left[G_{SH}^{(m)}(s, k_\perp; \nu_{SH})\right]^2 \\
&= \frac{\nu_{SH}^2}{4\pi}(\nu_{SH} b) K_1(\nu_{SH} b).
\end{aligned}
\tag{6.23}
$$

In analogy with expression (6.19), in the case of the dipole one is led to

$$W_{SH}^{(d)}(s, b; \nu_{SH}) = \frac{\nu_{SH}^2}{96\pi}(\nu_{SH} b)^3 K_3(\nu_{SH} b). \tag{6.24}$$

Notice that, as mentioned earlier, semi-hard interactions dominate at high energies. Thus, it was considered an energy-dependence behaviour for the spatial distribution exclusively in the case of $W_{SH}(s, b)$. In this way, the soft overlap densities $W_{soft}^+(s, b)$ and $W_{soft}^-(s, b)$ will merge only from the "static" dipole form factor, *i.e.*, from expressions (6.19) and (6.20), whereas the semi-hard overlap density $W_{SH}(s, b)$ will be directly associated with expressions (6.23) and (6.24). Moreover, in the semi-hard sector there is another form in which the eikonal can be factorised into the QCD parton model, since now $\text{Re}\,\chi_{SH} = \frac{1}{2}W_{SH}(s, b)\,\sigma_{QCD}(s)$.

6.2.2 Integral dispersion relations and high-energy eikonal

The analyticity of the scattering amplitude $f(s, t)$ leads to dispersion relations with crossing symmetry condition. In the case of elastic processes in the forward direction, the crossing variable is the energy E of the incident particle in the laboratory frame [39]. For an even amplitude, the real and the imaginary parts of $f^+(E)$ are connected by the dispersion relation,

$$\text{Re}\, f^+(E) = \frac{2}{\pi} \mathcal{P} \int_m^\infty dE' \left[\frac{E'}{E'^2 - E^2}\right] \text{Im}\, f^+(E). \tag{6.25}$$

The eikonals are written in terms of even and odd eikonal parts connected by crossing symmetry, namely $\chi_{pp}^{\bar{p}p} = \chi^+ \pm \chi^-$, where χ^+ and χ^- are therefore real analytic functions of E, i.e. they take real values on a real-axis segment, with the same cut structure as f^+ and f^-, respectively. Hence, taking the limit $E \gg m$ and changing the variables from $E \to s$,

one finds that the even eikonal also satisfies the reverse dispersion relation,

$$\text{Im}\,\chi^+(s,b) = -\frac{2s}{\pi}\,\mathcal{P}\int_0^\infty ds'\,\frac{\text{Re}\,\chi^+(s,b)}{s'^2-s^2}, \quad \text{in the limit at } s \gg m. \tag{6.26}$$

Thus, integrating by parts,

$$
\begin{aligned}
\text{Im}\,\chi^+(s,b) &= \lim_{\substack{\epsilon\to 0 \\ s''\to\infty}} -\frac{2s}{\pi}\left[\int_0^{s-\epsilon} ds'\,\frac{\text{Re}\,\chi^+(s',b)}{s'^2-s^2} + \int_{s+\epsilon}^{s''} ds'\,\frac{\text{Re}\,\chi^+(s',b)}{s'^2-s^2}\right] \\
&= \lim_{s''\to\infty} \frac{1}{\pi}\left[\text{Re}\,\chi^+(s'',b)\ln\left(\frac{s''+s}{s''-s}\right) - \int_0^\infty ds'\,\ln\left(\frac{s'+s}{|s'-s|}\right)\frac{d\,\text{Re}\,\chi^+(s',b)}{ds'}\right] \\
&= -\frac{1}{\pi}\int_0^\infty ds'\,\ln\left(\frac{s'+s}{|s'-s|}\right)\frac{d\,\text{Re}\,\chi^+(s',b)}{ds'}, \tag{6.27}
\end{aligned}
$$

where in the last step we have observed that the first term vanishes in the limit $s'' \to \infty$, and it was used,

$$\frac{s}{s'^2-s^2} = \frac{1}{2(s'+s)} - \frac{1}{2(s'-s)}. \tag{6.28}$$

Applying this dispersion relation to $\text{Re}\,\chi_{SH}(s,b) = \text{Re}\,\chi_{SH}^+(s,b) = \frac{1}{2}W_{SH}(s,b)\,\sigma_{QCD}(s)$, one finds,

$$
\begin{aligned}
\text{Im}\,\chi_{SH}(s,b) = &-\frac{1}{2\pi}\int_0^\infty ds'\,\ln\left(\frac{s'+s}{|s'-s|}\right)\left[\sigma_{QCD}(s')\frac{dW_{SH}(s',b)}{ds'}\right] \\
&-\frac{1}{2\pi}\int_0^\infty ds'\,\ln\left(\frac{s'+s}{|s'-s|}\right)\left[W_{SH}(s',b)\frac{d\sigma_{QCD}(s')}{ds'}\right]. \tag{6.29}
\end{aligned}
$$

The second integral on the *rhs* involves the derivatives of the QCD cross section $\sigma_{QCD}(s')$. One should at this point notice that the s' dependence in $d\hat{\sigma}_{ij}/d|\hat{t}|$ terms can be ignored, since their derivatives are of order $1/s'^2$. In this way, the only energy dependence appears in the Heaviside function $\Theta(x-y)$, in which

$$\frac{d}{ds'}\Theta\left(\frac{\hat{s}'}{2} - |\hat{t}|\right) = \frac{d}{ds'}\Theta\left(s' - \frac{2|\hat{t}|}{x_1 x_2}\right) = \delta\left(s' - \frac{2|\hat{t}|}{x_1 x_2}\right), \tag{6.30}$$

where $\hat{s} = x_1 x_2 s$ e $\hat{s}' = x_1 x_2 s'$. The δ-function removes the integration over ds', thus, the second integral can be expressed as

$$
\begin{aligned}
I_2(s,b) &= -\frac{1}{2\pi}\int_0^\infty ds'\,\ln\left(\frac{s'+s}{|s'-s|}\right)W_{SH}(s',b)\frac{d\sigma_{QCD}(s')}{ds'} \\
&= -\frac{1}{2\pi}\sum_{ij}\frac{1}{1+\delta_{ij}}W_{SH}\left(\frac{2|\hat{t}|}{x_1 x_2},b\right)\int_0^1 dx_1\int_0^1 dx_2\int_{Q_{min}^2}^\infty d|\hat{t}|\,\frac{d\hat{\sigma}_{ij}}{d|\hat{t}|}(\hat{s},\hat{t}) \\
&\quad \times f_{i/A}(x_1,|\hat{t}|)f_{j/B}(x_2,|\hat{t}|)\ln\left(\frac{\hat{s}/2+|\hat{t}|}{\hat{s}/2-|\hat{t}|}\right). \tag{6.31}
\end{aligned}
$$

The energy-dependent form factor $W_{SH}(s, b)$ can have a monopole or a dipole form, namely $W_{SH}^{(m)}(s, b; \nu_{SH})$ or $W_{SH}^{(d)}(s, b; \nu_{SH})$, see expressions (6.23) and (6.24). In the case of a monopole-like form, the first integral on *rhs* of (6.29) can be rewritten as

$$
\begin{aligned}
I_1^{(m)}(s, b) &= -\frac{1}{2\pi} \int_0^\infty ds' \ln\left(\frac{s' + s}{|s' - s|}\right) \sigma_{QCD}(s') \frac{dW_{SH}^{(m)}(s', b; \nu_{SH})}{ds'} \\
&= -\frac{b}{8\pi^2} \sum_{ij} \frac{1}{1 + \delta_{ij}} \int_0^\infty \frac{ds'}{s'} \ln\left(\frac{s' + s}{|s' - s|}\right) \int_0^1 dx_1 \int_0^1 dx_2 \int_{Q_{min}^2}^\infty d|\hat{t}| \frac{d\hat{\sigma}_{ij}}{d|\hat{t}|}(\hat{s}', \hat{t}) \\
&\quad \times f_{i/A}(x_1, |\hat{t}|) f_{j/B}(x_2, |\hat{t}|) \left[b\nu_2\nu_{SH}^3 K_0(\nu_{SH} b) - 2\nu_2\nu_{SH}^2 K_1(\nu_{SH} b)\right] \Theta\left(\frac{\hat{s}'}{2} - |\hat{t}|\right), \quad (6.32)
\end{aligned}
$$

and in the case of a dipole-like form factor one finds,

$$
\begin{aligned}
I_1^{(d)}(s, b) &= -\frac{1}{2\pi} \int_0^\infty ds' \ln\left(\frac{s' + s}{|s' - s|}\right) \sigma_{QCD}(s') \frac{dW_{SH}^{(d)}(s', b; \nu_{SH})}{ds'} \\
&= -\frac{b^3}{192\pi^2} \sum_{ij} \frac{1}{1 + \delta_{ij}} \int_0^\infty \frac{ds'}{s'} \ln\left(\frac{s' + s}{|s' - s|}\right) \int_0^1 dx_1 \int_0^1 dx_2 \int_{Q_{min}^2}^\infty d|\hat{t}| \frac{d\hat{\sigma}_{ij}}{d|\hat{t}|}(\hat{s}', \hat{t}) \\
&\quad \times f_{i/A}(x_1, |\hat{t}|) f_{j/B}(x_2, |\hat{t}|) \left[b\nu_2\nu_{SH}^5 K_2(\nu_{SH} b) - 2\nu_2\nu_{SH}^4 K_3(\nu_{SH} b)\right] \Theta\left(\frac{\hat{s}'}{2} - |\hat{t}|\right). \quad (6.33)
\end{aligned}
$$

The soft eikonal is needed only to describe the lower-energy forward data, since the main contribution to the asymptotic behaviour of the hadron-hadron total cross-section comes from parton-parton semi-hard collisions. Therefore, it is enough to build an instrumental parametrisation for the soft eikonal with terms dictated by the Regge-Gribov phenomenology [66–68, 176, 177]. For the even part of the soft eikonal it was taken,

$$
\chi_{soft}^+(s, b) = \frac{1}{2} W_{soft}^+(b; \mu_{soft}^+) \left\{ A' + \frac{B'}{(s/s_0)^\gamma} e^{i\pi\gamma/2} - i\, C' \left[\ln\left(\frac{s}{s_0}\right) - i\frac{\pi}{2}\right] \right\}, \quad (6.34)
$$

where $\sqrt{s_0} \equiv 5$ GeV and A', B', C', γ and μ_{soft}^+ are fitting parameters. The phase factor $e^{i\pi\gamma/2}$, which ensures the correct analyticity properties of the amplitude, is a result of the integral dispersion relation (6.25).

The odd eikonal $\chi^-(s, b)$ which accounts for the difference between pp and $\bar{p}p$ channels and vanishes at high-energy, is given by

$$
\chi^-(s, b) = \frac{1}{2} W_{soft}^-(b; \mu_{soft}^-) D' \frac{e^{-i\pi/4}}{\sqrt{s/s_0}}, \quad (6.35)
$$

where D', the strength of the odd term, is also a fitting parameter. The expression (6.35) was written with its correct analyticity property, since the phase factor $e^{-i\pi/4}$ is a result of

the dispersion relation,

$$\mathrm{Im}\,\chi^-(s,b) = -\frac{2s^2}{\pi}\mathcal{P}\int_0^\infty ds'\,\frac{\mathrm{Re}\,\chi^-(s',b)}{s'(s'^2 - s^2)}, \quad \text{valid at } s \gg m. \tag{6.36}$$

6.2.3 The role of gluons

The calculation of the QCD cross-section implies the sum over all possible parton types, but it is sufficiently accurate for our purpose in this new version of the DGM model to fix the number of flavors $n_f = 4$ and keep only the gluon g and the quarks u, d, s and c. As a matter of fact $\mathrm{Re}\,\chi_{SH}(s,b)$ and $\mathrm{Im}\,\chi_{SH}(s,b)$ have to be determined taking into account all the heavy quarks, where each heavy quarks $h = c, b, t$ with mass M_h is effectively decoupled from physical cross-section at momenta scales below the threshold $Q_h = M_h$, n_f being an increasing function of Q_h.

However, our numerical results show that the contributions of the quarks b and t to χ_{SH} are very small indeed. In fact even the charm contribution is tiny, and was included only for high-precision purposes. Hence, there is no fundamental role for heavy quarks $(m_q \approx M_h,\ h = c, b, t)$ in our analyses, and this result can be understood as follows: heavy quarks are produced, perturbatively, from the splitting of gluons into $\bar{h}h$ pairs at energies above the threshold $Q_h = M_h$. At sufficiently small-x, the ratio of the heavy-quarks parton distribution function, $h(x, Q^2)$, to the gluon one, $g(x, Q^2)$, is [178–181]

$$\frac{h(x, Q^2)}{g(x, Q^2)} \sim \frac{\alpha_s(Q^2)}{2\pi}\ln\left(\frac{Q^2}{M_h^2}\right), \tag{6.37}$$

where $h(x, Q^2) = 0$ at $Q = M_h$. However, the angular dependencies of the dominant subprocesses in (6.12) are very similar and all dominated by the t-channel angular distribution. As a consequence, the parton-parton differential cross-sections vary essentially as $d\hat{\sigma}_{ij}/d|\hat{t}| \sim 1/Q^4$. Hence, the effects of distribution functions as well as current masses of heavy quarks on $\sigma_{QCD}(s)$ are absolutely negligible.

In order to obtain $\chi_{SH}(s,b)$ it was selected parton-parton scattering processes containing at least one gluon in the initial state. The reason for this choice comes from the behaviour of the partonic splitting dictated by DGLAP evolution equations at leading order [116–119], in which the gluon splitting functions $P_{gq} \to 4/(3z)$ and $P_{gg} \to 6/z$ are singular as $z \to 0$. As a result, the gluon distribution becomes very large as $x \to 0$ (in the convolution integrals $z < x$), and its role in the evolution of parton distributions becomes central. Thus, taking into account the mechanism of dynamical mass generation in QCD, it was selected the following required parton-parton processes for calculating $\sigma_{QCD}(s)$:

i. gluon-gluon elastic scattering,

$$\frac{d\hat{\sigma}}{d\hat{t}}(gg \to gg) = \frac{9\pi\bar{\alpha}_s^2}{2\hat{s}^2}\left(3 - \frac{\hat{t}\hat{u}}{\hat{s}^2} - \frac{\hat{s}\hat{u}}{\hat{t}^2} - \frac{\hat{t}\hat{s}}{\hat{u}^2}\right), \tag{6.38}$$

ii. quark-gluon elastic scattering,

$$\frac{d\hat{\sigma}}{d\hat{t}}(qg \to qg) = \frac{\pi\bar{\alpha}_s^2}{\hat{s}^2}\left(\hat{s}^2 + \hat{u}^2\right)\left(\frac{1}{\hat{t}^2} - \frac{4}{9\hat{s}\hat{u}}\right), \tag{6.39}$$

iii. gluon fusion into a quark pair,

$$\frac{d\hat{\sigma}}{d\hat{t}}(gg \to \bar{q}q) = \frac{3\pi\bar{\alpha}_s^2}{8\hat{s}^2}\left(\hat{t}^2 + \hat{u}^2\right)\left(\frac{4}{9\hat{t}\hat{u}} - \frac{1}{\hat{s}^2}\right), \tag{6.40}$$

where $\hat{s} = x_1 x_2 s$ and $\hat{t} = -Q^2$. The gluon-gluon and quark-gluon scattering processes in fact dominate at high energies. For example, at $\sqrt{s} = 7$ TeV and with $Q_{min} = 1.3$ GeV, their relative contribution to the cross section $\sigma_{QCD}(s)$ is around 98.84% (98.66%) for the CTEQ6L (MSTW) set of parton distributions. The relative contribution of the process $gg \to \bar{q}q$ is rather tiny, nevertheless, it was included just for completeness.

In the limit of large enough Q^2, the expressions (6.38-6.40) reproduce their pQCD counterparts. In these expressions the kinematic constraints under consideration are given by $\hat{s}+\hat{t}+\hat{u} = 4M_g^2(Q^2)$ in the case of gluon-gluon scattering, and $\hat{s}+\hat{t}+\hat{u} = 2M_g^2(Q^2)+2M_q^2(Q^2)$ in the case of quark-gluon scattering and gluon fusion into a quark pair. Here, $M_q^2(Q^2)$ is the dynamical quark mass,

$$M_q(Q^2) = \frac{m_q^3}{Q^2 + m_q^2}, \tag{6.41}$$

which assumes a nonzero infrared mass scale m_q, to be phenomenologically adjusted. Notice that the effective mass for quarks is a sum of the dynamical mass and the running one. However, as discussed, only the contributions of lighter quarks are relevant in calculating $\sigma_{QCD}(s)$ and as a result the effective mass behaviour is dominated by the dynamical part. The expression (6.41), which rapidly decreases with increasing Q, is the simplest *Ansatz* for a dynamical quark mass in agreement with OPE [182–189]. According to the OPE the dynamical mass is a function of the quark condensate $\langle\bar{\psi}\psi\rangle$. More specifically, $M_q(P^2) \propto \langle\bar{\psi}\psi\rangle/P^2$, where $P^2 = -p^2$ is the momentum in Euclidean space. The quark mass scale m_q can be related to the quark condensate ($\langle\bar{\psi}\psi\rangle \propto m_q^3$ by dimensional considerations) and general constraints are satisfied for $m_q \in [100; 250]$ MeV. The simple power-law behaviour of $M_q(Q^2)$ is finally obtained by introducing the factor m_q^2 in the denominator in order to get the right infrared limit $M_q(Q^2 \to 0) = m_q^2$.

6.3 The parton distribution functions

Although the QCD-inspired eikonal models have passed through many changes and in the phenomenological point of view evolved in some other aspects in the last couple of decades, the gluon distribution function usually adopted is still based on (naive) parametrisations of the form $g(x) \propto (1-x)^5/x^J$, where the parameter $J = \alpha_{\mathbb{P}}(0) = 1 + \epsilon$, with $\epsilon > 0$, controls the evolution of the gluon distribution at small-x. The quark-quark and quark-gluon contributions are written by means of parametrisations based on Regge-Gribov phenomenology. In the Regge language the quantity J controls the asymptotically behaviour of the total cross-section and is the so-called intercept of the Pomeron. Hence, the total cross-section should behave asymptotic as a Pomeron power-law s^{J-1}, and a consistent value of J should be determined by fitting forward quantities data by means of a Regge pole model.

However, the validity of the functional form of $g(x)$ is approximately correct only in the limits at $x \to 0$ and $x \to 1$, whereas in intermediate x regions it does not reproduce the behaviour of any other distribution function $g(x, Q^2)$ running with Q^2, whatever the values of the momentum scale Q^2 and the parameter J. The coupling $\alpha_s(Q^2)$ is one of the basic parameter in QCD, since its dependence with Q reflects the property of asymptotic freedom of QCD. Thus, by fixing the coupling $\alpha_s(Q^2)$, as some models used to do, it represents a very unsatisfactory approximation for the partonic distribution. This resembles to a loss of bond to the QCD parton model, is such a way that it turned out to be contested the terminology "QCD-inpired model". The partonic distributions must run with the momentum scale Q according to the DGLAP equations [116–119], thus allowing to determine the distribution in x and Q by means of an initial scale Q_0. It is extremely important that PDF's should exhibit a dependence with the momentum scale.

In the literature there are a great variety of different kinds of PDF's, where some authors usually named the "first generation" the distributions set formed by EHLQ [190] and DO [191], respectively. But this first generation set of PDF's are now obsolete when compared to the rigorous calculations necessary to describe hadronic processes, since both theoretical and experimental developments have had breakthroughs in the last few years. The modern generation is compounded by distribution sets obtained by means of the most recent DIS structure functions data and other related processes, where in this set of PDF's one finds for instance the following ones: ABM [192–195], CTEQ [196–202], GRV/GJR [203–205], MRS/MRST/MSTW/MMHT [206, 207, 209–211], NNPDF [212]. These distributions differ from each other basically by the experimental data used, the types of parametrisations initially adopted, the different choices of the initial momentum scale Q_0 and the statistical treatment of the systematic errors.

In what follows, it will be discussed in general lines two different sets of PDF's, namely

CTEQ6 and MSTW. The main objective is to give a hint on it so that one can understand its basics features, to show its functional forms, to discuss the limits of applicability as well as some general aspects.

6.3.1   The partonic distribution CTEQ6

The development of PDF's through global analysis of hard scattering processes is extremely important to the search for a theoretical description involving the QCD parton model phenomenology, and also the search for new Physics in lepton-hadron and hadron-hadron colliders. Over the past few years there have been efforts beyond the conventional analysis used by the most popular PDF's [196–199, 203, 204, 206, 207]. One of the most recent distribution was developed by the CTEQ Collaboration and it extends the previous generations, mainly due to the treatment between previous and new experimental data, and the treatment of the systematic uncertainties associated with partonic distributions and its physical predictions. In this new updated set, namely CTEQ6 [200–202], the conventional strategy methodology of producing the best global fit to the data was largely improved introducing new statistical tools which allow to characterise the partonic distribution space parameter around the global minimum. Within this new methodology [213–215] it turned out to be possible to explore the systematical uncertainties in the partonic distributions and its physical predictions, resulting in a better understanding of the hadronic content, mostly the gluon distribution.

The functional form of the partonic parametrisations used in CTEQ6 with initial momentum scale fixed in $Q_0 = 1.3$ GeV is given by [200–202]

$$xf(x, Q_0) = A_0\, x^{A_1}(1 - x)^{A_2}\, e^{A_3 x}\, (1 + e^{A_4}\, x)^{A_5}, \qquad (6.42)$$

with independent parameters for the parton combinations $u_V \equiv u - \bar{u}$, $d_V \equiv d - \bar{d}$, g e $\bar{u} + \bar{d}$. The functional behaviour of expression (6.42) at $x = 0$ and $x = 1$ represents the singularity associated with Regge-Gribov phenomenology at small-x and to the quark counting rule at bigger values of x, respectively.

Since the previous distribution set, CTEQ5 [216], a great quantity of new experimental data have contributed to the statistical analysis of an updated PDF. More specifically, it was very important in this new analysis the recent measurements of structure function in DIS with neutral currents by H1 [217,218] and ZEUS [219,220] experiments, the measurements of inclusive jets cross-section at DØ [221,222], the measurements of Drell-Yan deuteron/proton ratio at FNAL E866/NuSea [223] and the reanalysed measurements of F_2 at CCFR [224].

In the CTEQ6 distribution, the QCD coupling constant $\alpha_s(Q^2)$ is written in its LO and

NLO forms. Respectively, for the case where one uses CTEQ6L1,

$$\alpha_s^{LO}(Q^2) = \frac{4\pi}{\beta_0 \ln(Q^2/\Lambda^2)}, \tag{6.43}$$

and for the case of CTEQ6L,

$$\alpha_s^{NLO}(Q^2) = \frac{4\pi}{\beta_0 \ln(Q^2/\Lambda^2)} \left[1 - \frac{\beta_1}{\beta_0^2} \frac{\ln\ln(Q^2/\Lambda^2)}{\ln(Q^2/\Lambda^2)} \right]. \tag{6.44}$$

An effective number of quarks n_f could be fixed if they were massless, in this case expressions (6.43) and (6.44) would be determined by only one Λ. However, the decoupling theorem [225] says that each heavy quark with mass m_i decouples from the physical cross-sections at energy scales $\mu < m_i$. Thus, the effective number of quark flavors depends on the renormalisation scale μ implying that the resolution of the strong coupling α_s and the determination of Λ are not unique in the presence of massive quarks, *i.e.* it depends on the renormalisation scheme adopted. One natural choice is based on the requirement that $\alpha_s(\mu)$ is a continuous function of μ, but respectively the values of Λ are discontinuous at $\mu = m_i$.

The u, d and s quarks are considered massless in the CTEQ6 distribution[1], and the mass scales are defined by the masses of c and b quarks, with $m_c = 1.3$ GeV and $m_b = 4.5$ GeV. The leading order coupling is determined by the M_Z scale where $\alpha_s^{LO}(M_Z^2) = 0.130$ and Λ's are defined as $\Lambda_4 = 215$ MeV and $\Lambda_5 = 165$ MeV. In the next-to-leading order case, $\alpha_s^{NLO}(M_Z^2) = 0.118$ with $\Lambda_4 = 326$ MeV and $\Lambda_5 = 226$ MeV.

6.3.2 The partonic distribution MSTW

The year of 2008 was the 20th anniversary of the first publication of MRS distribution, which contained the first NLO global analysis of the partonic distributions [120]. It is natural that new experimental data and new theoretical methods to treat these data imply in the development of more sophisticated PDF's. The MRST98 [207] was the first updated set of MRS to use the new measurements of structure function obatained at HERA. Moreover, the MRST98 is also known for being the first one to apply the study of heavy quarks in the partonic analysis.

One of the recent distribution sets, originally based on MRS, extends the previous versions such as MRST2001 LO [211], MRST2004 NLO [226], MRST2006 NNLO [227]. In the recent set, namely MSTW [209], the technique used to obtain the best fit to the data presents some improvements because of the advances in the study of error propagations, hence implying in a better understanding of the partonic distribution uncertainties.

---

[1] $m_u \approx 1.7 - 3.1$ MeV, $m_d \approx 4.1 - 5.7$ MeV and $m_s \approx 80 - 130$ MeV.

The functional form of the partonic parametrisations used in MSTW with initial momentum scale fixed in $Q_0 = 1.0$ GeV is given by the following expressions [209]

$$xu_V(x, Q_0^2) = A_u x^{\eta_1}(1-x)^{\eta_2}(1 + \epsilon_u\sqrt{x} + \gamma_u x), \tag{6.45}$$

$$xd_V(x, Q_0^2) = A_d x^{\eta_3}(1-x)^{\eta_4}(1 + \epsilon_d\sqrt{x} + \gamma_d x), \tag{6.46}$$

$$xS(x, Q_0^2) = A_S x^{\delta_S}(1-x)^{\eta_S}(1 + \epsilon_S\sqrt{x} + \gamma_S x), \tag{6.47}$$

$$x\Delta(x, Q_0^2) = A_\Delta x^{\eta_\Delta}(1-x)^{\eta_S+2}(1 + \gamma_\Delta x + \delta_\Delta x^2), \tag{6.48}$$

$$xg(x, Q_0^2) = A_g x^{\delta_g}(1-x)^{\eta_g}(1 + \epsilon_g\sqrt{x} + \gamma_g x) + A_{g'} x^{\delta_{g'}}(1-x)^{\eta_{g'}}, \tag{6.49}$$

$$x(s + \bar{s})(x, Q_0^2) = A_+ x^{\delta_S}(1-x)^{\eta_+}(1 + \epsilon_S\sqrt{x} + \gamma_S x), \tag{6.50}$$

$$x(s - \bar{s})(x, Q_0^2) = A_- x^{\delta_-}(1-x)^{\eta_-}(1 - x/x_0), \tag{6.51}$$

where $\Delta = \bar{d} - \bar{u}$, $q_V = q - \bar{q}$ and the light sea quarks are defined as $S \equiv 2(\bar{u} + \bar{d}) + s + \bar{s}$. The above expressions are constrained by four normalisations, the counting rules

$$\int_0^1 dx\, u_V(x, Q_0^2) = 2, \tag{6.52}$$

$$\int_0^1 dx\, d_V(x, Q_0^2) = 1, \tag{6.53}$$

$$\int_0^1 dx\, s_V(x, Q_0^2) = 0, \tag{6.54}$$

and the conservation of momentum

$$\int_0^1 dx\, x\, \left[u_V(x, Q_0^2) + d_V(x, Q_0^2) + S(x, Q_0^2) + g(x, Q_0^2)\right] = 1. \tag{6.55}$$

In the MSTW the u, d and s quarks are considered massless and the mass scales are defined by the mass of c and b quarks, with $m_c = 1.40$ GeV and $m_b = 4.75$ GeV. As stressed out by the authors [209], to obtain the best fit at LO, then the second term in the *rhs* of expression (6.49) should not be considered.

6.4   Results so far

First, in order to determine the model parameters, we fix $n_f = 4$ and set the values of the gluon and quark mass scales to $m_g = 400$ MeV and $m_q = 250$ MeV, respectively. These choices for the mass scales are not only consistent with our LO procedures, but are also the ones usually obtained in other calculations of strongly interacting processes

[24–27, 30–32, 228, 229]. Next, a global fit to high-energy forward pp and $\bar{p}p$ scattering data was carried out above $\sqrt{s} = 10$ GeV, namely, the total cross-section $\sigma_{tot}^{pp,\bar{p}p}$ and the ratio of the real to imaginary part of the forward scattering amplitude $\rho^{pp,\bar{p}p}$.

It was used data sets compiled and analysed by the Particle Data Group [35] as well as the recent data at the LHC from the TOTEM Collaboration, with the statistical and systematical errors added in quadrature. The TOTEM data set includes the first and the second measurements of the total pp cross-section at $\sqrt{s} = 7$ TeV, $\sigma_{tot}^{pp} = 98.30 \pm 2.80$ mb [17] and $\sigma_{tot}^{pp} = 98.58 \pm 2.23$ mb [18], both using the optical theorem together with the luminosity provided by the CMS [52], the luminosity-independent measurements at $\sqrt{s} = 7$ TeV, $\sigma_{tot}^{pp} = 98.0 \pm 2.50$ mb [19], the ρ-independent measurements at $\sqrt{s} = 7$ TeV, $\sigma_{tot}^{pp} = 99.10 \pm 4.30$ mb [19], and the luminosity-independent measurement at $\sqrt{8}$ TeV, $\sigma_{tot}^{pp} = 101.70 \pm 2.90$ [20]. The data set includes the first estimate for the ρ-parameter made by the TOTEM Collaboration in their ρ-independent measurement at $\sqrt{s} = 7$ TeV, namely $\rho^{pp} = 0145 \pm 0.091$ [19]. Unfortunately, this version of the DGM model [28, 29] does not include the corresponding total cross-section data at $\sqrt{s} = 8$ TeV, namely $\sigma_{tot}^{pp} = 102.90 \pm 2.30$ [21] and $\sigma_{tot}^{pp} = 103.00 \pm 2.30$ [21] and the corresponding ρ-parameter at $\sqrt{s} = 8$ TeV, namely $\rho^{pp} = 0.120 \pm 0.030$ [21], because when the paper was published, these data were not available yet. So, it was decided just for completeness to maintain the results as given in Reference [29].

In all the fits performed was used a χ^2 fitting procedure, assuming an interval $\chi^2 - \chi_{min}^2$ corresponding, in the case of normal errors, to the projection of the χ^2 hypersurface containing 90% of probability. In this DGM version (8 fitting parameters) this corresponds to the interval $\chi^2 - \chi_{min}^2 = 13.36$.

In our analysis we have investigated the effects of some updated sets of PDFs on the high-energy cross-sections. In performing the fits one uses tree-level formulas for the parton-parton cross-sections. In this way we have to choose PDF's evolved with LO splitting functions, as in case of LO sets CTEQ6L, CTEQ6L1 and MSTW. For the coupling $\alpha_s(Q^2)$ it is usual to use either the LO formula for formal consistency or even the NLO one. In the specific case of CTEQ distributions [201, 202], the CTEQ6L1 uses LO formula for $\alpha_s(Q^2)$ with $\Lambda_{CTEQ6L1}^{(4flavor)} = 215$ MeV, whereas CTEQ6L uses NLO formula for $\alpha_s(Q^2)$ with $\alpha_s(M_Z) = 0.118$, consistent with the value $\Lambda_{CTEQ6L}^{(4flavor)} = 326$ MeV. Since the dynamical mass $M_g(Q^2)$ practically vanishes at scales where four flavors are active, we choose these same values of $\Lambda^{(4flavor)}$ in our effective charges $\bar{\alpha}_s^{LO}(Q^2)$ and $\bar{\alpha}_s^{NLO}(Q^2)$, where $\bar{\alpha}_s^{LO}$ is given by the expression (6.1) whereas $\bar{\alpha}_s^{NLO}(Q^2)$ is given by [32]

$$\bar{\alpha}_s^{NLO}(Q^2) = \frac{4\pi}{\beta_0 \ln\left[\left(Q^2 + 4M_g^2(Q^2)\right)/\Lambda^2\right]} \left[1 - \frac{\beta_1}{\beta_0^2} \frac{\ln\ln\left[\left(Q^2 + 4M_g^2(Q^2)\right)/\Lambda^2\right]}{\ln\left[\left(Q^2 + 4M_g^2(Q^2)\right)/\Lambda^2\right]}\right], \quad (6.56)$$

where $\beta_1 = 102 - \frac{38}{3}n_f$ and $\Lambda = \Lambda_{CTEQ6L}^{(4flavor)}$. This NLO non-perturbative coupling is built by saturating the two-loop perturbative strong coupling α_s^{NLO}, that is, by introducing the replacement $\alpha_s^{NLO}(Q^2) \to \bar{\alpha}_s^{NLO}(Q^2) = \alpha_s^{NLO}(Q^2 + 4M_g^2(Q^2))$ into the perturbative result. Notice that we are using the same dynamical mass $M_g^2(Q^2)$ expression for both LO and NLO couplings, since the results from Reference [32] give support to the statement that the dynamical mass scale m_g is not strongly dependent on the perturbation order. The MSTW set uses an alternative definition of α_s, where the renormalisation group equation for α_s is truncated at the appropriate order and solved starting from an initial value $\alpha_s(Q_0^2)$. This input value is one of their fit parameters and replaces the Λ parameter [209]. In the usual matching-prescription scheme the behaviour of $\alpha_{s_{MSTW}}(Q^2)$ can be properly reproduced from the choice $\Lambda_{MSTW}^{(4flavor)} \sim 319$ MeV.

The values of the fitted parameters are given in Tables 6.1 and 6.2. In Table 6.1 (6.2) it is shown the values of the parameters in the case of a monopole (dipole) form factor in the semi-hard sector. The χ^2/dof for all fits was obtained for 154 degrees of freedom. The sensitivity of the χ^2/dof to the cutoff Q_{min} is shown in Figured 6.1. We observe that the χ^2/dof is not very sensitive to Q_{min} in the interval $[1.0, 1.5]$ GeV for all PDFs we have considered. The results of the fits to σ_{tot} and ρ for both pp and $\bar{p}p$ channels are displayed in Figures 6.2-6.5, together with the experimental data. In Figure 6.6 we show the theoretical predictions for the pp cross-sections at cosmic-ray energies; the comparison of the curves with the AUGER experimental datum at $\sqrt{s} = 57$ TeV [49] and the Telescope Array datum at $\sqrt{s} = 95$ TeV [50] shows good agreement. The curves depicted in Figures 6.2-6.6 were all calculated using the cutoff $Q_{min} = 1.3$ GeV, the value of the CTEQ6 fixed initial scale Q_0. In the case of MSTW set the slightly lower value $Q_0 \equiv 1$ GeV is adopted, and the condition $Q_{min} \geq Q_0$ is always satisfied in our analysis. In the case of fits using the CTEQ6 set, calculations in the region $Q_{min} < Q \leq Q_0$ were carried out with PDFs fixed at the scale $Q = Q_0 = 1.3$ GeV. In Table 6.3 we show the theoretical predictions for the forward scattering quantities $\sigma_{tot}^{pp,\bar{p}p}$ and $\rho^{pp,\bar{p}p}$ using different sets of parton distributions.

6.5   Partial conclusions

The road so far shows that we have somewhat studied infrared contributions to semi-hard parton-parton interactions by considering LO and NLO effective QCD charges with finite infrared behaviour. We have investigated pp and $\bar{p}p$ scattering in the LHC energy region with the assumption that the observed increase of hadron-hadron total cross-sections arises exclusively from these semi-hard interactions.

In the calculation of $\sigma_{tot}^{pp,\bar{p}p}$ and $\rho^{pp,\bar{p}p}$ we have investigated the behaviour of the forward amplitude for a range of different cutoffs and parton distribution functions, namely

CTEQ6L, CTEQ6L1 and MSTW, and considered the phenomenological implications of a class of energy-dependent form factors for semi-hard partons. We introduce integral dispersion relations specially tailored to connect the real and imaginary parts of eikonals with energy-dependent form factors. In our analysis we have included the recent data at LHC from the TOTEM Collaboration available at that time [21].

We have paid attention to the sensitivity of the χ^2/dof to the cutoff Q_{min}, which restricts the parton-parton processes to semi-hard interactions. Our results show that very good descriptions of $\sigma_{tot}^{pp,\bar{p}p}$ and $\rho^{pp,\bar{p}p}$ data are obtained by constraining the cutoff to the interval $1.0 \leq Q_{min} \lesssim 1.5$ GeV. The χ^2/dof for the best global fits lie in the range [1.05;1.06] for 154 degrees of freedom. This good statistical result shows that our eikonal model, where non-perturbative effects are naturally included via a QCD effective charge, is well suited for detailed predictions of the forward quantities to be measured at higher energies. In fact our predictions for pp total cross-section are statistically compatible with the AUGER result at $\sqrt{s} = 57$ TeV, namely $\sigma_{tot}^{pp} = [133 \pm 13\,(\text{stat})_{-20}^{+17}\,(\text{syst}) \pm 16\,(\text{Glauber})]$ mb [49], as well as with the Telescope Array result at $\sqrt{s} = 95$ TeV, namely $\sigma_{tot}^{pp} = [170_{-44}^{+48}\,(\text{stat})_{-19}^{+17}\,(\text{syst})]$ mb [50]. However it is worth noting that both results are model dependent, since they come from the conversion of the proton-air production cross-section via a Glauber calculation. Moreover, as stressed by AUGER group, the total uncertainty of converting the proton-air to pp cross-section may be larger than the published. Clearly new results from AUGER and Telescope Array at higher energies would be extremely informative.

The uncertainty in our theoretical predictions for the forward observables at $\sqrt{s} = 8, 13, 14, 57$ and 95 TeV, see Table 6.3, have been estimated by varying the gluon mass scale within a typical uncertainty δm_g while keeping all other model parameters constant, and by exploring the uncertainties of parton distributions on production cross-sections. This procedure does not determines the formal uncertainty in σ_{tot} and ρ, since the variance-covariance matrix method, necessary for proving this quantity, was not employed. However, at high energies the forward observables are dominated by semi-hard interactions represented by the eikonal term $\chi_{SH}(s,b)$, which depends only on 3 parameters, namely ν_1, ν_2 and m_g.

In all χ^2 analyses we have observed that the correlation coefficients of these parameters are very small. Moreover, the values of σ_{tot} and ρ are actually more sensitive to the gluon mass scale than to variations of others parameters of the model. A reliable estimate of δm_g, namely around 7.1% of the value of m_g, was obtained from the analysis of the proton structure function $F_2(x, Q^2)$ at small-x [32]. Hence in our case, where m_g was set at 400 MeV, the gluon mass uncertainty is $\delta m_g \sim 28$ GeV. In order to estimate the uncertainty of parton distributions on the forward predictions we simply adopt the conservative stance that the PDFs uncertainties on the total cross-sections are of the same order of magnitude as the uncertainties on the production cross-sections of the W and Z bosons at the LHC. The

uncertainties on the production cross-sections are estimated to be $\pm 5\%$ by the CTEQ group [200–202, 213–216]. So, summarising, the total uncertainty of our theoretical predictions is obtained from the quadrature sum of the uncertainties coming from the gluon mass uncertainty δm_g and the parton distributions.

In the semi-hard sector we have considered a new class of form factors in which the average gluon radius increases with $\sqrt{s}$. With this assumption we have obtained another form in which the eikonal can be factored into the QCD parton model, namely $\mathrm{Re}\,\chi_{SH}(s,b) = \frac{1}{2}\,W_{SH}(s,b)\,\sigma_{QCD}(s)$. The imaginary part of this semi-factorisable eikonal was obtained by means of appropriate integral dispersion relations which take into account eikonals with energy-dependent form factors. Although these dispersion relations are quite accurate at high energies, detailed studies using derivative dispersion relations [69, 230, 231] would be needed to quantify the effect of dispersion-relation subtractions on the imaginary part of the eikonal.

	CTEQ6L	CTEQ6L1	MSTW
ν_1 [GeV]	1.712 ± 0.541	1.980 ± 0.745	1.524 ± 0.769
ν_2 [GeV]	$(3.376\pm1.314)\times10^{-2}$	$(5.151\pm1.627)\times10^{-2}$	$(9.536\pm8.688)\times10^{-3}$
A' [GeV^{-1}]	125.3 ± 14.7	107.3 ± 9.0	107.2 ± 13.6
B' [GeV^{-1}]	42.96 ± 24.91	28.73 ± 14.78	30.54 ± 16.20
C' [GeV^{-1}]	1.982 ± 0.682	1.217 ± 0.402	1.186 ± 0.466
γ	0.757 ± 0.189	0.698 ± 0.212	0.644 ± 0.250
μ^+_{soft} [GeV]	0.777 ± 0.176	0.407 ± 0.266	0.475 ± 0.300
D' [GeV^{-1}]	23.78 ± 1.97	21.37 ± 2.67	21.92 ± 2.83
χ^2/dof	1.060	1.063	1.049

Table 6.1: Values of the revised DGM model parameters from the global fit to the scattering pp and $\bar{p}p$ data. Results obtained using a monopole form factor in the semi-hard sector.

	CTEQ6L	CTEQ6L1	MSTW
ν_1 [GeV]	2.355 ± 0.620	2.770 ± 0.865	2.267 ± 0.845
ν_2 [GeV]	$(5.110 \pm 4.203) \times 10^{-2}$	$(7.860 \pm 5.444) \times 10^{-2}$	$(3.106 \pm 2.920) \times 10^{-2}$
A' [GeV^{-1}]	128.9 ± 13.9	108.9 ± 8.6	108.5 ± 11.5
B' [GeV^{-1}]	46.73 ± 26.13	30.19 ± 15.78	31.63 ± 16.16
C' [GeV^{-1}]	2.103 ± 0.669	1.260 ± 0.437	1.230 ± 0.467
γ	0.780 ± 0.170	0.719 ± 0.200	0.660 ± 0.227
μ^+_{soft} [GeV]	0.821 ± 0.150	0.457 ± 0.209	0.506 ± 0.236
D' [GeV^{-1}]	23.96 ± 1.92	21.73 ± 2.26	22.14 ± 2.38
χ^2/dof	1.064	1.062	1.047

Table 6.2: Values of the revised DGM model parameters from the global fit to the scattering pp and $\bar{p}p$ data. Results obtained using a dipole form factor in the semi-hard sector.

	$\sqrt{s}$ [TeV]	σ_{tot} [mb]		ρ	
		monopole	dipole	monopole	dipole
CTEQ6L	8.0	$100.9^{+8.6}_{-7.3}$	$101.0^{+8.6}_{-7.3}$	$0.115^{+0.009}_{-0.008}$	$0.106^{+0.009}_{-0.007}$
	13.0	$111.5^{+9.7}_{-8.4}$	$111.7^{+9.7}_{-8.4}$	$0.110^{+0.010}_{-0.008}$	$0.101^{+0.009}_{-0.008}$
	14.0	$113.2^{+9.9}_{-8.6}$	$113.5^{+9.9}_{-8.6}$	$0.110^{+0.010}_{-0.008}$	$0.100^{+0.009}_{-0.008}$
	57.0	$152.5^{+15.4}_{-14.7}$	$154.1^{+15.6}_{-14.9}$	$0.097^{+0.010}_{-0.010}$	$0.088^{+0.009}_{-0.009}$
	95.0	$170.3^{+17.2}_{-16.5}$	$172.9^{+17.5}_{-16.8}$	$0.092^{+0.010}_{-0.010}$	$0.083^{+0.009}_{-0.009}$
CTEQ6L1	8.0	$101.1^{+8.6}_{-7.3}$	$101.2^{+8.6}_{-7.3}$	$0.134^{+0.012}_{-0.009}$	$0.124^{+0.011}_{-0.009}$
	13.0	$112.4^{+9.8}_{-8.5}$	$112.9^{+9.8}_{-8.5}$	$0.131^{+0.012}_{-0.010}$	$0.120^{+0.011}_{-0.009}$
	14.0	$114.2^{+10.0}_{-8.7}$	$114.9^{+10.0}_{-8.7}$	$0.130^{+0.012}_{-0.010}$	$0.119^{+0.011}_{-0.009}$
	57.0	$159.3^{+16.1}_{-15.4}$	$163.7^{+16.5}_{-15.8}$	$0.117^{+0.012}_{-0.012}$	$0.106^{+0.011}_{-0.011}$
	95.0	$181.5^{+18.3}_{-17.6}$	$188.9^{+19.0}_{-18.4}$	$0.112^{+0.012}_{-0.012}$	$0.101^{+0.011}_{-0.011}$
MSTW	8.0	$101.3^{+8.6}_{-7.3}$	$101.3^{+8.7}_{-7.3}$	$0.142^{+0.013}_{-0.010}$	$0.131^{+0.012}_{-0.009}$
	13.0	$113.3^{+9.9}_{-8.5}$	$113.6^{+9.9}_{-8.5}$	$0.139^{+0.012}_{-0.011}$	$0.128^{+0.011}_{-0.010}$
	14.0	$115.4^{+10.1}_{-8.7}$	$115.7^{+10.1}_{-8.8}$	$0.139^{+0.013}_{-0.011}$	$0.128^{+0.012}_{-0.010}$
	57.0	$162.1^{+16.4}_{-15.6}$	$164.7^{+16.6}_{-15.9}$	$0.127^{+0.013}_{-0.013}$	$0.116^{+0.012}_{-0.011}$
	95.0	$183.0^{+18.5}_{-17.8}$	$187.3^{+18.9}_{-18.2}$	$0.123^{+0.013}_{-0.013}$	$0.112^{+0.012}_{-0.012}$

Table 6.3: Predictions for the forward scattering quantities $\sigma_{tot}^{pp,\bar{p}p}$ and $\rho^{pp,\bar{p}p}$ using different sets of parton distributions.
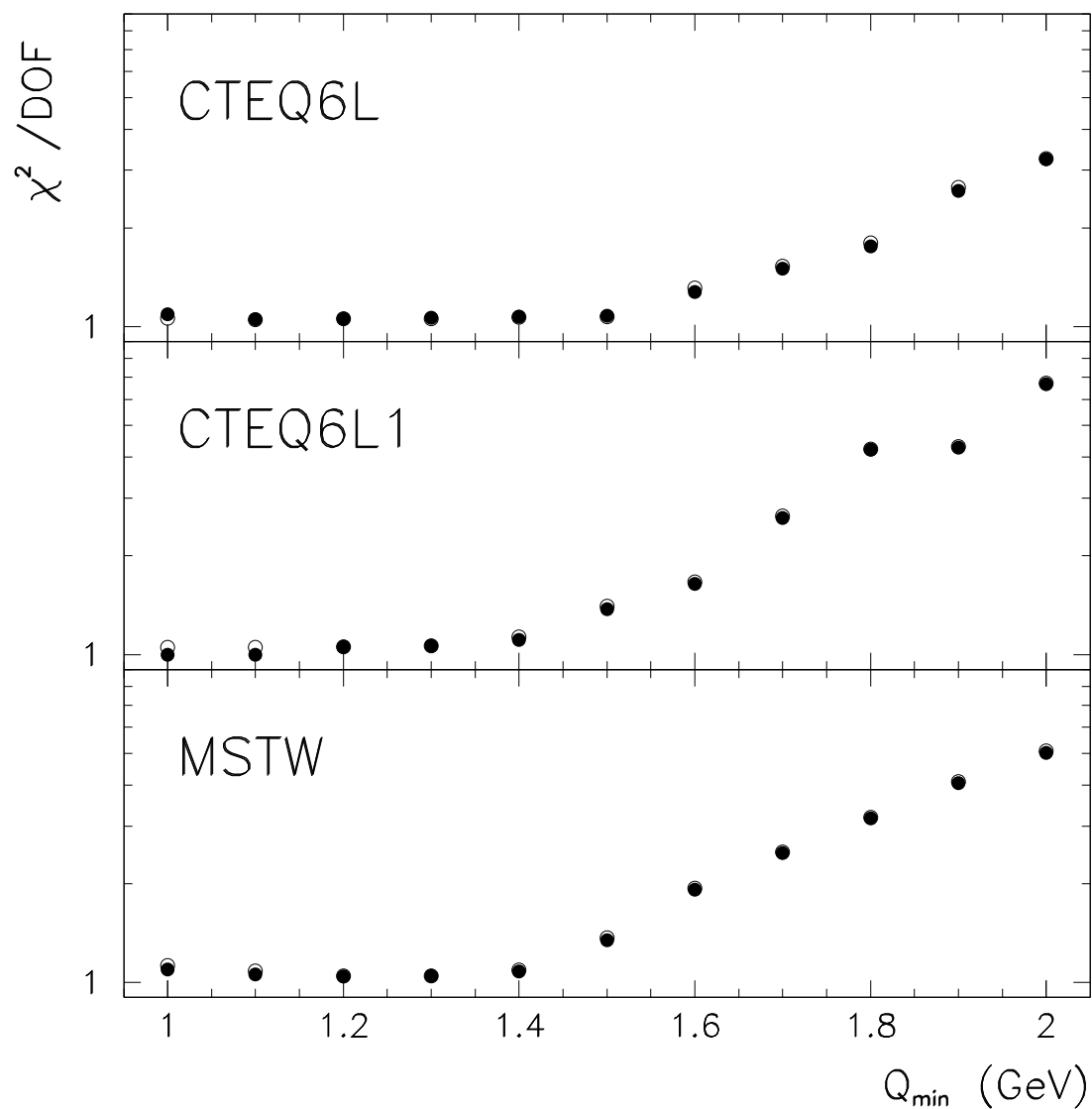
Figure 6.1: The χ^2/dof as a function of the cutoff Q_{min} for the monopole ($\circ$) and the dipole ($\bullet$) semi-hard form factor.
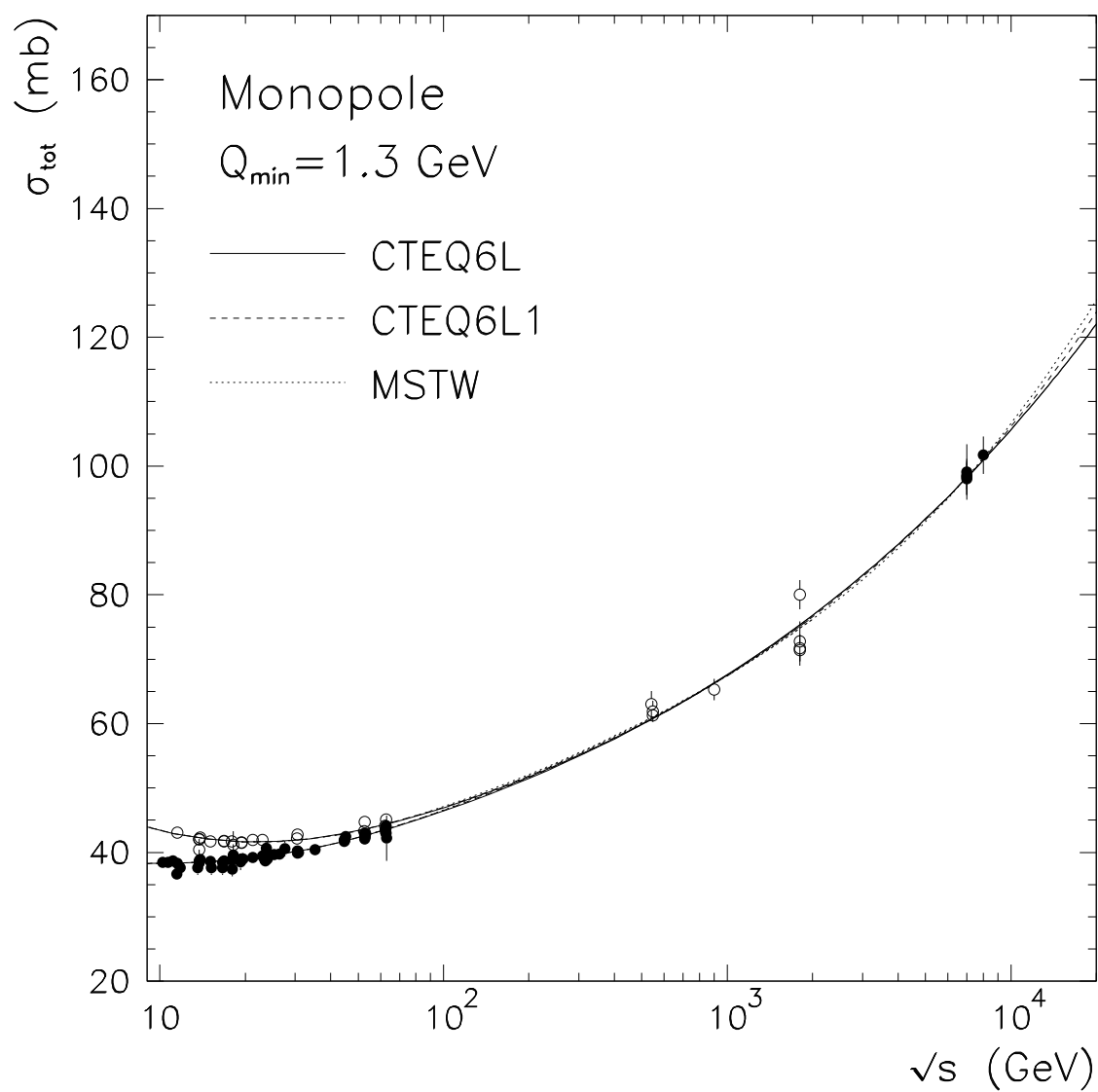
Figure 6.2: Total cross-section for pp ($\bullet$) and $\bar{p}p$ ($\circ$).
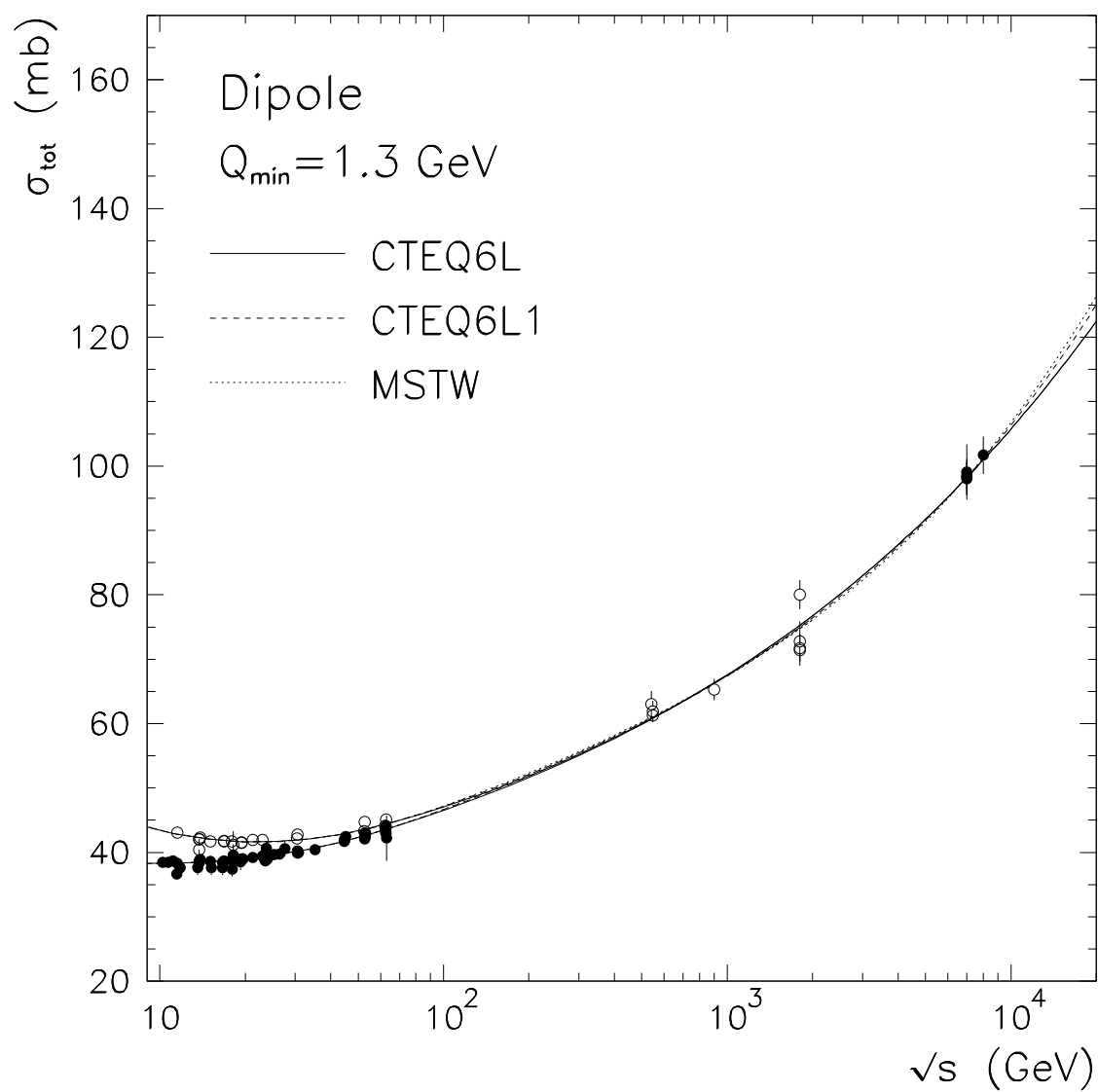
Figure 6.3: Total cross-section for pp ($\bullet$) and $\bar{p}p$ ($\circ$).
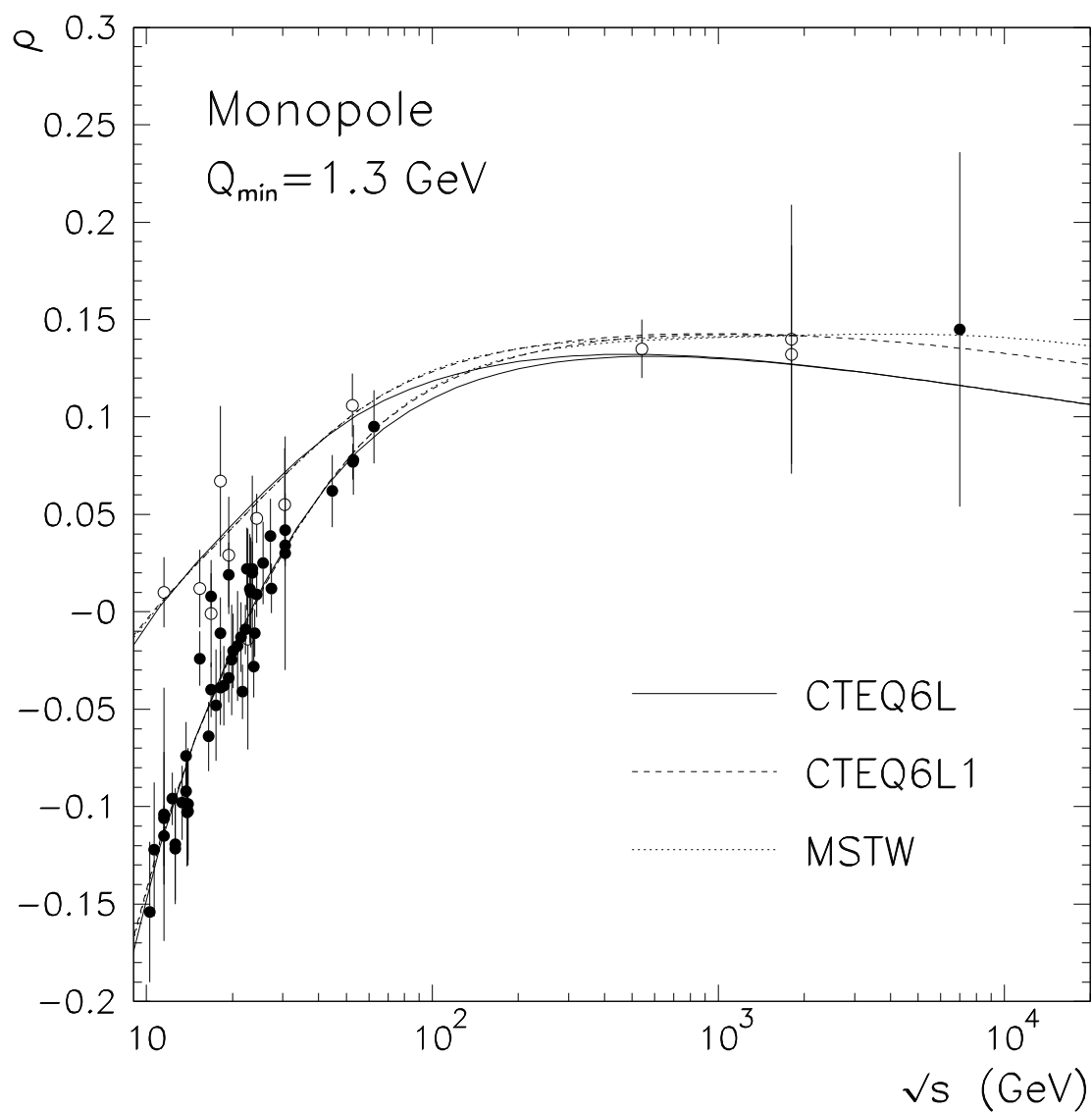
Figure 6.4: Ratio of the real to imaginary part of the forward scattering amplitude for pp ($\bullet$) and $\bar{p}p$ ($\circ$).
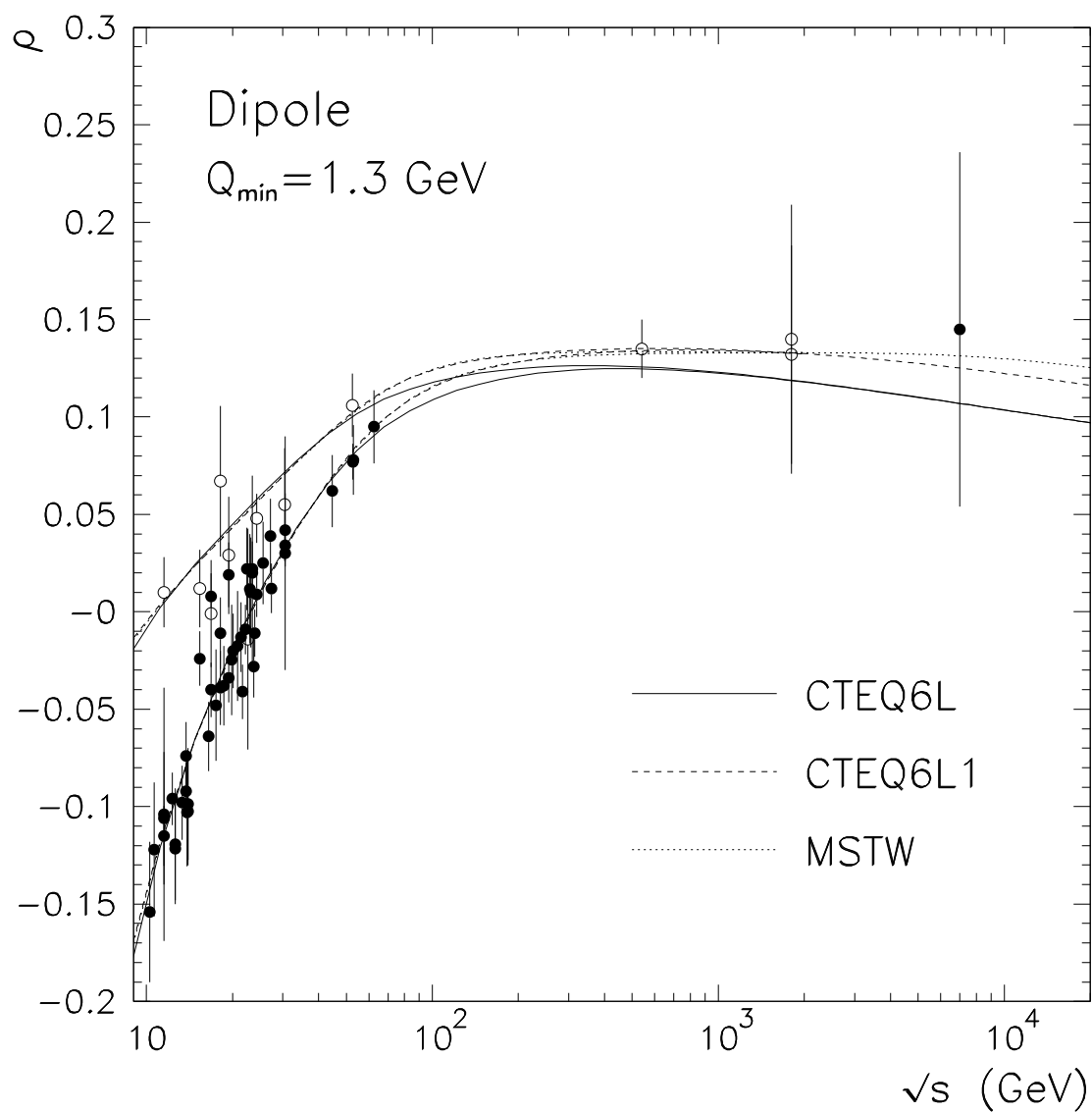
Figure 6.5: Ratio of the real to imaginary part of the forward scattering amplitude for pp ($\bullet$) and $\bar{p}p$ ($\circ$).
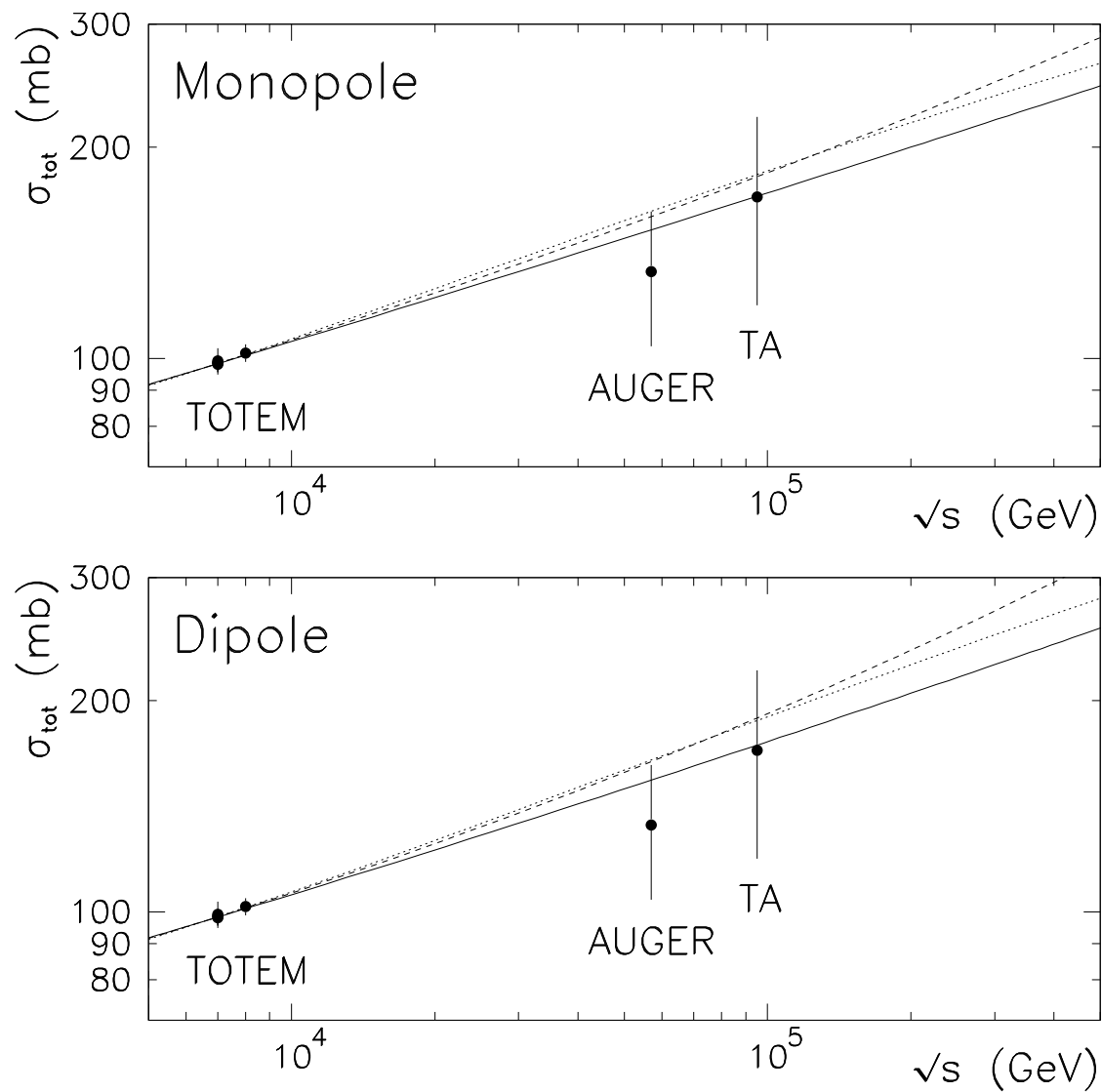
Figure 6.6: TOTEM, AUGER and Telescope Array (TA) results compared with theoretical expectations obtained using CTEQ6L (solid curve), CTEQ6L1 (dashed curve) and MSTW (dotted curve) parton distribution functions.

6.6 Differences from the previous model

There are some essential differences between this recent version of the DGM model [28, 29], which was discussed in details in the last couple of sections, and the one that was presented in my Master Thesis [232], whici it will be properly shown below.

The eikonal functions are assumed to be additive with respect to the soft and semi-hard parton interactions in hadronic collision, see expression (6.9). Moreover, it is written in terms of even and odd eikonal parts connected by crossing-symmetry. As it was already discussed, the crossing-odd eikonal receives no contribution from semi-hard processes at high energies. As a result, for our purposes it is sufficient to take $\chi_{SH}(s,b) = \chi_{SH}^+(s,b)$ and, consequently, $\chi^-(s,b) = \chi_{soft}^-(s,b)$. Hence the even eikonals

$$
\begin{aligned}
\chi^+(s,b) &= \chi_{soft}^+(s,b) + \chi_{SH}^+(s,b) \\
&= \frac{i}{2}\left[W_{soft}^+(b)\,\sigma_{soft}(s) + W_{SH}(b)\,\sigma_{QCD}(s)\right],
\end{aligned}
\tag{6.57}
$$

where $\sigma_{QCD}(s) = \operatorname{Re}\sigma_{QCD}(s) + i\operatorname{Im}\sigma_{QCD}(s)$, and $\sigma_{soft}(s) = \operatorname{Re}\sigma_{soft}(s) + i\operatorname{Im}\sigma_{soft}(s)$, with the real soft cross-section written as

$$
\operatorname{Re}\sigma_{soft}(s) = A' + C'\left(\frac{s}{s_0}\right)^{-\gamma}\cos\left(\frac{\pi\gamma}{2}\right),
\tag{6.58}
$$

and the corresponding imaginary soft cross-section term given by

$$
\operatorname{Im}\sigma_{soft}(s) = B' + C'\left(\frac{s}{s_0}\right)^{-\gamma}\sin\left(\frac{\pi\gamma}{2}\right).
\tag{6.59}
$$

The soft eikonal is needed only to describe the lower-energy forward data. Then, for the even part of the soft eikonal we therefore take

$$
\chi_{soft}^+(s,b) = \frac{i}{2}\,W_{soft}^+(b)\left[A' + i\,B' + C'\left(\frac{s}{s_0}\right)^{-\gamma}\right],
\tag{6.60}
$$

where $s_0 \equiv 1$ GeV^2 and A', B', C' and γ are fitting parameters. We ensure the correct analyticity properties of our model amplitudes by substituting $s \to se^{-i\pi/2}$ throughout the expression (6.60). The odd eikonal $\chi^-(s,b)$, that accounts for the difference between pp and $\bar{p}p$ channels and vanishes at high energy, is given by

$$
\chi^-(s,b) = \frac{1}{2}\,W_{soft}^-(b)\,D'\,\frac{e^{i\pi/4}}{\sqrt{s/s_0}},
\tag{6.61}
$$

where D', the strength of the odd term, is also a fitting parameter. The above expression was

written with its correct analyticity property. The energy-dependent form factor discussion, see section 6.2.1, is exactly the same, but here μ_{soft}^- is a constant to be fitted.

The biggest difference, and perhaps the only one that really matters, is in the imaginary part of the semi-hard eikonal function $\chi_{SH}(s, b)$. There is a common misconception in some QCD-based eikonal models, as for example in the Durand & Pi model [124–126], where the authors usually write the QCD cross-section as a complex quantity. Following exactly Durand *et al.* [126], and in the first drafts of this reviewed DGM model, the QCD cross-section used to be given by

$$
\mathrm{Re}\,\sigma_{QCD}(s) = \sum_{ij} \frac{1}{1 + \delta_{ij}} \int_{2Q^2/s}^{1} dx_1 \int_{2Q^2/x_1 s}^{1} dx_2 \int_{Q_{min}^2}^{\hat{s}/2} d|\hat{t}|\, \frac{d\hat{\sigma}_{ij}}{d|\hat{t}|}(\hat{s}, \hat{t}) f_{i/A}(x_1, |\hat{t}|) f_{j/B}(x_2, |\hat{t}|),
$$

(6.62)

and as previously shown it follows from the QCD parton model that the eikonal term $\chi_{SH}^+(s, b)$ can be factorised as [124–126]

$$
\mathrm{Re}\,\chi_{SH}^+(s, b) = \frac{1}{2} W_{SH}(b)\,\mathrm{Re}\,\sigma_{QCD}(s).
$$

(6.63)

The breaking point here is that one can easily be induced to write a similar expression for the imaginary part of $\chi_{SH}^+(s, b)$,

$$
\mathrm{Im}\,\chi_{SH}^+(s, b) = \frac{1}{2} W_{SH}(b)\,\mathrm{Im}\,\sigma_{QCD}(s),
$$

(6.64)

where it can be properly obtained by means of an integral dispersion relation, see expression (6.26), thus

$$
\begin{aligned}
\mathrm{Im}\,\sigma_{QCD}(s) &= -\frac{1}{\pi} \sum_{ij} \frac{1}{1 + \delta_{ij}} \int_0^1 dx_1 \int_0^1 dx_2 \int_{Q_{min}^2}^{\hat{s}/2} d|\hat{t}|\, \frac{d\hat{\sigma}_{ij}}{d|\hat{t}|}(\hat{s}, \hat{t}) \\
&\times\ f_{i/A}(x_1, |\hat{t}|) f_{j/B}(x_2, |\hat{t}|) \ln\left(\frac{\hat{s}/2 + |\hat{t}|}{\hat{s}/2 - |\hat{t}|}\right).
\end{aligned}
$$

(6.65)

It follows that, and as pointed out by Professor Márcio J. Menon, when one actually applies the integral dispersion relation into expression (6.63) all the dynamical energy-dependence considered by means of the two different *Ansätze* for the energy-dependent form factors was simply lost, see expression (6.21)-(6.24). Because it was not even considered in the calculation in the first place, and it makes all the difference. In what follows, it will be shown the results obtained using this first draft of the revised DGM model, also known as the work which was properly presented in my Master Thesis.

In all the fits performed we used a χ^2 fitting procedure, assuming an interval $\chi^2 - \chi_{min}^2$ corresponding, in the case of normal errors, to the projection of the χ^2 hypersurface

containing 90% of probability. In this version of the DGM model (9 fitting parameters) this corresponds to the interval $\chi^2 - \chi^2_{min} = 14.68$.

The values of the fitted parameters are given in Tables 6.4 and 6.5. In Table 6.4 (6.5) we show the values of the parameters in the case of a monopole (dipole) form factor in the semi-hard sector. The χ^2/dof for all fits was obtained for 153 degrees of freedom. The sensitivity of the χ^2/dof to the cutoff Q_{min} is shown in Figure 6.7. We observe that the χ^2/dof is not very sensitive to Q_{min} in the interval $[1.0, 1.5]$ GeV for all PDFs we have considered. The results of the fits to σ_{tot} and ρ for both pp and $\bar{p}p$ channels are displayed in Figures 6.8-6.11, together with the experimental data. The curves depicted in Figures 6.8-6.11 were all calculated using the cutoff $Q_{min} = 1.3$ GeV, the value of the CTEQ6 fixed initial scale Q_0. Thus, in the case of fits using the CTEQ6 set, PDFs at $Q_0 = 1.3$ GeV were used in the calculations with $Q_{min} < Q_0$. In the case of MSTW set the slightly lower value $Q_0 \equiv 1$ GeV is adopted, and the condition $Q_{min} \geq Q_0$ is always satisfied. In the case of fits using the CTEQ6 set, calculations in the region $Q_{min} < Q \leq Q_0$ were carried out with PDFs fixed at the scale $Q = Q_0 = 1.3$ GeV. In Table 6.6 we show the theoretical predictions for the forward scattering quantities $\sigma_{tot}^{pp,\bar{p}p}$ and $\rho^{pp,\bar{p}p}$ using different sets of parton distributions.

	CTEQ6L	CTEQ6L1	MSTW
ν_1 [GeV]	2.079 ± 0.842	2.006 ± 0.879	1.387 ± 0.824
ν_2 [GeV]	$(4.890 \pm 4.135) \times 10^{-2}$	$(4.467 \pm 3.817) \times 10^{-2}$	$(0.162 \pm 24.526) \times 10^{-2}$
A' [GeV^{-1}]	107.7 ± 7.7	106.5 ± 8.6	107.7 ± 11.4
B' [GeV^{-1}]	-5.33 ± 1.90	-5.14 ± 1.83	-4.98 ± 1.86
C' [GeV^{-1}]	727.6 ± 602.2	624.8 ± 547.5	556.3 ± 498.2
γ	0.832 ± 0.117	0.799 ± 0.129	0.759 ± 0.143
μ_{soft}^{+} [GeV]	0.452 ± 0.216	0.439 ± 0.252	0.525 ± 0.254
D' [GeV^{-1}]	108.8 ± 49.0	119.0 ± 112.9	109.1 ± 73.7
μ_{soft}^{-} [GeV]	0.216 ± 0.324	0.176 ± 0.286	0.430 ± 2.786
χ^2/dof	1.084	1.080	1.062

Table 6.4: Values of the first draft of the revised DGM model parameters from the global fit to the scattering pp and $\bar{p}p$ data. Results obtained using a monopole form factor in the semi-hard sector.

	CTEQ6L	CTEQ6L1	MSTW
ν_1 [GeV]	2.953 ± 0.987	2.862 ± 0.990	2.1947 ± 0.48503
ν_2 [GeV]	$(7.560 \pm 5.218) \times 10^{-2}$	$(7.037 \pm 5.286) \times 10^{-2}$	$(2.2591 \pm 2.7787) \times 10^{-2}$
A' [GeV^{-1}]	109.0 ± 7.0	107.9 ± 7.7	108.2 ± 3.3
B' [GeV^{-1}]	-5.42 ± 1.96	-5.24 ± 1.95	-5.12 ± 1.76
C' [GeV^{-1}]	773.3 ± 603.8	669.0 ± 560.9	581.9 ± 331.6
γ	0.842 ± 0.109	0.811 ± 0.121	0.76417 ± 0.079687
μ_{soft}^{+} [GeV]	0.489 ± 0.173	0.479 ± 0.193	0.53665 ± 0.07098
D' [GeV^{-1}]	107.2 ± 98.3	106.39 ± 85.99	146.34 ± 119.59
μ_{soft}^{-} [GeV]	0.416 ± 3.867	0.394 ± 3.862	0.13375 ± 0.11705
χ^2/dof	1.095	1.090	1.075

Table 6.5: Values of the first draft of the revised DGM model parameters from the global fit to the scattering pp and $\bar{p}p$ data. Results obtained using a dipole form factor in the semi-hard sector.

	$\sqrt{s}$ [TeV]	σ_{tot} [mb]		ρ	
		monopole	dipole	monopole	dipole
CTEQ6L	8.0	$100.7^{+8.6}_{-7.3}$	$101.0^{+8.6}_{-7.4}$	$0.101^{+0.009}_{-0.007}$	$0.094^{+0.008}_{-0.007}$
	13.0	$111.7^{+9.8}_{-8.4}$	$112.4^{+9.8}_{-8.5}$	$0.100^{+0.009}_{-0.008}$	$0.092^{+0.008}_{-0.007}$
	14.0	$113.5^{+9.9}_{-8.6}$	$114.3^{+10.0}_{-8.7}$	$0.099^{+0.009}_{-0.008}$	$0.092^{+0.008}_{-0.007}$
CTEQ6L1	8.0	$100.9^{+8.6}_{-7.4}$	$101.0^{+8.6}_{-7.4}$	$0.103^{+0.009}_{-0.007}$	$0.095^{+0.008}_{-0.007}$
	13.0	$111.7^{+9.8}_{-8.4}$	$112.2^{+9.8}_{-8.5}$	$0.101^{+0.009}_{-0.008}$	$0.093^{+0.008}_{-0.007}$
	14.0	$113.5^{+10.0}_{-8.6}$	$114.1^{+10.0}_{-8.6}$	$0.101^{+0.009}_{-0.008}$	$0.093^{+0.008}_{-0.007}$
MSTW	8.0	$101.0^{+8.6}_{-7.4}$	$101.1^{+8.6}_{-7.4}$	$0.102^{+0.009}_{-0.007}$	$0.096^{+0.008}_{-0.007}$
	13.0	$112.7^{+9.8}_{-8.5}$	$113.0^{+9.9}_{-8.5}$	$0.099^{+0.009}_{-0.007}$	$0.094^{+0.008}_{-0.007}$
	14.0	$114.6^{+10.1}_{-8.7}$	$115.0^{+10.1}_{-8.7}$	$0.099^{+0.009}_{-0.007}$	$0.093^{+0.008}_{-0.007}$

Table 6.6: Predictions for the forward scattering quantities $\sigma_{tot}^{pp,\bar{p}p}$ and $\rho^{pp,\bar{p}p}$ using different sets of parton distributions.
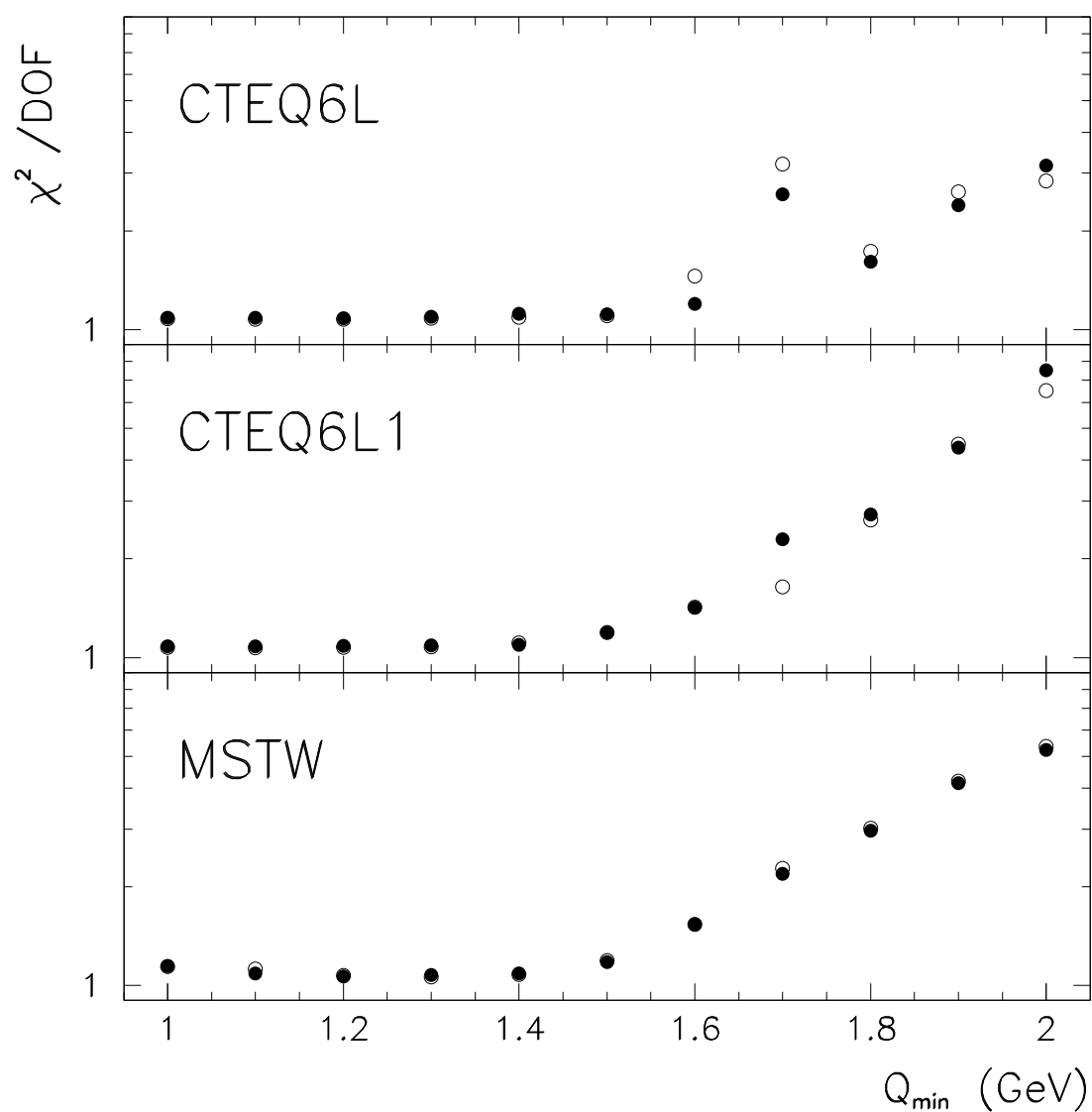
Figure 6.7: The χ^2/dof as a function of the cutoff Q_{min} for the monopole ($\circ$) and the dipole ($\bullet$) semi-hard form factor. Master Dissertation result [232].
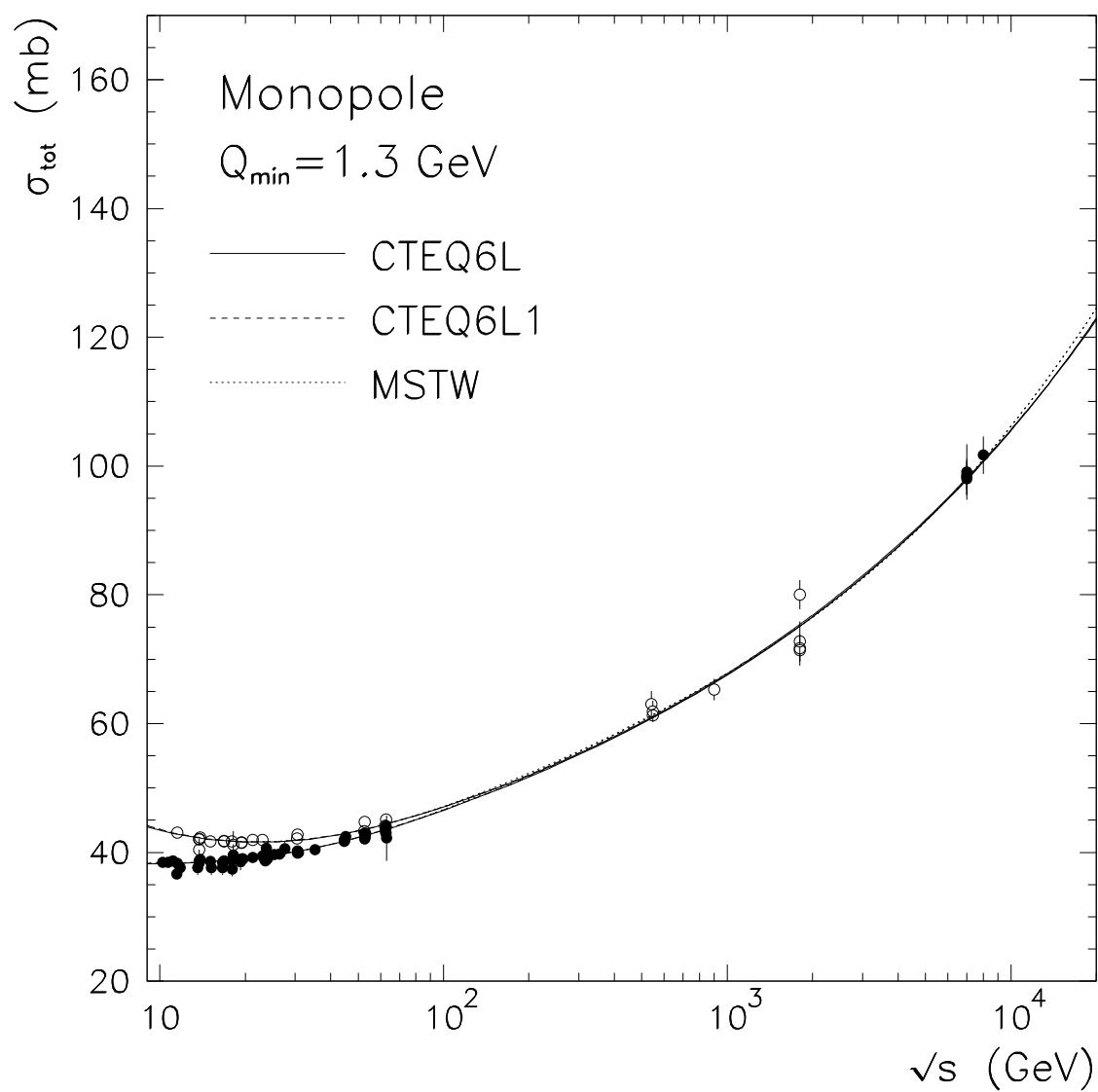
Figure 6.8: Total cross-section for pp ($\bullet$) and $\bar{p}p$ ($\circ$). Master Dissertation result [232].
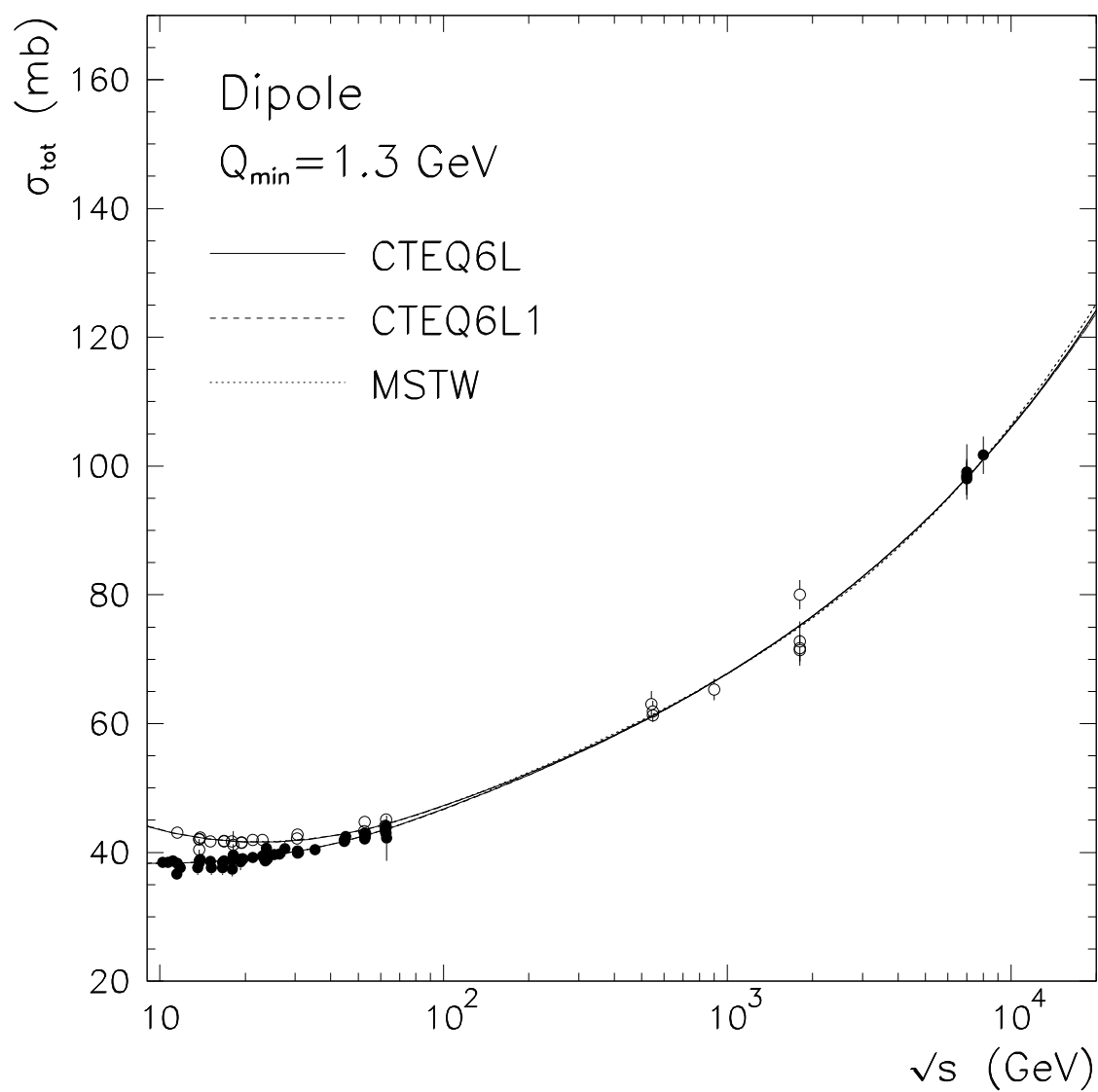
Figure 6.9: Total cross-section for pp ($\bullet$) and $\bar{p}p$ ($\circ$). Master Dissertation result [232].
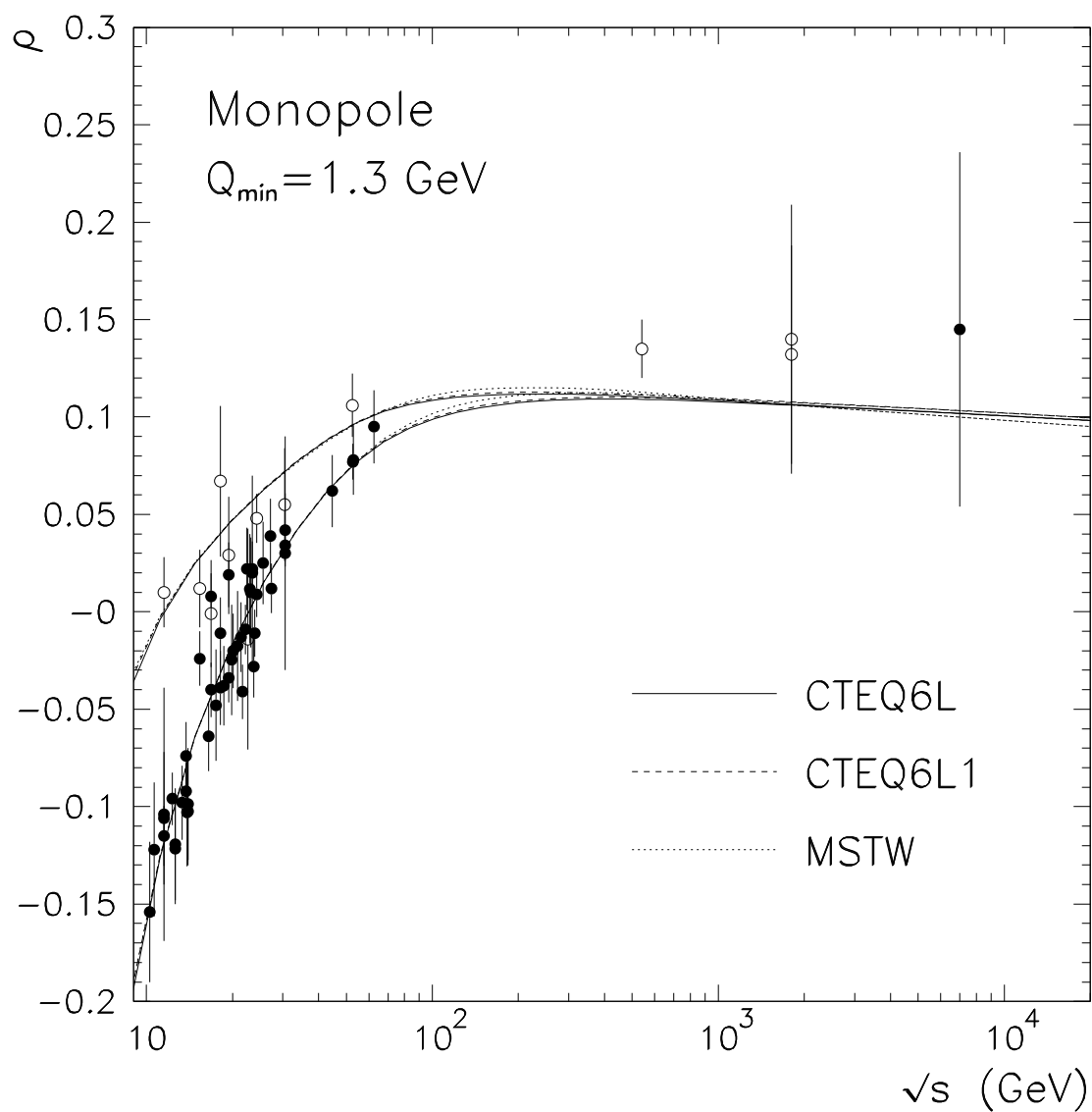
Figure 6.10: Ratio of the real to imaginary part of the forward scattering amplitude for pp (•) and $\bar{p}p$ (○). Master Dissertation result [232].
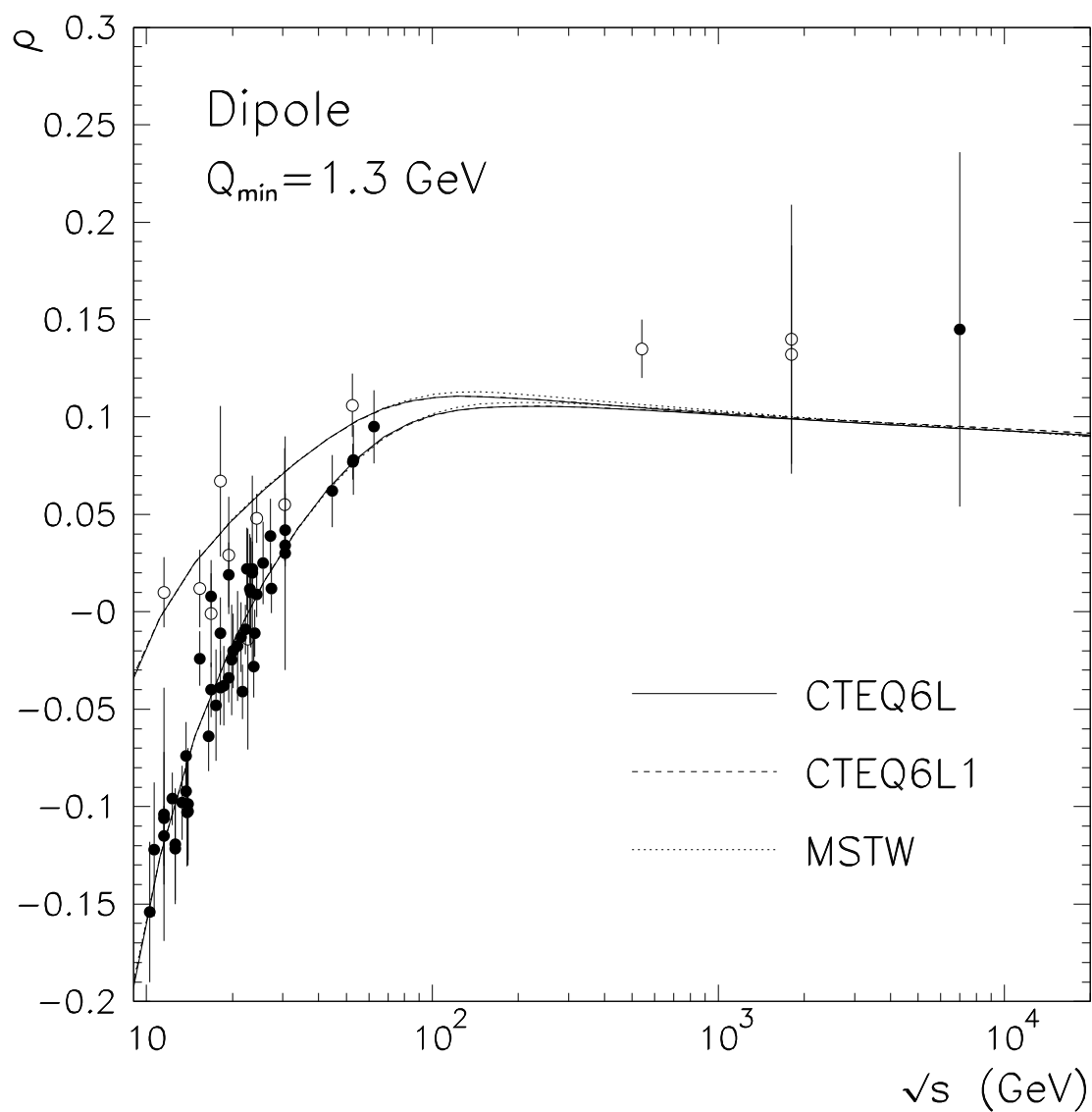
Figure 6.11: Ratio of the real to imaginary part of the forward scattering amplitude for pp ($\bullet$) and $\bar{p}p$ ($\circ$). Master Dissertation result [232].

Chapter 7

Perspectives and work in progress

To work with phenomenology Physics is like taking the risk to make mistakes everyday. The work presented here was divided in two parts. Two different approaches which in essence describe the same thing. The first part concerns to our Regge-Gribov based model, which was initially based on some ideas of Covolan *et al* [65] and also inspired by the guidelines of KMR model from the Durham Group [74–77]. It started just as a toy-model, just as an exercise to tune our numerical codes, our QIM numerical codes. As time goes by, we saw that perhaps it was possible to study the constraints of the Pomeron intercept in a very fresh way by means of the recent LHC released data. And last, but not least, our QCD-inspired eikonal model [28, 29, 233], based on a revised version of the original DGM model [24, 27], where it was introduced a whole class of energy-dependent form factors which account for the dynamics of the semi-hard partonic collisions at high energies, and updated sets of particle distribution functions. These two revised analysis are our "little mistakes" per se, and for the time being those are my biggest, and only, contributions to Physics, more specifically in the field of particle Physics phenomenology.

7.1 Future prospects in the Regge-Gribov inspired model

This is a very brand new study, and for this reason we still does not have so many changes to perform, but rather there are some ideas. Most of them were actually our first choices to begin with calculations, but we decided to give a step backward and not to overcomplicate the analysis right in the first draft. However, in what follows is discussed some specific possible changes, in fact some of them was already performed in Reference [233].

I. The signature factor

As it was shown and discussed in Chapter 4, in order to simplify the numerical calculations we decided to use the asymptotic form of the signatures at very low-t region. Indeed,

these asymptotic forms led to faster numerical coding, however if we decide to study the elastic hadron-hadron scattering at higher values of t, then we have to use the signature factors as given in expression (4.2). Within the full signature, the Born-level amplitude again will be separated into its real and imaginary parts, respectively. For the Pomeron term,

$$
\begin{aligned}
A_{\mathbb{P}}(s,t) &= -\beta_{\mathbb{P}}^2(t) \frac{1 + \cos(\pi\alpha_{\mathbb{P}}(t))}{\sin(\pi\alpha_{\mathbb{P}}(t))} \left(\frac{s}{s_0}\right)^{\alpha_{\mathbb{P}}(t)} + i\beta_{\mathbb{P}}^2(t) \left(\frac{s}{s_0}\right)^{\alpha_{\mathbb{P}}(t)} \\
&= -\beta_{\mathbb{P}}^2(t) \frac{\cos\left(\frac{\pi}{2}\alpha_{\mathbb{P}}(t)\right)}{\sin\left(\frac{\pi}{2}\alpha_{\mathbb{P}}(t)\right)} \left(\frac{s}{s_0}\right)^{\alpha_{\mathbb{P}}(t)} + i\beta_{\mathbb{P}}^2(t) \left(\frac{s}{s_0}\right)^{\alpha_{\mathbb{P}}(t)},
\end{aligned}
\tag{7.1}
$$

for Reggeons with $C = +1$,

$$
\begin{aligned}
A_+(s,t) &= -\beta_+^2(t) \frac{1 + \cos(\pi\alpha_+(t))}{\sin(\pi\alpha_+(t))} \left(\frac{s}{s_0}\right)^{\alpha_+(t)} + i\beta_+^2(t) \left(\frac{s}{s_0}\right)^{\alpha_+(t)} \\
&= -\beta_+^2(t) \frac{\cos\left(\frac{\pi}{2}\alpha_+(t)\right)}{\sin\left(\frac{\pi}{2}\alpha_+(t)\right)} \left(\frac{s}{s_0}\right)^{\alpha_{\mathbb{P}}(t)} + i\beta_+^2(t) \left(\frac{s}{s_0}\right)^{\alpha_+(t)},
\end{aligned}
\tag{7.2}
$$

and the contribution of Reggeons with $C = -1$,

$$
\begin{aligned}
A_-(s,t) &= -\beta_-^2(t) \frac{1 - \cos(\pi\alpha_-(t))}{\sin(\pi\alpha_-(t))} \left(\frac{s}{s_0}\right)^{\alpha_-(t)} - i\beta_-^2(t) \left(\frac{s}{s_0}\right)^{\alpha_-(t)} \\
&= -\beta_-^2(t) \frac{\sin\left(\frac{\pi}{2}\alpha_-(t)\right)}{\cos\left(\frac{\pi}{2}\alpha_-(t)\right)} \left(\frac{s}{s_0}\right)^{\alpha_-(t)} - i\beta_-^2(t) \left(\frac{s}{s_0}\right)^{\alpha_-(t)},
\end{aligned}
\tag{7.3}
$$

justifying the vertex transformations shown in expression (4.14). The full Born-level amplitude will be given by expression (4.12) and it is separated, respectively, as

$$
A_B(s,t) = \operatorname{Re} A_B(s,t) + i \operatorname{Im} A_B(s,t),
\tag{7.4}
$$

where now, on the contrary, τ flips sign when going from $pp\,(\tau = +1)$ to $\bar{p}p\,(\tau = -1)$, because of the negative sing which appears in the imaginary part of the amplitude for the contribution of Reggeons with $C = -1$.

II. Derivative dispersion relations

Following the work from the Durham Group [74–77], they argue that the ratio between the real to the imaginary part of the amplitude, $\operatorname{Re} A_B(s,t)/\operatorname{Im} A_B(s,t)$, is small, and for simplicity they omit the real part of the Born-level amplitude, since they are not interested in the ρ-parameter, which is typically the real component of the forward amplitude and the elastic differential cross-section is analysed in values of t way far from the dip-region.

Therefore, it can be evaluated via dispersion relation whenever necessary.

However, by looking carefully to the real part of the amplitude, one sees that there are singularities on it, because the full signature factor behaves as $\operatorname{Re}\eta_i(t) \propto 1/\sin(\pi\alpha_i(t))$. Moreover, in our analysis we are carrying out the best global fit to the data by means of the χ^2 fitting procedure, then $\alpha_i(t)$ might take real integer values such that the amplitude could eventually diverge, $\operatorname{Re}A_B(s,t) \to \infty$. For these reasons, we are considering the possibility to neglect this real part of the amplitude, but instead to use a derivative dispersion relation to properly find its correct analytical form.

Therefore, returning to the task in hand, in the large s-limit in a two-body scattering process $1 + 2 \to 3 + 4$, it will be considered, for single Regge exchange, an imaginary Born-level amplitude given by [233]

$$A_i(s,t) = i\xi\beta_i^2(t)\left(\frac{s}{s_0}\right)^{\alpha_i(t)}, \tag{7.5}$$

where $\xi = \pm 1$ stands for the positive or negative signature Reggeons. The complete imaginary Born-level amplitude is written according to expression (4.19), the total cross-section and the ρ-parameter are given by expressions (4.27) and (4.29), respectively.

The connection between the real and imaginary parts of expression (7.4) at $t = 0$ is obtained by means of dispersion relations. Defining,

$$2A_\pm(s,t) = A_{\bar{p}p}(s,t) \pm A_{pp}(s,t), \tag{7.6}$$

these relations read, see expressions (A.69) and (A.76),

$$\operatorname{Re}A_+(s,t=0) = K + s\tan\left[\frac{\pi}{2}\frac{d}{d\ln s}\right]\frac{\operatorname{Re}A_+(s,t=0)}{s}, \tag{7.7}$$

$$\operatorname{Re}A_-(s,t=0) = s\tan\left[\frac{\pi}{2}\left(1+\frac{d}{d\ln s}\right)\right]\frac{\operatorname{Im}A_-(s,t=0)}{s}, \tag{7.8}$$

where K is the subtraction constant, here defined to be zero. Within this formalism one obtains, see Appendix B.3,

$$\rho(s)\sigma_{tot}(s) = Xs^\epsilon\tan\left(\frac{\pi}{2}\epsilon\right) - Y_+s^{-\eta+}\tan\left(\frac{\pi}{2}\eta_+\right) + \tau Y_-s^{-\eta-}\cot\left(\frac{\pi}{2}\eta_-\right). \tag{7.9}$$

where $X \equiv 4\pi\beta_P^2(0)s_0^{-(1+\epsilon)}$ and $Y_\pm \equiv 4\pi\beta_\pm^2(0)s_0^{-(1-\eta_\pm)}$. The elastic differential cross-section is expressed in terms of the complex amplitude $A(s,t)$, where we assume that the derivative dispersion relations are valid for $t \leq 1$ GeV^2,

$$\operatorname{Re}A_+(s,t) = K + s\tan\left[\frac{\pi}{2}\frac{d}{d\ln s}\right]\frac{\operatorname{Re}A_+(s,t)}{s}, \tag{7.10}$$

$$\frac{\operatorname{Re} A_-(s,t)}{s} = \tan\left[\frac{\pi}{2}\left(1 + \frac{d}{d\ln(s)}\right)\right]\frac{\operatorname{Im} A_-(s,t)}{s}, \tag{7.11}$$

and a straightforward calculation shows that, see Appendix B.3,

$$\begin{aligned}
\operatorname{Re} A_B^{pp,\bar{p}p}(s,t) = {}&X s^{1+\epsilon'}\left[\frac{\pi}{2}\left(\alpha_{\mathbb{P}}' t + \Phi\right) + \tan\left(\frac{\pi}{2}\epsilon\right)\right] \\
&- Y_+ s^{1-\eta_+'}\left[-\frac{\pi}{2}\alpha_+' t + \tan\left(\frac{\pi}{2}\eta_+\right)\right] \\
&+ \tau Y_- s^{1-\eta_-'}\left[\frac{\pi}{2}\alpha_-' t + \cot\left(\frac{\pi}{2}\eta_-\right)\right],
\end{aligned} \tag{7.12}$$

where it was defined $\epsilon' = \epsilon + \alpha_{\mathbb{P}}' t + \Phi$, $\eta_+' = \eta_+ - \alpha_+' t$ and $\eta_-' = \eta_- - \alpha_-' t$. The quantity Φ stands for the non-linear correction in the Pomeron trajectory. Notice that for $t = 0$ one recovers the forward expression (7.9).

7.2 On QIM future insights

Although we have obtained some very good descriptions of the forward experimental data, namely $\sigma_{tot}^{pp,\bar{p}p}$ and $\rho^{pp,\bar{p}p}$, as previously shown in the result's section 6.4, we cannot say that our QIM [28,29] is fully complete and also that our results and predictions, respectively, are undoubtedly correct. But things are moving on, as for example when Professor Márcio J. Menon pointed out that we were losing the dynamical energy-dependence of the form factors when applying the integral dispersion relation, see expressions (6.64) and (6.65). We are already working on a few sets of modifications and there are also some calculations under analysis. In the following it will be presented a short remark list of what comes next.

I. The functional form of the dynamical gluon mass

Of course that this effective momentum-dependent mass is not a bare one, and its signal is erased from the physical amplitudes just at some few GeV, which merge into the perturbative QCD calculations. As it was mentioned before, the gluons mass generation mechanism is a purely dynamical effect, for this reason the formal approach for tackling this non-perturbative problem is provided by Dyson-Schwinger equations [150, 151]. The generation of a dynamical gluon mass is associated with infrared finite solutions of the gluon propagator [147, 234–238], where in covariant gauges it has the form

$$\Delta_{\mu\nu}(q^2) = -i\left[P_{\mu\nu}(q)\Delta(q^2) + \xi\frac{q_\mu q_\nu}{q^4}\right], \tag{7.13}$$

where ξ stands for the gauge-fixing parameter and $P_{\mu\nu}(q) = g_{\mu\nu} - q_\mu q_\nu/q^2$. Massive propagators of the form $\Delta^{-1}(q^2) = q^2 + M_g^2(q^2)$ can properly fit infrared finite solutions ($\Delta^{-1}(0) > 0$), where $M_g^2(q^2)$ is the dynamical gluons mass. In a recent study of a non-linear Dyson-

Schwinger equation for the gluon self-energy it was shown that $M_g^2(q^2)$ might have two distinct behaviours [239], where it runs as an inverse power of a logarithm and one where it drops as an inverse power of momentum.

The log-running of the dynamical mass has been found in previous studies of linearised Dyson-Schwinger equation to behave as $M_g^2(Q^2) \sim (\ln Q^2)^{-1-\gamma}$, with $\gamma > 1$ [147, 240]. In the non-linear case this behaviour is given by [239]

$$M_g^2(Q^2) = m_g^2 \left[\frac{\ln\left[\left(Q^2 + \rho M_g^2(Q^2)\right)/\Lambda^2\right]}{\ln\left(\rho m_g^2/\Lambda^2\right)} \right]^{-1-\gamma_1}, \tag{7.14}$$

with $\gamma_1 = -6(1+c_2-c_1)/5$, c_1 and c_2 are parameter of the *Ansatz* for the three-gluon vertex used in the numerical analysis of the gluon self-energy [32]. Their values are constrained by a mass condition which controls the behaviour of the dynamical mass in the ultraviolet region, and the values of ρ and m_g, which controls the behaviour of the dynamical mass in the infrared region, are also constrained by this same condition. Hence, one finds that for the logarithm running these parameters are restricted to the intervals [239]

$$c_1 \in [0.15; 0.4],$$
$$c_2 \in [-1.07; -0.92],$$
$$\rho \in [1.0; 8.0],$$
$$m_g \in [300; 800] \text{ MeV},$$

within the possible values of c_1 and c_2, then $-1-\gamma_1$ has an upper and a lower limit. Just for a better understanding, defining a quantity $\varepsilon_{log} = -1 - \gamma_1$, hence $\varepsilon_{log}^{up} = -1.084$ and $\varepsilon_{log}^{low} = -1.564$.

A power-law running behaviour for the dynamical gluon mass was envisaged for the first time by Cornwall & Hou [241], and according to OPE the most probable asymptotic behaviour of the running gluon mass is proportional to $1/Q^2$ [189]. In the non-linear case this behaviour is given by

$$M_g^2(Q^2) = \frac{m_g^4}{Q^2 + m_g^2} \left[\frac{\ln\left[\left(Q^2 + \rho M_g^2(Q^2)\right)/\Lambda^2\right]}{\ln\left(\rho m_g^2/\Lambda^2\right)} \right]^{\gamma_2-1}, \tag{7.15}$$

where $\gamma_2 = (4 + 6c_1)/5$. For the power-law running the mass condition imposes that

$$c_1 \in [0.7; 1.3],$$
$$\rho \in [1.0; 8.0],$$
$$m_g \in [300; 800] \text{ MeV},$$

and within the possible values of c_1, and defining $\varepsilon_{pl} = \gamma_2 - 1$ then $\varepsilon_{pl}^{up} = 1.360$ and $\varepsilon_{pl}^{low} = 0.639$.

So far we have used in our calculations the functional form which was found for the first time by Cornwall [146, 147], see expression (6.2), where the infrared mass scale m_g is phenomenologically determined and is typically to be of the order $m_g = 500 \pm 200$ MeV. It is worth mentioning that the Cornwall expression is a special case of the logarithm-running expression (7.14) by fixing $\rho = 4$ and $\gamma_1 = 1/11$. Beyond the usual Cornwall expression for the dynamical gluon mass, we are studying the possibility of implementing expressions (7.14) and (7.15) as new sets for the DGM functional form. We chose to keep $\rho = 4$ for both log- and power-like behaviours, and we also decided to study the behaviour of both dynamical mass forms on its respective $\varepsilon_{(log,pl)}^{(up,low)}$ values. Following Luna *et al.* in Reference [32], we see that the infrared mass scale values were obtained by means of the best χ^2 fitting procedure through out global fits to the nucleon structure function $F_2(x, Q^2)$ at low-Q^2 measured in the previously unexplored small-x regime at the HERA collider. In the case of the logarithm running it was found that $m_g = 364 \pm 26$ MeV, and as for the power-law running mass $m_g = 355 \pm 27$ MeV. Therefore, we decided to use these mass scales when we in fact incorporate these alternative forms of the dynamical gluon mass, and the value of $m_g = 400$ MeV which was previouly used will be kept just as a matter of comparison. As before, our results and prediction will be calculated using updated sets of PDF's, namely MSTW and CTEQ6, and physically motivated cutoffs that restrict the parton-level processes to semi-hard ones. We opted to set Q_{min}, *i.e.* the minimum momentum transfer in the semi-hard scattering, as $Q_{min} = 2m_g$. For this reason we expect an increase in the elementary partonic cross-section at high energies since $Q_{min} = 2m_g$ is the limit for two-gluon production.

Figures 7.1 and 7.2 show the behaviour of different functional forms for the dynamical gluons mass, respectively, see expressions (6.2), (7.14) and (7.15). In Figure 7.1, the curves were obtained using the same infrared mass scale, $m_g = 400$ MeV, for all $M_g^2(Q^2)$, just as a matter of comparison between them, and of course because $m_g = 400$ MeV was in fact the infrared mass scale value used in our QCD-eikonal based model [28, 29]. In Figure 7.2, the curves were depicted following the infrared mass scale obtained by Luna *et al.* [32] for each $M_g^2(Q^2)$, namely, in the case of the logarithm running $m_g = 364$ MeV, and in the case of the power-law running $m_g = 355$ MeV. Of course that for the Cornwall expression (6.2), the infrared mass scale value used was $m_g = 400$ MeV. In both Figures 7.1 and 7.2 the curves were depicted using $\Lambda = 326$ MeV [32].

II. Prescription

As mentioned before in section 6.2, we chose to use in our calculations the corresponding Durand & Pi model prescription for the scattering amplitude. There is nothing wrong in

this kind of prescription, but the only reason why we actually have decided to use it was because we were following the work of Durand *et al.* [124–126].

In the attempt to maintain some kind of a stronger connection to the original DGM model [24, 27], and for this reason to state that our model is in fact a "smooth evolution" of the original one, we have decided to modify our prescription [28, 29]. Thus, once again the scattering amplitude will be written as, see expressions (2.101) and (2.102).

$$F(s,t) = i \int_0^\infty db\, b\, J_0(b\sqrt{-t}) \left[1 - e^{i\chi(s,b)}\right], \tag{7.16}$$

where the cross-sections, ρ-parameter and B-slope are respectively given by expressions (2.108-2.113), instead of expressions (6.5-6.7).

This change of prescription implies that $\operatorname{Re}\chi \to -\operatorname{Im}\chi$ and $\operatorname{Im}\chi \to \operatorname{Re}\chi$ in expressions (6.5-6.7), but for consistency we will apply it also in expression (6.10), hence it follows from the QCD parton model that the eikonal $\chi_{SH}(s,b)$ can be factored as [124–126]

$$\operatorname{Im}\chi_{SH}(s,b) = -\frac{1}{2} W_{SH}(b)\, \sigma_{QCD}(s), \tag{7.17}$$

and then the dispersion relation will be properly used to generate the real part of the eikonal function.

III. The dispersion relation

It is not an easy task to implement integral dispersion relations, such as expressions (6.29-6.33), into the numerical code. This is one of the reasons why we are considering the possibility to start using derivative dispersion relations with one subtraction constant in our next generation DGM model.

In the high-energy limit, the integral dispersion relation for even and odd scattering amplitudes are given by [69, 230, 231], see Appendix A.1.1,

$$\operatorname{Re} f^+(s) = K + \frac{2s^2}{\pi} \mathcal{P} \int_{s_0}^\infty ds' \frac{\operatorname{Im} f^+(s)}{s'\left(s'^2 - s^2\right)}, \tag{7.18}$$

and

$$\operatorname{Re} f^-(s) = \frac{2s}{\pi} \mathcal{P} \int_{s_0}^\infty ds' \frac{\operatorname{Im} f^-(s)}{s'^2 - s^2}. \tag{7.19}$$

It is straightforward to show that one can obtain the following expressions as the derivative dispersion relations of the aforementioned expressions [69, 230, 231], for further

details in the formal derivation see Appendix A.1.2,

$$\begin{aligned}
\mathrm{Re}\, f^+(s) &= K + s \tan\left[\frac{\pi}{2}\frac{d}{d\ln s}\right]\frac{\mathrm{Im}\, f^+(s)}{s} \\
&\simeq K + s\frac{\pi}{2}\frac{d}{d\ln s}\frac{\mathrm{Im}\, f^+(s)}{s},
\end{aligned} \tag{7.20}$$

and

$$\begin{aligned}
\mathrm{Re}\, f^-(s) &= \tan\left[\frac{\pi}{2}\frac{d}{d\ln s}\right]\mathrm{Im}\, f^-(s) \\
&\simeq \frac{\pi}{2}\frac{d}{d\ln s}\,\mathrm{Im}\, f^-(s),
\end{aligned} \tag{7.21}$$

and one can easily show that these approximate relation can be obtained through the expansion of the tangent operator $\tan[x] = x + x^3/3 + 2x^5/15 + ...$, where it was considered just up to the first order, see Appendix A.1.2. Terms of higher orders $\mathcal{O}(x^3)$ and so on, give an irrelevant contribution.

Bearing in mind that the eikonals are written as a linear combination of crossing-even and crossing-odd eikonal parts, and that χ^+ and χ^- are therefore real analytic functions of E, thus they have the same cut structure as f^+ and f^-, respectively, see Appendix A.2. Hence, one finds that for the even eikonal,

$$\mathrm{Re}\,\chi^+(s,b) = K + s \tan\left[\frac{\pi}{2}\frac{d}{d\ln s}\right]\frac{\mathrm{Im}\,\chi^+(s,b)}{s}, \tag{7.22}$$

as for the odd eikonal $\chi^-(s,b)$, it accounts just for the difference between pp and $\bar{p}p$ channels and vanishes at high-energy, thus it is enough to parametrise it in a similar way as expression (6.35). As before, the soft eikonal is needed to describe the lower-energy forward data, therefore the even part of the soft eikonal will be parametrised with terms dictated by the Regge-Gribov phenomenology. We are not yet sure of its parametrisation, but see expression (6.34) as a reference.

Within expression (7.22), it is not so difficult to generate the real part of the semi-hard eikonal function from expression (7.17). Thus after some tedious math, one finds

$$\begin{aligned}
\mathrm{Re}\,\chi^+_{SH}(s,b) = K + \frac{\pi}{4}W_{SH}(s,b;\nu_{SH})\,\sigma_{QCD}(s) + \\
-s\frac{\pi}{4}W_{SH}(s,b;\nu_{SH})\frac{d\sigma_{QCD}(s)}{ds} - s\frac{\pi}{4}\sigma_{QCD}(s)\frac{dW_{SH}(s,b;\nu_{SH})}{d\nu_{SH}}\frac{d\nu_{SH}(s)}{ds},
\end{aligned} \tag{7.23}$$

where $\sigma_{QCD}(s)$ is given by expression (6.12) and $W_{SH}(s,b;\nu_{SH})$ is written following the monopole- and the dipole-like *Ansätze* and given by expressions (6.23) and (6.24), respectively. The final expression for the derivatives of the form factor with respect to ν_{SH}, in the

case of the monopole reads

$$\frac{dW_{SH}^{(m)}(s, b; \nu_{SH})}{d\nu_{SH}} = \frac{b}{4\pi} \left[2\nu_{SH}^2 K_1(\nu_{SH} b) - b\nu_{SH}^3 K_0(\nu_{SH} b) \right], \tag{7.24}$$

and for the monopole,

$$\frac{dW_{SH}^{(d)}(s, b; \nu_{SH})}{d\nu_{SH}} = \frac{b^3}{96\pi} \left[2\nu_{SH}^4 K_3(\nu_{SH} b) - b\nu_{SH}^5 K_2(\nu_{SH} b) \right]. \tag{7.25}$$

In the above expressions, it was used the following recurrence formulas for $K's$ functions [61],

$$\left(\frac{d}{xdx} \right)^m [x^n K_n(x)] = (-1)^m x^{n-m} K_{n-m}(x), \tag{7.26}$$

and also,

$$\left(\frac{d}{xdx} \right)^m \left[x^{-n} K_n(x) \right] = (-1)^m x^{-n-m} K_{n+m}(x). \tag{7.27}$$

For $m = 1$ and $x = \nu b$, then

$$\frac{d}{d\nu} [\nu^n K_n(\nu b)] = -b\nu^n K_{n-1}(\nu b), \tag{7.28}$$

and,

$$\frac{d}{d\nu} \left[\nu^{-n} K_n(\nu b) \right] = -b\nu^{-n} K_{n+1}(\nu b). \tag{7.29}$$

IV. Energy dependence

The semi-hard parton-parton scattering is directly associated with the increase of the total cross-sections at high energies. This high-energy dependence of the cross-sections is driven mainly by processes involving at least one gluon in the initial state of the elementary scattering subprocess. Thus, in our revised version of the DGM model, the semi-hard gluon, which dominates at high-energy, we have considered the possibility of a "broadening" of the spatial distribution suggesting an increase of the average gluon radius when $\sqrt{s}$ increases. Our assumption was properly implemented by means of phenomenological energy-dependent form factors, where ν_{SH} accounts for all of this energy dependence. Thus, we are considering the possibility to study different forms of ν_{SH}, as for example:

    i. double-log-like energy-dependence

$$\nu_{SH}(s) = \nu_1 - \nu_2 \ln(\ln s), \quad \text{then} \quad \frac{d\nu_{SH}(s)}{ds} = -\frac{\nu_2}{s \ln s}, \tag{7.30}$$

ii. root-log-like energy-dependence

$$\nu_{SH}(s) = \nu_1 - \nu_2 \ln^{1/2} s, \quad \text{then} \quad \frac{d\nu_{SH}(s)}{ds} = -\frac{\nu_2}{2s \ln^{1/2} s}, \tag{7.31}$$

iii. and of course, the original log-like energy-dependence

$$\nu_{SH}(s) = \nu_1 - \nu_2 \ln s, \quad \text{then} \quad \frac{d\nu_{SH}(s)}{ds} = -\frac{\nu_2}{s}. \tag{7.32}$$

V. Experimental data

As it was mentioned, we decided to maintain the results which was previously obtained in Reference [28,29]. This means that the most recent data set obtained at the LHC by the TOTEM Collaboration [21] were not considered. So, first of all this new data set must be included, namely $\sigma_{tot}^{pp} = 102.9 \pm 2.30$ mb and $\sigma_{tot}^{pp} = 103.0 \pm 2.30$ mb at $\sqrt{s} = 8$ TeV [21], and also the ratio of the real to the imaginary part of the forward scattering amplitude $\rho^{pp} = 0.120 \pm 0.030$ also at $\sqrt{s} = 8$ TeV [21].

In the attempt to obtain a better shape of the ρ-parameter at middle energies, because there are not any data sets for pp collisions at this energy region, there is an effort at the LHC to measure, as a TOTEM request in a special run, total cross-sections at energies $\sqrt{s} = 900$ GeV and perhaps later at $\sqrt{s} = 450$ GeV [242], respectively for 2018. There are also some preliminary data at the energy $\sqrt{s} = 2.76$ TeV, namely $\sigma_{tot}^{pp} = 84.7 \pm 3.3$ mb [242] using $\rho = 0.145$ [51]. Perhaps, should be interesting to give some predictions for the total cross-section and the ρ-parameter at this middle energy region and also at $\sqrt{s} = 2.76$ TeV in our forthcoming work, and also to take into account these "new set" in our Regge-Gribov based model. It is expected that by the end of this year, 2017, the TOTEM Collaboration at the LHC releases the corresponding data set at $\sqrt{s} = 13$ TeV [243].

The corresponding differential cross-section data sets were not included in our analysis, because our energy-dependent form factors are not "strong enough" to treat the dip-shoulder region, as well as the behaviour in the region of higher values of t. We are still studying some different ways of introducing a better t-dependence in our energy-dependent form factors. We have some ideas, but just ideas that does not worth to be mentioned yet.

Speaking of differential cross-section, some years ago I briefly presented part of my initial work in the RETINHA-XXV workshop. Figure 7.3 shows our fitting to the differential cross-section at $\sqrt{s} = 7$ TeV [244]. At that time, our even eikonal function was written as the sum of quark-quark, quark-gluon and gluon-gluon contributions, respectively [24, 27], and each one of them parametrised on its own way. For the gluon-gluon contribution,

$$\chi_{gg}(s,b) = \sigma_{gg}(s)W(b;\mu_{gg}), \tag{7.33}$$

where $W(b; \mu_{gg})$ was a monopole or a dipole form factor with no energy dependence,

$$\sigma_{gg}(s) = \frac{1}{2} C_{gg} \int_{2Q^2/s}^{1} dx_1 \int_{2Q^2/x_1s}^{1} dx_2 \int_{4m_g^2}^{\hat{s}/2} d|\hat{t}| \, \frac{d\hat{\sigma}_{gg}}{d|\hat{t}|}(\hat{s}, |\hat{t}|) \, g_1(x_1, Q^2) g_2(x_2, Q^2), \qquad (7.34)$$

and $g(x, Q^2)$ stands for the gluon distribution function, namely CTEQ6L distribution, the elementary differential cross-section is given by expression (6.38). The C_{gg} ($= 0.026 \pm 0.012$) was just a fitting parameter, but it actually gives a reasonable fit to the differential cross-section, although it has, in principle, no physical meaning. Perhaps we should go back a few steps and try to reinterpret this parameter, and see its statistical weight in our revised DGM model. I do not know, it is just a thought.
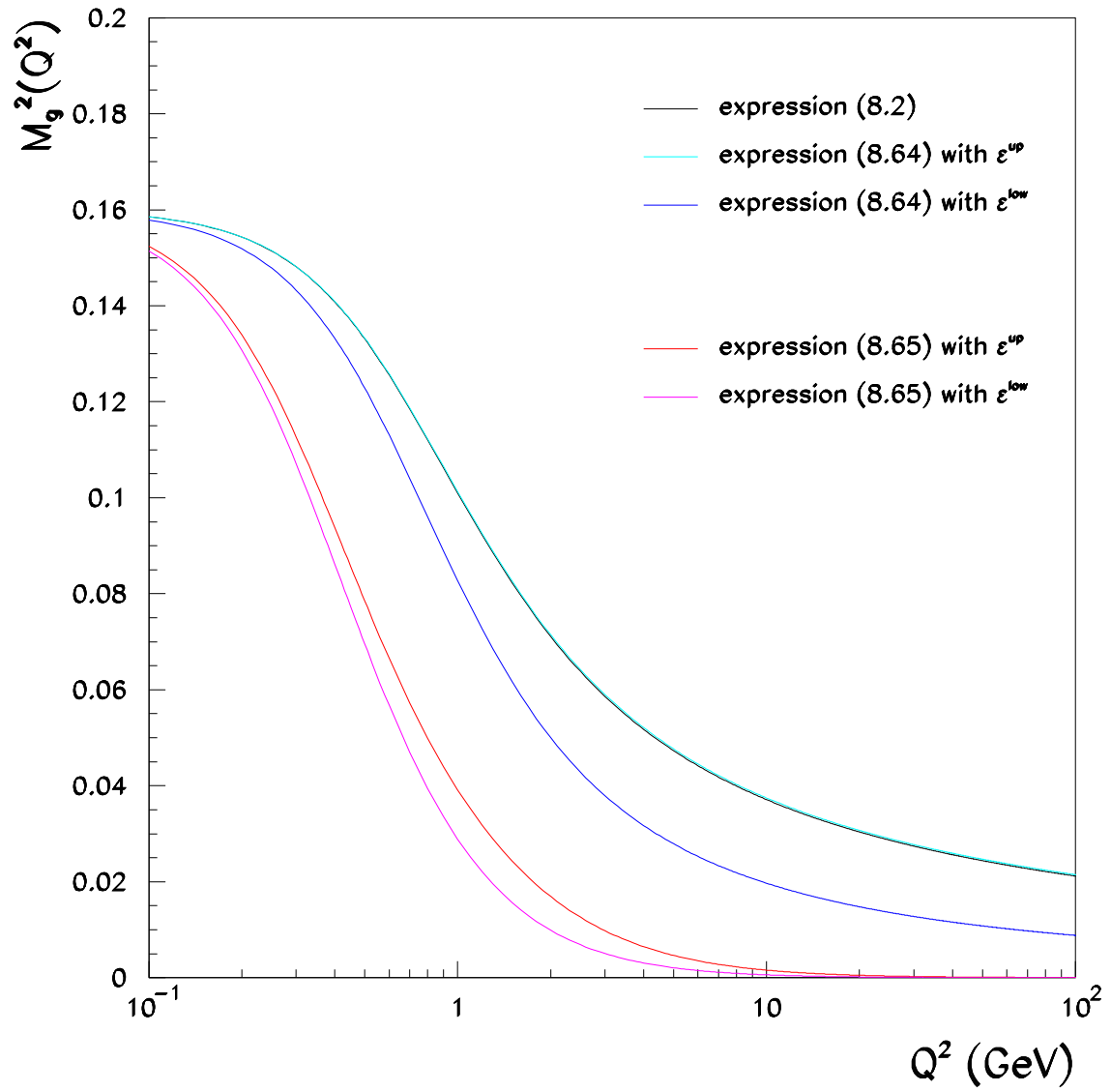
Figure 7.1: Pictorical form of different kinds of dynamical gluon mass with infrared mass scale $m_g = 400$ MeV and $\Lambda = 326$ MeV.
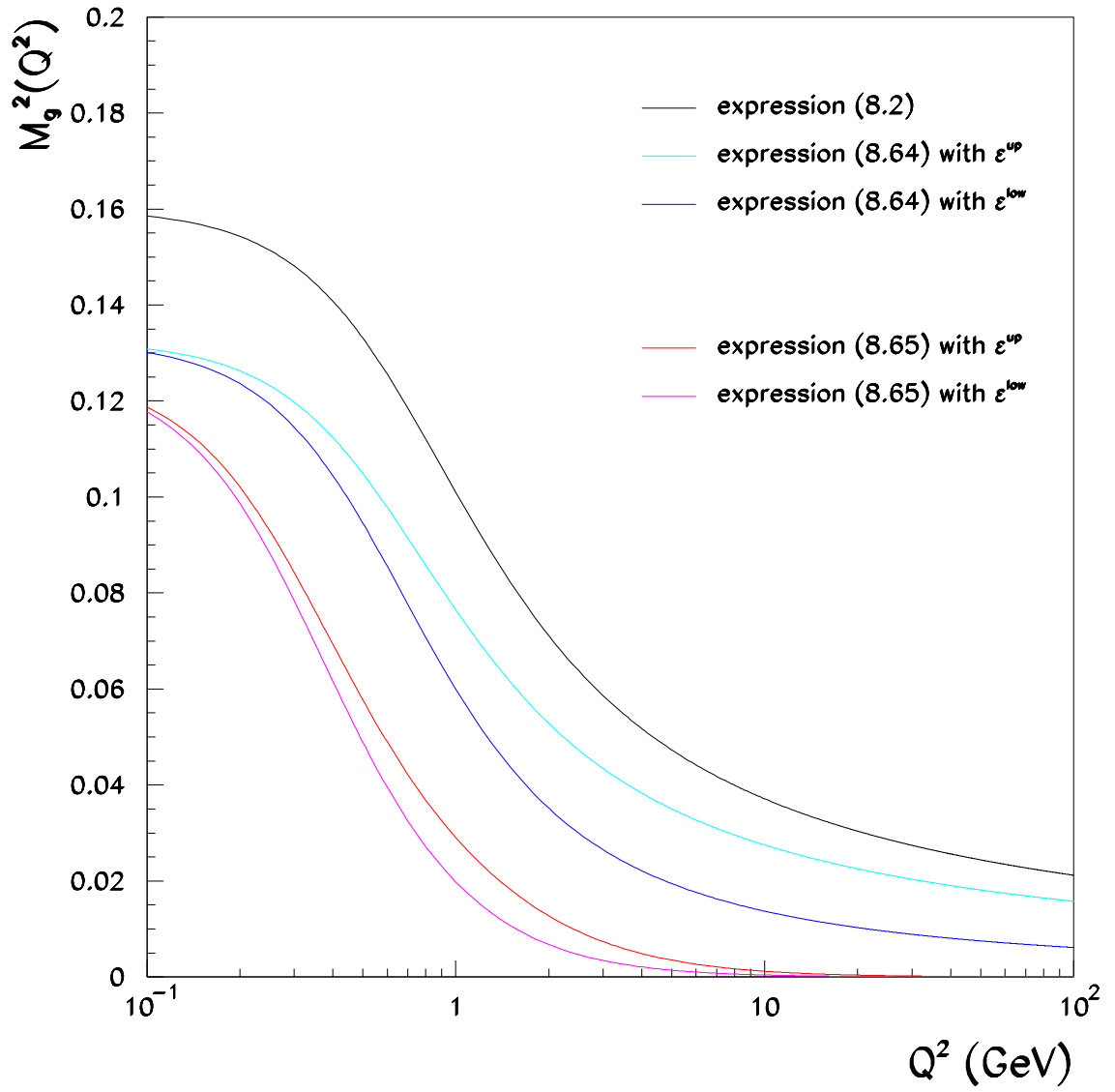
Figure 7.2: Pictorical form of different kinds of dynamical gluon mass with infrared mass scale $m_g = 400$ in the case of the usual Cornwall expression, and $m_g = 364$ ($m_g = 355$) MeV for the logarithm (power-law) running with $\Lambda = 326$ MeV.
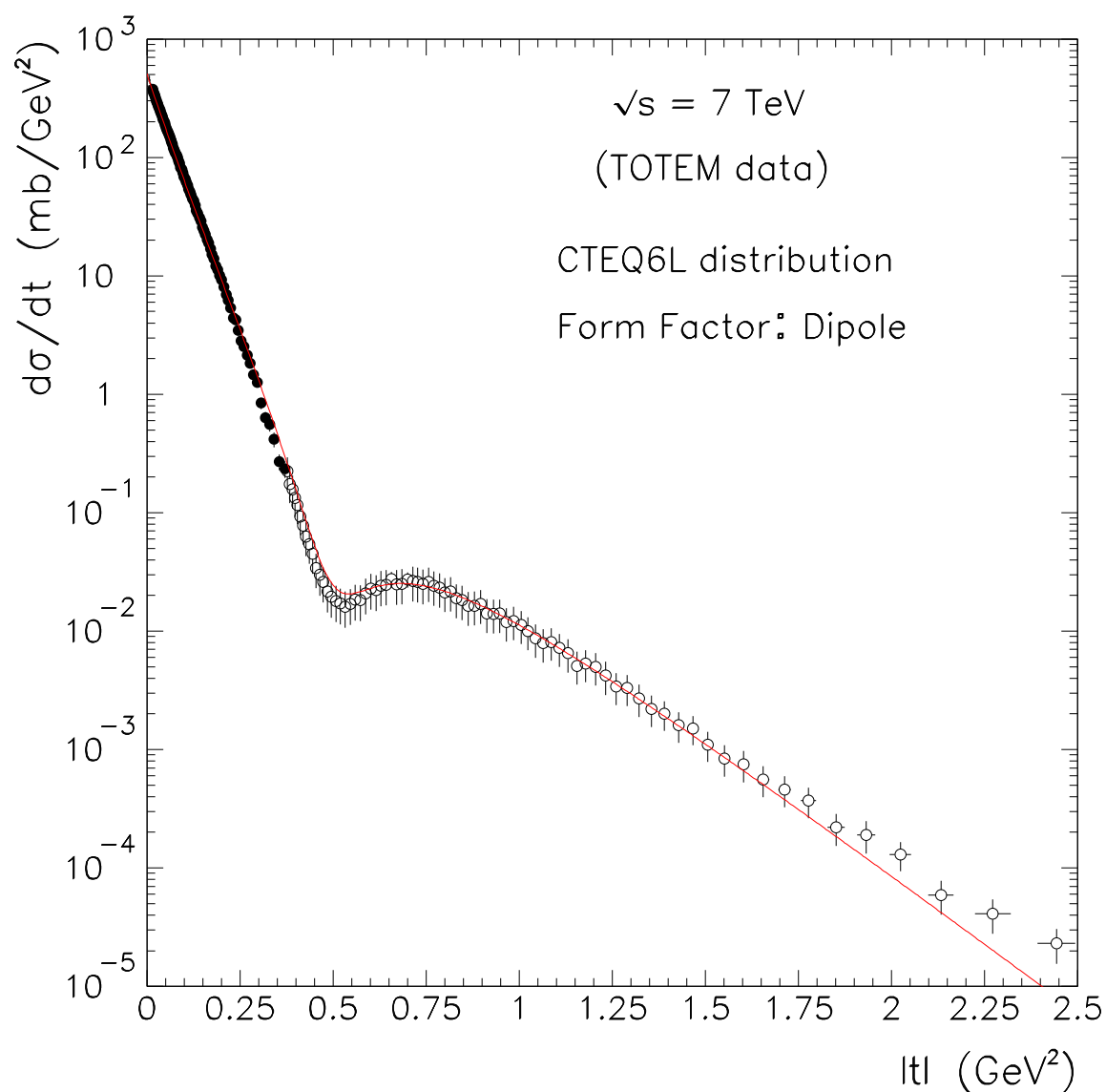
Figure 7.3: The fitting to the differential cross-section at $\sqrt{s} = 7$ TeV presented in RETINHA-XXV workshop [244].

Appendix A

General properties of the scattering amplitude

In the early 60's the scattering S-matrix program was an attempt to pursue a theoretical approach towards a complete description of strong interactions and as motivation the belief that scattering should become simpler as the energy increases. At high-energy, it is known that a huge number of partial waves is involved, and therefore an accurate knowledge of each one of them becomes unpractical and a small number of parameters should be enough to satisfactorily describe high-energy collisions. At present, the low-momentum transfer processes which contribute to most of the total cross-section and to diffractive reactions cannot be treated perturbatively and calculated in a reliable way only within QCD [122]. The original program of S-matrix failed as it was first conceived, but its fundamental principles remain even today in the background of hadronic physics.

In principle it would be possible to reconstruct the entire dynamics of the interaction processes if, and only if, one has the full knowledge of the S-matrix. Basically, it is an unitary operator, $S^\dagger S = S S^\dagger = \mathbb{1}$, which transforms an initial state $|i\rangle$ into the final state $|f\rangle$ of a given scattering processes,

$$S|i\rangle = |f\rangle, \tag{A.1}$$

where these states are defined at the time $t_i \to -\infty$ and $t_f \to +\infty$, respectively. Therefore they represent free particles before and after the interaction, and form a complete set of states.

The S-matrix can be related to the time evolution unitary operator $U(t_i, t_f)$, which connects a state at a given time t_i to time t_f,

$$S = U(-\infty, +\infty), \tag{A.2}$$

and in quantum field theory is given by the Dyson series,

$$S = \mathbb{1} + \sum_{n=1}^{\infty} \frac{i^n}{n!} \int d^4x_1...d^4x_n \tau(H'_{int}(x_1)...H'_{int}(x_n)), \tag{A.3}$$

where τ stands for the time-ordered product and H'_{int} is the interaction Hamiltonian.

In addition to relativistic invariance, which means that the S-matrix elements must depend on Lorentz-invariant combinations of the kinematic variables, the other fundamental principles which are usually assumed in this context are given by the following:

i. Unitarity of the S-matrix, which is a consequence of the principle of conservation of probability. The probability that after the interaction process the system, which is initially in the in-state $|i\rangle$, passes to the out-state $|f\rangle$ is given by

$$P_{i \to f} = |\langle i|S|f\rangle|^2, \tag{A.4}$$

moreover, if one takes an orthonormal basis of vectors $|k\rangle$, the probability to go from an arbitrarily initial state to any of the states $|k\rangle$ must sum up to unity,

$$\sum_k P_{i \to k} = \sum_k |\langle i|S|k\rangle|^2 = \sum_k \langle i|S|k\rangle \langle k|S|i\rangle = \langle i|S^\dagger S|i\rangle = 1. \tag{A.5}$$

ii. Analyticity, which originates from the principle of causality. It states that the S-matrix elements when expressed as functions of the kinematic variables can be analytically continued to the complex domain and the resulting analytic function has a simples singularity structure or at least the simplest one which is consistent with unitarity.

iii. Crossing symmetry, which states that the same invariant amplitudes describing elastic scattering in the s, u and t channels are actually embodied in a single analytic function $F(s,t,u)$.

A.1 Dispersion relations

A direct and very important consequence of analyticity are the dispersion relations, which relate the real and the imaginary part of the scattering amplitude. The first appearance of dispersion relations in Physics was in the 20's through out the work from H.A. Kramers and R. Kronig about the scattering of light by a dispersive medium. That is the reason why it is known as dispersion relations. Over the years this type of relations have been used in many different areas of modern physics and have found its way into particle physics.

A.1.1 Integral dispersion relations

Complex functions of real variables are usually found in physical systems. Although sometimes one can obtain informations about the general properties of a system if the argument of the function is complex, in physics, however, the experimental data are represented by real arguments. Therefore, it is important to verify if it is possible to connect quantities with actual physical meaning. This connection can be properly done by means of the Hilbert transform, or either known as Sokhotski-Plemelj theorem [245].

Let $f(z)$ be an analytic function in the upper semi-plane of a complex plane and over the x-axis such that $|f(z)| \to 0$ at $|z| \to \infty$, and also let C be a smooth closed curve,

$$i\pi f(\alpha) = \lim_{\substack{R \to \infty \\ r \to 0}} \left\{ \int_{-R}^{\alpha - r} dx \, \frac{f(x)}{x - \alpha} + \int_{\alpha + r}^{+R} dx \, \frac{f(x)}{x - \alpha} \right\}, \tag{A.6}$$

where R defines the range of the contour over the complex plane and r defines the ratio of the contour over the pole. The sum of the integrals represents the principal value of Cauchy,

$$i\pi f(\alpha) = \mathcal{P} \int_{-\infty}^{+\infty} dx \, \frac{f(x)}{x - \alpha}, \tag{A.7}$$

where α represents a simple pole. Since $f(x)$ is a complex function of a real value, there is no reason why one cannot write $f(x) \equiv \operatorname{Re} f(x) + i \operatorname{Im} f(x)$. Thus equating one finds a relation between the real and imaginary parts of the complex function,

$$\operatorname{Re} f(\alpha) = \frac{1}{\pi} \mathcal{P} \int_{-\infty}^{+\infty} dx \, \frac{\operatorname{Im} f(x)}{x - \alpha}, \tag{A.8}$$

and the inverse relation,

$$\operatorname{Im} f(\alpha) = -\frac{1}{\pi} \mathcal{P} \int_{-\infty}^{+\infty} dx \, \frac{\operatorname{Re} f(x)}{x - \alpha}, \tag{A.9}$$

However, in some situations physical systems demand a change in the limits of integration like $(-\infty, +\infty) \to [0, +\infty)$. Therefore, $f(x)$ must obey the symmetrical relations imposed by the Schwartz reflection principle which states that if $f(z)$ is an analytic complex function, then $f^*(z) = f(z^*)$. More specifically, scattering amplitudes in the case of pp and $\bar{p}p$ scatterings are written in terms of even and odd functions connected by crossing

symmetry where $f_{\bar{p}p}^{pp} = f^+ \pm f^-$. Thus, the complex function $f(z)$ can be written as

$$
\begin{aligned}
f(z) &= \operatorname{Re} f(z) + i \operatorname{Im} f(z) \\
&= [\operatorname{Re} f_+(z) + \operatorname{Re} f_-(z)] + i \, [\operatorname{Im} f_+(z) + \operatorname{Im} f_-(z)] \\
&= [\operatorname{Re} f_+(z) + i \operatorname{Im} f_+(z)] + [\operatorname{Re} f_-(z) + i \operatorname{Im} f_-(z)] \\
&= f_+(z) + f_-(z).
\end{aligned}
\tag{A.10}
$$

In the case of the even part of $f(z)$, *i.e* when the even complex function behaves as $f_+(z) = f_+(-z)$, the Schwartz reflection principle implies that,

$$
f_+^*(z) = f_+(-z^*),
\tag{A.11}
$$

and by applying it to the real x-axis,

$$
f_+^*(x) = f_+(-x^*) = f_+(-x),
\tag{A.12}
$$

which gives,

$$
f_+^*(x) = \operatorname{Re} f_+(x) - i \operatorname{Im} f_+(x),
\tag{A.13}
$$

$$
f_+(-x) = \operatorname{Re} f_+(-x) + i \operatorname{Im} f_+(-x),
\tag{A.14}
$$

and by means of equation (A.12), one arrives at the symmetrical relations for the even term of the complex function $f(z)$,

$$
\operatorname{Re} f_+(x) = \operatorname{Re} f_+(-x),
\tag{A.15}
$$

$$
\operatorname{Im} f_+(x) = -\operatorname{Im} f_+(-x).
\tag{A.16}
$$

Similarly, in the case of the odd part of $f(z)$, *i.e.* $f_-(z) = -f_-(-z)$, then

$$
f_-^*(z) = -f_-(-z^*),
\tag{A.17}
$$

$$
f_-^*(x) = -f_-(-x^*) = -f_-(-x).
\tag{A.18}
$$

which gives,

$$
f_-^*(x) = \operatorname{Re} f_-(x) - i \operatorname{Im} f_-(x),
\tag{A.19}
$$

$$
f_-(-x) = \operatorname{Re} f_-(-x) + i \operatorname{Im} f_-(-x),
\tag{A.20}
$$

and by means of equation (A.12), similarly one arrives at the odd symmetrical relations,

$$
\operatorname{Re} f_-(x) = -\operatorname{Re} f_-(-x),
\tag{A.21}
$$

$$\text{Im}\, f_-(x) = \text{Im}\, f_-(-x). \tag{A.22}$$

By returning to expressions (A.8) and (A.9), separating the limits of integration into two intervals and considering the even function,

$$\text{Re}\, f_+(\alpha) = \frac{1}{\pi} \mathcal{P} \int_{-\infty}^{0} dx\, \frac{\text{Im}\, f_+(x)}{x - \alpha} + \frac{1}{\pi} \mathcal{P} \int_{0}^{+\infty} dx\, \frac{\text{Im}\, f_+(x)}{x - \alpha}, \tag{A.23}$$

$$\text{Im}\, f_+(\alpha) = -\frac{1}{\pi} \mathcal{P} \int_{-\infty}^{0} dx\, \frac{\text{Re}\, f_+(x)}{x - \alpha} - \frac{1}{\pi} \mathcal{P} \int_{0}^{+\infty} dx\, \frac{\text{Re}\, f_+(x)}{x - \alpha}, \tag{A.24}$$

thus by changing $x \to -x$ in the first integral on the *rhs* and within the even symmetrical relations, a straightforward calculation leads to the following integral dispersion relations,

$$\text{Re}\, f_+(\alpha) = \frac{2}{\pi} \mathcal{P} \int_{0}^{\infty} dx\, \frac{x}{x^2 - \alpha^2}\, \text{Im}\, f_+(x), \tag{A.25}$$

$$\text{Im}\, f_+(\alpha) = -\frac{2\alpha}{\pi} \mathcal{P} \int_{0}^{\infty} dx\, \frac{1}{x^2 - \alpha^2}\, \text{Re}\, f_+(x). \tag{A.26}$$

These expressions represent even integral dispersion relations with a single pole-like singularity in the real axis. The necessary condition adopted to obtain dispersion relations is the request that $f(z)$ be a well behaved function, *i.e.* $f(z)$ must be analytic at $\text{Im}\, z \geq 0$ and $|f(z)| \to 0$ at $|z| \to \infty$. A similar calculation for the odd function would therefore be written by the following relations,

$$\text{Re}\, f_-(\alpha) = \frac{2\alpha}{\pi} \mathcal{P} \int_{0}^{\infty} dx\, \frac{1}{x^2 - \alpha^2}\, \text{Im}\, f_-(x), \tag{A.27}$$

$$\text{Im}\, f_-(\alpha) = -\frac{2}{\pi} \mathcal{P} \int_{0}^{\infty} dx\, \frac{x}{x^2 - \alpha^2}\, \text{Re}\, f_-(x), \tag{A.28}$$

which represent odd integral dispersion relations with a single pole-like singularity in the real axis.

However, is common to work with complex functions $f(z)$ which are not well behaved, *i.e.* they do not converge at $|z| \to \infty$. Then the approach must be slightly modified. This is the case, for instance, of a limited function where asymptotically for $|z| \to \infty$, $|f(z)| = \text{constant}$. To begin with, it is necessary to find a function which is asymptotically well behaved, *i.e.* analytic in the upper-half complex plane and vanishes at large values of $|z|$. Thus defining a function $\varphi(z)$ such that,

$$\varphi(z) \equiv \frac{f(z) - f(\alpha_0)}{z - \alpha_0}, \tag{A.29}$$

where is not singular at $z = \alpha_0$ once it is stated that

$$\lim_{z \to \alpha_0} \frac{f(z) - f(\alpha_0)}{z - \alpha_0} = f'(\alpha_0), \tag{A.30}$$

thus implying that $\varphi(z)$ is analytic in the upper-half complex plane. By taking the limit for large values of $|z|$,

$$\lim_{|z| \to \infty} \varphi(z) = \lim_{|z| \to \infty} \frac{|f(z) - f(\alpha_0)|}{|z - \alpha_0|}, \tag{A.31}$$

and using the Cauchy-Schwartz inequality,

$$
\begin{aligned}
|A - B| &= |A| - |B|, \quad \text{if } B \geq 0, \\
|A - B| &> |A| - |B|, \quad \text{if } B < 0, \\
|A - B| &\geq |A| - |B|.
\end{aligned} \tag{A.32}
$$

then one is able to prove that,

$$\lim_{|z| \to \infty} \varphi(z) \leq \lim_{|z| \to \infty} \frac{|f(z) - f(\alpha_0)|}{|z| - |\alpha_0|} = 0. \tag{A.33}$$

Hence, expressions (A.20) and (A.23) show that $\varphi(z)$ has the required properties, so it can be written by means of a dispersion relation,

$$i\pi\varphi(\alpha) = \mathcal{P} \int_{-\infty}^{+\infty} dx \, \frac{\varphi(x)}{(x - \alpha)}, \tag{A.34}$$

which is exactly as

$$
\begin{aligned}
f(\alpha) - f(\alpha_0) &= \frac{\alpha - \alpha_0}{i\pi} \mathcal{P} \int_{-\infty}^{+\infty} dx \, \frac{f(x) - f(\alpha_0)}{(x - \alpha)(x - \alpha_0)} \\
&= \frac{\alpha - \alpha_0}{i\pi} \mathcal{P} \int_{-\infty}^{+\infty} dx \, \frac{f(x)}{(x - \alpha)(x - \alpha_0)} + \frac{f(\alpha_0)}{i\pi} \mathcal{P} \int_{-\infty}^{+\infty} dx \left[\frac{1}{(x - \alpha)} - \frac{1}{(x - \alpha_0)} \right].
\end{aligned} \tag{A.35}
$$

It is easy to see that the second integral in the *rhs* vanishes because of

$$\int_{-\infty}^{+\infty} dx \, \frac{1}{x - y} = \lim_{\epsilon \to \infty} \int_{-\epsilon}^{+\epsilon} dx \, \frac{1}{x - y} = \lim_{\epsilon \to +\infty} \ln |\epsilon - y| - \lim_{\epsilon \to +\infty} \ln |\epsilon + y| = 0. \tag{A.36}$$

By means of the above result, the dispersion relation takes the form,

$$f(\alpha) = f(\alpha_0) + \frac{\alpha - \alpha_0}{i\pi} \mathcal{P} \int_{-\infty}^{+\infty} dx \, \frac{f(x)}{(x - \alpha)(x - \alpha_0)}, \tag{A.37}$$

and by following the same procedure as before, one arrives at the relation between the real and the imaginary parts of the complex function,

$$\operatorname{Re} f(\alpha) = \operatorname{Re} f(\alpha_0) + \frac{\alpha - \alpha_0}{\pi} \mathcal{P} \int_{-\infty}^{+\infty} dx \, \frac{\operatorname{Im} f(x)}{(x - \alpha)(x - \alpha_0)}, \tag{A.38}$$

and the inverse relation,

$$\operatorname{Im} f(\alpha) = \operatorname{Re} f(\alpha_0) - \frac{\alpha - \alpha_0}{\pi} \mathcal{P} \int_{-\infty}^{+\infty} dx \, \frac{\operatorname{Re} f(x)}{(x - \alpha)(x - \alpha_0)}. \tag{A.39}$$

These expressions define the so-called class of single-subtracted integral dispersion relations. In general, for those cases where the complex function behaves as $|f(z)| \sim z^\lambda$ at $|z| \to \infty$, then in principle it is necessary to make N subtractions so that $f(z)$ converges asymptotically for large $|z|$. As before, by changing the limits of integration to physical limits, *i.e.*, to $(-\infty, +\infty) \to [0, +\infty)$, and using the even and odd symmetrical relation imposed by Schwartz's reflection principle, a straightforward calculation for the even function would easily give,

$$\operatorname{Re} f_+(\alpha) = \operatorname{Re} f_+(\alpha_0) + \frac{2}{\pi} \mathcal{P} \int_0^{+\infty} dx \, \frac{x(\alpha^2 - \alpha_0^2)}{(x^2 - \alpha^2)(x^2 - \alpha_0^2)} \operatorname{Im} f_+(x), \tag{A.40}$$

and also,

$$\operatorname{Im} f_+(\alpha) = \operatorname{Im} f_+(\alpha_0) - \frac{2}{\pi} \mathcal{P} \int_0^{+\infty} dx \, \frac{(\alpha - \alpha_0)(x^2 - \alpha\alpha_0)}{(x^2 - \alpha^2)(x^2 - \alpha_0^2)} \operatorname{Re} f_+(x). \tag{A.41}$$

Just for curiosity, by changing $\alpha \to s$, $x \to s'$ and $\alpha_0 \to 0$, one arrives at the energy integral dispersion relations for the scattering amplitude with one subtraction constant, respectively,

$$\operatorname{Re} f_+(s) = \operatorname{Re} f_+(0) + \frac{2s^2}{\pi} \mathcal{P} \int_0^{+\infty} ds' \, \frac{\operatorname{Im} f_+(s')}{s'(s'^2 - s^2)}, \tag{A.42}$$

and also,

$$\operatorname{Im} f_+(s) = \operatorname{Im} f_+(0) - \frac{2s}{\pi} \mathcal{P} \int_0^{+\infty} ds' \, \frac{\operatorname{Re} f_+(s')}{s'^2 - s^2}. \tag{A.43}$$

As for the case of the odd function, one arrives at

$$\operatorname{Re} f_-(\alpha) = \operatorname{Re} f_-(\alpha_0) + \frac{2}{\pi} \mathcal{P} \int_0^{+\infty} dx \, \frac{(\alpha - \alpha_0)(x^2 - \alpha\alpha_0)}{(x^2 - \alpha^2)(x^2 - \alpha_0^2)} \operatorname{Im} f_-(x), \tag{A.44}$$

and,

$$\operatorname{Im} f_-(\alpha) = \operatorname{Im} f_-(\alpha_0) - \frac{2}{\pi} \mathcal{P} \int_0^{+\infty} dx \, \frac{x(\alpha^2 - \alpha_0^2)}{(x^2 - \alpha^2)(x^2 - \alpha_0^2)} \operatorname{Re} f_-(x), \tag{A.45}$$

and finally applying the same changing prescription,

$$\operatorname{Re} f_-(s) = \operatorname{Re} f_-(0) + \frac{2s}{\pi} \mathcal{P} \int_0^{+\infty} ds' \, \frac{\operatorname{Im} f_-(s')}{s'^2 - s^2}, \tag{A.46}$$

and also,

$$\operatorname{Im} f_-(s) = \operatorname{Im} f_-(0) - \frac{2s^2}{\pi} \mathcal{P} \int_0^{+\infty} ds' \, \frac{\operatorname{Re} f_-(s')}{s'(s'^2 - s^2)}. \tag{A.47}$$

Before pressing on, if $\mathcal{F}(E)$ is the analytic continuation of the forward elastic scattering amplitude, $f(E, t = 0)$, the pp and $\bar{p}p$ forward amplitudes are the limits of the analytic function $\mathcal{F}$ according to

$$f_{pp}^{\bar{p}p}(E, t = 0) = \lim_{\epsilon \to 0} \mathcal{F}(\mp E \mp i\epsilon, t = 0). \tag{A.48}$$

The Cauchy theorem implies that

$$\mathcal{F}(E) = \frac{1}{2\pi i} \oint dE' \, \frac{\mathcal{F}(E')}{E' - E}, \tag{A.49}$$

and after choosing an appropriate contour, see Figure A.1, the above expression can be written as

$$\mathcal{F}(E) = \frac{1}{2\pi i} \left[\int_m^R dE' \, \frac{\mathcal{F}(E' + i\epsilon) - \mathcal{F}(E' - i\epsilon)}{E' - E} + \int_{-R}^{-m} dE' \, \frac{\mathcal{F}(E' + i\epsilon) - \mathcal{F}(E' - i\epsilon)}{E' - E} \right], \tag{A.50}$$

where $E = -m$ and $E = m$ are cuts on the real axis and $R \to \infty$. For an even amplitude, $\mathcal{F} = \mathcal{F}^+$, i.e. $\mathcal{F}(E' + i\epsilon) = \mathcal{F}(-E' - i\epsilon)$, thus [39],

$$\mathcal{F}^+(E) = \frac{1}{\pi} \int_m^\infty dE' \left[\frac{1}{E' - E} + \frac{1}{E' + E} \right] \operatorname{Im} \mathcal{F}^+(E' + i\epsilon), \tag{A.51}$$

and for an odd amplitude, $\mathcal{F} = \mathcal{F}^-$, i.e. $\mathcal{F}(E' + i\epsilon) = -\mathcal{F}(-E' - i\epsilon)$,

$$\mathcal{F}^-(E) = \frac{1}{\pi} \int_m^\infty dE' \left[\frac{1}{E' - E} - \frac{1}{E' + E} \right] \operatorname{Im} \mathcal{F}^-(E' + i\epsilon), \tag{A.52}$$

where the Schwartz reflection principle implies that

$$\mathcal{F}(E' + i\epsilon) - \mathcal{F}(E' - i\epsilon) = \mathcal{F}(E' + i\epsilon) - \mathcal{F}^*(E' + i\epsilon) = 2i \operatorname{Im} \mathcal{F}(E' - i\epsilon). \tag{A.53}$$

The real and imaginary parts of $f(E)$ are connected by the dispersion relations,

$$\operatorname{Re} f^+(E) = \frac{2}{\pi} \mathcal{P} \int_m^\infty dE' \, \frac{E'}{E'^2 - E^2} \operatorname{Im} f^+(E'), \tag{A.54}$$

and

$$\operatorname{Re} f^-(E) = \frac{2}{\pi} \mathcal{P} \int_m^\infty dE' \, \frac{E}{E'^2 - E^2} \operatorname{Im} f^-(E'), \tag{A.55}$$

which is exactly expression (A.25) and (A.27), except for the lower limit of integration. Hence, taking the limit $E \gg m$ and changing the variable from $E \to s$,

$$\operatorname{Re} f^+(s) = \frac{2}{\pi} \mathcal{P} \int_{s_0}^\infty ds' \, \frac{s'}{s'^2 - s^2} \operatorname{Im} f^+(s'), \tag{A.56}$$

and

$$\operatorname{Re} f^-(s) = \frac{2}{\pi} \mathcal{P} \int_{s_0}^\infty ds' \, \frac{s}{s'^2 - s^2} \operatorname{Im} f^-(s'). \tag{A.57}$$

And by means of the same procedure, the single-subtracted integral dispersion relations are given by,

$$\operatorname{Re} f^+(s) = \operatorname{Re} f^+(0) + \frac{2s^2}{\pi} \mathcal{P} \int_{s_0}^{+\infty} ds' \, \frac{\operatorname{Im} f^+(s')}{s'(s'^2 - s^2)}, \tag{A.58}$$

$$\operatorname{Re} f^-(s) = \operatorname{Re} f^-(0) + \frac{2s}{\pi} \mathcal{P} \int_{s_0}^{+\infty} ds' \, \frac{\operatorname{Im} f^-(s')}{s'^2 - s^2}. \tag{A.59}$$

The same thing goes to obtain the reverse dispersion relations, but applying the Cauchy theorem into an even function such as $\phi^+(E) = (m^2 = E^2)^{-1/2} \mathcal{F}^+(E)$ [39].
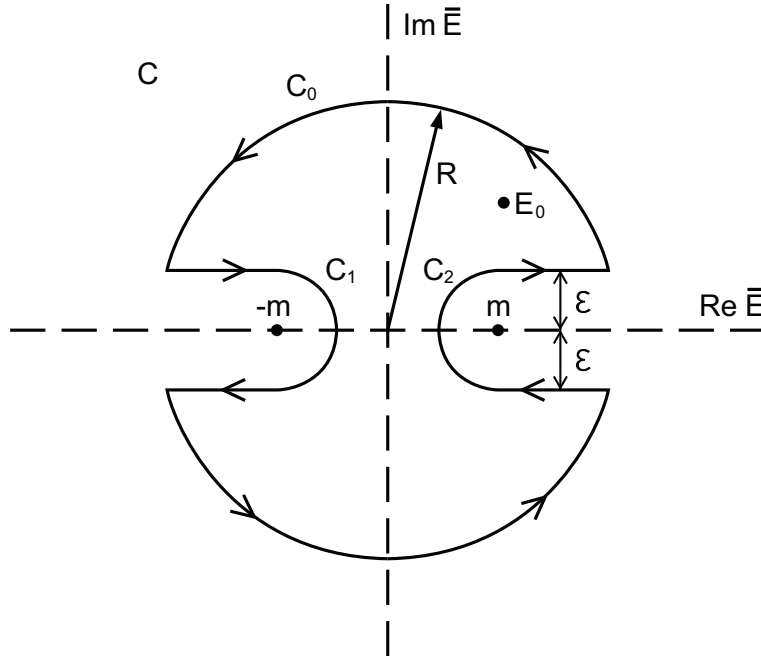

Figure A.1: Complex E-plane and the contour over the pole singularities in the real axis.

A.1.2 Derivative dispersion relations

Although the smooth increase of the total cross-section experimental data at energies above $\sqrt{s} \sim 20$ GeV, roughly as $\sim \ln^2 s$ and that $\sigma_{tot}^{\bar{p}p} - \sigma_{tot}^{pp} \sim 0$, suggest the use of integral dispersion relations with only one subtraction constant, its non-local character limits the class of functions which allows analytical integration [231]. Under some conditions, the integral dispersion forms may be replaced by quasi-local ones, expressed in a derivative form. This is named derivative dispersion relation or either sometimes called by analyticity relations.

By considering the even amplitude in expression (A.58) and rewriting $s' = e^{\xi'}$, $s = e^{\xi}$ and $g(\xi') = \operatorname{Im} f^+(e^{\xi'})/e^{\xi'}$,

$$
\begin{aligned}
\operatorname{Re} f^+(e^{\xi}) - K &= \frac{2e^{\xi'}}{\pi} \mathcal{P} \int_{\ln s_0}^{\infty} d\left(e^{\xi'}\right) \frac{\operatorname{Im} f^+(e^{\xi'})}{e^{\xi'}\left(e^{\xi'2} - e^{2\xi}\right)}, \\
&= \frac{e^{\xi}}{\pi} \mathcal{P} \int_{\ln s_0}^{\infty} d\xi' \frac{g(\xi')}{\sinh(\xi' - \xi)},
\end{aligned} \tag{A.60}
$$

where K stands for the subtraction constant. In the case that $g(x)$ is an analytic function of its argument, then it can be expanded as

$$
g(x') = \sum_{n=0}^{\infty} \frac{d^n}{dx'^n} g(x') \bigg|_{x'=x} \frac{(x' - x)^n}{n!}. \tag{A.61}
$$

Within the above expansion and also by considering the high-energy limit where the mass of the particles can be neglected, $s_0 \to 0$, thus expression (A.60) reads

$$
\operatorname{Re} f^+(e^{\xi}) - K = \frac{e^{\xi}}{\pi} \sum_{n=0}^{\infty} \frac{g^{(n)}(\xi)}{n!} \mathcal{P} \int_{-\infty}^{\infty} d\xi' \frac{(\xi' - \xi)^n}{\sinh(\xi' - \xi)}. \tag{A.62}
$$

The above expression can be put into the following form if one defines $y = (\xi' - \xi)$,

$$
\operatorname{Re} f^+(e^{\xi}) - K = e^{\xi} \sum_{n=0}^{\infty} \frac{g^{(n)}(\xi)}{n!} I_n(y), \tag{A.63}
$$

where

$$
I_n(y) = \frac{\mathcal{P}}{\pi} \int_{-\infty}^{\infty} dy \frac{y^n}{\sinh y}. \tag{A.64}
$$

For even values of n, the integrand will always be an odd function, therefore $I_n = 0$. However, consider the following integral for odd values of n,

$$
J(a) = \frac{\mathcal{P}}{\pi} \int_{-\infty}^{\infty} dy \frac{e^{ay}}{\sinh y} = \tan\left(\frac{a\pi}{2}\right), \tag{A.65}
$$

in such a way that

$$I_n(y) = \frac{d^n}{da^n} J(a)\Big|_{a=0} = \frac{\mathcal{P}}{\pi} \int_{-\infty}^{\infty} dy \, \frac{y^n e^{ay}}{\sinh y}\Big|_{a=0}, \tag{A.66}$$

and then, one arrives at

$$\mathrm{Re}\, f^+(e^\xi) - K = e^\xi \sum_{n=0}^{\infty} \frac{1}{n!} \frac{d^n}{da^n} \tan\left(\frac{a\pi}{2}\right)\Big|_{a=0} \frac{d^n}{d\xi'^n} g(\xi')\Big|_{\xi'=\xi}. \tag{A.67}$$

Hence, by expanding the $\tan(x)$ function, differentiating it n-times with respect to a and collecting together the survival terms when performed $a = 0$ with the n-derivatives of $g(\xi')$ at $\xi' = \xi$, one is led to

$$\mathrm{Re}\, f^+(e^\xi) - K = e^\xi \tan\left[\frac{\pi}{2}\frac{d}{d\xi}\right] g(\xi), \tag{A.68}$$

notice that the tangent operator acts as a differential operator and covers the series expansion. Therefore, by means of the prescription defined before, it leads to

$$\frac{\mathrm{Re}\, f^+(s)}{s} = \frac{K}{s} + \tan\left[\frac{\pi}{2}\frac{d}{d\ln s}\right] \frac{\mathrm{Im}\, f^+(s)}{s}. \tag{A.69}$$

This expression represents the derivative dispersion relation for an even scattering amplitude. By means of an analogous procedure, the odd relation is written as

$$\mathrm{Re}\, f^-(s) = \tan\left[\frac{\pi}{2}\frac{d}{d\ln s}\right] \mathrm{Im}\, f^-(s), \tag{A.70}$$

where it was neglected the contribution of the subtraction constant, because the odd amplitude accounts for the differences between the pp and $\bar{p}p$ data at low energies.

It is possible to show that by defining $x = \ln s$ and $e^x = s$, then,

$$\mathrm{Im}\, f^-(s) = \left(\frac{\mathrm{Im}\, f^-(e^x)}{e^x}\right) e^x \equiv G(x)\, e^x, \tag{A.71}$$

by expanding the tangent operator,

$$\frac{d}{dx}\left[G(x)\, e^x\right] = G'(x)\, e^x + G(x)\, e^x = e^x\left[G'(x) + G(x)\right], \tag{A.72}$$

$$\frac{d^2}{dx^2}\left[G(x)\, e^x\right] = G''(x)\, e^x + G'(x)\, e^x + G'(x)\, e^x + G(x)\, e^x$$
$$= e^x\left[G''(x) + 2G'(x) + G(x)\right], \tag{A.73}$$

$$\frac{d^3}{dx^3}\left[G(x)\, e^x\right] = e^x\left[G'''(x) + 3G''(x) + 3G'(x) + G(x)\right], \tag{A.74}$$

and collecting terms,

$$
\begin{aligned}
\tan\left[\frac{\pi}{2}\frac{d}{dx}\right][G(x)\,e^x] &= e^x\left\{\frac{\pi}{2}\left[G'(x)+G(x)\right]+\frac{1}{3}\left(\frac{\pi}{2}\right)^3\left[G''(x)+2G'(x)+G(x)\right]+\ldots\right\}\\
&= e^x\left\{\frac{\pi}{2}\left[1+\frac{d}{dx}\right]G(x)+\frac{1}{3}\left(\frac{\pi}{2}\right)^3\left[1+\frac{d}{dx}\right]^3 G(x)+\ldots\right\}\\
&= e^x\tan\left[\frac{\pi}{2}\left(1+\frac{d}{dx}\right)\right]G(x).
\end{aligned}
\tag{A.75}
$$

Therefore, this result implies that expression (A.70) can be rewritten as

$$
\frac{\operatorname{Re} f^-(s)}{s} = \tan\left[\frac{\pi}{2}\left(1+\frac{d}{d\ln(s)}\right)\right]\frac{\operatorname{Im} f^-(s)}{s}.
\tag{A.76}
$$

Within an analogous calculation, it is possible to show that for the even scattering amplitude, the following expression,

$$
s\operatorname{Re} f^+(s) = sK + \tan\left[\frac{\pi}{2}\frac{d}{d\ln(s)}\right]\left[s\operatorname{Im} f^+(s)\right],
\tag{A.77}
$$

is similar to expression (A.69). By using the same prescription,

$$
\operatorname{Im} f^+(s) = \left(\frac{\operatorname{Im} f^+(e^x)}{e^x}\right)e^x \equiv G(x)\,e^x,
\tag{A.78}
$$

and again expanding tangent operator,

$$
\frac{d}{dx}\left[G(x)\,e^{2x}\right] = G'(x)\,e^{2x}+2G(x)\,e^x = e^{2x}\left[G'(x)+2G(x)\right],
\tag{A.79}
$$

$$
\begin{aligned}
\frac{d^2}{dx^2}\left[G(x)\,e^{2x}\right] &= G''(x)\,e^{2x}+2G'(x)\,e^{2x}+2G'(x)\,e^{2x}+4G(x)\,e^{2x}\\
&= e^{2x}\left[G''(x)+4G'(x)+4G(x)\right],
\end{aligned}
\tag{A.80}
$$

$$
\frac{d^3}{dx^3}\left[G(x)\,e^x\right] = e^{2x}\left[G'''(x)+6G''(x)+12G'(x)+8G(x)\right].
\tag{A.81}
$$

Thus, collecting terms, one arrives at the following relation,

$$
\begin{aligned}
\tan\left[\frac{\pi}{2}\frac{d}{dx}\right]\left[G(x)\,e^{2x}\right] &= e^{2x}\left\{\left[\pi+\frac{\pi}{2}\frac{d}{dx}\right]G(x)+\frac{1}{3}\left[\pi+\frac{\pi}{2}\frac{d}{dx}\right]^3 G(x)+\ldots\right\}\\
&= e^{2x}\tan\left[\frac{\pi}{2}\left(\pi+\frac{\pi}{2}\frac{d}{dx}\right)\right]G(x).
\end{aligned}
\tag{A.82}
$$

And then,

$$s\mathrm{Re}\, f^+(s) = sK + s^2 \tan\left[\pi + \frac{\pi}{2}\frac{d}{d\ln(s)}\right]\frac{\mathrm{Im}\, f^+(s)}{s}. \tag{A.83}$$

By rewriting the tangent operator as,

$$\tan\left[\pi + \frac{\pi}{2}\frac{d}{d\ln(s)}\right] = \frac{\tan(\pi) + \tan\left(\frac{\pi}{2}\frac{d}{d\ln(s)}\right)}{1 - \tan(\pi)\tan\left(\frac{\pi}{2}\frac{d}{d\ln(s)}\right)}, \tag{A.84}$$

where $\tan(\pi) = 0$, thus,

$$\tan\left[\pi + \frac{\pi}{2}\frac{d}{d\ln(s)}\right] = \tan\left[\frac{\pi}{2}\frac{d}{d\ln(s)}\right]. \tag{A.85}$$

Therefore, expression (A.83) is written exactly as expression (A.69) which completes the proof.

A.2   Relation between the eikonal function and the scattering amplitude

As it was already mentioned before, the physical amplitude for a pp and $\bar{p}p$ scattering is written by means of even and odd terms connected by crossing symmetry,

$$F_{pp}^{\bar{p}p}(s,t) = F^+(s,t) \pm F^-(s,t). \tag{A.86}$$

So, the even and odd amplitudes can be written as

$$F^\pm(s,t) = \frac{F_{\bar{p}p}(s,t) \pm F_{pp}(s,t)}{2}. \tag{A.87}$$

By means of the Durand & Pi prescription, $\Gamma(s,b) = 1 - e^{-\chi(s,b)}$, and expression (2.101), the forward physical scattering amplitude is written as,

$$F(s, t=0) = i\int_0^\infty db\, b\left[1 - e^{-\chi_{pp}^{\bar{p}p}(s,b)}\right], \tag{A.88}$$

where $\chi_{pp}^{\bar{p}p}(s,b) = \chi^+(s,b) \pm \chi^-(s,b)$. In the case of even amplitude, one finds,

$$
\begin{aligned}
2F^+(s) &= i\int_0^\infty db\, b\left[1 - e^{-\chi_{\bar{p}p}(s,b)}\right] + i\int_0^\infty db\, b\left[1 - e^{-\chi_{pp}(s,b)}\right] \\
&= i\int_0^\infty db\, b\left[1 - e^{-\left(\chi^+ + \chi^-\right)}\right] + i\int_0^\infty db\, b\left[1 - e^{-\left(\chi^+ - \chi^-\right)}\right],
\end{aligned} \tag{A.89}
$$

by expanding the exponential,

$$
2F^+(s) = i \int_0^\infty db\, b \left\{ 1 - \left[1 + (\chi^+ + \chi^-) + \frac{(\chi^+ + \chi^-)^2}{2!} + \frac{(\chi^+ + \chi^-)^3}{3!} + \dots \right] \right\} +
$$
$$
+ i \int_0^\infty db\, b \left\{ 1 - \left[1 - (\chi^+ - \chi^-) + \frac{(\chi^+ - \chi^-)^2}{2!} + \frac{(\chi^+ - \chi^-)^3}{3!} + \dots \right] \right\},
$$

(A.90)

and neglecting higher order terms $\mathcal{O}(\chi^2)$, then

$$
\begin{aligned}
F^+(s) &= \frac{i}{2} \int_0^\infty db\, b \left\{ (\chi^+ + \chi^-) + (\chi^+ - \chi^-) \right\} \\
&= i \int_0^\infty db\, b \left\{ 2\chi^+ \right\} \\
&= i \int_0^\infty db\, b \left\{ \chi_R^+ + i\chi_I^+ \right\} \\
&= \underbrace{\int_0^\infty db\, b \left[-\chi_I^+ \right]}_{\mathrm{Re}\, F^+(s)} + i \underbrace{\int_0^\infty db\, b \left[\chi_R^+ \right]}_{\mathrm{Im}\, F^+(s)},
\end{aligned}
$$

(A.91)

Bearing in mind that $F^+(s) = \mathrm{Re}\, F^+(s) + i\, \mathrm{Im}\, F^+(s)$, then at first-order of the eikonal expansion,

$$
\mathrm{Re}\, F^+(s) \longleftrightarrow -\mathrm{Im}\, \chi^+(s, b),
$$

$$
\mathrm{Im}\, F^+(s) \longleftrightarrow \mathrm{Re}\, \chi^+(s, b).
$$

This means that only in first-order of approximation the eikonal function has the same cut structure as the scattering amplitude. Thus justifying the inverse integral dispersion relation in expression (6.26). Following the same procedure, in the case of an odd scattering amplitude,

$$
\begin{aligned}
2F^-(s) &= i \int_0^\infty db\, b \left\{ (\chi^+ + \chi^-) - (\chi^+ - \chi^-) \right\} \\
&= i \int_0^\infty db\, b \left\{ 2\chi^- \right\},
\end{aligned}
$$

(A.92)

then,

$$
\begin{aligned}
F^-(s) &= i \int_0^\infty db\, b\, \chi^- \\
&= i \int_0^\infty db\, b \left\{ \chi_R^- + i\chi_I^- \right\} \\
&= \underbrace{\int_0^\infty db\, b \left[-\chi_I^- \right]}_{\mathrm{Re}\, F^-(s)} + i \underbrace{\int_0^\infty db\, b \left[\chi_R^- \right]}_{\mathrm{Im}\, F^-(s)},
\end{aligned}
$$

(A.93)

therefore leading to a similar result,

$$\mathrm{Re}\,F^-(s) \longleftrightarrow -\mathrm{Im}\,\chi^-(s,b),$$

$$\mathrm{Im}\,F^-(s) \longleftrightarrow \mathrm{Re}\,\chi^-(s,b).$$

If, however, the profile function is written according to the usual DGM prescription, which is exactly the one in expression (2.102), the relation between the eikonal function and the scattering amplitude will slightly change. Therefore, it is not difficult to show that, under this prescrition condition, the relation between the even parts of the eikonal function and the scattering amplitude reads

$$\mathrm{Re}\,F^+(s) \longleftrightarrow \mathrm{Re}\,\chi^+(s,b),$$

$$\mathrm{Im}\,F^+(s) \longleftrightarrow \mathrm{Im}\,\chi^+(s,b),$$

as for the case of its odd parts,

$$\mathrm{Re}\,F^-(s) \longleftrightarrow \mathrm{Re}\,\chi^-(s,b),$$

$$\mathrm{Im}\,F^-(s) \longleftrightarrow \mathrm{Im}\,\chi^-(s,b),$$

then, justifying expression (7.22).

Appendix B

Some useful calculations in the Regge-Gribov based model

This Appendix was written as an attempt to clarify some aspects in the calculations presented in Chapter 4 that may have not been very well discussed. The reader may skip this brief discussion if so desires.

B.1   Reggeon signatures

The reggeon signature factor is given by expression (4.5), and it appears as a consequence of crossing symmetry when calculating the s-channel partial wave scattering amplitude by means of the Watson-Sommerfeld transform in the Froissart-Gribov projection [3, 11–14]. Thus, the signature factor can be rewritten as

$$
\begin{aligned}
\eta(t) &= -\frac{1 + \xi \left[\cos \pi \alpha(t) - i \sin \pi \alpha(t)\right]}{\sin \pi \alpha(t)} \\
&= -\frac{1 + \xi \left[\cos \left(\frac{\pi}{2} \alpha(t) + \frac{\pi}{2} \alpha(t)\right) - i \sin \left(\frac{\pi}{2} \alpha(t) + \frac{\pi}{2} \alpha(t)\right)\right]}{\sin \left(\frac{\pi}{2} \alpha(t) + \frac{\pi}{2} \alpha(t)\right)} \\
&= -\frac{1 + \xi \left[\cos^2 \frac{\pi}{2} \alpha(t) - \sin^2 \frac{\pi}{2} \alpha(t) - 2i \sin \frac{\pi}{2} \alpha(t) \cos \frac{\pi}{2} \alpha(t)\right]}{2 \sin \frac{\pi}{2} \alpha(t) \cos \frac{\pi}{2} \alpha(t)}.
\end{aligned} \tag{B.1}
$$

In the case of reggeons with positive-signature $\xi = +1$, one easily finds

$$
\begin{aligned}
\eta(t) &= -\frac{2 \cos^2 \frac{\pi}{2} \alpha(t) - 2i \sin \frac{\pi}{2} \alpha(t) \cos \frac{\pi}{2} \alpha(t)}{2 \sin \frac{\pi}{2} \alpha(t) \cos \frac{\pi}{2} \alpha(t)} \\
&= -\frac{\cos \frac{\pi}{2} \alpha(t) - i \sin \frac{\pi}{2} \alpha(t)}{\sin \frac{\pi}{2} \alpha(t)} \\
&= -\frac{e^{-i\pi \alpha_i(t)/2}}{\sin \frac{\pi}{2} \alpha_i(t)},
\end{aligned} \tag{B.2}
$$

and for negative-signatures $\xi = -1$,

$$
\begin{aligned}
\eta(t) &= -\frac{2\sin^2\frac{\pi}{2}\alpha(t) + 2i\sin\frac{\pi}{2}\alpha(t)\cos\frac{\pi}{2}\alpha(t)}{2\sin\frac{\pi}{2}\alpha(t)\cos\frac{\pi}{2}\alpha(t)} \\
&= -i\,\frac{-i\sin\frac{\pi}{2}\alpha(t) + \cos\frac{\pi}{2}\alpha(t)}{\cos\frac{\pi}{2}\alpha(t)} \\
&= -i\,\frac{e^{-i\pi\alpha_i(t)/2}}{\cos\frac{\pi}{2}\alpha_i(t)}.
\end{aligned}
\tag{B.3}
$$

B.2   Asymptotic low-t signatures

By means of the extent that $|t|$ is small and considering linear trajectories $\alpha(t) \simeq \alpha(0) + \alpha' t$, it is possible to find the asymptotic form of the signatures at the region of very low-t. Hence, for $\xi = +1$,

$$
\begin{aligned}
\eta(t) &= -\frac{e^{-i\pi(\alpha(0)+\alpha't)/2}}{\sin\frac{\pi}{2}\left(\alpha(0)+\alpha't\right)} \\
&= --\frac{e^{-i\pi(\alpha(0)+\alpha't)/2}}{\sin\frac{\pi}{2}\alpha(0)\cos\frac{\pi}{2}\alpha't + \sin\frac{\pi}{2}\alpha't\sin\frac{\pi}{2}\alpha(0)},
\end{aligned}
\tag{B.4}
$$

where for low-t values $\cos\frac{\pi}{2}\alpha't \sim 1$ and $\sin\frac{\pi}{2}\alpha't \sim \frac{\pi}{2}\alpha't$, therefore $\sin\frac{\pi}{2}\left(\alpha(0)+\alpha't\right) \sim t$. Neglecting the t-dependence of the denominator in expression (B.4),

$$
\eta(t) = -e^{-i\pi\alpha_i(t)/2}.
\tag{B.5}
$$

Similarly, for $\xi = -1$,

$$
\begin{aligned}
\eta(t) &= -i\,\frac{e^{-i\pi(\alpha(0)+\alpha't)/2}}{\cos\frac{\pi}{2}\left(\alpha(0)+\alpha't\right)} \\
&= -i\,\frac{e^{-i\pi(\alpha(0)+\alpha't)/2}}{\cos\frac{\pi}{2}\alpha(0)\cos\frac{\pi}{2}\alpha't - \sin\frac{\pi}{2}\alpha't\sin\frac{\pi}{2}\alpha(0)},
\end{aligned}
\tag{B.6}
$$

where for low-t values $\cos\frac{\pi}{2}\left(\alpha(0)+\alpha't\right) \sim -t$. And as before, neglecting the t-dependence of the denominator in expression (B.6),

$$
\eta(t) = ie^{-i\pi\alpha_i(t)/2}.
\tag{B.7}
$$

B.3   Dispersion relation calculus

From expression (7.6), one can write the real and the imaginary part of the even and odd terms of the physical amplitudes,

$$\operatorname{Re} A^{\bar{p}p}_{pp}(s,t) = \operatorname{Re} A^+(s,t) \pm \operatorname{Re} A^-(s,t), \tag{B.8}$$

$$\operatorname{Im} A^{\bar{p}p}_{pp}(s,t) = \operatorname{Im} A^+(s,t) \pm \operatorname{Im} A^-(s,t), \tag{B.9}$$

and defining even and odd cross-sections such that,

$$
\sigma^+(s) = \frac{4\pi}{s} \operatorname{Im} A^+(s, t=0) = \frac{4\pi}{s} \left[\frac{\operatorname{Im} A_{\bar{p}p}(s,t) + \operatorname{Im} A_{pp}(s,t)}{2} \right]
$$
$$
= \frac{1}{2} \left[\sigma^{\bar{p}p}_{tot}(s) + \sigma^{pp}_{tot}(s) \right], \tag{B.10}
$$

$$
\sigma^-(s) = \frac{4\pi}{s} \operatorname{Im} A^-(s, t=0) = \frac{1}{2} \left[\sigma^{\bar{p}p}_{tot}(s) - \sigma^{pp}_{tot}(s) \right]. \tag{B.11}
$$

By means of expressions (7.7) and (7.8), and with the above results, one can rewrite expression (B.8) in terms of the dispersion relations,

$$
\begin{aligned}
\operatorname{Re} A^{pp}_B(s) &= \frac{s}{8\pi} \tan\left[\frac{\pi}{2} \frac{d}{d\ln s} \right] \left\{ \sigma^{\bar{p}p}_{tot}(s) + \sigma^{pp}_{tot}(s) \right\} + \\
&\quad - \frac{s}{8\pi} \tan\left[\frac{\pi}{2} \left(1 + \frac{d}{d\ln s} \right) \right] \left\{ \sigma^{\bar{p}p}_{tot}(s) - \sigma^{pp}_{tot}(s) \right\} \\
&= s \tan\left[\frac{\pi}{2} \frac{d}{d\ln s} \right] \left\{ X s^\epsilon + Y_+ s^{-\eta_+} \right\} + s \tan\left[\frac{\pi}{2} \left(1 + \frac{d}{d\ln s} \right) \right] \left\{ Y_- s^{-\eta_-} \right\}, \tag{B.12}
\end{aligned}
$$

Applying the tangent operator and collecting the terms corresponding to the intercept of the Reggeons one finds that,

$$
\operatorname{Re} A^{pp}_B(s) = X s^{1+\epsilon} \tan\left[\frac{\pi}{2} \epsilon \right] - Y_+ s^{1-\eta_+} \tan\left[\frac{\pi}{2} \eta_+ \right] + Y_- s^{1-\eta_-} \tan\left[\frac{\pi}{2} (1-\eta_+) \right]. \tag{B.13}
$$

And similarly for $\bar{p}p$ scattering,

$$
\operatorname{Re} A^{\bar{p}p}_B(s) = X s^{1+\epsilon} \tan\left[\frac{\pi}{2} \epsilon \right] - Y_+ s^{1-\eta_+} \tan\left[\frac{\pi}{2} \eta_+ \right] - Y_- s^{1-\eta_-} \tan\left[\frac{\pi}{2} (1-\eta_+) \right]. \tag{B.14}
$$

Now, int the case where the dispersion relations are valid for $t \le 1 \text{ GeV}^2$,

$$
\begin{aligned}
\operatorname{Re} A^{pp}_B(s,t) &= s \tan\left[\frac{\pi}{2} \frac{d}{d\ln s} \right] \frac{\operatorname{Im} A_{\bar{p}p}(s,t) + \operatorname{Im} A_{pp}(s,t)}{2s} + \\
&\quad - s \tan\left[\frac{\pi}{2} \left(1 + \frac{d}{d\ln s} \right) \right] \frac{\operatorname{Im} A_{\bar{p}p}(s,t) - \operatorname{Im} A_{pp}(s,t)}{2s}, \tag{B.15}
\end{aligned}
$$

thus,

$$
\mathrm{Re}\, A_B^{pp}(s,t) = s\tan\left[\frac{\pi}{2}\left(1 + \frac{d}{d\ln s}\right)\right]\left\{s^{\epsilon'}Y_+ s^{-\eta'_+}\right\} + s\tan\left[\frac{\pi}{2}\left(1 + \frac{d}{d\ln s}\right)\right]\left\{Y_- s^{-\eta'_-}\right\}.
$$

$$(\mathrm{B.16})$$

By expanding the tangent operator, again collecting the intercept-Reggeon terms, but now considering the t-dependence only in first order terms of the expansion, then one arrives at,

$$
\begin{aligned}
\mathrm{Re}\, A_B^{pp}(s,t) = {}& X s^{1+\epsilon'}\left[\frac{\pi}{2}\left(\alpha'_{\mathbb{P}}t + \Phi\right) + \tan\left(\frac{\pi}{2}\,\epsilon\right)\right] \\
& - Y_+ s^{1-\eta'_+}\left[-\frac{\pi}{2}\,\alpha'_+ t + \tan\left(\frac{\pi}{2}\,\eta_+\right)\right] \\
& + Y_- s^{1-\eta'_-}\left[\frac{\pi}{2}\,\alpha'_- t + \tan\left(\frac{\pi}{2}\,(1-\eta_-)\right)\right],
\end{aligned}
$$

$$(\mathrm{B.17})$$

and for the case of the $\bar{p}p$ scattering,

$$
\begin{aligned}
\mathrm{Re}\, A_B^{pp}(s,t) = {}& X s^{1+\epsilon'}\left[\frac{\pi}{2}\left(\alpha'_{\mathbb{P}}t + \Phi\right) + \tan\left(\frac{\pi}{2}\,\epsilon\right)\right] \\
& - Y_+ s^{1-\eta'_+}\left[-\frac{\pi}{2}\,\alpha'_+ t + \tan\left(\frac{\pi}{2}\,\eta_+\right)\right] \\
& - Y_- s^{1-\eta'_-}\left[\frac{\pi}{2}\,\alpha'_- t + \tan\left(\frac{\pi}{2}\,(1-\eta_-)\right)\right].
\end{aligned}
$$

$$(\mathrm{B.18})$$

Appendix C

Some useful calculations in QIM

Perhaps in Chapter 6, which presents the newest version of the original dynamical gluon mass model, one probably felt a sort of a lack of mathematical rigorous demonstrations. And this is exactly the reason why this Appendix was written, to tie up these loose ends.

C.1   The overlap density function

The hadron overlap density function at impact-parameter b is written as

$$A(b) = \int d^2\mathbf{b}' \, \rho_A(|\mathbf{b} - \mathbf{b}'|)\rho_B(b'), \tag{C.1}$$

and normalisation[1]

$$N \int d^2\mathbf{b} \, A(b) = 1. \tag{C.2}$$

However, if one writes the parton density function $\rho_B(b')$ as the Fourier Transform of the form factor $G(q^2)$

$$\rho_B(b') = \frac{1}{2\pi} \int d^2\mathbf{q} \, G(q^2) \, \mathrm{e}^{i\,\mathbf{q}\cdot\mathbf{b}'} = \frac{1}{2\pi} \int_0^{2\pi} d\phi \int_0^\infty dq \, q \, G(q^2) \, \mathrm{e}^{i\,q\,b'\cos\phi}, \tag{C.3}$$

it is easy to see that by means of the integral form of the Bessel function,

$$\rho_B(b') = \int_0^\infty dq \, q \, J_0(qb) \, G(q^2). \tag{C.4}$$

Moreover, the inverse Fourier Transform also defines $G(q^2)$,

$$G(q^2) = \frac{1}{2\pi} \int d^2\mathbf{b}' \, \rho_B(b')\mathrm{e}^{-i\mathbf{q}\cdot\mathbf{b}'}. \tag{C.5}$$

---

[1] In reference [123] the eikonal function takes its form from the contribution from each of the nine pairs of valence (anti)quarks that corresponds to each of the two (anti)protons, and the contribution of all reactions initiated by a pair of gluons even though this number cannot be determined. Then, the overlap density function for valence quarks is normalised to 9, and for the gluons it is fixed as an effective number which is obtained by a fitting parameter.

Now considering that $b'' = |\mathbf{b} - \mathbf{b}'|$, and following the exactly same procedure,

$$
\begin{aligned}
\rho_A(|\mathbf{b} - \mathbf{b}'|) &= \frac{1}{2\pi} \int d^2\mathbf{q}\, G(q^2)\, e^{i\,\mathbf{q}\cdot(\mathbf{b}-\mathbf{b}')} \\
&= \int_0^\infty dq\, q\, J_0(qb)\, G(q^2)\, e^{-i\,\mathbf{q}\cdot\mathbf{b}'},
\end{aligned}
\tag{C.6}
$$

so, $A(b)$ can be rewritten as

$$
A(b) = \int_0^\infty dq\, q\, J_0(qb)\, G(q^2) \int d^2\mathbf{b}'\, \rho_B(b')\, e^{-i\,\mathbf{q}\cdot\mathbf{b}'}.
\tag{C.7}
$$

The second integral in the rhs of (C.7) is simply the form factor $G(b')$, which it finally gives

$$
\begin{aligned}
A(b) &= 2\pi \int_0^\infty dq\, q\, J_0(qb) \left[G(q^2)\right]^2 \\
&= \int d^2\mathbf{q}\, J_0(qb) \left[G(q^2)\right]^2.
\end{aligned}
\tag{C.8}
$$

C.2 The distribution function

The distribution function at impact-parameter b, $W(b; \mu)$, is defined as the overlap density function multiplied by the normalisation factor N,

$$
W(b; \mu) = N A(b; \mu).
\tag{C.9}
$$

Different form factors implies different distribution functions, since in essence it is simply written as the Hankel Transform of $G(q^2)$, also know as Fourrier-Bessel transform.

C.2.1 Monopole-like form factor

A monopole distribution is defined as

$$
G(q^2) = \left(1 + \frac{q^2}{\mu^2}\right)^{-1},
\tag{C.10}
$$

and using that $\langle(...)\rangle \equiv \int_0^\infty dq\, q J_0(qb)(...)$, where it is simply not to overload the notation, then the distribution function reads

$$
\frac{A(b)}{2\pi} = \left\langle \left(\frac{\mu^2}{q^2 + \mu^2}\right)^2 \right\rangle = \mu^4 \left\langle \left(\frac{1}{q^2 + \mu^2}\right)^2 \right\rangle.
\tag{C.11}
$$

It is well known that the Hankel transform of an Yukawa-type distribution is given by a simple modified Bessel function[2] of the second kind and zeroth order,

$$\left\langle \frac{1}{q^2 + \mu^2} \right\rangle = K_0(\mu b), \tag{C.12}$$

and moreover, there are different ways that higher orders of K_α functions can be generated from lower ones [61], *e.g.*,

$$\frac{d}{dx} \left[x^{-n} K_n(x) \right] = -x^{-n} K_{n+1}(x), \tag{C.13}$$

and if $x = \mu b$, then

$$\partial_\mu \left[\mu^{-n} K_n(\mu b) \right] = -b \, \mu^{-n} K_{n+1}(\mu b), \tag{C.14}$$

where $\partial_\mu = \partial/\partial\mu$. Now, it is easy to find out that for the monopole-like form factor the overlap distribution function can be written as

$$A(b) = 2\pi \frac{\mu^2}{2} (\mu b) \, K_1(\mu b), \tag{C.15}$$

whilst that

$$
\begin{aligned}
\left\langle \left(\frac{1}{q^2 + \mu^2} \right)^2 \right\rangle &= -\frac{1}{2\mu} \partial_\mu \left\langle \frac{1}{q^2 + \mu^2} \right\rangle \\
&= -\frac{1}{2\mu} \partial_\mu K_0(\mu b) \\
&= \frac{b}{2\mu} K_1(\mu b).
\end{aligned}
\tag{C.16}
$$

The normalisation of the distribution function as it was mentioned in expressions (C.2) and (C.9), follows as $\int d^2b \, W(b;\mu) = N \int d^2b \, A(b) = 1$, then

$$
\begin{aligned}
N \int d^2b \, A(b) &= N \int_0^{2\pi} d\phi \int_0^\infty db \, b \, A(b) = N \, 2\pi \, 2\pi \frac{\mu^3}{2} \int_0^\infty db \, b^2 \, K_1(\nu b) \\
&= N \, (2\pi)^2 \, \Gamma(2) \, \Gamma(1) = 1.
\end{aligned}
\tag{C.17}
$$

Hence, the normalisation is given by the value $N = 1/4\pi^2$. To calculate the integral of the K_α function, it was used the following relation [61]

$$\int_0^\infty dx \, x^\mu \, K_\nu(ax) = 2^{\mu-1} \, a^{-\mu-1} \Gamma\left(\frac{1+\mu+\nu}{2} \right) \Gamma\left(\frac{1+\mu-\nu}{2} \right), \tag{C.18}$$

$$\text{Re}\{\mu + 1 \pm \nu\} > 0 \text{ e Re} > 0,$$

---

[2] Or occasionally called as the hyperbolic Bessel function.

where the Euler gamma function is $\Gamma(n+1) = n!$. Finally, the normalised distribution function for the monopole model is written as

$$W(b;\mu) = \frac{\mu^2}{4\pi}(\mu b)K_1(\mu b). \tag{C.19}$$

C.2.2 Dipole-like form factor

A dipole distribution is defined as

$$G(q^2) = \left(1 + \frac{q^2}{\nu^2}\right)^{-2}, \tag{C.20}$$

and within the same procedure as before,

$$
\begin{aligned}
\frac{A(b)}{2\pi} &= \left\langle \left(\frac{\nu^2}{q^2+\nu^2}\right)^4 \right\rangle \\
&= \nu^8 \left\langle \left(\frac{1}{q^2+\nu^2}\right)^2 \left(\frac{1}{q^2+\nu^2}\right)^2 \right\rangle \\
&= \frac{\nu^6}{4} \left\{ \frac{1}{2}\partial_\nu\partial_\nu \left\langle \left(\frac{1}{q^2+\nu^2}\right)^2 \right\rangle - \left\langle \left(\frac{1}{q^2+\nu^2}\right)\partial_\nu^2\left(\frac{1}{q^2+\nu^2}\right) \right\rangle \right\}.
\end{aligned}
\tag{C.21}
$$

The math here is basically the same, but it will be shown step by step. The first term in curly brackets in the *rhs* of expression (C.21) can be written as a linear combination of K_α functions,

$$
\begin{aligned}
\frac{1}{2}\partial_\nu\partial_\nu \left\langle \left(\frac{1}{q^2+\nu^2}\right)^2 \right\rangle &= \frac{1}{2}\partial_\nu\partial_\nu \left(\frac{b}{2\nu}K_1(\nu b)\right) \\
&= \frac{b^4}{4}\left[\frac{K_3(\nu b)}{\nu b} - \frac{K_2(\nu b)}{(\nu b)^2}\right],
\end{aligned}
\tag{C.22}
$$

and similarly for the second term in the *rhs*,

$$
\begin{aligned}
\left\langle \left(\frac{1}{q^2+\nu^2}\right)\partial_\nu^2\left(\frac{1}{q^2+\nu^2}\right) \right\rangle &= \left\langle \frac{8\nu^2}{(q^2+\nu^2)^4} \right\rangle - \left\langle \frac{2}{(q^2+\nu^2)^3} \right\rangle \\
&= \left\langle \frac{8\nu^2}{(q^2+\nu^2)^4} \right\rangle - \frac{b^2}{4\nu^2}K_2(\nu b).
\end{aligned}
\tag{C.23}
$$

Finally, substituting these last two expression into (C.21),

$$\nu^8 \left\langle \left(\frac{1}{q^2+\nu^2}\right)^4 \right\rangle = \frac{\nu^5 b^3}{16}K_3(\nu b) - 2\nu^8 \left\langle \left(\frac{1}{q^2+\nu^2}\right)^4 \right\rangle, \tag{C.24}$$

and then the non-normalised overlap density function is found as

$$A(b) = \left\langle \left(\frac{\nu^2}{q^2 + \nu^2} \right)^4 \right\rangle = 2\pi \frac{\nu^2}{48} (\nu b)^3 K_3(\nu b). \tag{C.25}$$

All it is left, is to determine the normalisation factor for the dipole-like model. Then following the same procedure as before, one finds that the normalisation N is given respectively by

$$
\begin{aligned}
N \int d^2b\, A(b) &= N \int_0^{2\pi} d\phi \int_0^\infty db\, b\, A(b) = 2\pi\, 2\pi \frac{\nu^5}{48} \int_0^\infty db\, b^4\, K_3(\nu b) \\
&= (2\pi)^2 \frac{1}{6} \Gamma(4)\, \Gamma(1) = 1.
\end{aligned}
\tag{C.26}
$$

Hence, again, the normalisation is given by the value $N = 1/4\pi^2$. Thus, the normalised distribution function for the dipole model is written as

$$W(b; \nu) = \frac{\nu^2}{96\pi} (\nu b)^3 K_3(\nu b). \tag{C.27}$$

Perhaps one might see that there is a quicker way to calculate the Hankel transform within the infinite integral [61]

$$\int_0^\infty dq\, q\, J_0(qb) \left(\frac{1}{q^2 + \mu^2} \right)^{\alpha+1} = \left(\frac{b}{2\mu} \right)^\alpha \frac{K_\alpha(\mu b)}{\Gamma(\alpha+1)}, \tag{C.28}$$

but the procedure shown here is very easy to apply for different kinds of form factors, more complicated ones, when there are no closed forms for the Hankel Transform, *e.g.* the Durand-Pi form factor where the gluons in a proton are assumed to be distributed around the valence quarks in a Yukawa-type (monopole) distribution, so that the gluon distribution in a proton is the convolution of a monopole and a dipole [126].

Just for completeness, it is interesting to show the following asymptotic limits for the $x^\alpha K_\alpha$ functions:

$$\lim_{x \to \infty} x K_1(x) = 0, \tag{C.29}$$

$$\lim_{x \to 0} x K_1(x) = 1, \tag{C.30}$$

$$\lim_{x \to \infty} x^3 K_3(x) = 0, \tag{C.31}$$

$$\lim_{x \to 0} x^3 K_3(x) = 8. \tag{C.32}$$

These asymptotic behaviour limits can be seen in Figure C.1, where, for a better pictorical purpose, the typical monopole distribution function was multiplied by a factor of 100 whilst the dipole by a factor of 10.
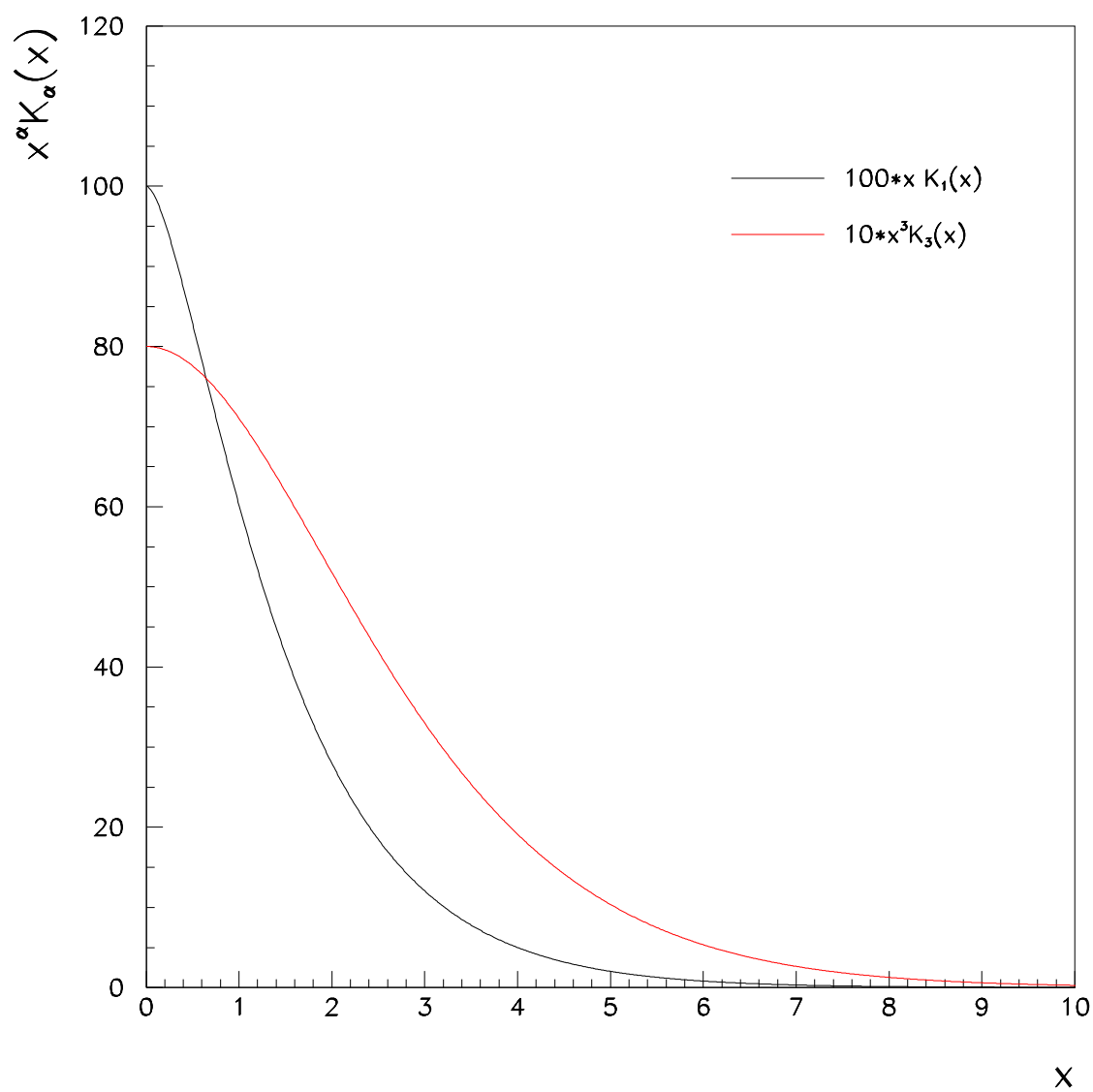
Figure C.1: Comparison between the asymptotic behaviour limits of typical monopole and dipole distribution functions.

Appendix D

List of publications

D.1 Articles in scientific journals

1. C.A.S. Bahia, M. Broilo and E.G.S. Luna, *Nonperturbative QCD effects in forward scattering at the LHC*, **Phys.Rev.D92 (2015) no.7 074039.**
   DOI: 10.1103/PhysRevD.92.074039.

2. C.A.S. Bahia, M. Broilo and E.G.S. Luna, *Energy-dependent dipole form factor in a QCD-inspired model*, **J.Phys.Conf.Ser. 706 (2016) no.5 052006.**
   DOI: 10.1088/1742-6596/706/5/052006.

3. C.A.S. Bahia, M. Broilo and E.G.S. Luna, *Regge phenomenology at LHC energies*, **Int.J.Mod.Phys. Conf.Ser. vol.45 (2017) 1760064.**
   DOI: 10.1142/S2010194517600643.

Bibliography

[1] Ellis, R.K., Stirling, W.J., Webber, B.R. *QCD and collider physics.* **Cambridge University Press, 1996.**

[2] Muta, T., *Foundations of quantum chromodynamics: an introduction to perturbative methods in gauge theories.* **Singapore: World Scientific 2009.**

[3] Barone, V., Predazzi, E., *High-energy particle diffraction.* **Springer-Verlag Berlin Heidelberg 2002.**

[4] Politzer, H.D., *Reliable pertubative results for strong interactions?.* **Phys.Rev.Lett. 30 (1973) 1346.**

[5] Gross, D.J., Wilczek, F., *Ultraviolet behavior of non-abelian gauge theories.* **Phys.Rev.Lett. 30 (1973) 1343.**

[6] Regge, T., *Introduction to complex orbital momenta.* **Nuovo Cimento 14 (1959) 951.**

[7] Regge, T., *Bound states, shadow states and Mandelstam representation.* **Nuovo Cimento 18 (1960) 947.**

[8] Gribov, V.N., *Analytic properties of the partial wave amplitudes and the asymptotic behavior of the scattering amplitude.* **Sov.Phys. JETP 15 (1962) 873.**

[9] Gribov, V.N., *A Reggeon Diagram Technique.* **Sov.Phys. JETP 26 (1968) 414.**

[10] Gribov, V.N., *Inelastic processes at super high-energies and the problem of nuclear cross-sections.* **Sov.J.Nucl.Phys. 9 (1969) 369.**

[11] Collins, P.D.B., *Regge heory and high energy physics.* **Cambriedge University Press, Cambriedge, (1977).**

[12] Gribov, V.N., *The theory of complex angular momenta.* **Cambriedge University Press, Cambriedge, (2003).**

[13] Donnachie, S., Dosch, G., Landshoff, P., Nachtmann, O., *Pomeron physics and QCD.* **Cambriedge University Press, Cambriedge, (2002).**

[14] Forshaw, J.R., Ross, D.A., *Quantum Chromodynamics and the Pomeron.* **Cambridge University Press, Cambridge, 1997.**

[15] Foldy, Leslie L., Peierls, Ronald F., *Isotopic spin of exchanged systems.* **Phys.Rev. 130 (1963) 1585.**

[16] Donnachie, A., Landshoff, P.V., *Total cross sections.* **Phys.Lett.B296 (1992) 227.**

[17] Antchev, G., *et al.*, *First measurement of the total proton-proton cross-section at the LHC energy of $\sqrt{s} = 7$ TeV.* **Eur.Phys.Lett. vol.96, (2011) 21002.**

[18] Antchev, G., *et al.*, *Measurement of proton-proton elastic scattering and total cross-section at $\sqrt{s} = 7$ TeV.* **Eur.Phys.Lett. vol.101 (2013) 21002.**

[19] Antchev, G., *et al.*, *Luminosity-independent measurements of total, elastic and inelastic cross-sections at $\sqrt{s} = 7$ TeV.* **Eur.Phys.Lett. vol.101 (2013) 21004.**

[20] Antchev, G., *et al.*, *Luminosity-independent measurements of the proton-proton total cross-sections at $\sqrt{s} = 8$ TeV.* **Phys.Rev.Lett. vol.111 (2013) 012001.**

[21] Antchev, G., *et al.*, *Measurement of elastic pp scattering at $\sqrt{s} = 8$ TeV in the Coulomb-nuclear interference region – Determination of the ρ-parameter and the total cross-section.* **Eur.Phys.J. C76 (2016) 661.**

[22] Antchev, G., *et al.*, *Proton-proton elastic scattering at the LHC energy of $\sqrt{s} = 7$ TeV.* **Eur.Phys.Lett. vol.95 (2011) 41001.**

[23] Anselm, A.A., Gribov, V.N., *Zero pion mass limit in interaction at very high energies.* **Phys.Lett.B40 (1972) 487.**

[24] Luna, E.G.S., Martini, A.F., Menon, M.J., Mihara, A., Natale, A.A., *Influence of a dynamical gluon mass in the pp and $\bar{p}p$ forward scattering.* **Phys.Rev.D72 (2005) 034019.**

[25] Luna, E.G.S., *Survival probability of large rapidity gaps in a QCD model with a dynamical infrared mass scale.* **Phys.Lett.B641 (2006) 171.**

[26] Luna, E.G.S., Natale, A.A., *γp and $\gamma\gamma$ scattering from $\bar{p}p$, pp forward amplitudes in a QCD eikonal model with a dynamical gluon mass.* **Phys.Rev.D73 (2006) 074019.**

[27] Fagundes, D.A., Luna, E.G.S., Menon, M.J., Natale, A.A., *Aspects of a dynamical gluon mass approach to elastic hadron scattering at LHC.* **Nucl.Phys.A886 (2012) 48.**

[28] Bahia, C.A.S., Broilo, M., Luna, E.G.S., *Energy-dependent dipolo form factor in a QCD-inspired model.* **J.Phys.Conf.Ser. 706 (2016) no.5 052006.**

[29] Bahia, C.A.S., Broilo, M., Luna, E.G.S., *Nonperturbative QCD effects in forward scattering at the LHC.* **Phys.Rev.D92 (2015) no.7 074039.**

[30] Luna, E.G.S., *Nucleon and delta sigma-terms.* **Braz.J.Phys. 37 (2007) 84.**

[31] Luna, E.G.S., Beggio, P.C., *Cross sections, multiplicity and moment distributions at the LHC.* **Nucl.Phys.A929 (2014) 230.**

[32] Luna, E.G.S., dos Santos, A.L., Natale, A.A., *QCD effective charge and the structure function F_2 at small-x.* **Phys.Lett.B698 (2011) 52.**

[33] Brodsky, S.J., *QCD phenomenology and light front wavefunctions.* **Acta Phys.Pol. B 32 (2001) 4013.**

[34] Brodsky, S.J., *The Heisenberg matrix formulation of quantum field theory.* **Fortschr.Phys. 50 (2002) 503.**

[35] Patrignani. C., *et al. Review of particle physics.* **Chin.Phys.C40 (2016) 100001.**

[36] Good, W.L., Walker, W.D., *Diffraction disssociation of beam particles.* **Phys.Rev. 120 (1960) 1857.**

[37] Bjorken, J.D., *Rapidity gaps and jets as a new physics signature in very high-energy hadron hadron collisions.* **Phys.Rev.D47 (1993) 101.**

[38] Sakurai, J. J., Tuan, S. F., *Modern quantum mechanics, revised edition.* **Addison Wesley Longman, 1994.**

[39] Block. M.M., Cahn, R.N., *High-enery $p\bar{p}$ and pp forward elastic scattering and total cross sections.* **Reviews of Modern Physics 57 (1985) no.2 563.**

[40] Froissart, M., *Asymptotic behavior and subtractions in the Mandelstam representation.* **Phys.Rev. 123 (1961) 1053.**

[41] Martin, A., *Extension of the axiomatic analyticity domain of scattering amplitudes by unitarity.* **Nuovo Cim.A42 (1965) 930.**

[42] Łukaszuk, L., Martin, A., *Absolute upper bounds for pi pi scattering* . **Nuovo Cim.A52 (1967) 122.**

[43] Pomaranchuk, I.Ya., *Equality of the nucleon and antinucleon total interaction cross section at high energies.* **Zh.Eksp.Teor.Fiz. 34 725 [Sov.Phys. – JETP 7 (1958) 499].**

[44] Eden, R.J., *Use of unitarity in proving pomeranchuk's theorem on cross sections at high energies.* **Phys.Rev.Lett. 16 (1966) no.1 39.**

[45] Grunberg, G., Truong, T.N., *Proof of the pomeranchuk theorem for unbounded total cross sections.* **Phys.Rev.Lett. 31 (1973) 63.**

[46] Cornille, H., Martin, A., *A pomeranchuk theorem for elastic diffraction peaks.* **Phys.Lett.B31 (1972) 671.**

[47] Halzen, F., Martin, A. D., *Quarks & Leptons: an introductory course in modern particle physics.* **John Wiley, 1984.**

[48] Mandelstam, S., *Determination of the pion-nucleon Scattering amplitude from dispersion relations and unitarity. General theory.* **Phys.Rev. 112 (1958) 1344.**

[49] Abreu, P., *et al.. Measurement of the proton-air cross-section at $\sqrt{s} = 57$ TeV with the Pierre Auger Observatory.* **Phys.Rev.Lett. 109 (2012) 062002.**

[50] Abbasi, R.U., *et al.. Measurement of the proton-air cross section with Telescope Array's Middle Drum detector and surface array in hybrid mode.* **Phys.Rev.D92 (2015) 032007.**

[51] Cudell, J.R., *et al.. Benchmarks for the Forward Observables at RHIC, the Tevatron-run II and the LHC.* **Phys.Rev.Lett. 89 (2002) 201801.**

[52] CMS Collaboration, Performance Analysis Note CMS-PAS-EWK-10-004 (2010); CMS Collaboration, Detector Performance Note CMS-DP-2011-000 C (2011).

[53] Amaldi, U., Schubert, K.R. *Impact parameter interpretation of proton proton scattering from a critical review of all ISR data.* **Nuclear Physics B 166 (1980) 301.**

[54] Amos, N.A., *et al., Measurement of small angle $\bar{p}p$ and proton proton elastic scattering at the CERN Intersecting Storage Rings.* **Nuclear Physics B 262 (1985) 686.**

[55] Breakstone, A., *et al.*, *A measurement of anti-p p and p p elastic scattering at ISR energies.* **Nuclear Physics B 248 (1984) 253.**

[56] Breakstone, A., *et al.*, *A measurement of anti-p p and pp elastic scattering in the dip region at $\sqrt{s} = 53$ GeV.* **Phys.Rev.Lett. 54 (1985) 2180.**

[57] Ambrosio, M., *et al.*, *Measurement of elastic scattering in anti-proton - proton collisions at 52.8 GeV center of mass energy.* **Phys.Lett. B115 (1982) 495.**

[58] Fagundes, D.A., Grau, A., Pacetti, S., Pancheri, G., Srivastava, Y.N., *Elastic pp scattering from the optical point to past the dip: An empirical parametrization from ISR to the LHC.* **Phys.Rev. D88 (2013) no.9 094019.**

[59] Titchmarsh, E.C., *The theory of functions.* **Oxford University Press, 2nd edition, Oxford, (1939).**

[60] Butkov, E., *Mathematical Physics.* Addison-Wesley, (1968).

[61] Bateman Manuscript Project, *Higher transcendental functions, vols. 1, 2 and 3.* **McGraw-Hill Book Company, Inc, 1953.**

[62] Chew, G.F., Frautschi, C., *Principle of equivalence for all strongly interacting particles within the S matrix framework.* **Phys.Rev.Lett 7 (1961) 394.**

[63] Chew, G.F., Frautschi, C., *Regge trajectories and the principle of maximum strength for strong interactions.* **Phys.Rev.Lett 8 (1962) 41.**

[64] Cudell, J.R., Kang, K., Kim, S.K., *Bounds on the Soft Pomeron Intercept.* **Phys.Lett.B395 (1997) 311.**

[65] Covolan, R.J.M., Montanha, J., Goulianos, K., *A new determination of the soft pomeron intercept.* **Phys.Lett.B389 (1996) 176.**

[66] Luna, E.G.S., Menon, M.J., *Extrema bounds for the soft Pomeron intercept.* **Phys.Lett.B565 (2003) 123.**

[67] Luna, E.G.S., Menon, M.J., Montanha, J., *An analysis on extrema and constrained bounds for the soft pomeron intercept.* **Nucl.Phys.A745 (2004) 104.**

[68] Luna, E.G.S., Menon, M.J., Montanha, J., *Extensions of the extrema bounds for the pomeron intercept to meson-proton, gamma-proton and gamma-gamma scattering.* **Braz.J.Phys. 34 (2004) 268.**

[69] Ávila, R.F., Luna, E.G.S., Menon, M.J., *Analytic models and forward scattering from accelerator to cosmic-ray energies.* **Phys.Rev.D67 054020 (2003) 054020.**

[70] Derrick, M., *et al.*, *A Measurement of sigma(tot) (gamma p) at s**(1/2) = 210-GeV.* **Phys.Lett.B293 (1992) 465.**

[71] Ahmed, T., *et al.*, *Observation of deep inelastic scattering at low x.* **Phys.Lett.B299 (1993) 385.**

[72] Breitweg, J., *et al.*, *Measurement of the diffractive structure function F2(D(4)) at HERA.* **Eur.Phys.J.C1 (1998) 81.**

[73] Baker, M., Ter-Martirosyan, K.A., *Gribov's Reggeon Calculus: Its Physical Basis and Implications.* **Phys.Rept. 28 (1976) 1.**

[74] Khoze, V.A., Martin, A.D., Ryskin, M.G., *Soft diffraction and the elastic slope at Teavatron and LHC energies: a multi-Pomeron approach.* **Eur.Phys.J.C 18 (2000) 167.**

[75] Luna, E.G.S.,Khoze, V.A., Martin, A.D., Ryskin, M.G., *Diffractive dissociation re-visited for predictions at the LHC.* **Eur.Phys.J.C 59 (2009) 1.**

[76] E.G.S. Luna, V.A. Khoze, A.D. Martin, and M.G. Ryskin, *The Possibility That the Triple-pomeron Coupling Vanishes at $q_t = 0$* **Eur.Phys.J.C 69 (2010) 95.**

[77] Khoze, V.A., Martin, A.D., Ryskin, M.G., *t dependence of the slope of the high energy elastic pp cross section.* **J.Phys.G42 (2015) 025003.**

[78] Capossoli, E.F., Boschi-Filho, H. *Odd spin glueball masses and the Odderon Regge trajectories from the holographic hardwall model.* **Phys.Rev.D88 (2013) 026010.**

[79] Ballon-Bayona, A., Quevedo, R.C., Costa, M.S., Djurić, M., *Soft Pomeron in Holographic QCD.* **Phys.Rev.D93 (2016) 035005.**

[80] Capossoli, E.F., Li, D., Boschi-Filho, H. *Pomeron and Odderon Regge Trajectories from a Dynamical Holographic Model.* **Phys.Lett.B760 (2016) 101.**

[81] Capossoli, E.F., Boschi-Filho, H. *Glueball spectra and Regge trajectories from a modified holographic softwall model.* **Phys.Lett.B753 (2016) 419.**

[82] Rodrigues, D.M., Capossoli, E.F., Boschi-Filho, H. Phys. *Twist two operator approach for even spin glueball masses and Pomeron Regge trajectory from the Hardwall model.* **Phys.Rev.D95 (2017) 076011.**

[83] Good, M.L., Walker, W.D., *Diffraction disssociation of beam particles.* **Phys.Rev.D120 (1960) 1857.**

[84] Khoze, V.A., Martin, A.D., Ryskin, M.G., *Can the Higgs be seen in rapidity gap events at the Tevatron or the LHC?*. **Eur.Phys.J.C14 (2000) 525.**

[85] Gotsman, E., Levin, E., Maor, U., *A Two channel calculation of screening corrections.* **Phys.Lett.B452 (1999) 387.**

[86] Gotsman, E., Levin, E., Maor, U., *Large rapidity gaps in p p collisions.* **Phys.Lett.B309 (1993) 199.**

[87] Donnachie, A., Landshoff, P.V., *pp and $\bar{p}p$ total cross sections and elastic scattering* . **Phys.Lett.B727 500 (2013) 500.**

[88] Desgrolard, P., Jenkovszky, L., Struminsky, B., *Where is the black disc limit?* **Eur.Phys.J.C11 (1999) 145**.

[89] Giffon, M., Martynov, E., Predazzi, E., *Generalized eikonalization and unitarity.* **Z.Phys.C76 (1997) 155.**

[90] Troshin, S.M., Tyurin, N.E., *The new elastic scattering measurements of TOTEM — are there hints for asymptotics?*. **Eur.Phys.J.A53 (2017) 57.**

[91] Bowman, P.O., Heller, U.M., Leinweber, D.B., Parappilly, M.B., Williams, A.G., *Unquenched gluon propagator in Landau gauge.* **Phys.Rev.D70 (2004) 034509.**

[92] Sternbeck, A., Ilgenfritz, E.-M., Muller-Preussker, M., *Spectral properties of the Landau gauge Faddeev-Popov operator in lattice gluodynamics.* **Phys.Rev.D73 (2006) 014502.**

[93] Boucaud, Ph., Brüntjen, T., Leroy, J. P., Le Yaouanc, A., Lokhov, A., Micheli, J., Pène, O., Rodriguez-Quintero, J., *Is the QCD ghost dressing function finite at zero momentum?* **J.High Energy Phys. 0606 (2006) 001.**

[94] Bowman, P.O., Heller, U.M., Leinweber, D.B., Parappilly, M.B., Sternbeck, A., von Smekal, L., Williams, A.G., Zhang, J. *Scaling behavior and positivity violation of the gluon propagator in full QCD.* **Phys.Rev.D76 (2007) 094505.**

[95] Bogolubsky, I.L., Ilgenfritz, E.-M., Muller-Preussker, M., Sternbeck, A., *Lattice gluodynamics computation of Landau-gauge Green's functions in the deep infrared.* **Phys.Lett.B676 (2009) 69.**

[96] Oliveira, O., Silva, P.J., *The lattice infrared Landau gauge gluon propagator: from finite volume to the infinite volume.* **Proc.Sci., QCD- TNT09 (2009) 033, arXiv:0911.1643.**

[97] Cucchieri, A., Mendes, T., Santos, E.M.S., *Covariant gauge on the lattice: a new implementation.* **Phys.Rev.Lett. 103 (2009) 141602.**

[98] Cucchieri, A., Mendes, T., *Landau-gauge propagators in Yang-Mills theories at $\beta = 0$: Massive solution versus conformal scaling.* **Phys.Rev.D81 (2010) 016005.**

[99] Dudal, D., Oliveira, O., Vandersickel, N., *Indirect lattice evidence for the refined Gribov-Zwanziger formalism and the gluon condensate $\langle A^2 \rangle$ in the Landau gauge.* **Phys.Rev.D81 (2010) 074505.**

[100] Cucchieri, A.,Dudal, Mendes, T.,Vandersickel, N., *Modeling the gluon propagator in Landau gauge: Lattice estimates of pole masses and dimension-two condensates.* **Phys.Rev.D85 (2012) 094513.**

[101] Cucchieri, A.,Dudal, Mendes, T.,Vandersickel, N., *BRST-symmetry breaking and Bose-ghost propagator in lattice minimal Landau gauge.* **Phys.Rev.D90 (2014) 051501.**

[102] Aguilar, A.C., Binosi, D., Papavassiliou, J., Rodriguez-Quintero, J., *Nonperturbative comparison of QCD effective charges.* **Phys.Rev.D80 (2009) 085018.**

[103] Ryder, L., *Quantum field theory 2ed.* **Cambridge University Press, 1996.**

[104] Faddeev, L.D., Popov, V.N., *Feynman diagrams for Yang-Mills Field.* **Phys.Lett.B v. B 25, no.1, (1967).**

[105] Faddeev, L.D., Slavnov, A.A., *Gauge Felds: introduction to quantum theory 2.ed..* **Redwood City: Addison-Wesley, 1991.**

[106] Caswell, W.E., *Asymptotic behavior of non-abelian gauge theories to two-loop order.* **Phys.Rev.Lett. 33 (1974) 244.**

[107] Barger, V.D., Phillips, R.J.N., *Collider physics.* **Addison-Wesley Publishing Company, 1997 (updated edition).**

[108] Taylor, R.E., Kendall, H.W., Friedman, J.I., *Deep inelastic scatterin: acknowledgements.* **Rev.Mod.Phys. 63 (1991) 573.**

[109] ZEUS Collaboration, CHEKANOV, S., *et al.*, *ZEUS next-to-leading-order QCD analysis of data on deep inelastic scattering.* **Phys.Rev.D67 (2003) 012007.**

[110] Bjorken, J.D., *Asymptotic Sum Rules at Infinite Momentum.* **Phys.Rev. 179 (1969) 1547.**

[111] Bjorken, J.D., Paschos, E.A., *Inelastic electron-proton scattering and the structure of the nucleon.* **Phys.Rev. 185 no.5 (1969) 1975.**

[112] Miller, G., *et al.*, *Inelastic electron-proton scattering at large momentum transfers and the inelastic structure functions of the proton.* **Phys.Rev.D5 no.3 (1972) 528.**

[113] Callan, C.G., Gross, D.J., *High-energy electroproduction and the constitution of the electric current.* **Phys.Rev.Lett. 22 no.4 (1969.) 156.**

[114] Aaron, F.D., *et al.*, *Combined measurement and QCD analysis of the inclusive $e^{\pm}p$ scattering cross sections at HERA.* **JHEP vol.2010 no.1 (2010) 1.**

[115] Altarelli, G., *A QCD primer.* **AIP Conf.Proc. 631 (2002) 70.**

[116] Gribov, V.N., Lipatov, L.N., *Deep inelastic ep scattering in perturbation theory.* **Yad. Fiz. 15, 781 (1972) [Sov.J.Nucl.Phys. 15 (1972) 438].**

[117] Lipatov, L.N., *The parton model and perturbation theory.* **Yad. Fiz. 20, 181 (1974) [Sov.J.Nucl.Phys. 20 (1975) 94].**

[118] Altarelli, G., Parisi, G., *Asymptotic freedom in parton language.* **Nucl.Phys.B126 (1977) 298.**

[119] Dokshitzer, Y.L., *Calculation of the structure functions for deep inelastic scattering and $e^+ e^-$ annihilation by perturbation theory in quantum chromodynamics.* **Zh. Eksp. Teor. Fiz. 73, 1216 (1977) [Sov.Phys. JETP 46 (1977) 641].**

[120] Martin, A.D., Roberts, R.G., Stirling, W.J., *Structure-function analysis and Ψ, jet, W, and Z production: Determining the gluon distribution.* **Phys.Rev.D37 (1988) 1161.**

[121] Halzen, F., *Summary talk – Blois V workshop on elastic and diffractive scattering.* **arxiv.org/abs/hep-ph/9307237v1 (1993).**

[122] Matthiae, G., *Proton and antiproton cross sections at high energies.* **Rep. Prog. Phys. 57 (1994) 743.**

[123] L'Heureux, P., Margolis, B., Valin, P., *Quark-gluon model for diffraction at high-energies.* **Phys.Rev.D32 (1985) no.7 1681.**

[124] Durand, L., Pi, H., *QCD and and rising cross section.* **Phys.Rev.Lett. 58 (1987) no.4 303.**

[125] Durand, L., Pi, H., *High-energy nucleon-nucleus scattering and cosmic-ray cross sections.* **Phys.Rev.D38 (1988) no.1 78.**

[126] Durand, L., Pi, H., *Semihard QCD and high-energy pp and $\bar{p}p$ scattering.* **Phys.Rev.D40 (1989) no.5 1436.**

[127] Cheng, H., Wu, T.T., *Limit of cross section at infinite energy.* **Phys.Rev.Lett. 24 (1970) 1456.**

[128] Low, F.E., *A model of the bare pomeron.* **Phys.Rev.D12 (1975) 163.**

[129] Nussinov, S., *Colored quark version of some hadronic puzzles.* **Phys.Rev.Lett. 34 (1975) 1286.**

[130] Landshoff, P.V., Nachtmann, O., *Vacuum structure and diffraction scattering.* **Z.Phys.C35 (1987) 405.**

[131] Gribov, L.V., Levin, E.M., Ryskin, M.G., *Semihard preocesses in QCD.* **Phys.Rep. 100 (1983) 1.**

[132] Levin, E.M., Ryskin, M.G., *High energy hadron collision in QCD.* **Phys.Rep. 189 (1990) 268.**

[133] Abou-El-Naga, N., Geiger, K., Müller, B., *QCD phenomenology of nucleon-nucleon cross sections.* **J.Phys.G18 (1992) 797.**

[134] Cheung, M.F., Chiu, C.B., *Classical color field modified minijet model for pp and $\bar{p}p$ total cross section.* **arXiv:1111.6957 [hep-ph].**

[135] Šauli, V., *Confined gluon from Minkowski space continuation of the PT-BFM SDE solution.* **J.Phys.G39 (2012) 035003.**

[136] Jia, S., Huang, F., *Scale dependencies of proton spin constituents with a nonperturbative α_s.* **Phys.Rev.D86 (2012) 094035.**

[137] Jia, S., Huang, F., *Interpretation of the measurements of total, elastic, and diffractive cross sections at LHC.* **Eur.Phys.J.C73 (2013) 2630.**

[138] Giannini, A.V., Durães, F.O., *Nonlinear effects and the behavior of total hadronic and photonic cross sections.* **Phys.Rev.D88 (2013) 114004.**

[139] Sidorov, A.V., Solovtsova, O.P., *The QCD analysis of xF_3 structure function based on the analytic approach.* **Nonlin.Phenom.Complex Syst. 16 397 (2013) 397.**

[140] Gomez, J.D., Natale, A.A., *Scalar coupling evolution in a non-perturbative QCD resummation scheme.* **Phys.Lett.B747 541 (2015) 541.**

[141] Ayala, C., Cvetič, G., *anQCD: A Mathematica package for calculations in general analytic QCD models.* **Comput.Phys.Commun. 190 (2015) 182.**

[142] Cvetič, G., *Techniques of evaluation of QCD low-energy physical quantities with running coupling with infrared fixed point.* **Phys.Rev.D89 (2014) 036003.**

[143] Allendes, P., Ayala, C., Cvetič, G., *Gluon propagator in fractional analytic perturbation theory.* **Phys.Rev.D89 (2014) 054016.**

[144] Aguilar, A.C., Natale, A.A., Rodrigues da Silva, P.S. *Relating a gluon mass scale to an infrared fixed point in pure gauge QCD.* **Phys.Rev.Lett. 90 (2003) 152001.**

[145] Forshaw, J.R., Papavassiliou, J., Parrinello, C., *Massive Yang-Mills model and diffractive scattering.* **Phys.Rev.D59 074008 (1999) 074008.**

[146] Cornwall, J.M., *Confinement and chiral-symmetry breakdown: Estimates of F_π and of effective quark masses.* **Phys.Rev.D22 (1980) 1452.**

[147] Cornwall, J.M., *Dynamical mass generation in continuum quantum chromodynamics.* **Phys.Rev.D26 1453 (1982) 1453.**

[148] Cornwall, J.M., Soni, A., *Glueballs as bound states of massive gluons.* **Phys.Lett.B120 (1983) 431.**

[149] Cornwall, J.M., Soni, A., *Couplings of low-lying glueballs to light quarks, gluons, and hadrons.* **Phys.Rev.D29 (1984) 1424.**

[150] Dyson, F.J., *The S Matrix in Quantum Electrodynamics.* **Phys.Rev.D75 (1949) 1736.**

[151] Schwinger, J.S., *On the Green's functions of quantized fields. I.* **Proc.Natl. Acad.Sci. 37 452 (1951) 452.**

[152] Aguilar, A.C., Mihara, A, Natale, A. A., *Freezing of the QCD coupling constant and solutions of Schwinger-Dyson equations.* **Phys.Rev. D65 (2002) 054011.**

[153] Aguilar, A.C., Mihara, A, Natale, A. A., *Phenomenological tests for the freezing of the QCD running coupling constant.* **Int. J. Mod.Phys. A19 (2004) 249.**

[154] Aguilar, A.C., Natale, A. A., *A Dynamical gluon mass solution in Mandelstam's approximation.* **Int.J.Mod.Phys.A20 (2005) 7613.**

[155] Stefanis, N.G., *Taming Landau singularities in QCD perturbation theory: The analytic approach* 2.0. **Phys.Part.Nucl. 44 (2013) 494.**

[156] Shirkov, D.V., Solovtsov, I.L., *Analytic model for the QCD running coupling with universal $\bar{\alpha_s}(0)$ value.* **Phys.Rev.Lett. 79 (1997) 1209.**

[157] Webber, B.R., *QCD power corrections from a simple model for the running coupling.* **J. High Energy Phys. 10 (1998) 012.**

[158] Nesterenko, A.V., *Quark-antiquark potential in the analytic approach to QCD.* **Phys.Rev.D62 (2000) 094028.**

[159] Nesterenko, A.V., Papavassiliou, J., *Massive analytic invariant charge in QCD.* **Phys.Rev.D71 (2005) 016009.**

[160] Alekseev, A.I., *Synthetic Running Coupling of QCD.* **Few-Body Syst.Suppl.X40 (2006) 57.**

[161] Cvetič, G., Valenzuela, C., *An approach for the evaluation of observables in analytic versions of QCD.* **J.Phys.G32 (2006) L27.**

[162] Cvetič, G., Valenzuela, C., *Various versions of analytic QCD and skeleton-motivated evaluation of observables.* **Phys.Rev.D74 (2006) 114030.**

[163] Cvetič, G., Valenzuela, C., *Analytic QCD: A Short review.* **Braz.J.Phys.38 371 (2008) 371.**

[164] Cvetič, G., Kögerler, R., Valenzuela, C., *Reconciling the analytic QCD with the ITEP operator product expansion philosophy.* **Phys.Rev.D82 (2010) 114004.**

[165] Cvetič, G., Villavicencio, C., *Operator product expansion with analytic QCD in τ decay physics.* **Phys.Rev.D86 116001 (2012) 116001.**

[166] Ayala, C., Cvetič, G., *Calculation of binding energies and masses of quarkonia in analytic QCD models.* **Phys.Rev.D87 054008 (2013) 054008.**

[167] Contreras, C., Cvetič, G., Kögerler, R., Kröger, P., Orellana, O., *Perturbative QCD in acceptable schemes with holomorphic coupling.* **Int.J.Mod.Phys.A30 (2015) 1550082.**

[168] Cvetič, G., *Evaluations of low-energy physical quantities in QCD with IR freezing of the coupling.* **Few-Body Syst.Suppl.X55 (2012) 567.**

[169] Carreras, B., White, J.N.J., *High energy diffraction slopes and the Chou-Yang model.* **Nucl.Phys.B42 95 (1972) 95.**

[170] White, J.N.J., *A comment on the ISR diffraction slope and the proton dipole form factor.* **Nucl.Phys.B51 (1973) 23.**

[171] Menon, M.J., *Phenomenological description of pp and pp elastic scattering above 10 GeV.* **Nucl.Phys.B,Proc.Suppl. 25 (1992) 94.**

[172] Menon, M.J., *Blackening and expansion in elastic hadron scattering.* **Can.J.Phys. 74 (1996) 594.**

[173] Beggio, P.C., Menon, M.J., Valin, P., *Scaling violations: connections between elastic and inelastic hadron scattering in a geometrical approach.* **Phys.Rev.D61 (2000) 034015.**

[174] Lipari, P., Lusignoli, M., *Multiple parton interactions in hadron collisions and diffraction.* **Phys.Rev.D80 (2009) 074014.**

[175] Fagundes, D.A., Grau, A., Pacetti, S., Pancheri, G., Srivastava, Y.N., *Elastic pp scattering from the optical point to past the dip: an empirical parametrization from ISR to the LHC.* **Phys.Rev.D88 (2013) 094019.**

[176] Luna, E.G.S., Khoze, V.A., Martin, A.D., Ryskin, M.G., *Diffractive dissociation re-visited for predictions at the LHC.* **Eur.Phys.J.C59 (2009) 1.**

[177] Luna, E.G.S., Khoze, V.A., Martin, A.D., Ryskin, M.G., *The possibility that the triple-Pomeron coupling vanishes at $q_t = 0$.* **Eur.Phys.J.C69 (2010) 95.**

[178] Barnett, R.M., Haber, H.E., Soper, D.E., *Ultra-heavy particle production from heavy partons at hadron colliders.* **Nucl.Phys.B306 (1988) 697.**

[179] Olness, F.I., Tung, W.-K., *When is a heavy quark not a parton? Charged Higgs production and heavy quark mass effects in the QCD-based parton model.* **Nucl.Phys.B308 (1988) 813.**

[180] Aivazis, M.A.G., Collins, J.C., Olness, F.I., Tung, W.-K., *Leptoproduction of heavy quarks. II. A unified QCD formulation of charged and neutral current processes from fixed-target to collider energies.* **Phys.Rev.D50 3102 (1994) 3102;**

[181] Stelzer, T., Sullivan, Z., Willenbrock, S., *Single-top-quark production via W-gluon fusion at next-to-leading order.* **Phys.Rev.D56 5919 (1997) 5919.**

[182] Politzer, H.D., *Effective quark masses in the chiral limit.* **Nucl.Phys.B117 (1976) 397.**

[183] Pascual, P., de Rafael, E., *Gluonic corrections to quark vacuum condensate contributions to two-point functions in QCD.* **Z.Phys.C12 (1982) 127.**

[184] Shifman, M.A., Vainshtein, A.I., Voloshin, M.B., Zakharov, V.I., *η_c puzzle in quantum chromodynamics.* **Phys.Lett. 77B 80 (1978) 80.**

[185] Vainshtein, A.I., Zakharov, V.I., Shifman, M.A., *Gluon Condensate And Lepton Decays Of Vector Mesons.* **Pisma Zh.Eksp.Teor.Fiz. 27 60 (1978) [JETP Lett. 27 (1978) 55].**

[186] Shifman, M.A., Vainshtein, A.I., Zakharov, V.I., *QCD and resonance physics. Theoretical foundations.* **Nucl.Phys.B147 (1979) 385.**

[187] Shifman, M.A., Vainshtein, A.I., Zakharov, V.I., *QCD and resonance physics. Applications.* **Nucl.Phys.B147 (1979) 448.**

[188] Lavelle, M., *Gauge-invariant effective gluon mass from the operator-product expansion.* **Phys.Rev.D44 (1991) R26.**

[189] Dudal, D., Gracey, J.A., Sorella, S.P., Vandersickel, N., Verschelde, H., *Refinement of the Gribov-Zwanziger approach in the Landau gauge: Infrared propagators in harmony with the lattice results.* **Phys.Rev.D78 (2008) 065047.**

[190] Eichten, E.J., Hinchliffe, I., Lane, K., Quigg, C., *Super collider physics.* **Rev.Mod.Phys. 56 (1984) 579.**

[191] Duke, D.W., Owens, J.F., *Q^2 dependent parametrizations of parton distribution functions.* **Phys.Rev.D30 (1984) 49.**

[192] Alekhin, S., *Extraction of parton distributions and α_s from DIS data within the baysian treatment of systematic errors.* **Eur.Phys.J.C10 (1999) 395.**

[193] Alekhin, S., *Statistical properties of the estimator using covariance matrix.* **hep-ex/0005042.**

[194] Alekhin, S., *Global fit to the charged leptons DIS data: α_s, parton distribution and high twists.* **Phys.Rev.D63 (2011).**

[195] Alekhin, S., *Parton distributions from deep inelastic scattering data.* **Phys.Rev.D68 (2003) 32.**

[196] CTEQ collabration, Botts, J., et al., *CTEQ parton distribution and flavor dependence of sea quarks.* **PhysLett.B304 (1993) 159.**

[197] CTEQ collaboration, Lai, H.L., et al., *Global QCD analysis and the CTEQ parton distribution.* **Phys.Rev.D51 (1995) 4763.**

[198] CTEQ collaboration, Lai, H.L., et al., *Improved parton distributions from global analysis of recent deep inelastic scattering and inclusive jet data.* **Phys.Rev.D55 (1997) 1280.**

[199] CTEQ collaboration, Lai, H. L., et al., *Global QCD analysis of parton structure of the nucleon: CTEQ5 parton distributions.* **Eur.Phys.J.C12 (2000) 375.**

[200] Pumplin, J., Stump, D.R., Huston, J., Lai, H.L., Tung, W.K., *New generation of parton distribution uncertainties from global QCD analysis.* **JHEP 07 (2002) 012.**

[201] Pumplin J., Stump, D.R., Huston,J., Lai, H.L., Nadolsky, P., Tung, W.K., *New Generation of Parton Distributions with Uncertainties from Global QCD Analysis.* **JHEP 0207 (2002) 012.**

[202] Stump, D.R., Huston, J., L., Tung, W.K., *Inclusive jet production, parton distributions, and the search for new physics.* **JHEP 12 (2003) 046.**

[203] Glück, M., Reya, E., Vogt, A., *Dynamical parton distributions of the proton ans small x physics.* **Z.PhysikC67 (1995) 433.**

[204] Glück, M., Reya, E., Vogt, A., *Dynamical parton distributions revisited.* **Eur.Phys.J.C5 (1998) 461.**

[205] Glück, M., Jimenez-Delgado, P., Reya, E., *Dynamical parton distributions of the nucleon and very small-x physics.* **Eur.Phys.J.C53 (2008) 355.**

[206] Martin, A.D., Roberts, R.G., Stirling, W.J., *Parton distributions of the proton.* **Phys.Rev.D50 (1994) 6734.**

[207] Martin, A.D., Roberts, R.G., Stirling, W.J., Thorne R.S., *Parton distribution: a new global analysis.* **Eur.Phys.J.C4 (1998) 463.**

[208] Martin, A.D., Roberts, R.G., Stirling, W.J., Thorne R.S., *Parton distribution and the LHC: W and Z production.* **Eur.Phys.J.C14 (2000) 133.**

[209] Martin, A.D., Stirling, W.J., Thorne, R.S., Watt, G., *Parton distributions for the LHC.* **Eur.Phys.J.C63 (2009) 189.**

[210] Harland-Lang, L.A., Martin, A.D., Motylinski, P., Thorne, R.S., *Parton distributions in the LHC era: MMHT 2014 PDFs.* **Eur.Phys.J.C75 (2015) 204.**

[211] Martin, A.D., Roberts, R.G. Stirling, W.J., Thorne, R.S., *NNLO global parton analysis.* **Phys.Lett.B531 (2002) 216.**

[212] Ball, R. D., Del Debbio, L., Forte, S., Guffanti, A., Latorre, J. I., Piccione, A., Rojo, J., Ubiali, M., *A determination of parton distributions with faithful uncertainty estimation.* **Nucl.Phys.B809 (2009) 1.**

[213] Pumplin, J., Stump, D.R., Tung, W.K., *Multivariate fitting and the error matrix in global analysis of data.* **Phys.Rev.D65 (2002) 014011.**

[214] Stump, D., Pumplin, J., Brock, R., Casey, D., Huston, J., Kalk, J., Lai, H.L., Tung, W. K., *Uncertainties of predictions from parton distribution functions. I. The Lagrange multiplier method.* **Phys.Rev.D65 (2001) 014012.**

[215] Pumplin, J., Stump, D., Brock, R., Casey, D., Huston, J., Kalk, J., Lai, H.L., Tung, W. K., *Uncertainties of predictions from parton distribution functions. II. The Hessian method.* **Phys.Rev.D65 (2002) 014013.**

[216] Lai, H.L., Huston, J., Kuhlmann, S., Morfin, J., Olness, F., Owens, J.F., Pumplin, J., Tung, W.K., *Global QCD analysis of parton structure of the nucleon: CTEQ5 parton distributions.* **Eur.Phys.J.C12 (2000) 375.**

[217] H1 collaboration, Adloff, C., et al., *Measurement of neutral and charged current cross-sections in positron proton collisions at large momentum transfer.* **Eur.Phys.J.C13 (2000) 609.**

[218] H1 collaboration, Adloff, C., et al., *Measurement of neutral and charged current cross-sections in electron proton collisions at high Q^2.* **Eur.Phys.J.C19 (2001) 269.**

[219] ZEUS collaboration, Chekanov, S., et al., *Measurement of neutral current cross sections an F_2 structure function for deep inelastic e^+p scattering at HERA.* **Eur.Phys.J.C21 (2001) 443.**

[220] Cooper-Sarkar, A., *Zeus NLO QCD fits.* bf hep-ph/0110386.

[221] D collaboration, Abbot, B., et al., *Inclusive jet production in $p\bar{p}$ collisions.* **Phys.Rev.Lett.86 (2001) 1707.**

[222] D collaboration, Abbot, B., et al., *High-p_T jets in $\bar{p}p$ collisions at $\sqrt{s} = 630\ GeV$ and $1800\ GeV$.* **Phys.Rev.D64 (2001) 032003.**

[223] FNAL E866/NuSea collaboration, Towell, R.S., et al., *Improved measurement of the $\frac{\bar{d}}{\bar{u}}$ asymmetry in the nucleon sea.* **Phys.Rev.D64 (2001) 052002.**

[224] CCFR/NuTeV collaboration, Yang, U.K., et al., *Measurements of F_2 and $xF_3^\nu - xF_3^{\bar\nu}$ from CCFR ν_μ-Fe and $\bar\nu_\mu$-Fe data in a physics model independent way.* **Phys.Rev.Lett. 86 (2001) 2742.**

[225] Appelquist, T., Carazzone, J., *Infrared singularities and massive fields.* **Phys.Rev.D11 (1975) 2856.**

[226] Martin, A.D., Roberts, R.G. Stirling, W.J., Thorne, R.S., *Uncertainties of predictions from parton distributions. I: Theoretical errors.* **Phys.lett.B604 (2004) 61.**

[227] Martin, A.D., Roberts, R. G. Stirling, W. J., Thorne, R. S., *Update of parton distributions at NNLO.* **Phys.lett.B652 (2007) 292.**

[228] Doff, A.,Luna, E.G.S., Natale, A.A., *The 125 GeV boson: A composite scalar?* **Phys.Rev.D88 (2013) 055008.**

[229] Luna, E.G.S., Natale, A.A., *Limit on the pion distribution amplitude.* **J.Phys.G42 (2015) 015003.**

[230] Ávila, R.F., Luna, E.G.S., Menon, M.J., *High-energy proton-proton forward scattering and derivative analyticity relations.* **Braz.J.Phys. 31 567 (2001) 567.**

[231] Ávila, R.F., Menon, M.J., *Critical analysis of derivative dispersion relations at high energies.* **Nucl.Phys.A744 249 (2004) 249.**

[232] Broilo., M., *Fatores de forma em modelos inspirados na Cromodinâmica Qunântica.* **Universidade Federal do Rio Grande do Sul, LUME, Digital Repository (2015).**
http://www.lume.ufrgs.br/bitstream/handle/10183/114831/000955700.pdf

[233] C.A.S. Bahia, M. Broilo and E.G.S. Luna, *Regge phenomenology at LHC energies,* **IJMP Conf.Ser. vol.45 (2017) 1760064.**

[234] Cornwall, J.M., Papavassiliou, J., *Gauge-invariant three-gluon vertex in QCD.* **Phys.Rev.D40 (1989) 3474.**

[235] Papavassiliou, J., Cornwall, J.M., *Coupled fermion gap and vertex equations for chiral-symmetry breakdown in QCD.* **Phys.Rev.D44 (1991) 1285.**

[236] Binosi, D., Papavassiliou, J., *New Schwinger-Dyson equations for non-Abelian gauge theories.* **JHEP 0811 (2008) 063.**

[237] Binosi, D., Papavassiliou, J., *Pinch Technique: theory and applications.* **Phys.Rep. 479 (2009) 1.**

[238] Aguilar, A.C., Papavassiliou, J., *Gluon mass generation without seagull divergences.* **Phys.Rev.D81 (2010) 034003.**

[239] Aguilar, A.C., Papavassiliou, J., *Power-law running of the effective gluon mass.* **Eur.Phys.J.A35 (2008) 189.**

[240] Aguilar, A.C., Papavassiliou, J., *Gluon mass generation in the PT-BFM scheme.* **JHEP 0612 (2006) 012.**

[241] Cornwall, J.M., Hou, W.S., *Extension of the gauge technique to broken symmetry and finite temperature.* **Phys.Rev.D34 (1986) 585.**

[242] Deile, M., *Elastic and total cross-section measurements by TOTEM.* 17th **conference on elastic and diffractive scattering, EDS Blois 2017, Prague, Czech Republic.**
https://indico.cern.ch/event/577066/contributions/2565986/attachments /1482376/2299352/eds2017.pdf

[243] Deile, M., **Private Communication.**

[244] Broilo., M., *Estudos de fatores de forma em modelos inspirados em QCD.* **XXV Reunião de Trabalho sobre Interações Hadrônicas, RETINHA XXV, Campinas, Brasil.**
http://sites.ifi.unicamp.br/retinhaxxv/files/2014/02/broilo.pdf

[245] Byron Jr., F.W., Fuller, R.W., *Mathematics of classical and quantum Physics.* **Dover, Nova York, 1992.**